

AN INTEGRATED STUDY OF EPIGENETIC GOLD
MINERALIZATION, DUBER LAKE AREA,
NORTHEASTERN NEWFOUNDLAND

CENTRE FOR NEWFOUNDLAND STUDIES

**TOTAL OF 10 PAGES ONLY
MAY BE XEROXED**

(Without Author's Permission)

RODNEY ALFRED CHURCHILL



National Library
of Canada

Acquisitions and
Bibliographic Services Branch

395 Wellington Street
Ottawa, Ontario
K1A 0N4

Bibliothèque nationale
du Canada

Direction des acquisitions et
des services bibliographiques

395, rue Wellington
Ottawa (Ontario)
K1A 0N4

Your file - Votre référence

Our file - Notre référence

NOTICE

The quality of this microform is heavily dependent upon the quality of the original thesis submitted for microfilming. Every effort has been made to ensure the highest quality of reproduction possible.

If pages are missing, contact the university which granted the degree.

Some pages may have indistinct print especially if the original pages were typed with a poor typewriter ribbon or if the university sent us an inferior photocopy.

Reproduction in full or in part of this microform is governed by the Canadian Copyright Act, R.S.C. 1970, c. C-30, and subsequent amendments.

AVIS

La qualité de cette microforme dépend grandement de la qualité de la thèse soumise au microfilmage. Nous avons tout fait pour assurer une qualité supérieure de reproduction.

S'il manque des pages, veuillez communiquer avec l'université qui a conféré le grade.

La qualité d'impression de certaines pages peut laisser à désirer, surtout si les pages originales ont été dactylographiées à l'aide d'un ruban usé ou si l'université nous a fait parvenir une photocopie de qualité inférieure.

La reproduction, même partielle, de cette microforme est soumise à la Loi canadienne sur le droit d'auteur, SRC 1970, c. C-30, et ses amendements subséquents.

Canada

**AN INTEGRATED STUDY OF EPIGENETIC GOLD
MINERALIZATION, DUDER LAKE AREA,
NORTHEASTERN NEWFOUNDLAND.**

By

© Rodney Alfred Churchill, B.Sc. (Hons.)

*A Thesis Submitted to the School of Graduate Studies
in Partial Fulfilment of the Requirements for the Degree
of Master of Science.*

*Department of Earth Sciences,
Memorial University of Newfoundland*

St. John's

August, 1994

Newfoundland



National Library
of Canada

Acquisitions and
Bibliographic Services Branch

395 Wellington Street
Ottawa, Ontario
K1A 0N4

Bibliothèque nationale
du Canada

Direction des acquisitions et
des services bibliographiques

395, rue Wellington
Ottawa (Ontario)
K1A 0N4

Your file *Votre référence*

Our file *Notre référence*

THE AUTHOR HAS GRANTED AN IRREVOCABLE NON-EXCLUSIVE LICENCE ALLOWING THE NATIONAL LIBRARY OF CANADA TO REPRODUCE, LOAN, DISTRIBUTE OR SELL COPIES OF HIS/HER THESIS BY ANY MEANS AND IN ANY FORM OR FORMAT, MAKING THIS THESIS AVAILABLE TO INTERESTED PERSONS.

L'AUTEUR A ACCORDE UNE LICENCE IRREVOCABLE ET NON EXCLUSIVE PERMETTANT A LA BIBLIOTHEQUE NATIONALE DU CANADA DE REPRODUIRE, PRETER, DISTRIBUER OU VENDRE DES COPIES DE SA THESE DE QUELQUE MANIERE ET SOUS QUELQUE FORME QUE CE SOIT POUR METTRE DES EXEMPLAIRES DE CETTE THESE A LA DISPOSITION DES PERSONNE INTERESSEES.

THE AUTHOR RETAINS OWNERSHIP OF THE COPYRIGHT IN HIS/HER THESIS. NEITHER THE THESIS NOR SUBSTANTIAL EXTRACTS FROM IT MAY BE PRINTED OR OTHERWISE REPRODUCED WITHOUT HIS/HER PERMISSION.

L'AUTEUR CONSERVE LA PROPRIETE DU DROIT D'AUTEUR QUI PROTEGE SA THESE. NI LA THESE NI DES EXTRAITS SUBSTANTIELS DE CELLE-CI NE DOIVENT ETRE IMPRIMES OU AUTREMENT REPRODUITS SANS SON AUTORISATION.

ISBN 0-315-96089-2

Canada

FRONTISPIECE



Lush vegetation around Ten Mile Lake - the topographical expression of the Dog Bay Line fault system. Looking south from the hilly southeast shore of Duder Lake.

ABSTRACT

The Duder Lake area is located within the eastern Dunnage Zone of the Newfoundland Appalachians, being part of the volcano-sedimentary Exploits Subzone. The study area is underlain by a mixed succession of late Ordovician to middle Silurian sedimentary and volcanic rocks which are intruded by numerous small gabbroic dykes and sills of Silurian to Devonian age. These sills and dykes were emplaced late in the deformational history of the area, but exhibit features suggesting that emplacement coincided with movement along a major fault system termed the Dog Bay Line. All units preserve three phases of deformation as well as a low- to mid-greenschist facies metamorphic mineral assemblage.

Recent exploration activity in this area, and elsewhere in the eastern Dunnage Zone, has indicated that the gabbros and graphitic sedimentary rocks host gold-bearing pyrite and arsenopyrite mineralization. The sulphide mineralization in most instances is structurally controlled following low angle Riedel shears which appear to be late structures related to the Dog Bay Line fault system. Fluid/rock and $\text{CO}_2/\text{H}_2\text{O}$ ratios, as determined from alteration mineral assemblages, diminish away from the mineralized shear zones producing a distinctive alteration zonation that is characterized by sulphidation, carbonatization and silicification. The hydrothermal alteration overprints the regional metamorphic assemblages.

Detailed geochemical, isotopic and microthermometric studies suggest that the fluids responsible for the auriferous mineralization were derived from metamorphic

devolatilization reactions in both Gander Zone basement rocks and the overlying allochthonous cover rocks of the Dunnage Zone during a Silurian orogenic event. The fluids, having sampled lithologically complex and diverse country rocks, were enriched in CO₂, H₂O, Au, As and Sb and were focused into large, late structures transecting the crust.

Geochemical data suggest that the Au was transported as bisulphide complexes that were destabilized due to changes in redox conditions in the carrier fluid from reducing to relatively more oxidizing. The physico-chemical controls acting at the time of mineralization were such that Au precipitated simultaneously with As and S, resulting in its incorporation within arsenopyrite. As a result, gold at the Duder Lake occurrences is not free and is best described as *invisible*.

Similarities between the Duder Lake gold occurrences and others elsewhere in the Dunnage Zone with similar ages and geological relationships suggest that the processes inherent in the formation of the Duder Lake occurrences may have been of a regional extent. As such the Duder Lake genetic model may be applicable to these other occurrences as well.

ACKNOWLEDGEMENTS

Numerous individuals require acknowledgement for their contribution(s) to this study. First and foremost is Dr. Derek Wilton who proposed and supervised this study. His guidance and "open-door" policy was greatly appreciated as well as his sometimes failed excursions into the realm of humour. Not only has he fulfilled his capacity as graduate student supervisor, but he has also been a friend throughout the course of this study.

Mr. David Evans of the Newfoundland Department of Mines and Energy is acknowledged for his insightful discussions into the regional geology and metallogeny of the eastern Dunnage Zone. Dave should also be acknowledged as a pseudo-supervisor for skilfully "filling the boots" of one DW during sabbatical leave.

Noranda Exploration Company Limited (N.P.L.) is thanked for unlimited access to the Duder Lake property and drill core, as well as for all data associated with the area. In particular Mr. Ian Perry is acknowledged for his assistance.

Former Noranda geologist, fellow student and friend Peter "Mud" Tallman is sincerely thanked for his wet and wild tour of the Duder Lake area in the spring of 1991, and for his late night camp visits. His knowledge and discussion of the Duder Lake geology and mineralization proved invaluable.

The Newfoundland Department of Mines and Energy is thanked for logistical support and geochemical analyses. In particular Chris Finch and the lab staff are thanked for top-notch work. Similarly, the technical staff at MUN including Darryl Clarke (XRF/Computer support), Bev Chapman (ICP-MS), Pam King (ICP-MS), Simon Jackson (LAM-ICP-MS), Adrian Timbal (Stable Isotope Lab), Caroline Emerson (SEM), and Mervin Goodyear (computer support) are acknowledged for expert assistance. Doug Furey (Eastern Analytical) is acknowledged for quartz vein assays.

Geoscientific personnel from the Newfoundland Department of Mines and MUN are thanked for enlightened discussion and clarification on certain subjects. In particular Frank Blackwood, Brian O'Brien, John "Bib" Hayes and Lawson Dickson all of the Department of Mines and Hank Williams, Hugh Miller, Mark Wilson, George Jenner and Adam Szybinski of the Department of Earth Sciences are recognized.

Fellow students J. Saunders, C. Lee, M. Vaskovic, G. Thompson, P. Ivany, D. Ritcey, K. Deveau and S. Archibald made graduate life enjoyable and will be remembered for the early morning symposiums over coffee in X-2014.

Dale Phillips and Rob Lane provided excellent field assistance even when their boots fell apart or when the aroma in the truck became unbearable.

Finally I thank my wife Desma and son Matthew for their patience, support, encouragement and understanding during the long absences and late nights resulting from the course of this study.

If I have omitted anybody worthy of recognition - my apologies for the oversight.

TABLE OF CONTENTS

FRONTISPIECE	i
ABSTRACT	ii
ACKNOWLEDGEMENTS	iv
TABLE OF CONTENTS	v
LIST OF TABLES	x
LIST OF FIGURES	xiii
LIST OF PLATES	xviii
LIST OF ABBREVIATIONS AND SYMBOLS USED	xxii

CHAPTER 1 *INTRODUCTION*

1.1 Location and Access	1
1.2 Physiography, Vegetation and Glacial History	1
1.3 Previous Work	3
1.4 Methods	4
1.5 Purpose and Scope	13

CHAPTER 2 *GEOLOGICAL SETTING*

2.1 Regional Tectonic Setting	14
2.2 Geological Development of the Dunnage Zone	18
2.2.1 Pre-Accretion	19
2.2.2 Post-Accretion	20
2.3 Geology and Stratigraphy of the Eastern Notre Dame Bay Area	21
2.3.1 Dunnage Melange	22
2.3.2 Caradocian Shale	22
2.3.3 Davidsville Group	24
2.3.4 Indian Islands Group	26
2.3.5 Botwood Group	26
2.3.5.1 Goldson Conglomerate	26
2.3.5.2 Lawrenceton Formation	27
2.3.5.3 Wigwam Formation	27
2.3.6 Burnt Lake Pluton	31
2.3.7 Charles Cove Pluton	31
2.3.8 Loon Bay Batholith	32
2.3.9 Mafic to Intermediate Dykes and Sills	32
2.4 Faults	33
2.5 Deformational Fabrics	35
2.5.1 D ₁ Deformational Features	35

2.5.2 D ₂ Deformational Features	37
2.5.3 D ₃ Deformational Features	37
2.6 Summary	40

CHAPTER 3
PETROGRAPHY AND GEOCHEMISTRY OF VOLCANIC
AND SEDIMENTARY ROCKS AND INTERPRETATION
OF THEIR TECTONIC SETTING

3.1 Introduction	41
3.2 Mafic Volcanic Rocks	42
3.2.1 Petrography	43
3.2.2 Geochemistry and Tectonic Setting	45
3.3 Sedimentary Rocks	49
3.3.1 Petrography	50
3.3.1.1 Sedimentary Rocks of the Wigwam Formation	50
3.3.1.2 Sedimentary Rocks of the Davidsville Group	51
3.3.2 Geochemistry and Tectonic Setting	52
3.4 Summary	55

CHAPTER 4
ECONOMIC MINERALIZATION

4.1 Introduction	56
4.2 Classification of Mineralization	58
4.3 Geology of Showings	64
4.3.1 Flirt Showing	64
4.3.2 Stinger Prospect	66
4.3.3 Corvette Prospect	70
4.3.4 Goldstash Prospect	74
4.4 Structural Control on Mineralization	80
4.5 Geophysical Expression of Structures Inherent to Mineralization	85
4.6 Summary	89

CHAPTER 5
PETROGRAPHIC AND GEOCHEMICAL STUDIES
OF ALTERATION AND MINERALIZATION

5.1 Introduction	90
5.2 Petrography and Zonation of Alteration	92
5.2.1 The GMA-Zone	94
5.2.2 The A-Zone	97
5.2.2.1 The A1-Zone	97
5.2.2.2 The A2-Zone	100

5.2.3 The M-Zone	101
5.2.3.1 Ore Mineralogy	104
5.2.4 Mineral Chemistry	114
5.2.5 Alteration Paragenesis and Model for Alteration Systematics	119
5.2.6 Summary	122
5.3 Geochemistry of Alteration and Mineralization	124
5.3.1 Introduction	124
5.3.2 Lithophile Element Systematics	128
5.3.3 CO ₂ and Rare Metal Content as Indicators of Alteration Intensity	133
5.3.3.1 As, Au, Sb and S Systematics	135
5.3.3.2 CO ₂ , Molar Ratios and Alteration	140
5.3.4 Rare Earth Element (REE) Geochemistry	145
5.3.4.1 Petrogenesis and Tectonic Setting	147
5.3.4.2 Rare Earth Behaviour During Alteration and Mineralization	157
5.3.5 Quantification of Geochemical Losses and Gains	159
5.3.6 Microthermometry	168
5.3.7 Stable Isotope Studies	179
5.3.7.1 Carbon and Oxygen Isotopes	180
5.3.7.2 Sulphur Isotopes	186
5.3.8 Au-Sulphide Relationships	190
5.4 Summary	194

CHAPTER 6

DISCUSSION AND MODEL FOR GOLD MINERALIZATION

6.1 Introduction	196
6.2 Discussion of Mechanisms of Alteration	198
6.3 Discussion of Mechanisms of Mineralization	200
6.4 Physico-Chemical Conditions of Mineralizing Fluid and Postulations on Fluid Source Reservoirs	205
6.5 Genetic Model for Mineralization	207

REFERENCES	212
-----------------------------	-----

APPENDIX I
ANALYTICAL METHODS

I.1	Sample Preparation	A1
I.2	Scanning Electron Microscope (SEM) Determinations	A1
I.3	X-Ray Diffractometer (XRD) Mineral Identification	A2
I.4	Fluid Inclusion Techniques	A3
I.5	Stable Isotope Techniques	A4
	a. $\delta^{13}\text{C}$ and $\delta^{18}\text{O}$ Determinations from Carbonates	A4
	b. $\delta^{34}\text{S}$ Determinations from Sulphides	A7
	c. $\delta^{18}\text{O}$ Determinations from Quartz	A8
I.6	Laser Ablation Microprobe-Inductively Coupled Plasma-Mass Spectrometry (LAM-ICP-MS)	A8
I.7	Quartz Vein Assays	A10
	a. Fire Assay/Atomic Absorption (AA) Finish	A11
	b. Aqua Regia Digestion - Inductively Coupled Plasma-Mass Spectroscopy (AR-ICP)	A11
I.8	Infra-Red Determinations	A12
I.9	Multi-Element Direct Neutron Activation Analysis (NAA)	A13
I.10	Atomic Absorption Spectroscopy (AAS) Trace Element Determinations	A14
I.11	X-Ray Fluorescence (XRF) Trace Element Analyses	A16
I.12	Inductively Coupled Plasma-Emission Spectroscopy (ICP-ES) Major Oxide Determinations	A17
I.13	Inductively Coupled Plasma-Mass Spectrometry (ICP-MS) Techniques	A19
	References Cited In Appendices	A23

APPENDIX II
WHOLE ROCK GEOCHEMICAL ANALYSES

	Introduction	A25
II.a	Major- and trace-element data for mafic volcanic rocks of the Lawrenceton Formation	A27
II.b	Rare earth element data (ppm) for mafic volcanic rocks of the Lawrenceton Formation	A27
II.c	Major- and trace-element data for mafic plutonic rocks	A28
II.d	Rare earth element data for select mafic plutonic rocks	A39
II.e	Major- and trace-element data for sandstone and siltstone lithologies	A41
II.f	Major- and trace-element data for mineralized quartz-carbonate veins	A43
II.g	Gold assays and sample intervals for selected diamond drill core samples	A44

**APPENDIX III
SAMPLE LOCATIONS**

III.a	Trench and outcrop sample locations	A48
III.b	Location data for samples obtained from diamond drill core	A50

**APPENDIX IV
TRENCH MAPS**

TR-89-01	A54
TR-89-02	A55
TR-89-03	A56
TR-89-04	A57
TR-89-05	A58
TR-89-06	A59
TR-89-07	A60
TR-89-08	A61
TR-89-09A/B	A62

**APPENDIX V
SCHEMATIC VISUAL DRILL LOGS**

DL-90-01	A64
DL-90-02	A65
DL-90-03	A66
DL-90-04	A67
DL-90-05	A68
DL-90-06	A69
DL-90-07	A70
DL-90-08	A71

LIST OF TABLES

Chapter 1

Table 1.1: Compilation of relevant geoscientific research in the eastern Notre Dame Bay area with brief descriptive notes	5
-------------------------------------------------------------------------------------------------------------------------------------	---

Chapter 2

Table 2.1: Summary of geological features which support the division of the Dunnage Zone into two subzones	19
----------------------------------------------------------------------------------------------------------------------	----

Chapter 3

Table 3.1: Elements analyzed and numbers of samples per lithological type studied	42
---------------------------------------------------------------------------------------------	----

Table 3.2: Normalization factors for chondrite and geochemical data for continental flood basalt and MORB samples	49
-----------------------------------------------------------------------------------------------------------------------------	----

Chapter 5

Table 5.1: Elements analyzed and numbers of samples per lithological type studied	91
---------------------------------------------------------------------------------------------	----

Table 5.2: Some probable alteration and metamorphic mineral reactions that may have been important in the formation of the alteration zonation accompanying gold mineralization	103
-------------------------------------------------------------------------------------------------------------------------------------------------------------------------------------------	-----

Table 5.3: Compilation of minerals and mineral abundances of each of the four alteration zones based on optical observations	105
----------------------------------------------------------------------------------------------------------------------------------------	-----

Table 5.4: Mean oxide concentrations from SEM mineral analyses	118
--------------------------------------------------------------------------	-----

Table 5.5: Average major oxide and trace element compositions for mafic plutonic rocks from the (a) GMA-Zone, (b) A-Zone and (c) M-Zone	125
---------------------------------------------------------------------------------------------------------------------------------------------------	-----

Table 5.6: Average REE abundances for mafic plutonic rocks from each of the three zones	128
---------------------------------------------------------------------------------------------------	-----

Table 5.7: Element concentrations used in Figure 5.7	134
----------------------------------------------------------------	-----

Table 5.8: Normalization values for N-MORB (after Sun and McDonough, 1989) and primitive (adapted from Hofmann, 1988)	150
Table 5.9: Rare earth contents of aplite dyke sample (LB-0311) from Loon Bay (values from Burke, 1992) and for GSJ standard JGB-1 (values from Govindaraju, 1987)	152
Table 5.10: Average geochemical concentrations of fresh gabbros from the GMA-Zone (C°) and mineralized gabbros of the M-Zone (C*)	162
Table 5.11: Fluid inclusion sample descriptions	172
Table 5.12: Microthermometry data from fluid inclusions in quartz, calcite, and ankerite from variably altered gabbros and from quartz veins	173
Table 5.13: Volumetric, density and molar compositional data for fluid inclusions	174
Table 5.14: Stable isotope data from mineralized and non-mineralized samples	182
Table 5.15: Ranges of $\delta^{18}\text{O}$ and $\delta^{13}\text{C}$ isotopic compositions for selected lode gold deposits and isotopic reservoirs as well as the sources of data	184
Table 5.16: Tabulated $\delta^{18}\text{O}_{\text{H}_2\text{O}}$ values for each of the three lithotypes analyzed and information used in the calculation	186
Table 5.17: Ranges of $\delta^{34}\text{S}$ isotopic compositions for selected lode gold deposits and isotopic reservoirs as well as the sources of data	189
Table 5.18: Tabulated $\delta^{34}\text{S}_{\text{H}_2\text{S}}$ values for each of the three lithotypes analyzed as well as information used in the calculation of the value	189
 <i>Appendix I</i>	
Table I.1: Isotopic masses and natural abundances of isotopes used in LAM-ICP-MS determinations	A11
Table I.2: Limits of detection (LD) for elements analyzed by the AR-ICP technique	A12
Table I.3: Precision and accuracy for infra-red analyses	A13

Table I.4: Precision and accuracy for neutron activation analyses	A15
Table I.5: Precision and accuracy for AAS trace-element analyses	A16
Table I.6: Precision and accuracy for XRF analyses	A18
Table I.7: Precision and accuracy for major-oxide ICP-ES analyses	A19
Table I.8: Precision and accuracy for ICP-MS analyses	A22

Appendix II

Table II.1: Elements utilized from the different analytical techniques and which were used in all geochemical applications	A26
-----------------------------------------------------------------------------------------------------------------------------------------	-----

LIST OF FIGURES

Chapter 1

- Figure 1.1: Plan map showing location of Duder Lake, major routes, and Noranda claim blocks (CB) constituting part of their GRUB North exploration project 2

Chapter 2

- Figure 2.1: Tectonostratigraphic zonations and major tectonic boundaries of the Newfoundland Appalachians 15
- Figure 2.2: Regional geology of eastern Notre Dame Bay, Newfoundland 23
- Figure 2.3: Contoured, equal area, lower hemisphere, poles-to-planes stereographic projections for bedding and schistosity data 38

Chapter 3

- Figure 3.1: AFM plot of Irvine and Barager (1971) indicating the chemical affinity of the mafic volcanic rocks from Duder Lake, the Clutha gold prospect and Dan's Pond 46
- Figure 3.2: Irvine and Barager (1971) $\text{Na}_2\text{O} + \text{K}_2\text{O}$ versus SiO_2 plot illustrating the sub-alkaline nature of the mafic volcanic rocks 46
- Figure 3.3: Winchester and Floyd (1979) plot of Nb/Y versus Zr/Ti diagram which illustrates the composition of mafic volcanic rocks from the Duder Lake area 48
- Figure 3.4: Tectonic discrimination plot of Meschede (1986) indicating the tectonic affinity of volcanic rocks in the Duder Lake area 48
- Figure 3.5: Chondrite normalized REE profiles for mafic volcanic rocks from the Duder Lake area (shaded region, n=4) as well as typical continental flood basalts DT-13 and BCR-1 and mid-ocean ridge basalt sample BIR-1 53
- Figure 3.6: Roser and Korsch (1986) tectonic discrimination plot of SiO_2 (wt%) versus $\text{K}_2\text{O}/\text{Na}_2\text{O}$ for mudstone and sandstone suites with tectonic setting fields as labelled 53

Chapter 4

Figure 4.1: Simplified geological setting of gold occurrences in the eastern Dunnage Zone, central Newfoundland (modified from Evans, 1992) 57

Figure 4.2: Simplified grid geology of the area in the vicinity of the Corvette, Goldstash and Stinger prospects 59

Figure 4.3: Classification scheme for gold mineralization within the eastern Dunnage Zone (modified from Evans, 1993) 60

Figure 4.4: Simplified geology of the Flirt Showing with NTS grid reference and schematic trench maps 65

Figure 4.5: Geology of the Stinger Prospect with grid reference and location of drill hole DL-90-02 and trench TR-89-08 67

Figure 4.6: Log Au (ppb) assay values for diamond drill hole DL-90-02 from the Stinger Prospect 69

Figure 4.7: Geology of the Corvette Prospect with grid references and location of drill hole DL-90-03 and trenches TR-89-06 and TR-89-07 72

Figure 4.8: Log Au (ppb) assay values for diamond drill hole DL-90-03 from the Corvette Prospect 73

Figure 4.9: Geology of the Goldstash Prospect with grid references and location of drill holes and trenches 75

Figure 4.10: NE-SW oriented cross-section through the Goldstash Prospect showing topographic relief and lithological sub-units 77

Figure 4.11a: Log Au (ppb) assay values for diamond drill holes DL-90-01, DL-90-04 and DL-90-05 from the Goldstash Prospect with zones of economic mineralization delineated that coincides with visible pyrite and arsenopyrite mineralization observed in drill core 78

Figure 4.11b: Log Au (ppb) assay values for diamond drill holes DL-90-06, DL-90-07 and DL-90-08 from the Goldstash Prospect with zones of economic mineralization delineated that coincides with visible pyrite and arsenopyrite mineralization observed in drill core 79

Figure 4.12: Geomechanical representation of megascopic, second-order faults/shears associated with the Dog Bay Line 86

Figure 4.13: Geophysical expression of geological elements at Duder Lake 87

Chapter 5

Figure 5.1: Cumulative modal percentage plot for each of the alteration zonations defined for the Duder Lake gold showings 107

Figure 5.2: Ternary phase diagrams for (a) the FeO-Fe₂O₃-TiO₂ system showing three solid solution series including ulvospinel-magnetite and (b) the Fe-S-O system for low temperature assemblages 117

Figure 5.3: Semi-quantitative SEM analyses for (a) carbonates and (b) chlorites from the GMA-Zone (squares), A-Zone (triangles) and M-Zone (circles) 121

Figure 5.4: Alteration history and genetic model 123

Figure 5.5a: Covariant plots of K vs. Rb; K vs. Ba; K vs. Cs; K vs. Li; K/Rb vs. Rb and K/Ba vs. Ba for samples representative of the GMA-Zone (squares), A-Zone (triangles) and M-Zone (circles) 130

Figure 5.5b: Covariant plots of Sr vs. Rb; Ba vs. Rb; Ce vs. Th; U vs. Th; V vs. Ti and Ga vs. Al for samples from the three zones 131

Figure 5.6: Enrichment diagram for As, Au, S and Sb from each of the alteration zonations in the Duder Lake gold occurrences 134

Figure 5.7: Log frequency distribution diagrams for As, Au and Sb 136

Figure 5.8: Bivariate plots of S/Sb, S/As, S/Au, Sb/Au and As/Au which illustrate interelement relationships for As, Sb and Au 138

Figure 5.9: Plots of W versus Au, As and Sb showing correlation between increasing W contents and ore metal concentrations 139

Figure 5.10: Bivariate plots of CO₂ versus Au, As, Sb and W 142

Figure 5.11: Plots of molar ratio (CO_2/CaO) plotted against CO_2 (alteration index), K_2O (measure of potassic metasomatism) and Au (measure of mineralization)	144
Figure 5.12: Plots of $\text{CO}_2/\text{H}_2\text{O}$ alteration index plotted against the ore metals . . .	146
Figure 5.13: N-MORB normalized REE plot for fresh gabbros from the Duder Lake gold occurrences	149
Figure 5.14: N-MORB normalized REE plots for Loon Bay granodiorite (LB-0311), island arc gabbro (JGB-1) and the average REE content for unaltered Duder Lake gabbros (GMA-av)	149
Figure 5.15: Discrimination plots that illustrate the chemical affinity of the gabbros	153
Figure 5.16: Discrimination plots that support the concept of an arc component in the gabbros	154
Figure 5.17: Compilation of REE data for gabbros from the Gander River Complex (O'Neill, 1991), Big Pond and Clutha gold occurrences (unpublished data, Newfoundland Department of Mines and Energy) and unaltered gabbros from Duder Lake (this study)	156
Figure 5.18: Primitive normalized REE plots for gabbros from the (a) GMA-Zone, (b) A-Zone and (c) M-Zone	158
Figure 5.19: Compilation of primitive normalized REE data for each of the three lithotypes from the Duder Lake gold occurrences	160
Figure 5.20: Isocon diagrams for average analyses of unaltered gabbro and mineralized gabbro	163
Figure 5.21: Relative gains ("+" values) and losses ("- " values) calculated using the technique of Grant (1986) for changes observed between gabbros of the GMA- and M-Zones	165
Figure 5.22: Histograms of thermometric data collected from $\text{H}_2\text{O}(\ell)\text{-H}_2\text{O}(\text{v})$ (Type I) and $\text{CO}_2(\ell)\text{-CO}_2(\text{v})\text{-H}_2\text{O}(\ell)$ (Type IV) inclusions using heating and freezing experiments	175

Figure 5.23: H ₂ O-CO ₂ -NaCl ternary diagram for calculated molar compositions for fluid inclusions	178
Figure 5.24: Equivalent Wt. % NaCl versus homogenization temperature plot for microthermometric data from the Duder Lake gold occurrences	178
Figure 5.25: Carbon, oxygen and sulphur isotopic compositions for selected isotopic reservoirs as well as for numerous gold deposits which are similar in style to that of the Duder Lake occurrences	185
Figure 5.26: Deuterium versus oxygen isotope diagram illustrating the range of $\delta^{18}\text{O}$ data for calculated ore fluids	187
Figure 5.27: Oxygen versus carbon isotope diagram illustrating the range of $\delta^{18}\text{O}$ and $\delta^{13}\text{C}$ values for carbonate minerals	187
Figure 5.28: Plots of counts per second (c.p.s.) versus time for LAM-ICP-MS analyses of auriferous arsenopyrite representative of mineralization at Duder Lake	193
Chapter 6	
Figure 6.1: Calculated oxygen activity-sulphur activity diagram for the system Au-Fe-As-S-H ₂ O at 250°C and pH5	203
Figure 6.2: Schematic genetic model for gold mineralization in the Duder Lake area	208
Appendix I	
Figure I.1: Plan and cross-sectional views of the LAM-ICP-MS	A9
Map Appendix	
Figure MA-1: Duder Lake Geology	<i>In Back Pocket</i>

LIST OF PLATES

Chapter 2

Plate 2.1: Quartz veined, gossanous and pyrite mineralized Caradocian shale outcropping approximately 3km west of the community of Birchy Bay 25

Plate 2.2: Graphitic siltstones and shales of the Davidsville Group east of Duder Lake 25

Plate 2.3: Strongly deformed grey-green siltstones of the Stoneville Formation, Indian Islands Group 28

Plate 2.4: Clast supported polymictic conglomerate of the Goldson Conglomerate 28

Plate 2.5: Mafic agglomerate of the Lawrenceton Formation of the Botwood Group with rare felsic fragments (whitish colour) 30

Plate 2.6: Folded, convoluted bedded fine-grained sandstones of the Wigwam Formation possessing strong S_2 cleavage 30

Plate 2.7: Coarse-grained gabbro dyke with pegmatitic pods (right half of photograph) intruding red beds of the Wigwam Formation approximately 3km northeast of the northern extremity of Duder Lake 36

Plate 2.8: Overturned F_1 -fold in argillaceous siltstones of the lower part of the Wigwam Formation 36

Plate 2.9: Northeasterly-trending D_2 fabric developed in greenish siltstones of the lower part of the Wigwam Formation 39

Plate 2.10: S_3 crenulation cleavage kinking S_2 cleavage developed in maroon coloured sandstones of the Wigwam Formation located 4km east of the Birchy Bay turn-off 39

Chapter 3

Plate 3.1: Photomicrograph of metamorphosed basalt of the Lawrenceton Formation exhibiting a greenschist facies metamorphic mineral assemblage including calcite (cc), epidote (ep) and sericite (sr) in plagioclase (pl) 44

Plate 3.2: Photomicrograph of fine-grained quartzo-feldspathic sandstone from the Wigwam Formation 54

Plate 3.3: Photomicrograph of fine-grained argillaceous siltstone of the Davidsville Group 54

Chapter 4

Plate 4.1: Typical style of host rock replacement and mineralization associated with Type Ia mineralization 62

Plate 4.2: Thin, gossanous, quartz-carbonate veins (located below photo-scale) developed in gabbros at the Flirt Showing (TR-89-09) 63

Plate 4.3: Graphitic siltstones (black) from the Stinger Prospect with narrow sulphide veinlets (white) 63

Plate 4.4: Site of the Stinger Prospect 68

Plate 4.5: Recessively weathered, gossanous and mineralized section in trench TR-89-06 at the Corvette Prospect 71

Plate 4.6: "Blocky" joint/fracture pattern as seen in trench wall (TR-89-05) at the Goldstash Prospect 71

Plate 4.7: View of Riedel shear in trench TR-89-04 at the Goldstash Prospect . . . 82

Plate 4.8: Close-up of Riedel shear depicted in Plate 4.7 82

Plate 4.9: Deformation effects observed in albite having a "domino" appearance resulting from brittle fracturing and rigid rotation 84

Plate 4.10: Photomicrograph of fine-grained recrystallized quartz in narrow bands reminiscent of a ductile shear fabric 84

Chapter 5

Plate 5.1: Photomicrograph of "fresh" gabbro from the GMA-Zone exhibiting large euhedral pyroxene (Pyx) phenocrysts, albitized plagioclase (Alb) and minor chlorite (Chl) 96

Plate 5.2: Skeletal leucoxene (Lcx) pseudomorphing Fe-Ti oxides in a fresh gabbro from the GMA-Zone	96
Plate 5.3: Photomicrograph of gabbro from the A1-Zone showing uralite (Ur) bounding relict pyroxenes (Pyx)	99
Plate 5.4: Computer enhanced image of altered gabbro from the A1-Zone	99
Plate 5.5: Photomicrograph of altered gabbro from the A2-Zone	102
Plate 5.6: Photomicrograph of altered gabbro from the A2-Zone exhibiting fine-grained fibrous aggregates of sericite (blue) concentrated in millimetre wide bands	102
Plate 5.7: Photomicrograph of replacement features observed in leucoxene-anatase-rutile (brown) after titanomagnetite (yellow) as preserved in rocks of the M-Zone	106
Plate 5.8: Photomicrograph of a representative mineral assemblage from the M-Zone	106
Plate 5.9: Photomicrograph of pyrrhotite (brown) intergrown with pyrite (light brown)	109
Plate 5.10: Photomicrograph of simple intergrowth relationships between pyrite and arsenopyrite	109
Plate 5.11: Photomicrograph of bands of sulphide mineralization which parallel the shear foliation	111
Plate 5.12: Photomicrograph of pyrite megaclast (light brown, centre of photo) having an appearance best described as brecciated	111
Plate 5.13: Photomicrograph of large uralitized grain of pyroxene with visible cleavage traces occupied by sulphide grains	113
Plate 5.14: Annealed arsenopyrite grains (right of centre) exhibiting coalescence as well as the indicative 120° grain boundaries	113
Plate 5.15: Photomicrograph of chlorite (green) concentrated along shear bands with sulphides (black)	115

Plate 5.16: Photomicrograph of thin lamellae of exsolved ilmenite in a matrix of leucoxene (dark brown) and magnetite (Mgt)	115
Plate 5.17: Photomicrograph of relict magnetite (mgt), ilmenite (ilm), leucoxene (lcx) and arsenopyrite (asp)	116
Plate 5.18: Intimate association of arsenopyrite (yellow-brown) with skeletal leucoxene-magnetite-ilmenite intergrowth (dark brown)	116
Plate 5.19: Reflected light photomicrograph of undersaturated two phase $H_2O(l)$ - $H_2O(v)$ (Type I) inclusions associated with A-Zone alteration phases . . .	169
Plate 5.20: Reflected light photomicrograph of three phase $CO_2(l)$ - $CO_2(v)$ - $H_2O(l)$ (Type IV) inclusions associated with M-Zone alteration phases and mineralized quartz veins	169

LIST OF ABBREVIATIONS AND SYMBOLS USED

Weights and Measures

km	kilometre
m	metre
km ²	square kilometres
cm	centimetre
m ³	cubic metres
g/t	grams/tonne
ppb	parts per billion
nT	nano-teslas
μ	microns (10 ⁻⁶ m)
cps	counts per second
g	grams
cm ²	square centimetres
ml	millilitres
ppm	parts per million
wt. %	weight percent
kbars	kilobars
ρ	density

Mineral Abbreviations

cc	calcite
alb	albite
chl	chlorite
lcx	leucoxene
ank	ankerite
qtz	quartz
ep	epidote
sr	sericite
pl	plagioclase
mus	muscovite
pyx	pyroxene
ur	uralitized pyroxene
py	pyrite
asp	arsenopyrite
mgt	magnetite
Au	gold
hm	hematite
po	pyrrhotite

Microscopy

ppl	plane polarized light
XP	crossed polars

Organizations and Reference Standards

NDME	Newfoundland Department of Mines and Energy
MUN	Memorial University of Newfoundland
GSI	Geological Survey of Japan
U.S.G.S.	United States Geological Survey
NTS	National Topographic System
PDB	Pee Dee Belemnite
SMOW	Standard Mean Ocean Water
CDT	Canon Diablo Troctolite
UTM	Universal Transverse Mercator

Grammatical Expressions

viz.	that is to say, namely
et al.	and others
c.f.	compare
ie.	that is, to be precise
eg.	for example

Miscellaneous

VLF	very low frequency
IP	induced polarization
S.D.	standard deviation
Det.	lab determination
Pub.	published value
na	not analyzed
-	not detected

Geological Expressions and Notation

D ₁ , D ₂ , D ₃	deformational event with 1 being the oldest and 3 the youngest
F ₁ , F ₂ , F ₃	generation of folding with 1 being the oldest and 3 the youngest
S ₁ , S ₂ , S ₃	generations of schistosity with 1 being the oldest and 3 the youngest
S _o	bedding
Ma	million years old
P-MORB	plume mid-ocean ridge basalt
N-MORB	normal mid-ocean ridge basalt
MORB	mid-ocean ridge basalt
PM	passive margin
ACM	active continental margin
VMS	volcanogenic massive sulphides
W/R	water to rock ratio
MZ	M-Zone gabbro
AZ	A-Zone gabbro
MQV	mineralized quartz veins
MVT	Mississippi Valley type
WR	whole rock
MS	mineral separate
LCB	lower crustal block

Geochemical Expressions and Notation

REE	rare earth elements	C _i ^a	element concentration of altered rock
HREE	heavy rare earth elements	C _i ^o	" " of unaltered rock
LREE	light rare earth elements	LILE	large ion lithophile elements
LOI	loss on ignition	M _c	slope of constant volume isocon
FeO*	total Fe	M _c	slope of constant volume isocon
f _{CO₂}	the fugacity of CO ₂	M _v	slope of volume decrease isocon
ε _{Nd}	epsilon neodymium	M ^a	mass of altered sample
(ℓ)	Liquid Phase	M ^o	mass of unaltered sample
V ^a	volume of altered sample	ρ ^a	density of altered sample
V ^o	volume of unaltered sample	ρ ^o	density of unaltered sample
Mg#	Magnesium Number	T _h	homogenization temperature
(g)(v)	gaseous/Vapour Phase	T _t	trapping temperature
(s)	solid phase	clt	clathrate (CO ₂ · 5.75H ₂ O)
T _{mCO₂}	melting temperature of CO(s)	T _{hCO₂}	homogenization temperature of CO ₂ (g)
T _{mlce}	melting temperature of H ₂ O(s)	T _{mclt}	melting temperature of clathrate
LD	limits of detection		

Analytical Procedures

ICP-ES	Inductively Coupled Plasma Emission Spectroscopy
ICP-MS	Inductively Coupled Plasma Mass Spectroscopy
LAM-ICP-MS	Laser Ablation Microprobe - ICP-MS
AR-ICP	Aqua Regia Inductively Coupled Plasma Mass Spectrometer
AA	Atomic Absorption
NAA	Neutron Activation Analysis
XRF	X-Ray Fluorescence
SEM	Scanning Electron Microscope
XRD	X-Ray Diffractometer
AAS	Atomic Absorption Spectroscopy

Geological Divisions of the Newfoundland Appalachians

LRF	Long Range Fault	CRF	Cape Ray Fault
BDF	Bay d'Est Fault	RIL	Red Indian Line
BVL	Baie Verte Line	NPL	Noel Paul's Line
HF	Hermitage Fault	DF	Dover Fault
GRC	Gander River Complex	DBL	Dog Bay Line
RF	Reach Fault	DG	Davidsville Group
BG	Botwood Group	DM	Dunnage Melange
EG	Exploits Group	WBG	Wild Bight Group
VLG	Victoria Lake Group	BNG	Bay du Nord Group
BDG	Bay d'Espoir Group	PPC	Pipestone Pond Complex
CPC	Coy Pond Complex	GBC	Great Bend Complex
GRC	Gander River Complex	MPIS	Mount Peyton Intrusive Suite

GRUB Gander River Ultrabasic Belt

CHAPTER 1

INTRODUCTION

1.1 Location and Access

The study area is located in northeastern Newfoundland approximately 7 km east-southeast of the community of Birchy Bay, Notre Dame Bay (Figure 1). It is bounded by latitudes $49^{\circ} 21'N$ and $49^{\circ} 15'N$ and longitudes $54^{\circ} 41'E$ and $54^{\circ} 38'E$ within the Comfort Cove - Newstead map sheet, N.T.S. 2E/7. Access is available from Route 340 via a gravel surfaced logging road, beginning opposite the Birchy Bay turn-off, that parallels the north and east shorelines of Duder Lake and terminates approximately 2 km north of the exploration grid. A drill road originating at the end of the logging road provides access to the grid and gold showings. The cut grid comprises two north-south trending baselines with east-west lines spaced at 100 m intervals and provides good access to all parts of the property.

The gold showings are located in an 18 km² north-south trending area that separates Duder Lake from Rocky Pond to the east and Ten Mile Lake to the south. This area is underlain by three distinct north-south trending sedimentary units intruded by gabbroic dykes and sills which host gold mineralization.

1.2 Physiography, Vegetation, and Glacial History

The area separating all three lakes is characterized by approximately 30% bedrock

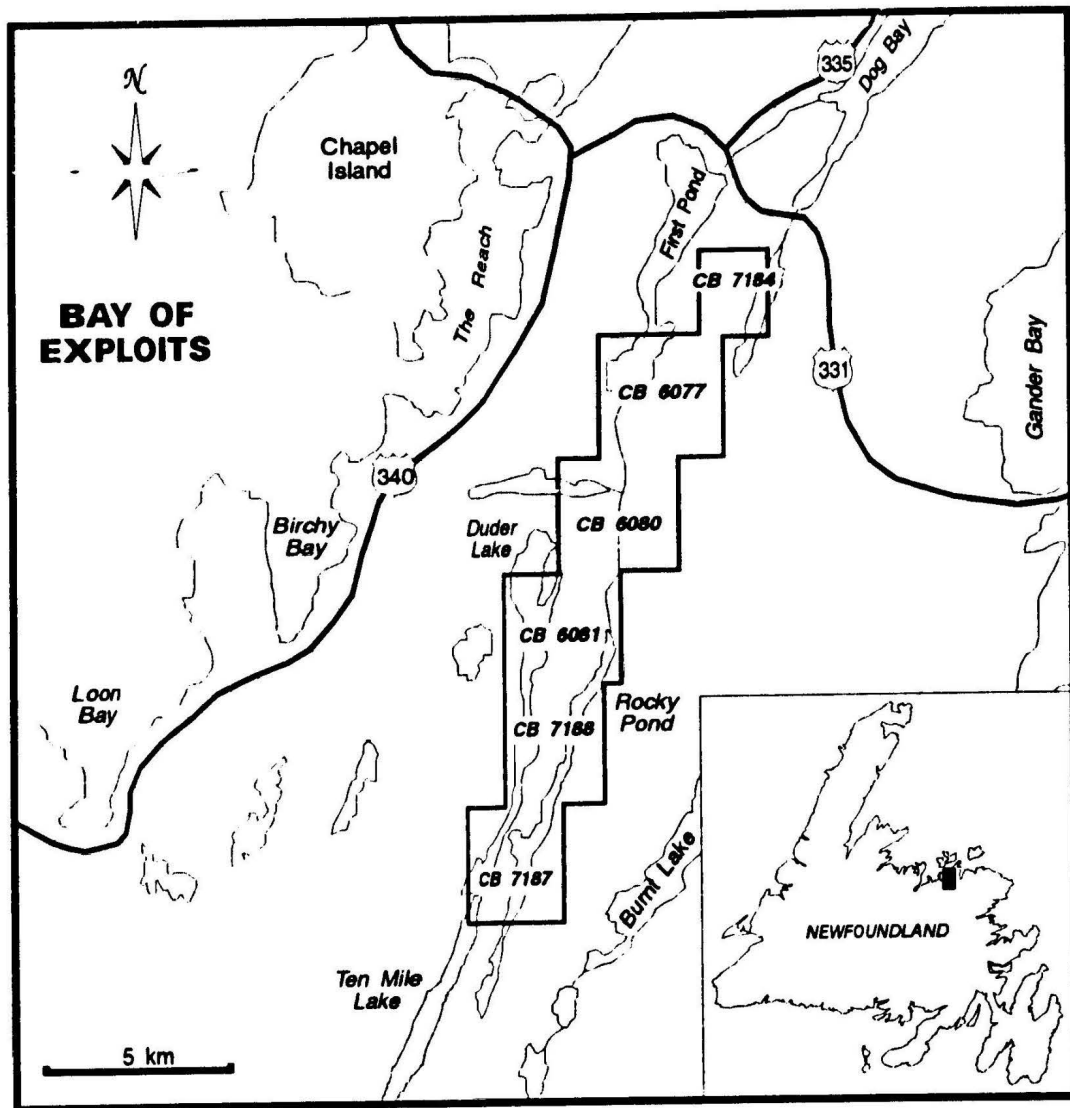


Figure 1.1: Plan map showing location of Duder Lake, major routes, and Noranda claim blocks (CB) constituting part of their GRUB North exploration project. (Modified from Tallman, 1990).

exposure and low relief with elongate ridges that appear to be controlled by the regional structures that transect the area. Areas of higher elevation are usually underlain by gabbros which form the elongate ridges while low lying areas are typified by bog and marsh which, in most instances, correspond to the surface traces of faults and shear zones. The morphologies of Duder Lake, Rocky Pond, and Ten Mile Lake to the south reflect the regional northeast-trending structural controls and bedrock grain.

Large stands of birch, poplar, and spruce are found in the heavily forested southern part of the area. Surrounding the boggy lowlands are dense thickets of alder. More northern areas have been cut over by recent logging leaving isolated stands of trees.

The region is covered in a thin, continuous, poorly sorted till veneer from 1.5 to 15 m in thickness with locally thick glacio-fluvial sand and gravel deposits present in the channelized surface of the till veneer (Liverman and Taylor, 1989). Several ice flow events (up to four with variable ice flow directions) during the Wisconsin glacial period are in evidence in the Duder Lake area. The numerous ice flow directions are attributed to the formation of smaller ice centres during deglaciation and repeated advance and retreat of ice during this period (St. Croix and Taylor, 1991).

1.3 Previous Work

Numerous regional stratigraphic, tectonic and structural studies have focused on the Silurian and Ordovician stratigraphy of north-central Newfoundland. Although these

studies were regionally orientated, their descriptions of the regional relationships of the Ordovician and Silurian strata and inferences regarding the deformational history are relevant to the study area. For ease of reference, Table 1.1 is a compilation of relevant geoscientific research in the Notre Dame Bay along with a brief description of the focus of research.

1.4 Methods

The initial stages of this project included four weeks of field mapping in the Duder Lake area. Maps on scales of 1:12 500 and 1:5 000 were produced from reconnaissance regional mapping and grid mapping respectively. In addition, maps on the scale of 1:500 were constructed for trenches at each of the gold showings. Representative samples were collected from selected lithologies in trenches and during the reconnaissance and grid mapping.

One week was spent at Noranda's office and storage compound in Grand Falls-Windsor examining Noranda-owned drill core from Duder Lake. Drill core samples were taken in 10 cm intervals on the basis of lithology, mineralization and alteration such that a representative sample set was obtained from the subsurface geology to complement the trench and mapping samples.

All samples were then transported to the Department of Earth Sciences, Memorial University of Newfoundland in St. John's where they were catalogued and selected for geochemical and/or petrographic analysis. Sample selection for analysis was

Table 1.1. Compilation of relevant geoscientific research in the eastern Notre Dame Bay area with brief descriptive notes.

STRUCTURAL STUDIES

Helwig (1972):	Defined three major phases of deformation in eastern Notre Dame Bay and related these to the development of major stratigraphic horizons and intrusions. Study bracketed the relative ages of several units which were previously problematic.
Dean and Strong (1977):	Correlated some of the major faults in the Notre Dame Bay area as continuous structures (viz. the Lobster Cove and Chanceport Faults). Also stated that some of the other major structures were originally thrust faults that were folded during Acadian deformation. In addition they noted that the Tommy's Arm and Reach Faults cut stratigraphy and structure making them post-Acadian.
Karlstrom <i>et al.</i> (1982):	Recognized three phases of deformation that affected rocks from Ordovician to middle Silurian in age implying that major portions of the Dunnage Zone may be allochthonous. Classified faults such as the Chanceport, Luke's Arm, Dildo and Reach as being post-D ₂ structures. Correlated the Dunnage, Carmanville and other mélanges in the area on the basis of F ₂ fabrics observed.
Currie <i>et al.</i> (1983):	Questioned some of the interpretations of Karlstrom <i>et al.</i> (1982) by asserting that some theories of the latter were based on incorrect interpretation of data and as such could not be applied to a regional model.
Karlstrom <i>et al.</i> (1983):	Reply to Currie <i>et al.</i> (1982) reaffirmed their findings based on better defined micro- and macroscopic structural relationships.
Williams (1984):	Based on overprinting of structural fabrics of different deformational events, recognized the presence of a pair of conjugate faults having transcurrent movement.
Van der Pluijm and Williams (1985):	Revision of stratigraphy due to modification by bedding parallel faults as well as folding.
Van der Pluijm <i>et al.</i> (1987):	Repetition of units, determined from fossil evidence, was the result of parallel faulting. Restoration of sections yielded a revised, simple lithostratigraphy.
Blewett and Pickering (1988):	Described transecting cleavages indicative of sinistral shear along major structures and which may have been associated with final closure of the Iapetus Ocean.

Table 1.1: cont...

- Calon and Szybinski (1988): Kinematic indicators suggest dextral shear sense for the Lobster Cove Fault. Paleontological and stratigraphic information suggests that movement along the fault may have been initiated during the Llandoveryan.
- Lafrance and Williams (1989): Dextral transcurrent movement along faults in the Notre Dame Bay area may have been initiated in the Silurian but the faults were active during the Acadian Orogeny.
- Elliot *et al.* (1991): U/Pb zircon age dates suggest deformation was continuous from the late Cambrian until the end of the Paleozoic. Age dates also bracketed age of intrusions (mafic, felsic and composite) thus providing age constraints on faulting as well as deposition of major sedimentary units (*e.g.* the Botwood Group).
- Goodwin and O'Neill (1991): Exploits and Gander Lake Subzone boundary gives evidence for two episodes of strike-slip and oblique-slip motion.
- Lafrance and Williams (1992): Silurian deformation was the result of south-directed thrusting of the Dunnage Zone over the Gander Zone which was followed by dextral ductile faulting. Closure of the Iapetus Ocean was oblique with a dextral, horizontal component.
- O'Brien (1993): Recognized four phases of deformation with D₁ and D₂ being thrust related and D₃ and D₄ associated with wrench movement.
- Piasecki (1993): Detailed structural study of the Dog Bay Line and associated structures on the Port Albert peninsula.
- Williams (1993): Suggested the presence of a major structural discontinuity in the vicinity of Duder Lake termed the Dog Bay Line, which had a dextral sense with possible offset of tens of kilometres.

TECTONIC STUDIES

- Kay (1967): One of the first attempts to correlate structural and stratigraphic features of northeast Newfoundland with similar features in the British Isles.
- Arnott *et al.* (1985): Deposition of terrestrial to marine sedimentary rocks was controlled by small fault-bounded basins and to movements along the Luke's Arm - Sop's Head Fault. Between the Baie Verte - Brompton Line and the Reach Fault there appears to be stratigraphic unity suggesting that the Reach Fault may represent the point

Table 1.1: cont...

- of closure of the Iapetus Ocean.
- Elliot and Williams (1986): Discussion on Arnott *et al.* (1985) paper. Authors state that important structural and deformational information was overlooked by Arnott *et al.* (1985) and as such, their tectonic and depositional inferences were incorrect.
- Wasowski and Jacobi (1986): Discussion on Arnott *et al.* (1985) paper. Authors state that although new paleontological finds by Arnott *et al.* suggests a stratigraphical continuity, geochemical and structural data suggest otherwise.
- Arnott *et al.* (1986): Reply to discussions by Wasowski and Jacobi (1986) and Elliot and Williams (1986) on the findings of Arnott *et al.* (1985).
- McKerrow and Cocks (1986): On the basis of faunal evidence, stated that site of the main Iapetus closure was the Reach Fault.
- Najjarpour and Upadhyay (1987): Major- and trace-element data for volcanic rocks on opposing sides of the Reach Fault yield contrasting geochemical signatures suggesting that the Reach Fault is the Iapetus Suture.
- O'Brien (1991): Findings include: (i) Ordovician and Silurian depocentres may have been controlled by a migrating crustal bulge or syndepositional arch. (ii) Post-Ilandoverly deformation was focused on basin-margin fault zones and (iii) Syndepositional faults were important structures that controlled the distribution of felsic pyroclastic rocks and base-metal mineralization.
- Colman-Sadd *et al.* (1992): Late Arenig orogenic event resulted in emplacement of ophiolitic rocks onto the Gondwanan margin (viz. Gander Zone). Metamorphism and plutonism of the Gander Zone were contemporaneous with volcanism in the overlying Exploits Subzone.
- Currie (1992): Arrangement of sedimentary sequences and plutonic belts, in the Carmanville area suggest the presence of two or more major southerly-directed thrust sheets within the Dunnage Zone.

STRATIGRAPHIC STUDIES

Twenhofel and Shrock (1937):

First systematic mapping of Silurian strata in the Exploits Valley - Notre Dame Bay areas which recognized: (i) structural overprinting, (ii) a Silurian deformational event with contemporaneous emplacement of dykes and sills, (iii) revised the stratigraphy on the basis of dominant lithologies present and ascribed coarser

Table 1.1: cont...

	grained units as being the product of emergent areas and (iv) suggested faunal links with Europe and eastern North America.
Kranck (1952):	Mapped three different localities in eastern Notre Dame Bay to fill gaps in previous mapping.
Patrick (1956):	Mapped the Comfort Cove-Newstead area and assigned rocks cropping-out in the Duder Lake area to the Siluro-Devonian Springdale Group.
Kay and Williams (1963):	On New World Island, Ordovician and Silurian stratigraphic belts appeared to be separated by a high-angle reverse fault or by a thrust-fault that was later tilted to higher angles.
Williams (1964):	Compiled the geology of the Botwood map area, investigated the mineral occurrences known in the area and completed mapping initiated by Patrick (1956).
Williams (1967):	Mapped the distribution of Silurian rocks in Newfoundland and divided all the Silurian strata into four units. Also stated that deposition was confined to fault-bound basins with the sedimentation punctuated by one or more volcanic episodes.
Horne and Helwig (1969):	Characterized Ordovician stratigraphy in the Notre Dame Bay area, tentatively assigning ages based on fossil evidence. Subdivided the stratigraphy on the basis of structural separation and dominant lithologies. Recognized an unconformity in some areas that separated middle Ordovician from overlying Silurian rocks.
Williams (1972):	Subdivided the Botwood Group into three formations: the basal Goldson Conglomerate, the Lawrenceton Formation and the upper Wigwam Formation.
McCann and Kennedy (1974):	Ascribed conglomeratic beds in the Horwood Bay area to ice-rafted glacio-marine deposits.
Currie (1980):	The Davidsville Group unconformably underlies the Silurian Indian Islands/Botwood Group west of Gander Bay. The Davidsville Group was partially equivalent to the Exploits Group and this correlation suggests that the northeastern part of the Dunnage Zone must be broadly synclinal.
Blackwood (1982):	As a result of a regional mapping project, observed that the contact between the Davidsville and Botwood Group varied from conformable, to faulted, and to conformable with fault modification.

Table 1.1: cont...

- Scheuing and Jacobi (1990): Used major- and trace-element data to subdivide rocks in eastern Notre Dame Bay into three intervals of differing age and environment of deposition.
- Currie (1993): Examined the stratigraphy between Gander Bay and Birchy Bay and divided major stratigraphic formations such as the Botwood Group into several formations based on lithological contrasts.
-

MÉLANGE STUDIES

- Hibbard *et al.* (1977): Fossil evidence affirmed that the Dunnage Mélange formed on a lower Paleozoic trench slope with an olistostromal origin.
- Hibbard and Williams (1979): Based on geological relationships, stated that the Dunnage Mélange is an olistostromal equivalent of the nearby Exploits Group and it tentatively formed in a fore-arc trough or rear-arc basin setting.
- Nelson (1981): Characterized mélangé development of the Boone's Point Complex and attributed its formation to an olistostromal event due to emergence of the Robert's Arm Group. The mélangé was deformed by both the Taconic and Acadian orogenic events.
- Wasowski and Jacobi (1984): Geochemistry of volcanic blocks within the Dunnage Mélange indicated both enriched-type ocean floor tholeiitic signatures and alkali basalt affinities. The chemistry of these blocks had similarities to basalts generated at bathymetric highs located off-centre at mid-ocean ridges.
- Blewett (1989): Described mélangé development and deformational control along the Luke's Arm - Sop's Head Fault (*viz.* Red Indian Line). Ascertained that five phases of deformation were concentrated along major faults such as the Red Indian Line.
- Williams (1992): Examined coticule occurrences in several mélanges of northeastern Newfoundland and proposed models for their formation as well as stating possible metallogenetic significance of their presence.
-

METALLOGENY STUDIES

- Snelgrove (1935): Compiled information on all known Newfoundland gold deposits including those occurrences in northeastern Newfoundland.

Table 1.1: cont...

Gibbons and Papezik (1970):	Study of volcanic rocks and arsenopyrite veins in the Moreton's Harbour area which made inferences on the physio-chemical conditions of mineralization.
Strong (1974):	Documentation of mineral occurrences in the Moreton's Harbour area focusing on As and Sb mineralization.
Kay (1975):	Documented the manganiferous chert prospects of the Campbellton area and their relationships with the Dunnage Mélange. Also stated that the Dunnage Mélange is the likely closure site of the Iapetus Ocean.
Dean (1977, 1978):	Compilation of the stratigraphy and mineralization of Notre Dame Bay. Study encompassed all known sulphide occurrences and revised the stratigraphy.
Kay (1982):	A geochemical and fluid inclusion study of the arsenopyrite-stibnite-gold mineralization that occurs at Moreton's Harbour.
Kay and Strong (1983):	Described some of the geologic and fluid controls of As-Sb-Au mineralization at Moreton's Harbour.
Evans (1991):	First systematic documentation and classification of gold mineralization in rocks of the eastern Dunnage Zone. Recognized a genetic link between gold mineralization and a complex network of northeast, north-northeast and northwest-trending linears.
Wilton and Evans (1991):	Geologically and geochemically compared two gabbro-hosted, mesothermal Au showings from opposing margins of the Dunnage Zone.
Churchill and Evans (1992):	Documentation of the Duder Lake gold prospects as well as preliminary mapping results.
Evans (1992):	Continuation of gold metallogeny study of rocks of the eastern Dunnage Zone.
Churchill <i>et al.</i> (1993):	Further documentation of the Duder Lake gold prospects. Study involved alteration and geochemical characteristics associated with mineralization.
Evans (1993):	Continuation of gold metallogeny project (<i>c.f.</i> Evans 1991; 1992) focusing on the examination of central Dunnage Zone gold occurrences.

Table 1.1: cont...

GEOPHYSICAL STUDIES

- Miller and Deutsch (1970): Gravity and magnetic study of rocks in eastern Notre Dame Bay. Study revealed a structural discontinuity near Change Islands (correlative with Williams' (1993) proposed Dog Bay Line?) and proposed the existence of an ultramafic layer at 5-10km depth to explain the overall positive character of the gravity data.
- Haworth and Miller (1982): Using gravity and magnetic geophysical data modelled the structure of basement rocks underlying Notre Dame Bay.
- Keen *et al.* (1986): Offshore deep seismic profiling across the Humber, Dunnage, Gander and Avalon Zones which characterized the nature of the terrane boundaries and yielded information on the lower crust to each of the different tectonostratigraphic zones.
- Quinlan *et al.* (1992): Onshore refraction seismic data better constrained the nature and structure of basement rocks underlying the Newfoundland tectonostratigraphic zones.
-

QUATERNARY STUDIES

- Ricketts and McGrath (1990): Granular aggregate-resource mapping in the eastern Notre Dame Bay area which indicated the presence of large glacio-fluvial deposits in excess of 500 000m³ in the vicinity of Birchy Bay.
- St. Croix and Taylor (1991): Reconnaissance striation mapping in the Notre Dame Bay area revealed a complex ice-flow history with four separate events preserved.
-

MISCELLANEOUS STUDIES

- Davenport and Nolan (1988): Regional lake-sediment geochemical data which defined anomalous Au, Sb and As concentrations over a wide area in the eastern Dunnage Zone.
- Green (1989): First year assessment report on grassroots exploration in the Duder Lake area.
- Tallman (1990): Second year assessment report on prospecting, mapping, trenching and diamond drilling in the Duder Lake area.
-
-

concentrated towards those samples possessing mineralization and alteration of the gabbroic gabbroic and sedimentary lithologies.

Major- and trace-element analyses were conducted on 85 samples by the Newfoundland Department of Mines and Energy (NDME) in St. John's (see Appendix I for analytical techniques and Appendix II for chemical analyses). Au assays (with a complementary suite of elements including As and Sb) on 72 samples were completed by Becquerel Labs for the NDME by Neutron Activation analysis. Trace and rare earth element analyses were performed at Memorial University using X-Ray Fluorescence (XRF) and Inductively Coupled Plasma - Mass Spectrometry (ICP-MS) techniques respectively.

Thin and polished thin sections were made and examined under transmitted and reflected light. Unknown minerals were analyzed by a Rigaku X-Ray Diffractometer (XRD). Several alteration phases (*viz.* carbonates and chlorites) were analyzed using a Scanning Electron Microscope (SEM) yielding qualitative trace and major element data and which differentiated between bulk mineral chemistry. In addition the SEM was utilized for microscopic examination of textural characteristics of sulphides and Au. Samples of fluid inclusions from mineralized gabbros and quartz veins as well as from post-mineralization quartz-carbonate veins were collected and analyzed so as to characterize some of the physio-chemical characteristics of the mineralizing fluid and environment. The fluid inclusion studies were performed on a standard fluid inclusion freezing\heating universal stage.

Isotopic studies were also carried out to aid in the characterization of the mineralizing event. Samples of syngenetic carbonate, quartz, and both pyrite and arsenopyrite were analyzed for ^{13}C , ^{18}O and ^{34}S respectively. The carbon and oxygen isotopes were analyzed on a Finnegan MAT-252 mass spectrometer while those of sulphur were analyzed using a VG-PRISM-903 mass spectrometer.

1.5 Purpose and Scope

Much of the gold mineralization appears to be related to alteration zones that bound low angle, second to third order, brittle-ductile Riedel shears cutting gabbros and/or Davidsville Group graphitic sedimentary rocks. Due to these relationships, the basis for this study involved definition and documentation of (1) the structural controls on alteration and mineralization, (2) the systematics of alteration, (3) possible compositions and source(s) of mineralizing fluid(s) (based on geochemical and isotopic studies), (4) affinity and character of the gabbroic bodies associated with the gold mineralization, and (5) synthesis of these data into a genetic model for the mineralization. This is used to interpret the regional significance of the Duder Lake gold showings and analogous gold and base-metal showings elsewhere in the eastern Dunnage Zone and the conclusion of a mesothermal origin for the fluids is the first documentation of this style of mineralization in the Dunnage Zone of the Newfoundland Appalachians. The findings of this research should provide insight into the metallogeny at convergent plate boundaries elsewhere in the Appalachian Orogen.

CHAPTER 2

GEOLOGICAL SETTING

2.1 Regional Tectonic Setting

The Appalachian Orogen in Newfoundland is composed of four northeast-trending late Precambrian to lower Paleozoic tectonostratigraphic zones (Williams, 1978a,b), the Humber, Dunnage, Gander, and Avalon Zones, which were classified on the basis of distinct structural, depositional, tectonic and volcanic-plutonic characteristics (Figure 2.1). Portions of these zones were deformed during the Precambrian Avalonian Orogeny (Hughes, 1970), the middle Ordovician Penobscot/ Taconic Orogeny (Rodgers and Neale, 1969; Stevens, 1970; Williams, 1975), the lower to middle Silurian Salinic Orogeny (Colman-Sadd, 1980, 1982; Karlstrom *et al.*, 1982; Dunning *et al.*, 1990), the Devonian Acadian Orogeny (Boucot *et al.*, 1964; Williams, 1983), and finally during the Carboniferous Alleghanian Orogeny (Bradley, 1982; Hyde *et al.*, 1988).

The Humber Zone records the development and subsequent destruction of an Atlantic-type passive continental margin on the southeast margin of Laurentia. The Dunnage Zone represents vestiges of the Iapetus Ocean and later accreted island arc systems and mélanges. Rocks of the Gander Zone record the development and destruction of a continental margin which was located to the east of the Iapetus Ocean and which possessed Celtic affinities (McKerrow and Cocks, 1977, 1986; Wonderly and Neuman, 1984). The rock record of the Avalon Zone relates to either rifting and

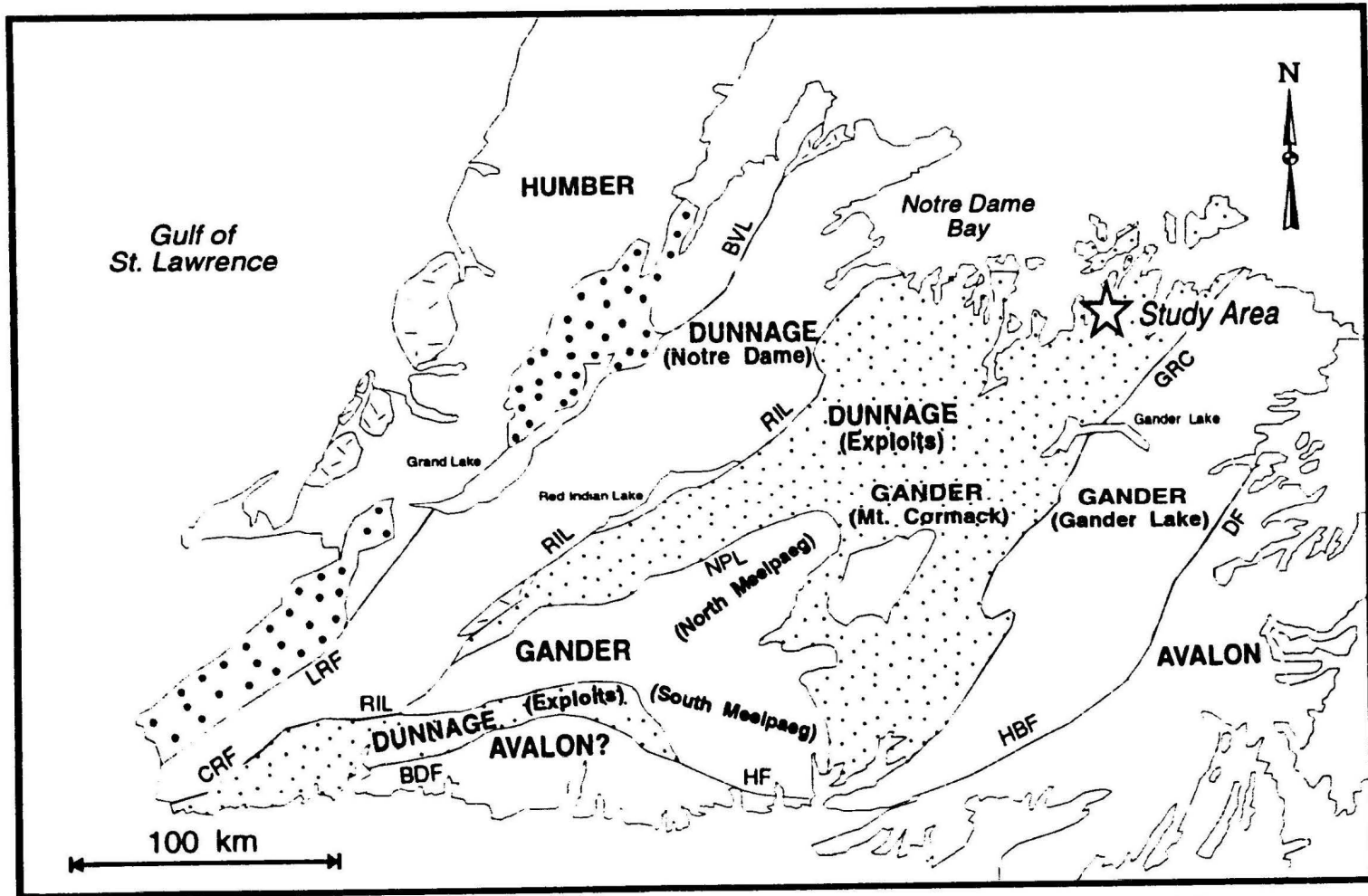


Figure 2.1: Tectonostratigraphic zonation and major tectonic boundaries of the Newfoundland Appalachians. Abbreviations are as follows: LCB = Lower Crustal Block, LRF = Long Range Fault, CRF = Cape Ray Fault, BDF = Bay d'Est Fault, RIL = Red Indian Line, BVL = Baie Verte Line, NPL = Noel Paul's Line, HF = Hermitage Flexure, HBF = Hermitage Bay Fault, DF = Dover Fault and GRC = Gander River Complex. Stippled area represents rocks of the Exploits Subzone, coarse dotted pattern denotes Carboniferous basins and hachured pattern denotes rocks of ophiolitic affinity. (Modified from Williams et al., 1988).

subsequent opening of Iapetus during Precambrian times (Papezik, 1972) or to a subduction cycle that predated opening of the Iapetus (Rast *et al.*, 1976). This zone was a stable marine platform during Cambro-Ordovician time, characterized by shallow water deposition of platform carbonates and siliciclastics.

With the exception of the Gander-Avalon boundary, the boundaries between the other zones are characterized by mélanges and ophiolite complexes. The Humber-Dunnage boundary is delineated by the Baie Verte - Brompton Line - Long Range Fault system (Williams and St. Julien, 1982) along which ophiolitic slivers such as the Flatwater Pond Complex (Hibbard, 1983) are found. The Gander and Avalon Zones are separated by the Gander River Ultrabasic Belt (Jenness, 1958) now formally known as the Gander River Complex (O'Neill, 1991). The Avalon - Gander boundary, the Dover Fault - Hermitage Flexure, is delineated by subvertical to vertical faults that contain broad zones of ductile deformation (Blackwood, 1976; Hanmer, 1981; Williams, 1982; Holdsworth, 1992).

Deep crustal seismic refraction studies across the Newfoundland Appalachians (Keen *et al.*, 1986; Quinlan *et al.*, 1992) have yielded valuable information about crustal basement to the different zones and subzones. Marine geophysical surveys by Keen *et al.* (1986) interpreted the existence of three lower crustal blocks (LCB) to the Newfoundland Appalachians: (from west to east) the Grenville LCB, Central LCB and Avalon LCB. The Grenville and Central LCBs were inferred to extend beneath the Dunnage Zone where they shared an apparent sutured contact (Keen *et al.*, 1986).

However, the notion that the boundary between the Avalon and Central LCBs cut the Moho (Keen *et al.*, 1986) has now been dismissed as new seismic modelling of the LCBs indicates the presence of two, not three, LCBs (Quinlan *et al.*, 1992). The present interpretation is that the easternmost block, the Gondwanan plate, has been underthrust as much as 200 km beneath the Laurentian plate to the west. The Laurentian plate correlates with Keen *et al.*'s. (1986) Grenville LCB, while the Central and Avalon LCBs are modelled as subdivisions of the Gondwanan plate.

Seismic data for the Baie Verte - Brompton Line and the Gander River Complex show that these major breaks do not extend to deeper crustal levels, compatible with earlier suggestions of Colman-Sadd and Swinden (1984) that the Dunnage Zone may be allochthonous on Humber and Gander Zone basement rocks (Keen *et al.*, 1986; Quinlan *et al.*, 1992). In addition, Quinlan *et al.* (1992) has shown that major structures such as Baie Verte - Brompton Line and Gander River Complex have shallowly dipping geometries consistent with ramp-flat style of deformation.

Williams *et al.* (1988) further subdivided the Dunnage and Gander Zones. The Dunnage Zone is divided into the Notre Dame and Exploits Subzones and the Gander Zone into the Gander Lake, Mount Cormack, and the North Meelpaeg and South Meelpaeg subzones (refer to Figure 2.1).

Within the Dunnage Zone volcanic, plutonic, and sedimentary rocks record the development and eventual destruction of the Iapetus Ocean during the early to middle Paleozoic. The southeastern part of the Dunnage Zone, the Exploits Subzone, is

characterized by deep marine sedimentary rocks of Ordovician age and by Silurian, shallow marine to fluviatile sedimentary rocks and subaerial volcanics, all of which were intruded by Siluro-Devonian granitoid and gabbroic bodies. Structural windows of inferred Gander Zone affinity (Colman-Sadd and Swinden, 1984), namely the Mount Cormack and Meelpaeg Subzones, are surrounded by the Exploits Subzone and outcrop along the south and southeast margins of the subzone (Figure 2.1).

The northwestern section of the Dunnage Zone, the Notre Dame Subzone, is underlain predominantly by metavolcanic rocks that were intruded by alkalic granitic bodies. Such bodies are distinctly different from those in the Exploits Subzone. Contrasts in stratigraphy, lithology, structure, faunas, plutonism, lead isotopic signatures in mineral deposits, and geophysics were used by Williams *et al.* (1988) to delineate the two subzones of the Dunnage Zone. A summary of the geological characteristics of each subzone is listed in Table 2.1.

The boundary between the Exploits and Notre Dame Subzones is delineated by a late rectilinear fault or fault system termed the Red Indian Line which, in some areas, is manifested as a mylonite zone locally punctuated by intrusions (Williams *et al.*, 1988).

2.2 Geological Development of the Dunnage Zone

Since the Dunnage Zone records the development and subsequent demise of the Iapetus Ocean during the late Cambrian to early Silurian, its development is best described in terms of pre- and post-accretionary geological events.

Table 2.1: Summary of geological features which support the division of the Dunnage Zone into two subzones (summarized from Williams *et al.*, 1988).

GEOLOGICAL FEATURE	EXPLOITS SUBZONE	NOTRE DAME SUBZONE
Stratigraphy and Lithology	Caradocian black shales overlain by upper Ordovician to Silurian marine greywackes and conglomerates. Silurian olistostromes and mélanges.	Lesser shales and other sedimentary rocks, subzone dominated by metavolcanic rocks.
Structure	Continuous Ordovician and Silurian sections. Less deformation along Red Indian Line. No major effects seen in subzone from the Taconic Orogeny.	Sub-Silurian unconformities. Strong deformation along the Red Indian Line. Strongly deformed by the Taconic Orogeny.
Faunas	Celtic affinities.	North American affinities.
Plutonism	Large Siluro-Devonian composite batholiths with granitic phases that cut mafic phases. (<i>e.g.</i> Mount Peyton, Hodges Hill).	Ordovician tonalites and middle Paleozoic alkali batholiths (<i>e.g.</i> Topsails Plutons).
Pb Isotopes	Radiogenic, corresponding with the orogene and upper crustal growth curves of Doe and Zartman (1981)	Non-radiogenic, plotting below the Doe and Zartman (1981) orogene growth curve
Geophysics	Lower magnetic and Bouger gravity anomalies.	Higher magnetic and Bouger gravity anomalies.

2.2.1 Pre-Accretion

Pre-accretionary events include the development of island arcs and back arc basins during the Cambrian to middle Ordovician. These arc systems contain both pre- and syn-

accretionary sedimentation manifested as distal turbidites. Cessation of volcanism during the middle Ordovician coincided with deposition of a black shale unit of Caradocian age (Dean, 1977). Continued closure of the Iapetus Ocean resulted in flyschoid sediment deposition within fault-bound basins of the east-central Dunnage Zone.

According to Blackwood (1982), the Davidsville Group (as named by Kennedy and McGonigal, 1972) is a thick sequence of distal, back-arc turbidites with detritus shed from older island arc systems to the west and deposited on allochthonous oceanic basement rocks of the Gander River Complex. Shelf-facies rocks of the Gander Zone pass conformably westwards into rocks of the Dunnage Zone in north-central Newfoundland.

2.2.2 Post-Accretion

Post-accretionary events include deposition of the Silurian Botwood and Indian Island groups. During the late Ordovician to middle Silurian, regional scale transcurrent faults were either activated or reactivated, causing the development of pull-apart basins (Williams, 1967; Arnott *et al.*, 1985; Szybinski *et al.*, 1990;) and crustal anatexis resulting in widespread epicontinental style volcanism (Coyle and Strong, 1987). Basin infilling was characterized by the deposition of polymictic conglomerates followed by deposition of fluvial to shallow marine facies sedimentary rocks and subaerial volcanism. These lithologies comprise the Botwood and Indian Island groups which are grouped as the Botwood Belt of Williams (1967) and Williams *et al.* (in press).

The Botwood Group consists of grey to red micaceous sandstone and siltstone, minor fossiliferous calcareous beds, and conglomerate (Williams, 1964). The Botwood Group is divided into three formations (Williams, 1972). The oldest unit is a polymictic conglomerate associated with initiation of basin infilling, termed the Goldson Conglomerate. Conformably overlying the Goldson Conglomerate are subaerial volcanic rocks of the Lawrenceton Formation which are seen sporadically in the stratigraphy of the Botwood Group intercalated with rocks of the Wigwam Formation (Williams, 1967). The youngest unit is the Wigwam Formation which represents the final stages of basin infilling and is characterized by red beds and shallow fluvial to marine sandstones and siltstones.

The Indian Islands Group is composed of phyllitic slates, quartzitic and calcareous sandstone, thin limestone lenses, and conglomerate (Baird, 1958). Patrick (1956) also identified minor felsic volcanic rocks intercalated with this unit. Current workers are in the process of redefining the stratigraphy of the Indian Islands Group (*c.f.* Currie, 1993).

All rocks in eastern Notre Dame Bay (and elsewhere in the eastern Dunnage Zone) exhibit intense deformational fabrics as well as numerous Siluro-Devonian plutons, suggesting a widespread Silurian orogenic event (Colman-Sadd 1980, 1982; Karlstrom *et al.*, 1982; Dunning *et al.*, 1990).

2.3 Geology and Stratigraphy of the eastern Notre Dame Bay Area

A compilation of the regional geology of the eastern Notre Dame Bay/Duder Lake

area (Figure 2.2) indicates that the geology is dominated by several northeast-southwest trending sedimentary, volcanic and plutonic rock units that are either in conformable or fault contact with one another. Eleven units are present, ranging in age from late Cambrian to early Devonian.

2.3.1 Dunnage Mélange

The oldest unit is Cambro-Ordovician in age and crops out in the northeast portion of Notre Dame Bay on an archipelago of islands, where it is observed to be intruded by the Loon Bay Batholith. The *mélange* is characterized by a black shaly matrix with polyolithic clasts as well as thin coticule layers (Williams, 1992). The *mélange* has been attributed to olistostromal mechanisms induced during collapse of the nearby Exploits Group (Hibbard and Williams, 1979) and was inferred to have formed on a lower Paleozoic trench slope (Hibbard *et al.*, 1977). Volcanic blocks in the *mélange* have geochemical signatures typical of basalts associated with bathymetric highs distal to mid-ocean ridge axis (Wasowski and Jacobi, 1984).

2.3.2 Caradocian Shale

The second oldest unit is Caradocian and is typified by black carbonaceous argillites and argillaceous siltstones, commonly cherty at the base, known as the Caradocian Shale (Plate 2.1). This unit is exposed to the west of Duder Lake where it has been intruded by the Loon Bay Batholith and has faulted contacts with the Goldson

LEGEND

SILURO-DEVONIAN

- | | | |
|---|---------------------|--------------------------------------------------------------------------------------------------------|
| 1 | LOON BAY BATHOLITH | Massive to locally foliated, medium to coarse grained, muscovite-biotite granite and quartz monzonite. |
| 2 | CHARLES COVE PLUTON | |
| 3 | BURNT LAKE PLUTON | |

SILURIAN

BOTWOOD GROUP

- | | | |
|---|-----------------------|--------------------------------------|
| 4 | WIGWAM FORMATION | Subaerial sandstones and siltstones. |
| 5 | LAWRENCETON FORMATION | Terrestrial mafic volcanic rocks. |
| 6 | GOLDSON CONGLOMERATE | Polymictic pebble conglomerate. |

INDIAN ISLANDS GROUP

- | | | |
|---|----------------------|------------------------------------------|
| 7 | STONEVILLE FORMATION | Phyllites, shales, +/- felsic volcanics. |
|---|----------------------|------------------------------------------|

ORDOVICIAN

- | | | |
|---|-------------------|-----------------------------------------|
| 8 | DAVIDSVILLE GROUP | Slates, siltstones and shales. |
| 9 | CARADOCIAN SHALE | Coticule-bearing black shale +/- chert. |

CAMBRO-ORDOVICIAN

- | | | |
|----|-----------------|--------------------------------------------|
| 10 | DUNNAGE MELANGE | Polymictic knockers in black shaly matrix. |
|----|-----------------|--------------------------------------------|

 Faults

Scale: 1cm = 1200m

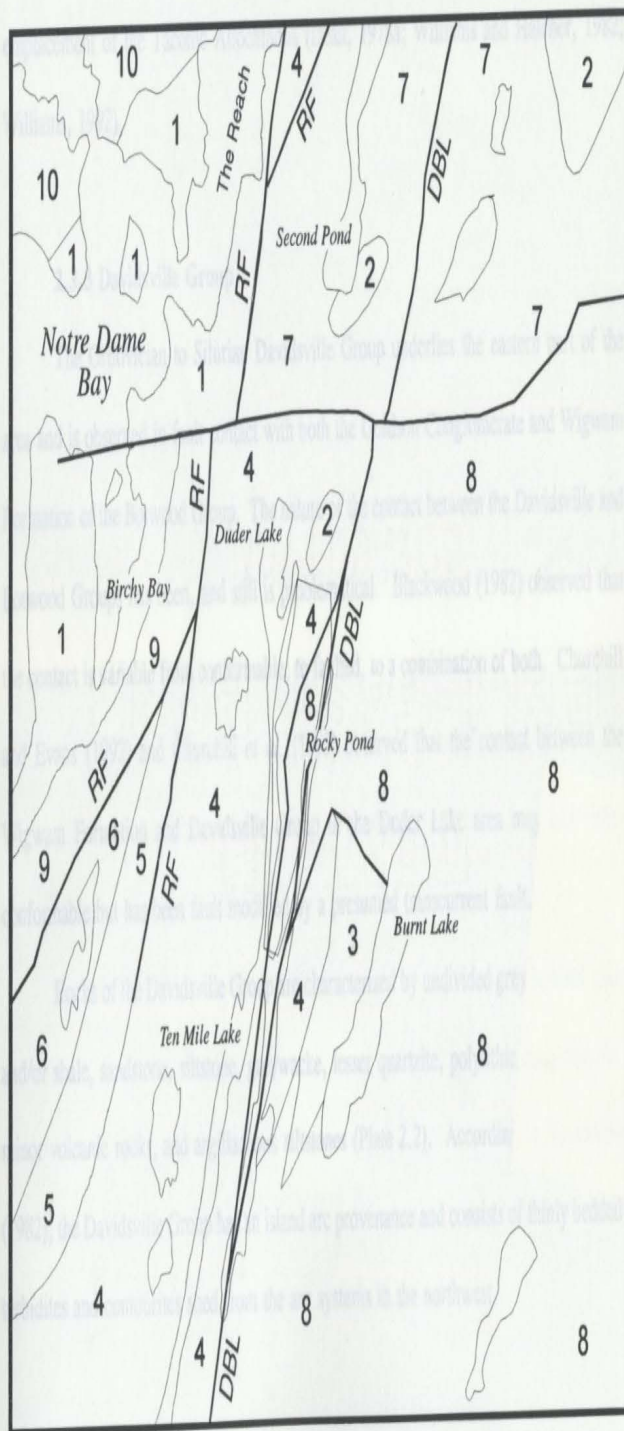


Figure 2.2: Regional geology of eastern Notre Dame Bay, Newfoundland. Geology compiled from Williams (1964), Dean (1978), Andrews (1980), Churchill (1992, 1993) and Williams (1993). Abbreviations used: RF = Reach Fault and DBL = Dog Bay Line. Polygon in the vicinity of Duder Lake delineates map area depicted on Figure MA-1.

Conglomerate and Wigwam Formation. The Caradocian Shale is found extensively throughout the Exploits Subzone and records the cessation of arc volcanism and emplacement of the Taconic Allochthons (Dean, 1978a; Williams and Hatcher, 1982; Williams, 1992).

2.3.3 Davidsville Group

The Ordovician to Silurian Davidsville Group underlies the eastern part of the area and is observed in fault contact with both the Goldson Conglomerate and Wigwam Formation of the Botwood Group. The nature of the contact between the Davidsville and Botwood Groups has been, and still is problematical. Blackwood (1982) observed that the contact is variable from conformable, to faulted, to a combination of both. Churchill and Evans (1992) and Churchill *et al.* (1993) observed that the contact between the Wigwam Formation and Davidsville Group in the Duder Lake area may have been conformable but has been fault modified by a presumed transcurrent fault.

Rocks of the Davidsville Group are characterized by undivided grey to black slate and/or shale, sandstone, siltstone, greywacke, lesser quartzite, polyolithic conglomerate, minor volcanic rocks, and argillaceous siltstones (Plate 2.2). According to Blackwood (1982), the Davidsville Group has an island arc provenance and consists of thinly bedded turbidites and contourites shed from the arc systems to the northwest.

Plate 2.1: Quartz veined, gossanous and pyrite mineralized Caradocian shale outcropping approximately 3km west of the community of Birchy Bay. Note rock hammer for scale.



Plate 2.2: Graphitic siltstones and shales of the Davidsville Group east of Duder Lake. Note northeast-trending slaty cleavage (S₂). The scale is 9cm long.



2.3.4 Indian Islands Group

Silurian rocks of the Stoneville Formation, Indian Islands Group, crops out in the northeast portion of the region and are separated from all other units by a major east-west trending fault that also truncates rocks of the Botwood and Davidsville Groups as well as the Caradocian Shale. The Stoneville Formation is typified by interbedded grey phyllites, slate, and sandy to fine-grained siltstones, minor coralline shales, and limestones (Plate 2.3). According to Currie (1980), the similarity of this unit with the temporally equivalent Botwood Group makes stratigraphic division between the two units extremely difficult. More recent studies (*c.f.* Currie, 1993) are in the process of better constraining the stratigraphy of the Indian Islands Botwood Groups.

2.3.5 Botwood Group

The Botwood Group predominates in the central portion of the study area. Three formations of the Botwood Group are present: an early Silurian basal conglomeratic unit called the Goldson Conglomerate, a volcanic unit known as the Lawrenceton Formation, and a sedimentary unit known as the Wigwam Formation.

2.3.5.1. Goldson Conglomerate

The Goldson Conglomerate outcrops in the western portion of the area. This unit is in fault contact with the Caradocian Shale and has a conformable contact with volcanic rocks of the Lawrenceton Formation. This unit consists of coarse, grey to red,

polymictic conglomerate, grey sandstone and quartzite, as well as minor, thin shale beds (Plate 2.4). The presence of this, and similar, conglomeratic units in the Notre Dame Bay is attributed to flyschoid sedimentation from the margins of fault-bounded basins (Williams, 1967; Arnott *et al.*, 1985; Szybinski *et al.*, 1990;). Initiation of these basins may have begun as a result of early Silurian wrench faulting, but basin development may have continued well into the late Silurian, or even early Devonian, when these transcurrent faults were still presumed to have been still active (Lafrance and Williams, 1989; O'Brien, 1991).

2.3.5.2 Lawrenceton Formation

Although the Lawrenceton Formation is faulted against the Wigwam Formation in the western portion of the map, the contact may originally have been conformable. Williams (1964) observed that the stratigraphic succession of the Botwood Group is locally punctuated by subaerial Silurian volcanic rocks. The volcanic rocks include coarse-grained, acidic to intermediate agglomerates; crystal and lithic tuffs; and red, green, purple, and black vesicular and amygdaloidal pillow basalts, breccias, and flows (Plate 2.5). These rocks may have formed in a manner analogous to the epicontinental style volcanic rocks that are observed in the Silurian Springdale Group (Coyle and Strong, 1987).

Geochemical studies on rocks of the Lawrenceton Formation indicate that they have a calc-alkaline signature (Najjarpour and Upadhyay, 1987, Churchill *et al.*, 1993)

Plate 2.3: Strongly deformed grey-green siltstones of the Stoneville Formation, Indian Islands Group. Note the abundance of tension gashes. Camera lens measures 51mm



Plate 2.4: Clast supported polymictic conglomerate of the Goldson Conglomerate. Exposure located approximately 6km southwest of Duder Lake.



which contrasts strongly with the tholeiitic signature of volcanic rocks located to the northwest in the New World Island area. This change in volcanic rock chemistry has led many researchers to believe that the fault separating the two volcanic packages may actually represent the Iapetus suture (*c.f.* Arnott *et al.*, 1985; McKerrow and Cocks, 1986; Najjarpour and Upadhyay, 1987).

2.3.5.3 Wigwam Formation

Rocks of the Wigwam Formation represent the final stages of basin infilling and are characterized by fluvial to shallow marine subaerial sedimentary rocks (Plate 2.6). A U/Pb zircon age date of 422 ± 2 Ma for a dyke intruding the Wigwam Formation on the Port Albert Peninsula north of Duder Lake constrains the upper age limit of the Botwood Group (Elliot *et al.*, 1991). The Wigwam Formation underlies the central portion of area to the west of Duder Lake and consists of undivided micaceous and siliceous, red, brown, grey, and green siltstone, sandstone, and shale with minor conglomerate, greywacke, and limestone. Minor, thin, tuffaceous horizons have also been observed. The contact with the Davidsville Group is faulted but several observations suggest that the contact may have originally been conformable:

- (i) From west to east (Wigwam Formation to Davidsville Group) there is a gradual change in facies from subaerial red beds to deeper water sedimentary rocks, demonstrated by a gradual colour change from reddish-brown, through greenish, to grey and by a gradual change from sandstone dominated to siltstone

Plate 2.5: Mafic agglomerate of the Lawrenceton Formation of the Borwood Group with rare felsic fragments (whitish colour). Exposure located 4km west of Ten Mile Lake.

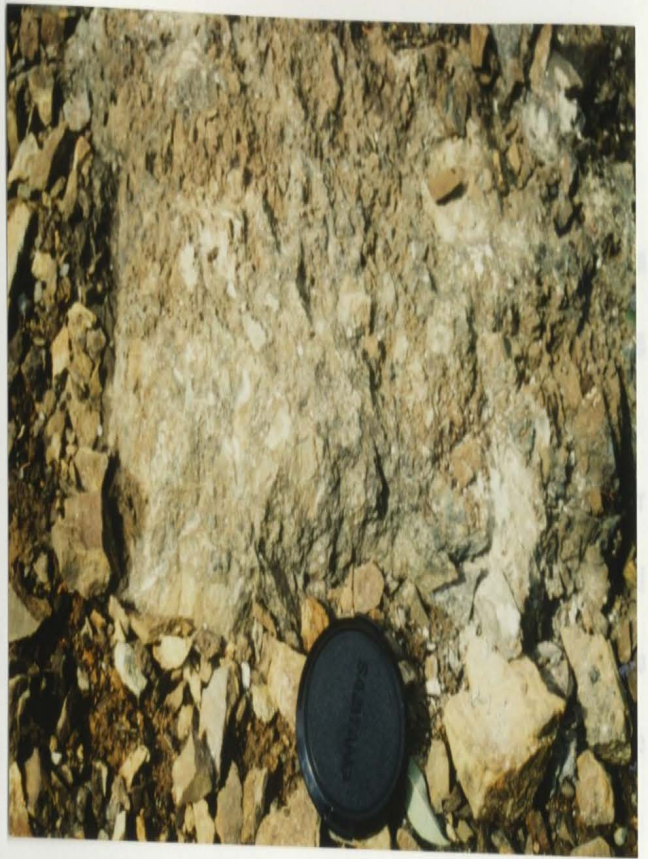


Plate 2.6: Folded, convoluted bedded fine-grained sandstones of the Wigwam Formation possessing strong S₂ cleavage. Location 2km northeast of Duder Lake.



and argillaceous siltstone dominated units.

(ii) The detrital mica content of the Wigwam Formation, inferred to have been derived from the gneissic Gander Lake Subzone, diminishes eastwards suggesting a change in provenance.

Sedimentary rocks from upper sections of the Davidsville Group and lower sections of the Wigwam Formation may record a bimodal provenance for detrital material - namely high-grade metamorphic gneisses of the Gander Lake Subzone and volcanic to volcanoclastic rocks of the Lower to Middle Ordovician aged island arc systems of the Notre Dame Subzone.

2.3.6 Burnt Lake Pluton

Late Silurian to early Devonian in age, this pluton crops out east of Duder Lake along the western shore of Burnt Lake. The Burnt Lake Pluton is composed of light-grey to light greenish-grey, medium-grained diorite, quartz-diorite, granodiorite, and gabbro. A fault contact is observed at its northern boundary with the Davidsville Group. Emplacement of this pluton as well as the Loon Bay Batholith and Charles Cove Pluton may reflect syn- to post-tectonic Siluro-Devonian magmatism related to the Silurian orogenic event (Dunning *et al.*, 1990).

2.3.7 Charles Cove Pluton

The Charles Cove Pluton comprises massive to locally foliated, medium- to

coarse-grained, muscovite-biotite granite and quartz monzonite of inferred Siluro-Devonian age. This pluton crops out in two localities, the first being in the vicinity of the northern end of Duder Lake while the second is a much larger intrusion located to the northeast of the study area (see Figure 2.2). The larger intrusion is known to be associated with tungsten mineralization (Dean, 1978b).

2.3.8 Loon Bay Batholith

The youngest unit present in the area is the Loon Bay Batholith (408 ± 2 Ma; Elliot *et al.*, 1991) and which intrudes the Dunnage Mélange, Caradocian Shale and Indian Islands Group. This batholith includes light-grey, medium to coarse-grained, hornblende-granodiorite, biotite-hornblende-granodiorite, and quartz-diorite. This intrusion predates movement along the east-west trending fault separating the Indian Islands Group from the other units in the area, thus constraining the age of movement along this fault as Devonian or younger.

2.3.9 Mafic to Intermediate Dykes and Sills

Although not depicted on Figure 2.2 on account of their small size, numerous small, fine to coarse-grained gabbroic (Plate 2.7), diabasic, and dioritic dykes and sills of probable late Silurian - early Devonian age are present proximal to, but not restricted to, the fault contact between the Wigwam Formation and Davidsville Group. Many of the intrusions are sub-parallel to parallel to the northeast-southwest trending structures

that transect the area, but others are orientated at angles to the same structures. The number of dykes and sills diminishes with increasing distance from the fault. These gabbros may be partial melts of lower crust induced by crustal thickening due to transpressional movement along these faults. This will be discussed in more detail in a later section.

These gabbro intrusions host gold-arsenopyrite-pyrite mineralization in the Duder Lake area (Churchill and Evans, 1992; Churchill *et al.*, 1993) as well as in several other localities in northeastern Newfoundland (Evans, 1991; 1992; 1993).

2.4 Faults

At least two generations of faults are present in the Duder Lake area. The major northeast trending, transcurrent faults include the Reach Fault (Dean, 1978a) and the Dog Bay Line (Williams, 1993) as well as numerous other smaller faults with the same geometry (Figure 2.2). These faults appear to have had latest Silurian or younger movement. The Dog Bay Line, located east of Duder Lake, is manifest as a series of northeast-trending faults that form a fault zone up to 1 kilometre in width with pronounced topographic expression.

The Reach Fault is a brittle structure having a sinistral sense of shear and displacements in excess of 15 km (Currie, 1993) and was long interpreted to delineate the point of final closure of the Iapetus Ocean (Arnott *et al.*, 1985; McKerrow and Cocks, 1986; Najjarpour and Upadhyay, 1987). Williams (1993) defined the Reach Fault

as the western boundary of the Botwood Belt.

The Dog Bay Line appears to be a major tectonic junction, but not a terrane boundary since there is faunal continuity across it (Williams, 1993). It has a curvilinear fault trace extending from the Indian Islands northeast of Gander Bay inland to Rocky Pond and has been inferred to extend as far south as the Mount Peyton Batholith with dextral transcurrent movement and dip-slip displacement (Williams, 1993).

Second generation faults are those east-west to northwest-southeast trending structures that cut stratigraphy as well as the major northeast-trending structures such as the Reach Fault and the Dog Bay Line. Movement along an unnamed east-west trending fault north of Duder Lake post-dated emplacement of the Loon Bay Batholith, making age of activation early Devonian or even Carboniferous. This inference is in agreement with the findings of Lafrance and Williams (1989) who stated that many of the east-west trending faults in the Notre Dame Bay area may have been initiated in the Silurian but may have remained active until the Devonian. It is also feasible that these faults may have been affected or even reactivated by a Carboniferous event.

The two major structures, the Reach Fault and the Dog Bay Line, have importance in the context of regional tectonics, but they also have relevance to regional metallogenesis since mineralization is closely related to faulting and directly controlled by second, and possibly third-order structures originating primarily from the Dog Bay Line.

2.5 Deformational Fabrics

Several structural studies have been undertaken in the Notre Dame Bay area, all of which have recognized the structural and resulting stratigraphic complexity (Helwig, 1972; Dean and Strong, 1977; Karlstrom *et al.*, 1982; Williams, 1984; Van der Pluijm and Williams, 1985; Van der Pluijm *et al.*, 1987; Goodwin and O'Neill, 1991; Lafrance and Williams, 1992; O'Brien, 1993).

According to O'Brien (1993), four phases of deformation are preserved in the rocks of the central Notre Dame Bay area - the D₁ and D₂ events are associated with thrusting of the volcanic terrane to the northwest (*viz.* the Robert's Arm Group of the Notre Dame Bay Subzone) upon rocks of the Exploits Subzone. The D₁ and D₄ events are associated with wrench movements along the major fault systems in the area.

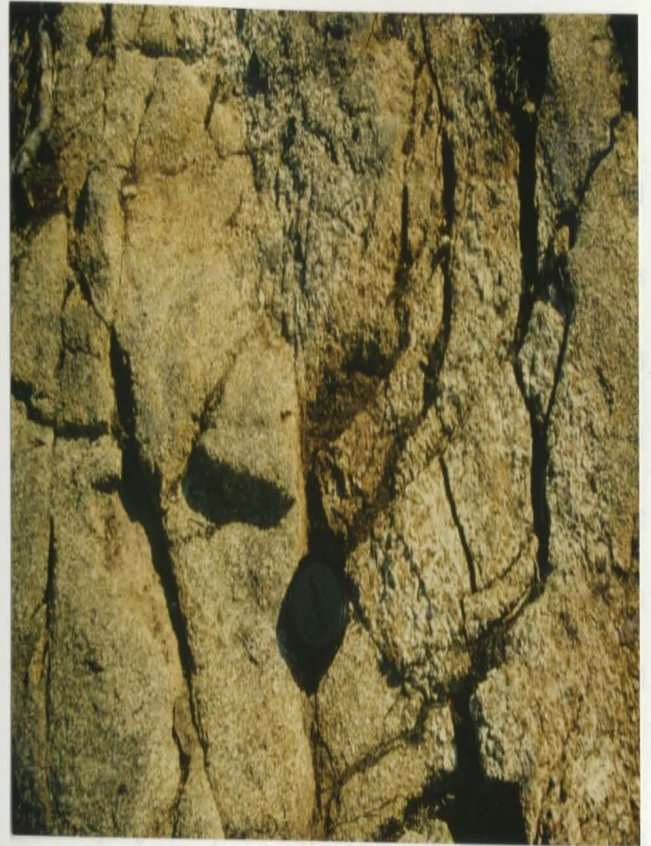
Only three deformational fabrics are observed in trench and outcrop exposures from the Duder Lake area. The D₂ fabrics are the most predominant structural features and the D₁ and D₃ features are seen only locally.

2.5.1 D₁ Deformational Features

The only evidence of a D₁ event is the presence of overturned beds and small recumbent folds that dip steeply to the southeast (Plate 2.8). F₁ structures have been inferred to be broad regional scale folds that were recumbent prior to F₂ folding (Karlstrom *et al.*, 1982) and which may not have had a well developed penetrative cleavage.

3.2 Deformational Features

Plate 2.7: Coarse-grained gabbro dyke with pegmatitic pods (right half of photograph) intruding red beds of the Wigwam Formation approximately 3km northeast of the northern extremity of Duder Lake.



of which have recognized the structural and resulting stratigraphic complexity (Folwell, 1972; Dean and Strong, 1977; Karstrom et al., 1982; Williams, 1984; Van der Pluijm and Williams, 1985; Van der Pluijm et al., 1987; Goodwin and O'Neill, 1991; LaFrance and Williams, 1992; O'Brien, 1993). According to O'Brien (1993), four phases of deformation are preserved in the rocks of the central Notre Dame Bay area - the D₁ and D₂ events are associated with thrusting of the volcanic terranes to the northwest (i.e., the Robert's Arm Group of the Notre Dame Bay Subzone) upon rocks of the Exploits Subzone. The D₁ and D₂ events are associated with wrench movements along the major fault systems in the area.

Plate 2.8: Overtaken F₁-fold in argillaceous siltstones of the lower part of the Wigwam Formation. Located 3km east of Duder Lake. D₁ fabric having an inclination of approximately 45° in photograph while the D₂ fabric is sub-vertical.



Only three deformational fabrics are observed in each and outcrop exposures and the D₁ and D₂ fabrics are seen only locally. The only evidence of a D₃ event is the presence of overturned beds and small recumbent folds that dip steeply to the southeast (Plate 2.8). F₂ structures have been inferred to be broad regional scale folds that were recumbent prior to F₁ folding (Karstrom et al., 1982) and which may not have had a well developed penetrative cleavage.

2.5.2 D₂ Deformational Features

Deformation within the Duder Lake area is recorded by a well developed penetrative cleavage (S₂) that parallels the regional fabric and is axial planar to F₂ folds produced during the regional deformation (Plate 2.9). Lower hemisphere projections (Figure 2.3b, 2.3d) of the structural data indicate that the S₂ cleavage is a northeast trending fabric with variable inclinations from shallowly dipping to sub-vertical. The bedding plane data (S₀) are quite varied in orientation and dip. However, a π -girdle can be constructed through the data points, leading to the inference of a gently plunging fold axis to the south (Figure 2.3a).

Comparing the two plots, it is apparent that the cleavage is axial planar to the folding, reaffirming the regional structural relationships defined by Karlstrom *et al.* (1982).

2.5.3 D₃ Deformational Features

These structures are only seen locally in the Duder Lake area and are manifested as kinking and crenulation of the S₂ cleavage (Plate 2.10). The S₃ cleavage planes are widely spaced (up to 10 cm) and were only observed in rocks of the Wigwam Formation. The orientations of the data are quite varied (Figure 2.3c) and S₃ development may in part be controlled by competency contrasts in the rock units.

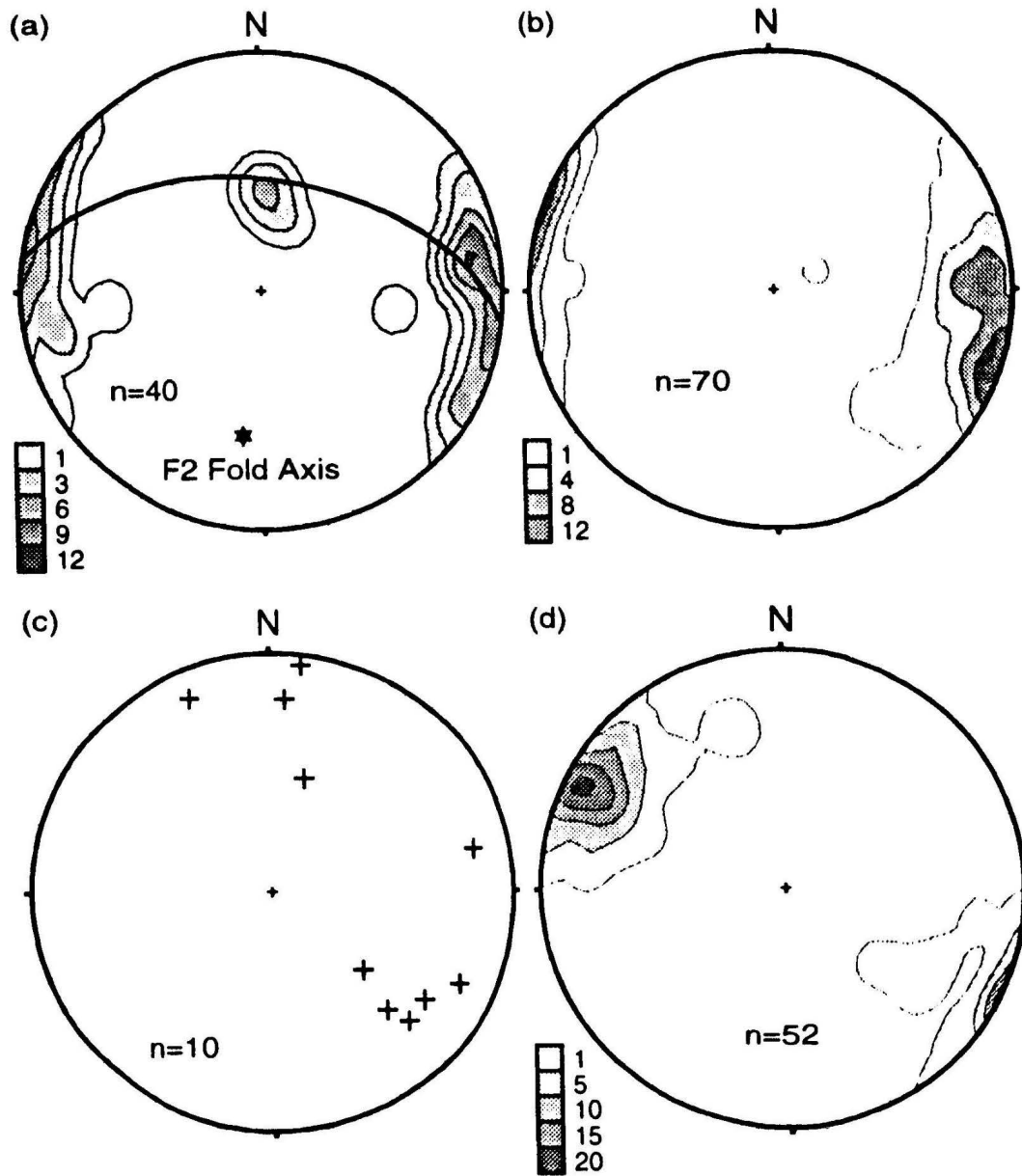


Figure 2.3: Contoured, equal area, lower hemisphere, poles-to-planes stereographic projections for bedding and schistosity data. (a) Bedding data for the Wigwam Formation. PI-girdle identifies an F2 fold axis with moderate south-southwest plunge. (b) S2 cleavage data from the Wigwam Formation illustrating the dominant northeast-trending cleavage. (c) S3 cleavage data from rocks of the Wigwam Formation showing variable orientations. (d) S2 cleavage data for the Davidsville Group showing strong northeast-trending orientation differing slightly from that of (b). Shift in orientation may be attributable to rigid block rotation post-dating cleavage development. Contour intervals as listed and n=number of observations.

Plate 2.9: Northeastery-trending D_2 fabric developed in greenish siltstones of the lower part of the Wigwam Formation. Located 1km west of Duder Lake.

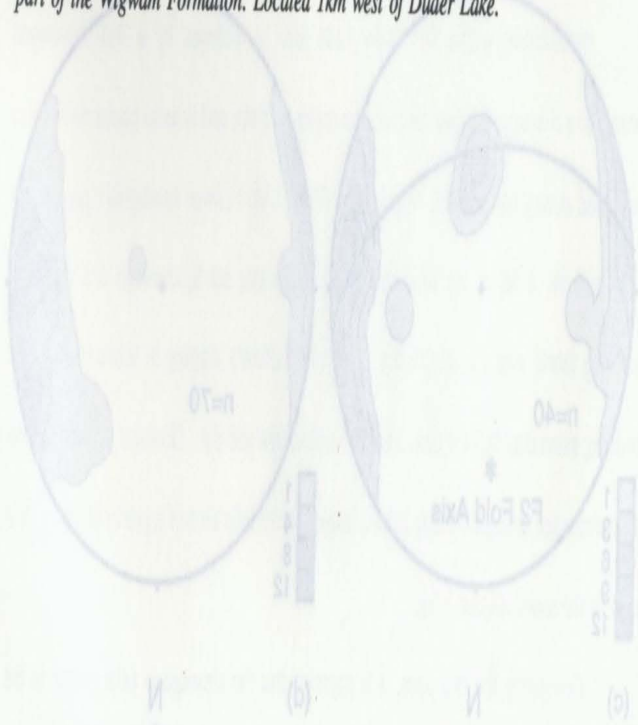


Plate 2.10: S_3 crenulation cleavage kinking S_2 cleavage developed in maroon-coloured sandstones of the Wigwam Formation located 4km east of the Birchy Bay turn-off.

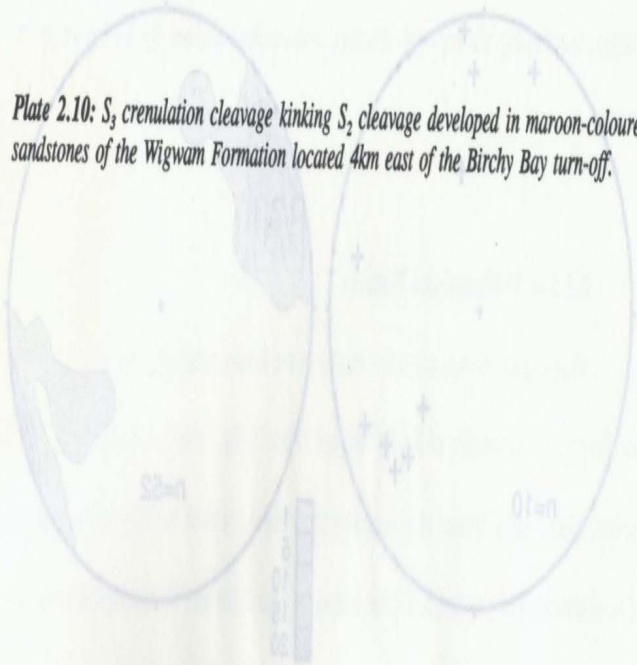


Figure 2.3: Contoured equal area lower hemisphere point-to-center stereographic projections for bedding and schistosity data for the Wigwam Formation. P-folds identified for bedding and schistosity data. (a) Bedding data for the Wigwam Formation. P-folds identified for bedding and schistosity data. (b) S_2 cleavage data from the Wigwam Formation showing the dominant northeast-trending cleavage. (c) S_3 cleavage data from the Wigwam Formation showing various orientations. (d) S_2 cleavage data for the Davidson Group showing strong northeast-trending orientation dipping slightly from flat to 60°. Both in crenulation may be attributable to high tectonic post-dating cleavage development. Contour intervals as listed and number of observations.

and can be constrained to have had a time of movement of lower Devonian or younger.

2.6 Summary

A sequence of Upper Ordovician to Upper Silurian marine and terrestrial sedimentary and volcanic rocks forms distinct, northeast trending outcrop belts in the Duder Lake area. Large Silurian and Devonian plutonic bodies intrude the sequence and parallel both stratigraphic and structural trends. In addition, numerous small gabbroic dykes and sills of probable Siluro-Devonian age intrude the Wigwam Formation and Davidsville Group close to the Dog Bay Line and some of the gabbroic intrusions are elongated parallel to this structural feature.

A series of northeast-trending faults forms contacts between several of the units. Later east-west and northwest-southeast trending faults offset the northeast-trending faults and can be constrained to have had a time of movement of lower Devonian or younger.

Three phases of deformation can be seen with D_1 and D_3 events only locally developed and a D_2 event defining the main structural fabric.

CHAPTER 3

PETROGRAPHY AND GEOCHEMISTRY OF VOLCANIC AND SEDIMENTARY ROCKS AND INTERPRETATION OF THEIR TECTONIC SETTING

3.1 Introduction

Although the focus of this study is to characterize the alteration and mineralization within gabbros, and to a lesser degree graphitic sandstones, of the Duder Lake area, unaltered samples were collected in an effort to characterize original compositions and/or tectonic settings. Of a total of 85 samples collected, 16 were classified as either unaltered volcanic (4 samples) or sedimentary rocks (12 samples). The remaining 62 samples constituted mineralized and vein samples. Table 3.1 gives specific information on elements analyzed for both volcanic and sedimentary lithologies. Major oxides were analyzed using ICP-OES techniques at the NDME laboratories and REE were analyzed via the ICP-MS techniques at MUN. Trace element contents were determined by one of three analytical methods including atomic absorption (AA) at the NDME labs, neutron activation analysis (NAA) at Becquerel Labs in Ontario under contract to the NDME and X-ray fluorescence (XRF) at MUN. Appendix I provides more detailed information on these different techniques.

In this section, the geochemistry is described for those rocks classified as unaltered, but which should be more properly termed least altered since all rocks from

Table 3.1: Elements analyzed and numbers of samples per lithological type studied.
Note that numbers in parentheses refer to the number of samples analyzed for the given analytical technique.

Sedimentary Rocks:

Total Number of Samples Collected = 12

Major Oxides (12): SiO₂, TiO₂, Al₂O₃, Fe₂O₃, MnO, MgO, CaO, Na₂O,
 K₂O, P₂O₅, H₂O, CO₂, LOI

Trace Elements (12): Cr, Ni, Co, Sc, V, Cu, Pb, Zn, Cd, W, Mo, S, As, Se, Sb,
 Au, Rb, Cs, Ba, Sr, Ga, Li, Ta, Nb, Hf, Zr, Y, Th, U, La,
 Ce, Sm, Eu, Tb, Dy, Yb, Lu, Cl, Br, Be

Volcanic Rocks:

Total Number of Samples Collected = 4

Major Oxides (4): SiO₂, TiO₂, Al₂O₃, Fe₂O₃, MnO, MgO, CaO, Na₂O,
 K₂O, P₂O₅, H₂O, CO₂, LOI

Trace Elements (4): Cr, Ni, Sc, V, Cu, Pb, Zn, S, As, Rb, Ba, Sr, Ga, Nb, Zr,
 Y, Th, U, Ce, Cl

REEs (4): Ba, Ta, Nb, Hf, Zr, Y, Th, La, Ce, Pr, Nd, Sm, Eu, Gd,
 Tb, Dy, Ho, Er, Tm, Yb, Lu

the study area have experienced at least lower- to mid-greenschist facies metamorphism. Thus, many of the diagrams used in this chapter to illustrate tectonic setting and/or petrographic classification will, for the most part, utilize those elements considered to be immobile under low grade metamorphic conditions including Ta, Nb, Hf, Zr, Ti, Y, Th and the HREE (Pearce and Cann, 1973; Myers and Breitkopf, 1989). The chemical analyses for the different rock types are listed in Appendices IIa through IIg.

3.2 Mafic Volcanic Rocks

Mafic volcanic rocks of the Lawrenceton Formation are only exposed in the

southern end of the study area. Two samples were collected from this area as well as one from the Clutha gold prospect (Evans, 1991) to the northeast of Duder Lake showings and one from the Dan's Pond area approximately 25km southwest of Duder Lake. These additional samples were collected so as to ascertain the geochemical nature of these mafic rocks on a regional scale and define whether they were a local phenomenon or were related to some larger episode of volcanism. Although the sample set is small, they are representative of the unit such that the following observations are valid for these rocks.

3.2.1 Petrography

The mafic volcanic rocks, some of which are pillowed, exhibit a variable degree of alteration. For the most part, these rocks have been pervasively chloritized, epidotized, and carbonatized perhaps the result of metamorphic effects of the lower to mid-greenschist facies. All samples exhibit intersertal textures defined by plagioclase laths set in a groundmass composed of epidote and chlorite. In addition, these rocks exhibit quartz and carbonate veining on both micro- and macroscopic scales. Generally, the rocks are very fine-grained with the largest relict igneous minerals < 1mm in size and consisting of 60% saussuritized plagioclase with minor amounts of metamorphic albite, 20% intersertal epidote, 10% intersertal and vein chlorite, and 10% mixed oxides and carbonate veins and patches (Plate 3.1).

3.1.2 Geochemistry and Tectonic Setting

Geochemical data for major and trace element as well as REEs are listed in Appendices IIa and IIb respectively. As indicated by the oxide data, the basaltic dykes have a range of SiO_2 contents from 49.57-59.07 wt. % corresponding to a basaltic to basaltic andesite composition (Cox *et al.*, 1974). There appears to be little variability in the alkali oxides (i.e. K_2O and Na_2O) which suggests that the contents may be the original. Figure 3.1 is an AFM plot of Irvine and Barager (1971) which indicates

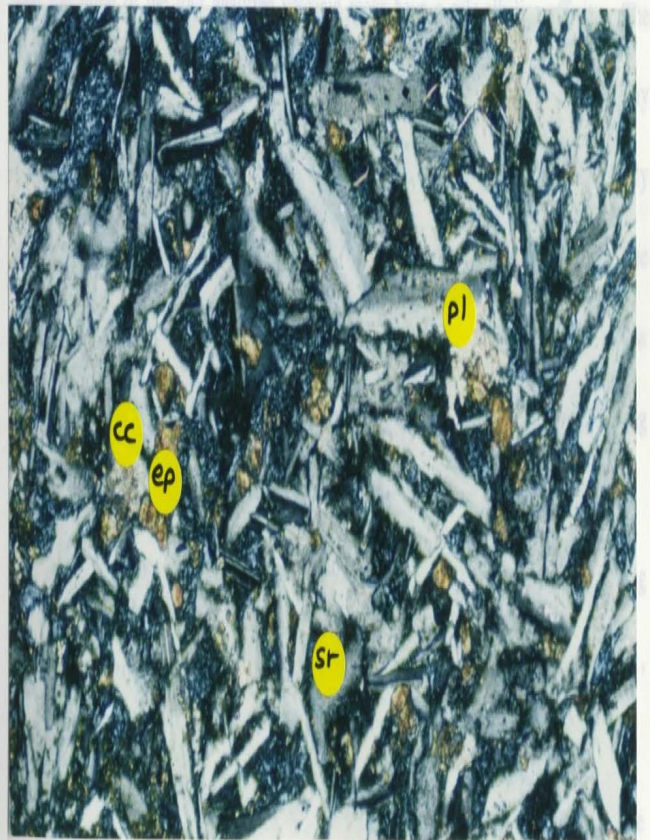


Plate 3.1: Photomicrograph of metamorphosed basalt of the Lawrenceton Formation exhibiting a greenschist facies metamorphic mineral assemblage including calcite (cc), epidote (ep) and sericite (sr) in plagioclase (pl). [XP at 10X magnification].

3.2.2 Geochemistry and Tectonic Setting

Geochemical data for major and trace element as well as REEs are listed in Appendices IIa and IIb respectively. As indicated by the oxide data, the basaltic lithologies have a range of SiO₂ contents from 49.57-59.07 wt. % corresponding to a basaltic to basaltic andesite composition (Cox *et al.*, 1979). There appears to be little variability in the alkali oxides (*ie.* K₂O and Na₂O) which suggests that the contents may be the original. Figure 3.1 is an AFM plot of Irvine and Barager (1971) which indicates that the three of the four analyzed volcanic rocks have a calc-alkaline affinity. The fourth sample (RC-92-04), being the most altered, has higher iron contents which may reflect the presence of hydrothermal pyrite. The Irvine and Barager (1971) alkalinity index of these rocks, indicates that they are variably subalkaline (Figure 3.2). The remaining oxide and trace element data show some variability attributed to either a low grade metamorphic alteration or to overprinting by the hydrothermal episode effecting gold mineralization, thus the original chemistry is not preserved .

Since some of the data may not reflect the original compositions, the following discussion will be based on those elements considered to be immobile, including Zr, Y, Nb and TiO₂.

The Winchester and Floyd (1979) plot of Zr/TiO₂ versus Nb/Y suggests that the mafic rocks have compositions which range from andesite to basaltic andesite (Figure 3.3). Studies on the volcanic rocks of eastern Notre Dame Bay by Najjarpour and Upadhyay (1987) also deduced that the volcanic rocks have a calc-alkaline affinity. One

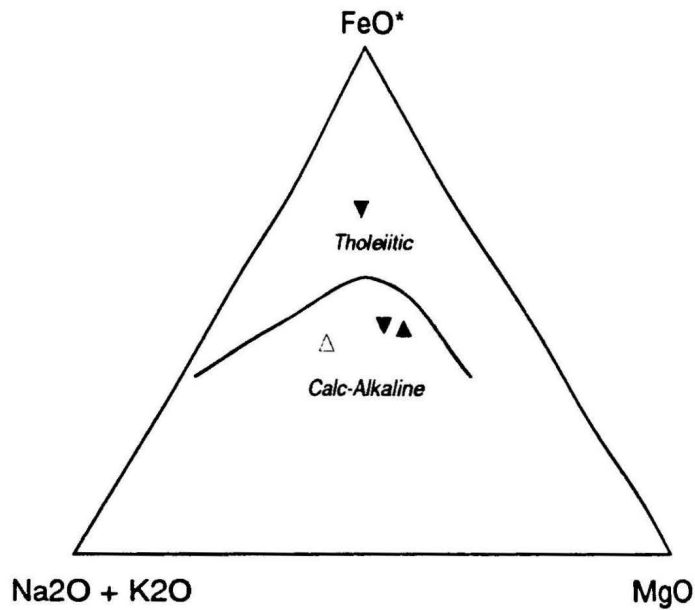


Figure 3.1: AFM plot of Irvine and Barager (1971) indicating the chemical affinity of the mafic volcanic rocks from Duder Lake (filled, inverted triangles) the Clutha gold prospect (filled triangle) and Dan's Pond (hollow triangle). Refer to text for discussion.

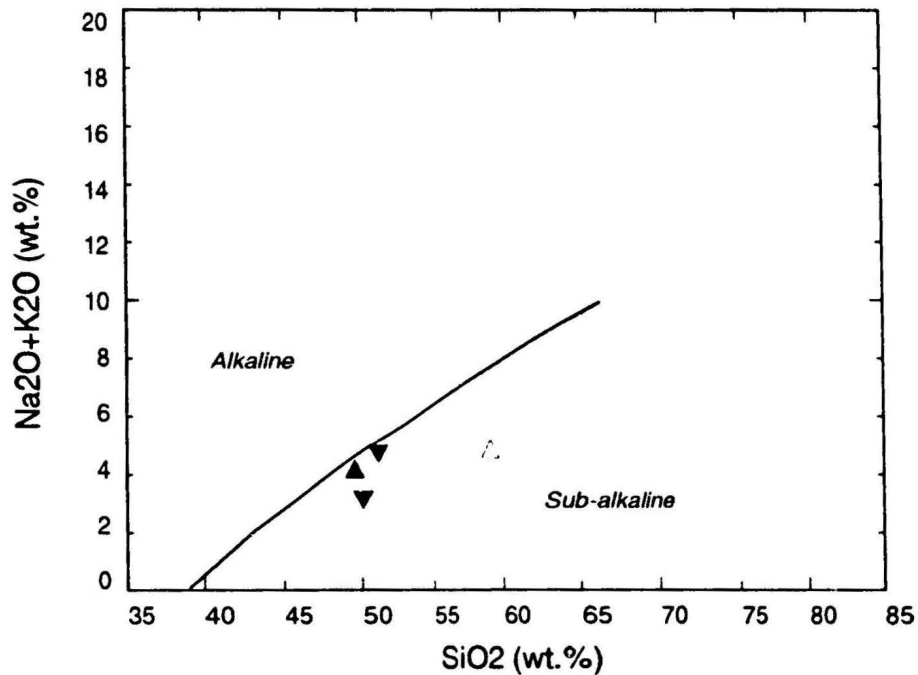


Figure 3.2: Irvine and Barager (1971) Na₂O+K₂O versus SiO₂ plot illustrating the sub-alkaline nature of the mafic volcanic rocks. Symbols as per Figure 3.1.

data point (RC-92-04) plots down and to the right of the other three, possibly due to the presence of a secondary alteration assemblage composed of chlorite, carbonate, and sericite which may have produced a limited mobility of these elements.

Incompatible elements can also be used to infer a probable tectonic setting for the basaltic lithologies. Figure 3.4 is Meschede's (1986) tectonic discrimination diagram which shows that the basalts have a calc-alkaline chemistry.

The normalized REE profile of the basalts can also yield information on the nature and origin of these rocks (Figure 3.5). The samples, normalized to Thompson *et al.*'s (1983) chondrite values all have similar morphologies defined by a LREE enrichment relative to HREE. This profile correlates with a continental-type REE chemistry as shown in Figure 3.5. Samples DT-13 and BCR-1 (refer to Table 3.2 for sample information and values) are continental flood basalts from the Deccan Traps, Indian and the Columbia River regions respectively. Also plotted is BIR-1 which is a mid-ocean ridge basalt and which bears no similarities to the Duder Lake samples thus discounting an oceanic affinity for the basalts. Therefore, since the samples from the Duder Lake area have similar normalized elemental abundances and morphologies to the continental flood basalts, the Duder Lake samples are probably of a continental origin. This interpretation agrees with Williams' (1962, 1972) suggestions that the Lawrenceton Formation rocks were subaerial volcanic rocks. As such they may represent a tectonic equivalent to the volcanic rocks of the Silurian Springdale Group (Coyle and Strong, 1987).

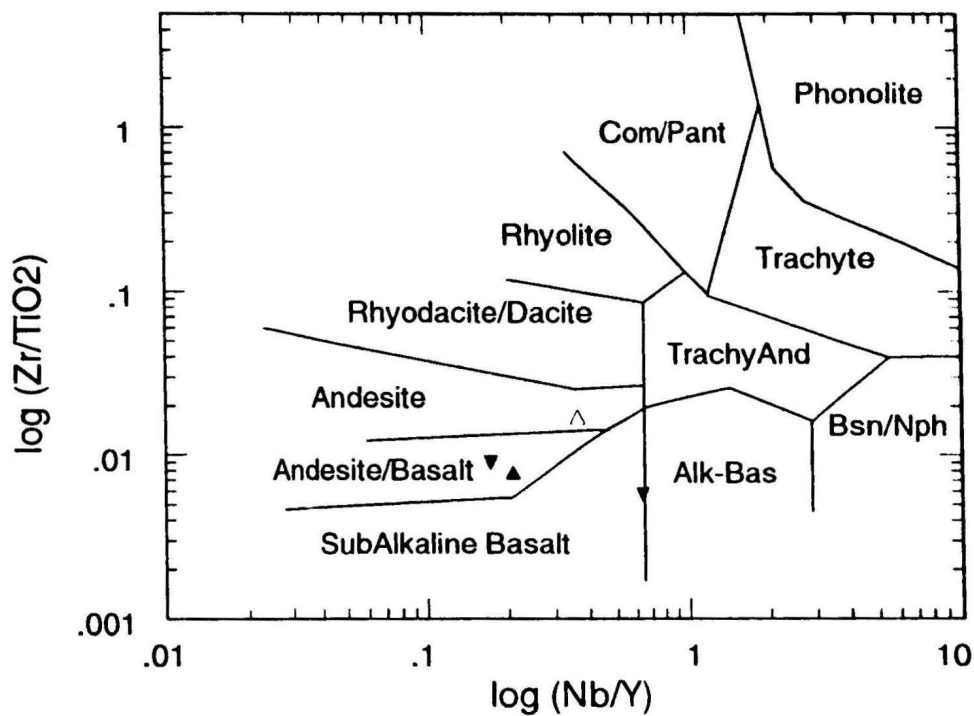


Figure 3.3: Winchester and Floyd (1979) plot of Nb/Y versus Zr/Ti diagram which illustrates the composition of mafic volcanic rocks from the Duder Lake area. Symbols as per Figure 3.1.

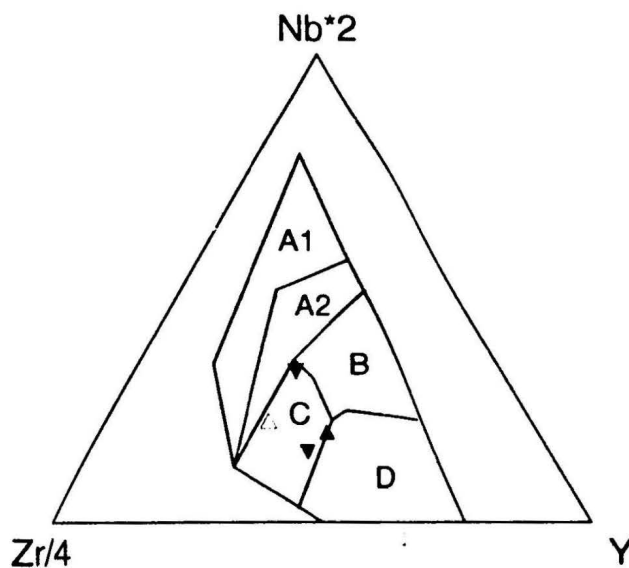


Figure 3.4: Tectonic discrimination plot of Meschede (1986) indicating the tectonic affinity of volcanic rocks in the Duder Lake area. Fields are as follows: A1= within-plate andesite; A2= within-plate tholeiite; B= P-MORB; C= volcanic-arc basalt; D= N-MORB. Symbols as per Figure 3.1.

Table 3.2: Normalization factors for chondrite and geochemical data for continental flood basalt and MORB samples.

	Norm ¹	DT-13 ²	BCR-1 ³	BIR-1 ⁴
Ba	6.9	239	681	7.7
Rb	0.35	15	47.2	1
Th	0.042	2.12	5.98	0.89
K	120	7720	14029	224
Nb	0.35	15.9	14	2
Ta	0.02	1.39	0.81	0.006
La	0.328	19.3	24.9	0.88
Ce	0.865	43	53.7	2.5
Sr	11.8	219	330	108
Nd	0.63	27.6	28.8	2.5
Sm	0.203	7.6	6.59	1.08
Zr	6.84	203	190	22
Hf	0.2	4.49	4.95	0.58
Ti	620	15407	13429	5755
Tb	0.052	-	1.05	0.41
Y	2	50	38	16
Tm	0.034	-	0.56	0.27
Yb	0.22	3.63	3.38	1.7

¹Norm values are for chondrite from Thompson *et al.* (1983)

²DT-13 is a tholeiitic basaltic andesite collected from Deccan, India (Muir, 1970)

³BCR-1 is an international basalt standard from the Bridal Veil Flow of the Columbia River Group (Govindaraju, 1989).

⁴BIR-1 is a sample of the Reykjavik Dolerites and also an international basalt standard for MORB-type basaltic rocks (Govindaraju, 1989).

3.3 Sedimentary Rocks

There is a wide variety of sedimentary rocks present at Duder Lake including subaerial sandstones, siltstones, argillaceous sandstone and siltstone, shales, and graphitic

fine-grained sandstones. A transect from the west to east sides of the Duder Lake study area defines a change in sedimentary lithologies and facies from subaerial rocks in the west to deeper marine rocks in the east. In addition, the rocks become increasingly graphitic eastwards which may be attributed to higher organic contents in a reducing environment.

3.3.1 Petrography

To simplify the petrographic descriptions of the diverse sedimentary lithologies, they will be divided into their respective units and discussed. The sedimentary rock samples studied belong to the Wigwam Formation (Botwood Group) and the Davidsville Group; the former is more quartzitic while the latter is dominated by clay minerals.

3.3.1.1 Sedimentary Rocks of the Wigwam Formation

Rocks of the Wigwam Formation are typically subaerial, oxidized shallow water fluviatile to fluvio-marine sandstones with subordinate siltstone horizons. Commonly these rocks illustrate a wide variety of bioturbation features, thixotrophic deformational structures, and varying degrees of sediment reworking.

Mineralogically, these rocks are composed primarily of quartz (upwards to 70% modally), abundant lithic fragments, and variable amounts of micas and chlorite which may have been produced/derived during metamorphism. Superimposed on the original clast mineralogy are later alteration phases such as carbonate and quartz veins, veinlets,

and replacement patches. The sandstones show a moderate degree of maturity with subrounded clasts indicative of a provenance which was relatively close to the site of deposition. One of the more interesting mineralogical features of these rocks is the presence of detrital micas that are predominantly muscovite (Plate 3.2). The presence of abundant detrital quartz and mica suggests a gneissic provenance and the most likely source rocks would be the high grade gneisses of the Gander Zone (Blackwood, 1982).

3.3.1.2 Sedimentary Rocks of the Davidsville Group

Protoliths of metasedimentary rocks of the Davidsville Group were submature to immature, fine-grained, dark-grey to black, graphitic sandstones, argillaceous siltstones and slates that are thinly interbedded and locally finely laminated. These rocks are characterized by an extremely fine overall grain size as well as a high proportion (>20% modal) of sericite and chlorite and rare quartz and feldspar clasts (Plate 3.3). Lithic fragments are rare and usually confined to the coarser grained lithologies such as the graphitic sandstones. Secondary matrix carbonate is also observed and is usually associated with sulphides suggesting carbonate and sulphide may have been the product of a common hydrothermal event.

Mineralogically these rocks are much different from those of the Botwood Group, and they may have been derived from the island-arc systems of the Notre Dame Bay Subzone to the north and west (Blackwood, 1982; Scheuing and Jacobi, 1990).

3.3.2 Geochemistry and Tectonic Setting

Geochemical analyses for the sedimentary rocks are listed in Appendix IIe. A total of twelve samples of sedimentary rocks were collected for analysis primarily to evaluate the extent of sulphide mineralization present. All samples were obtained from drill core, and as a result depict only Davidsville Group lithologies. Of the twelve samples collected, three represent finer-grained lithologies such as argillaceous siltstones whereas the remaining nine are coarser grained rocks such as sandstones and greywacke.

The argillaceous siltstones have SiO_2 values in the range of 45-53 wt. % and the Al_2O_3 values between 21 and 24 wt. % with one value as low as 10 wt. %. Other chemical characteristics include H_2O values around 5 wt. % and low CO_2 contents in the range of 0.29-2.83 wt. %. The combination of low SiO_2 and high Al_2O_3 , as well as slightly elevated alkalis contents in these samples, is a reflection of the high proportion of micas and chlorite in the argillaceous rocks. The remaining oxide percentages are somewhat variable.

The second set of rocks, the sandstones and greywackes, are higher in SiO_2 (62-73 wt. %), lower in Al_2O_3 (9-15 wt. %), lower H_2O (1-3 wt. %), and elevated CO_2 contents (3-6 wt. %). Neither the alkali oxides nor any of the remaining oxides exhibit any obvious correlation with the aforementioned chemical trends.

The chemistry of the sedimentary lithologies can be used to ascertain the tectonic environment of formation. Figure 3.6 is the plot of SiO_2 versus $\log (\text{K}_2\text{O}/\text{Na}_2\text{O})$ from Roser and Korsch (1986) which defines the tectonic setting of mudstone and sandstone

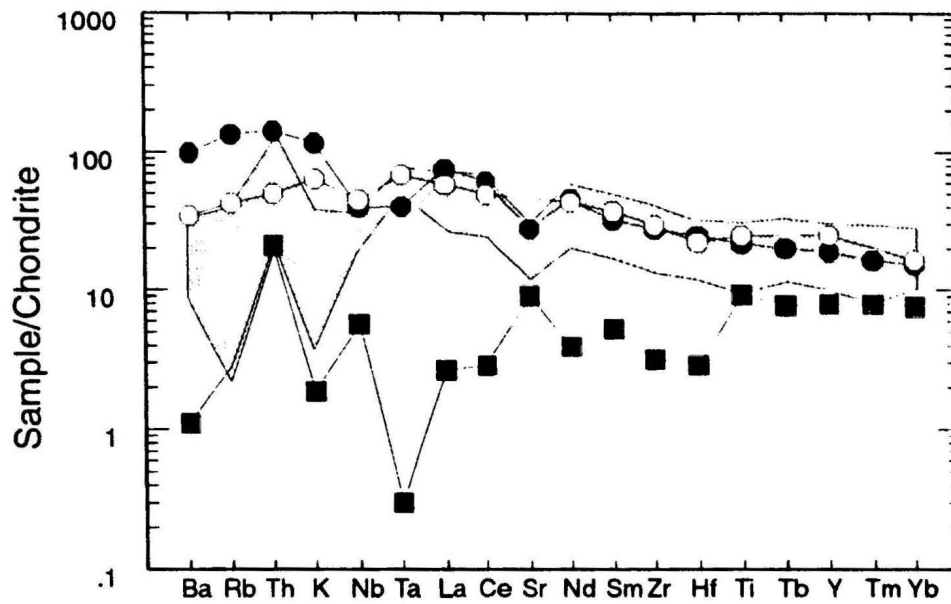


Figure 3.5: Chondrite normalized REE profiles for mafic volcanic rocks from the Duder Lake area (shaded region; n=4) as well as typical continental flood basalts DT-13 (hollow circles) and BCR-1 (filled circles) and mid-ocean ridge basalt sample BIR-1 (filled squares). Refer to text for discussion.

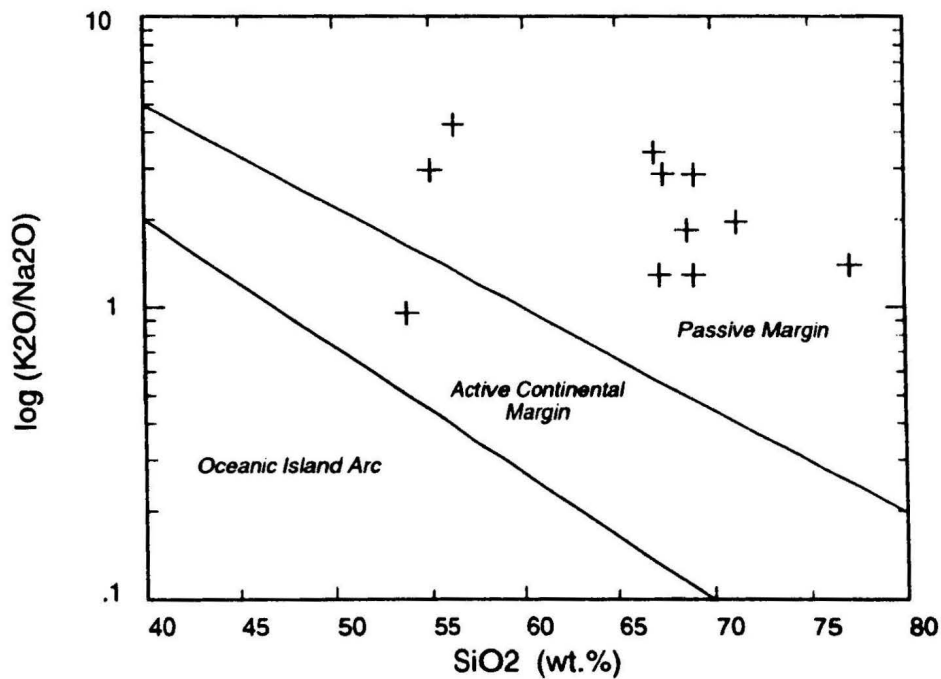


Figure 3.6: Roser and Korsch (1986) tectonic discrimination plot of SiO_2 (wt.%) versus $\text{K}_2\text{O}/\text{Na}_2\text{O}$ for mudstone and sandstone suites with tectonic setting fields as labelled.

Plate 3.2: Photomicrograph of fine-grained quartzofeldspathic sandstone from the Wigwam Formation. Note the presence of detrital micas (mus). [XP at 20X magnification].

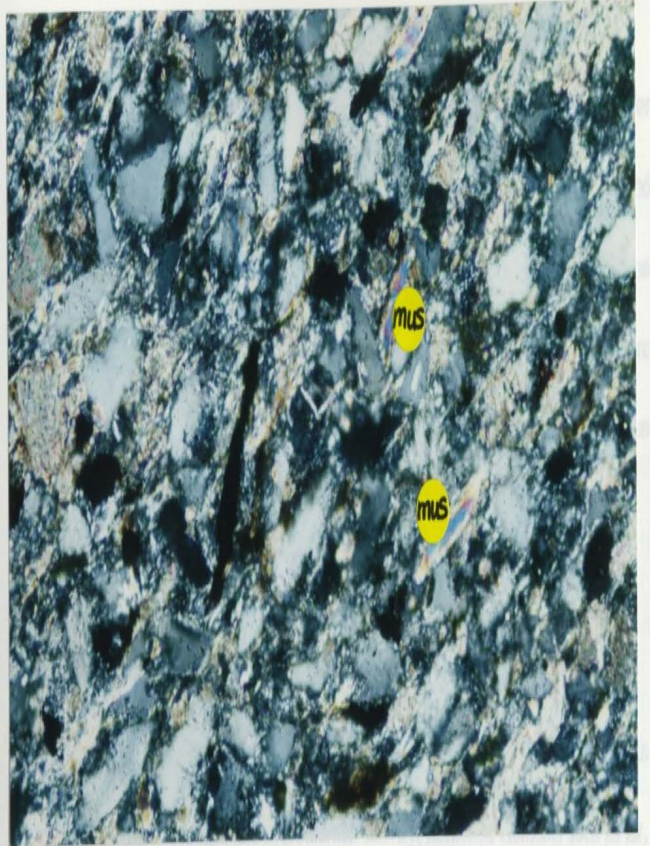
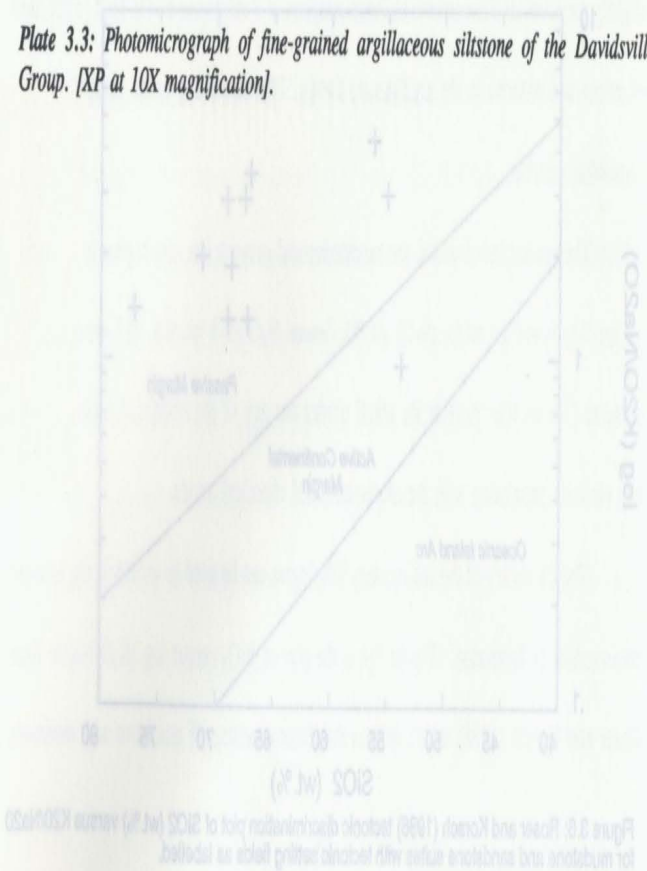


Plate 3.3: Photomicrograph of fine-grained argillaceous siltstone of the Davidsville Group. [XP at 10X magnification].



suites. All the Duder Lake samples cluster in the PM (passive margin) field except for one which plots in the ACM (active continental margin) field. According to Blackwood (1982), rocks of the Davidsville Group were deposited as turbidites and contourites on a continental margin, and as such volcanic detritus was derived from the island arc systems which were found to the north and west. Hence, the PM chemical classification has a geological basis.

3.4 Summary

Since oxide element compositions, especially those of the lithophile elements, can be affected by metamorphism and hydrothermal activity, immobile elements such as Zr, Nb, Y, and TiO_2 must be used to ascertain original compositions as well as tectonic settings. Interpretation of geochemical data for both mafic volcanic and sedimentary lithologies from Duder Lake indicate that the sedimentary rocks were deposited on a passive continental margin with syn-depositional volcanic episodes. This volcanic episode appears to have been calc-alkaline in nature (ie. andesitic to basaltic andesite in composition) and to have had a within-plate tectonic affinity.

These inferences reaffirm the findings of both Scheuing and Jacobi (1990), who stated that sedimentary rocks of eastern Notre Dame Bay were derived from a terrigenous source and deposited on a passive margin, and Najjarpour and Upadhyay (1987), who stated that the volcanic rocks in this area are dominantly calc-alkaline.

CHAPTER 4

ECONOMIC MINERALIZATION

4.1 Introduction

The gold potential of Ordovician-Silurian sequences in the eastern Dunnage Zone was unrecognized until vein-hosted gold was discovered in the Jonathan's Pond area in 1982 (Blackwood, 1982). In response to this discovery, the focus of mineral exploration shifted away from base metals to gold. Over the next ten years, a total of 55 significant epithermal- and mesothermal-like gold showings were discovered (Evans, 1992). In an attempt to document and classify the nature and setting of the mineralization, the Newfoundland Department of Mines and Energy initiated a metallogenic study in 1989 (*cf.* Evans, 1991; 1992; 1993). A compilation of all sites of mineralization is shown in Figure 4.1.

One of the more significant gold discoveries occurs at Duder Lake which is located approximately 7 km east-southeast of Birchy Bay, Notre Dame Bay. The mineralization is present in four pyrite-arsenopyrite-gold mineralized zones, all of which are inferred to be genetically related due to their spatial arrangement about a 4 km long shear zone (refer to Figure MA-1 in map appendix; Churchill and Evans, 1992).

The four mineralized zones have been named the Flirt showing (outside the area of Figure MA-1) and the Goldstash, Corvette and Stinger prospects (Figures MA-1 and 4.2) with each zone containing subtly different mineralization characteristics. As such

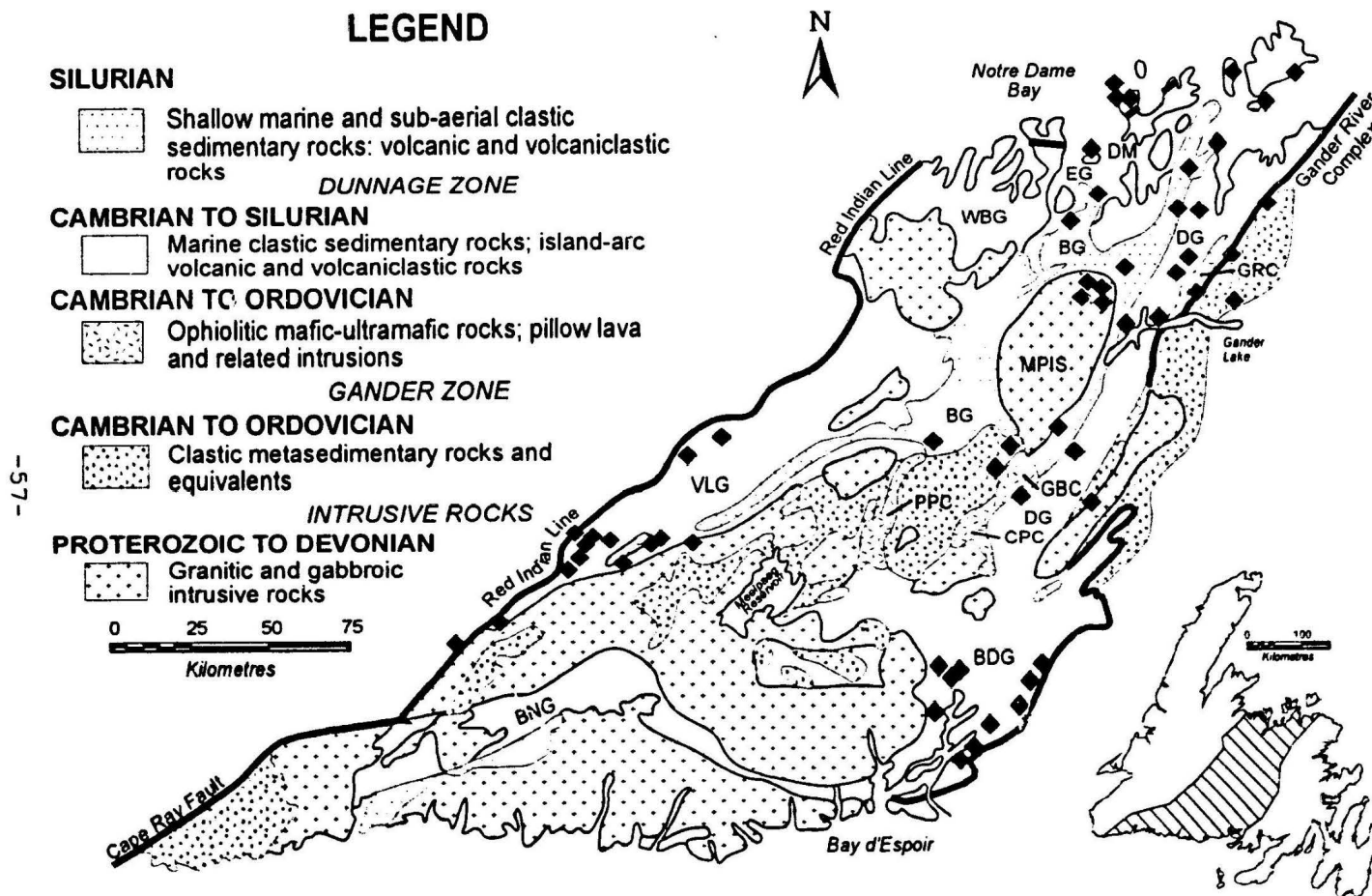


Figure 4.1: Simplified geological setting of gold occurrences in the eastern Dunnage Zone, central Newfoundland (modified from Evans, 1992). Gold occurrences depicted as solid diamonds. Note that not all gold mineralization is depicted due to scaling problems). Acronyms include: DG-Davidsville Group; BG-Botwood Group; DM-Dunnage Melange; EG-Exploits Group; WBG-Wild Bight Group; VLG-Victoria Lake Group; BNG-Bay du Nord Group; BDG-Baie d'Espoir Group; PPC-Pipestone Pond Complex; CPC-Coy Pond Complex; GBC-Great Bend Complex; GRC-Gander River Complex and MPIS-Mount Peyton Intrusive Suite.

they can be classified according to the scheme of Evans (1992) which is discussed in the following section.

4.2 Classification of Mineralization

The recently discovered examples of gold mineralization in the eastern Dunnage Zone are varied in geological setting, alteration character, style of mineralization and structural control. Evans (1992; 1993) has compiled information on all occurrences in an effort to classify them according to their inherent features. Figure 4.3 illustrates a preliminary classification scheme based on: (1) timing of mineralization relative to host rock formation, (2) structural controls, (3) mineralization category (e.g. VMS versus epithermal), (4) mode of mineralization and (5) main ore/indicator minerals. One of the subdivisions of Figure 4.3 pertains to the presence/absence of arsenopyrite as a major ore mineral constituent. Evans' (1992) examination of gold showings from both the western and eastern parts of the Exploits Subzone indicates that there are two mineralized belts, an eastern arsenopyrite-rich belt and a western arsenopyrite-poor belt, suggesting that there may have been a shift in fluid source-region between these two areas. Such inferences will be discussed in the following chapter with relevance to the Duder Lake mineralization.

Based on the classification of Evans (1992; 1993) as well as the concept of an eastern arsenopyrite-rich belt, the mineralization at Duder Lake can be classified as an arsenopyrite-rich, epigenetic, brittle-ductile, mesothermal-like, vein and wall rock style

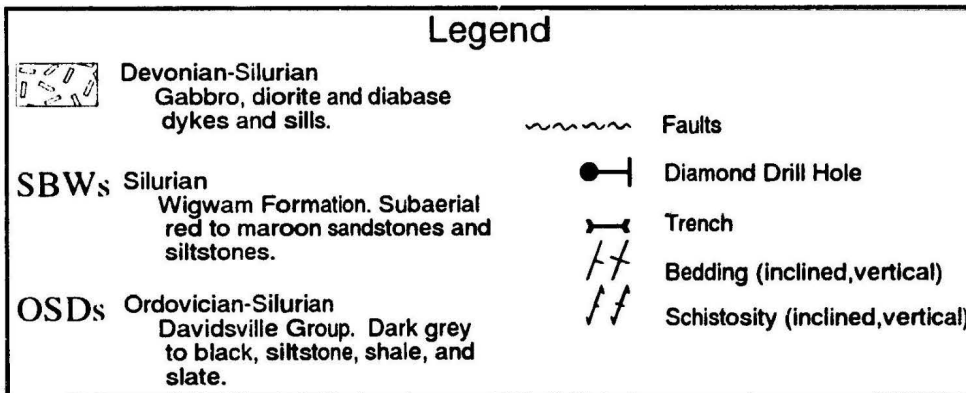
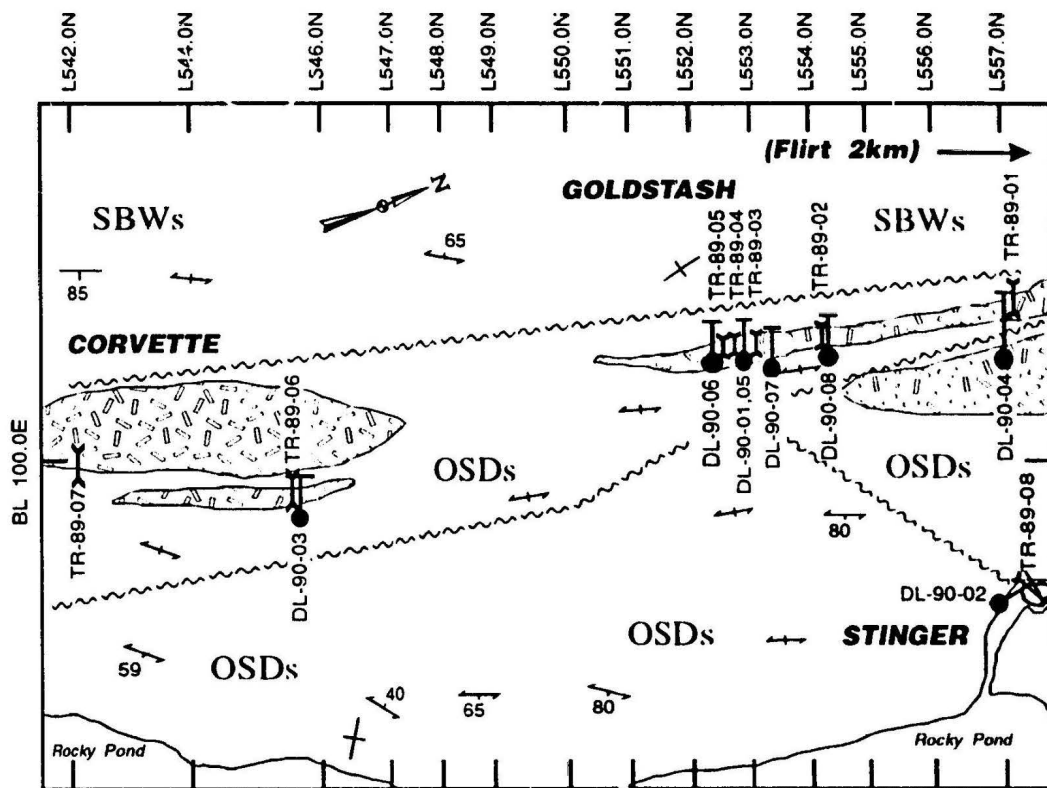


Figure 4.2: Simplified grid geology of the area in the vicinity of the Corvette, Goldstash and Stinger Prospects. Grid line spacing at 100m.

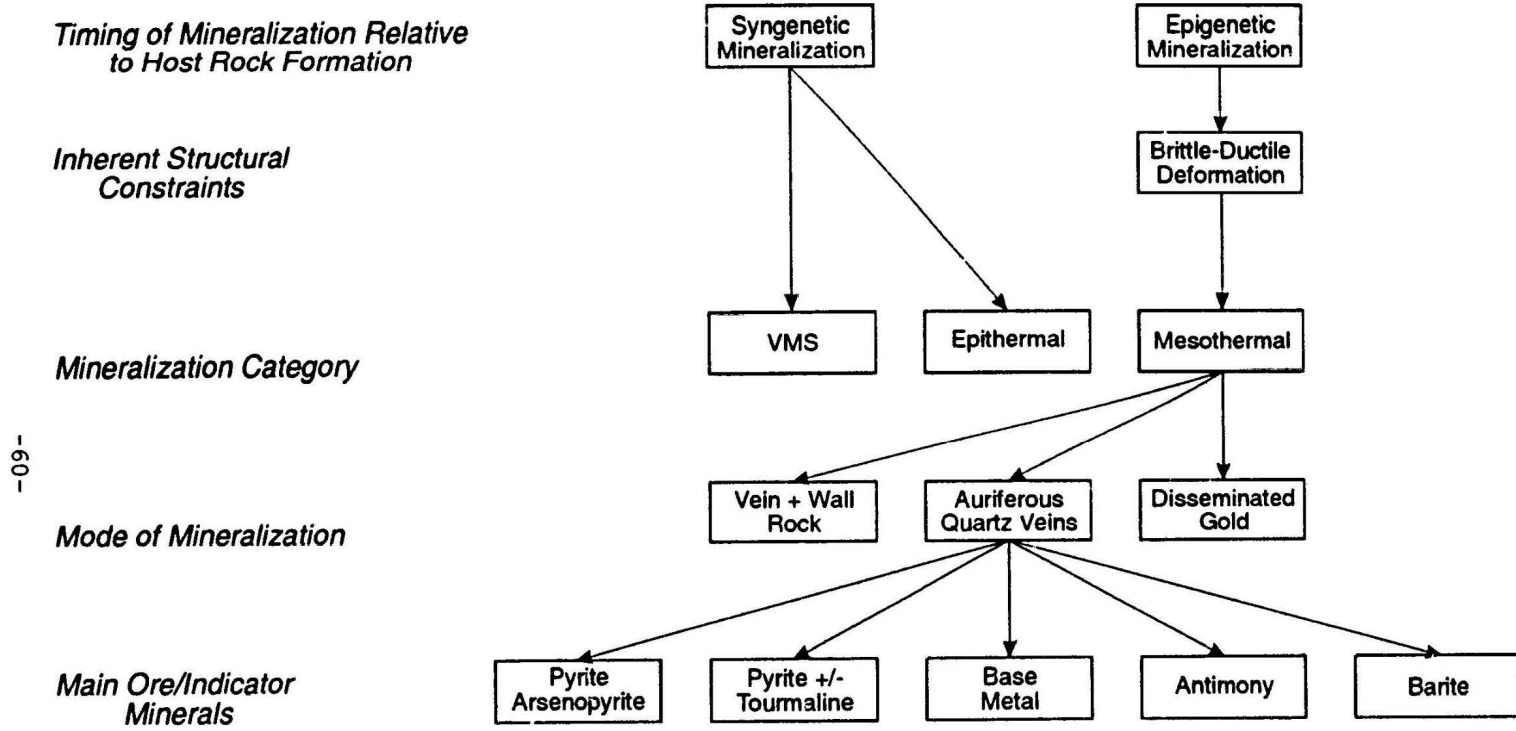


Figure 4.3: Classification scheme for gold mineralization within the eastern Dunnage Zone (modified from Evans, 1993).

of mineralization. This classification is a very broad assignment and based on subtle differences observed at Duder Lake, there are three different sub-classifications, Types Ia, Ib and II, which are described below.

Type I mineralization is present at the Flirt showing and the Corvette and Goldstash prospects. This class of occurrence is hosted by plutonic rocks of inferred Siluro-Devonian age and is structurally controlled by antithetic shears originating from a larger structure(s). This class of mineralization is further subdivided according to the mode of sulphide-gold occurrence. Type Ia (Corvette and Goldstash) represents shear-controlled sulphide disseminations in highly altered host (Plate 4.1) whereas Type Ib (Flirt) occurs as blebby sulphides (\pm gold) in dilational quartz-carbonate shear veins (Plate 4.2). This latter style of mineralization is manifested as thin, usually discontinuous, veins in weak to moderately altered host gabbro with both gold and arsenopyrite much less abundant than in Type Ia mineralization.

Type II mineralization is present at the Stinger prospect and is hosted by graphitic siltstones of the Davidsville Group. The mineralization is manifested as quartz-carbonate veins with variable thicknesses (up to 30cm) and/or hydrothermal breccia which contains coarse blebby sulphide patches and \pm gold. Also common are thin sulphide veinlets and stringers developed in fine-grained graphitic siltstones (Plate 4.3). Alteration along vein margins is confined to narrow centimetre-scale zones of minor sericitization and silicification of the host lithology.

of mineralization. This classification is a very broad assignment and based on subtle differences observed at Lower Lake, there are three different sub-classifications, Type I, II and III, which are described below.

Type I mineralization is present at the Flirt showing and the Corvette and Goldstar prospects. This class of occurrence is hosted by plutonic rocks of inferred Siluro-Devonian age and is structurally controlled by antiforms originating from a larger structure(s). This class of mineralization is further subdivided according to the mode of sulphide-gold occurrence. Type Ia (Corvette and Goldstar) represents shear-

controlled sulphide dissemination in highly sheared host (Plate 4.1) whereas Type Ib

Plate 4.1: Typical style of host rock replacement and mineralization associated with Type Ia mineralization. Sample from TR-89-06 (Corvette Prospect). Field of view measures 8cm across. Numbers on photo represent the following: (1) dilational tension gashes developed late in the history of the shear, (2) replacement groundmass composed of extremely fine-grained quartz and carbonate, (3) sulphides concentrated along foliation planes, (4) amorphous-like alteration minerals of varying colours including green carbonate-epidote-quartz intergrowths and (5) syn-mineralization and alteration foliation due to shearing. Also note on the extreme left of the photo an earlier quartz-carbonate vein which have been folded.

Type II mineralization is present at the Shogor prospect and is hosted by granitic

siltstones of the Davidsonville Group. The mineralization is manifested as quartz-carbonate

veins with variable thicknesses (up to 30cm) and/or hydrothermal breccias which contain

coarse bladed sulphide patches and ± gold. Also common are thin sulphide veins and

stringers developed in fine-grained granitic siltstones (Plate 4.2). Alteration along vein

margin is confined to narrow centimetre-scale zones of minor rehydration and

silicification of the host lithology.



Plate 4.2: Thin, gossanous, quartz-carbonate veins (located below photo-scale) developed in gabbros at the Flirt Showing (TR-89-09). Gradations on photo-scale are in centimetres.

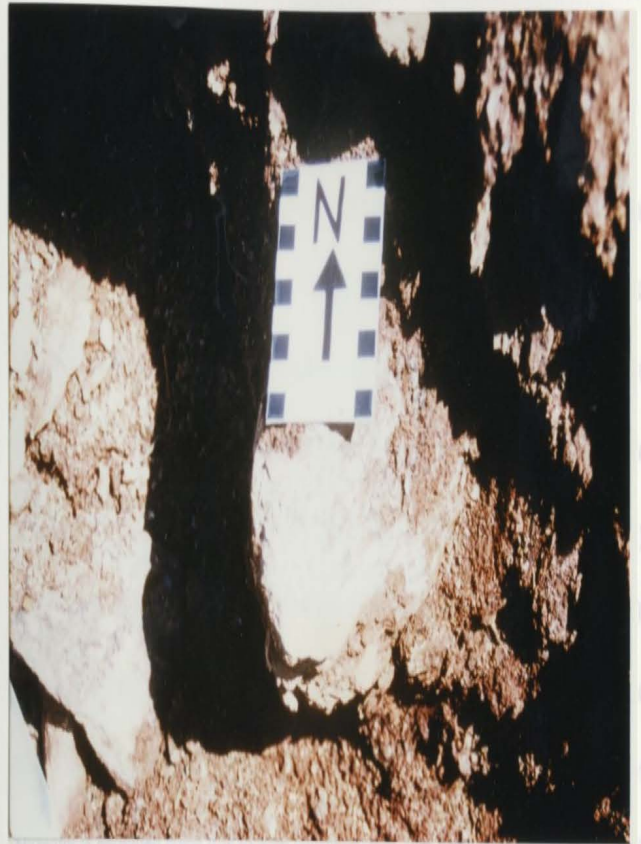
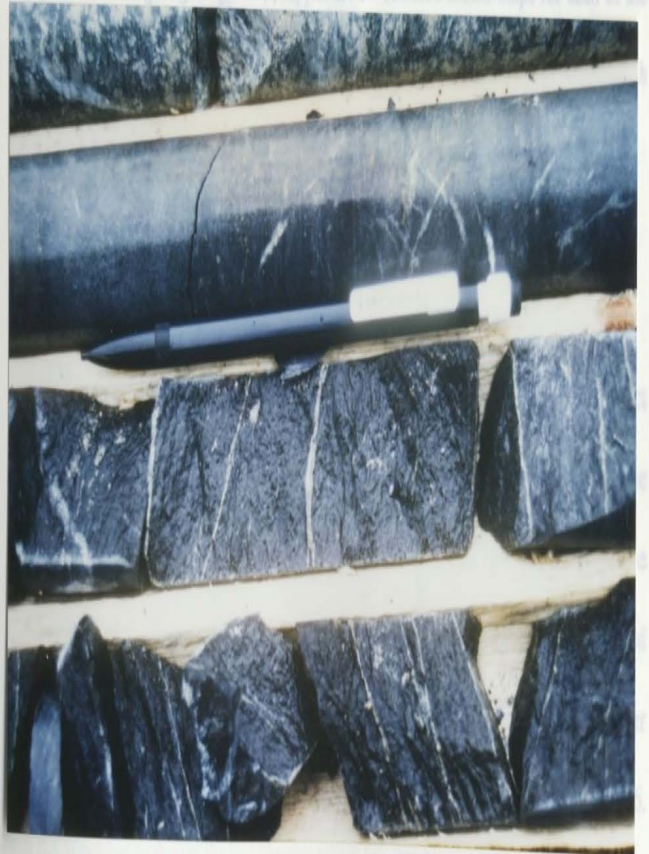


Plate 4.3: Graphitic siltstones (black) from the Singer Prospect with narrow sulphide veinlets (white). Sample from DL-90-02 at a depth of 13.2m. Note pencil for scale.



4.3 Geology of Showings

In this section, the local geological setting of each of the mineralized zones in the Duder Lake area is described, and relationships to nearby faults or shear systems, deformation fabrics, and subsurface spatial orientation of the mineralized zones are discussed (applicable only to the Goldstash Prospect since both the Stinger and Corvette Prospects were intersected in only one diamond drill hole each). A 1:5000 scale geology map is attached in the map appendix located at the back of the thesis (Figure MA-1). This map delineates the major lithological units, faults and shears and locations of the three main gold prospects - the Goldstash, Stinger, and Corvette Prospects. The Flirt Showing is excluded since it is located approximately 2km north of the exploration grid. In addition to the grid geology map, Appendix IV contains sketch maps for each of the trenches visited and sampled. Appendix V consists of schematic visual drill logs for each of the diamond drill holes in the Duder Lake Property.

4.3.1 The Flirt Showing

The Flirt Showing is located approximately 2km north of the Goldstash Prospect and occurs along the main logging road which parallels the east side of Duder Lake. The prospect comprises an excavation trending 135° that straddles the road (Figure 4.4). The mineralization at Flirt is classified as Type Ib and hosted by a sheared and altered gabbroic dyke trending 090°. The dyke intrudes greenish-grey siltstones of the lower part of the Wigwam Formation which exhibit strong S₂ cleavage with orientation 085/66.

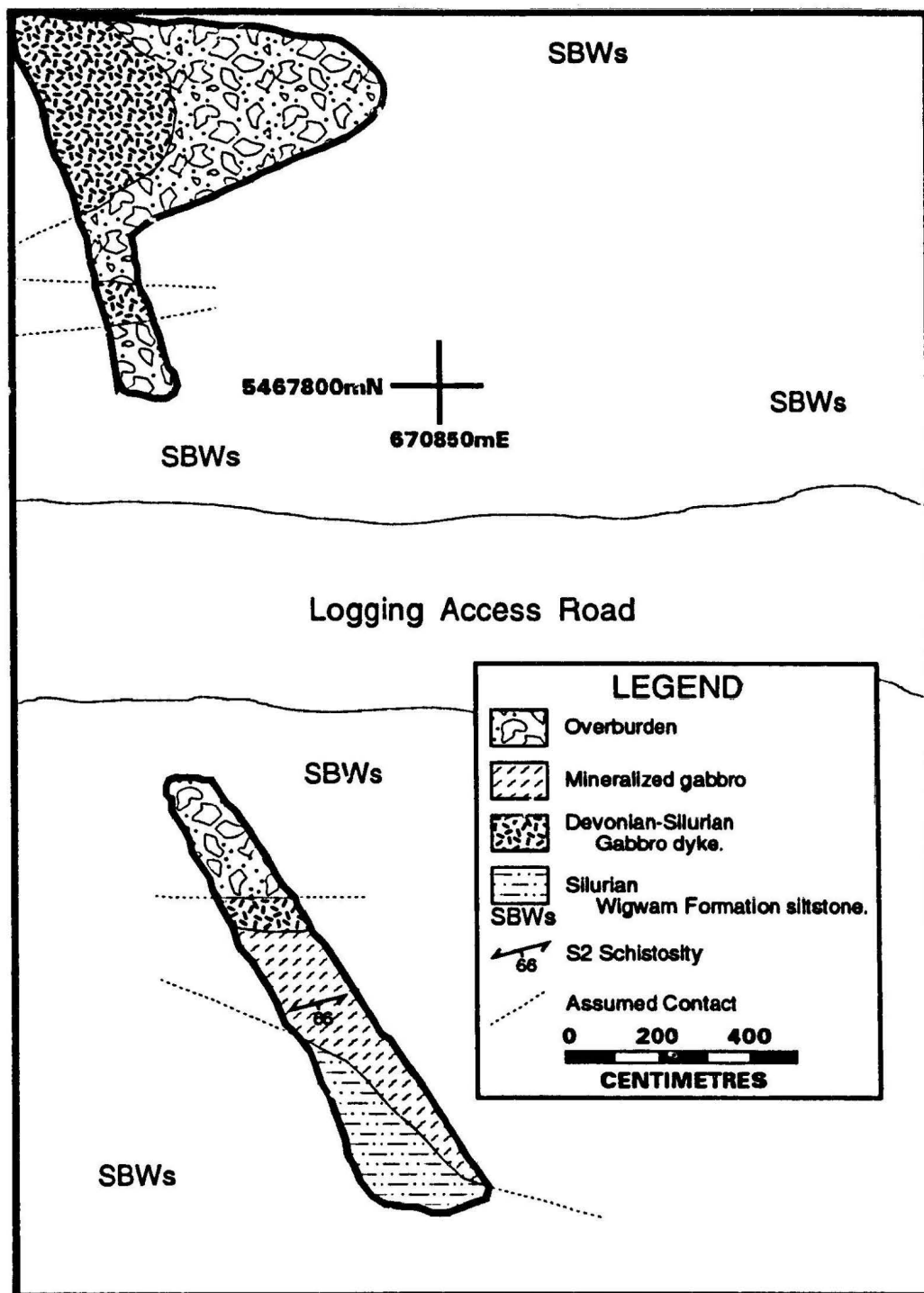


Figure 4.4: Simplified geology of the Flirt Showing with N.T.S. grid reference and schematic trench maps.

Tallman (1990) reports assays up to 9.3g/t Au from the sheared, altered gabbro containing quartz veins. Green (1989) and Tallman (1990) have correlated the Flirt mineralization with the other mineralized zones along a four kilometre long shear zone traceable from Flirt in the north to south of the Corvette Prospect. No drilling was undertaken at this site so subsurface orientation and extent of this mineralized zone is not known.

4.3.2 The Stinger Prospect

Discovered by Noranda geologists in the summer of 1990, the Stinger Prospect crops out in the Rocky Pond River bed (Figure 4.5). This zone comprises Type II mineralization which is hosted by quartz-carbonate veins in graphitic siltstones. Little is known about the surface geology of the Stinger Prospect since it was submerged by run-off waters during the author's stay at Duder Lake (Plate 4.4). However, Noranda geologists mapped the zone during 1990 and a copy of the map is present in Appendix IV. The rocks in the vicinity of the Stinger prospect belong to the Davidsville Group and are predominantly variably coloured (red to dark green) sandstones, siltstones, shales and slates. Cleavage in the area is strong with a northeasterly-trend and steep dip to the southeast. Two faults/shears have been mapped which bound mineralization (Figure 4.5) and create spectacular quartz-vein breccias which have yielded anomalous gold values.

Assays of quartz veins at Stinger yield values up to 30.1g/t Au from grab samples and returns of 2.1g/t Au over 2.8m in the best channel sample (Tallman, 1990). Gold

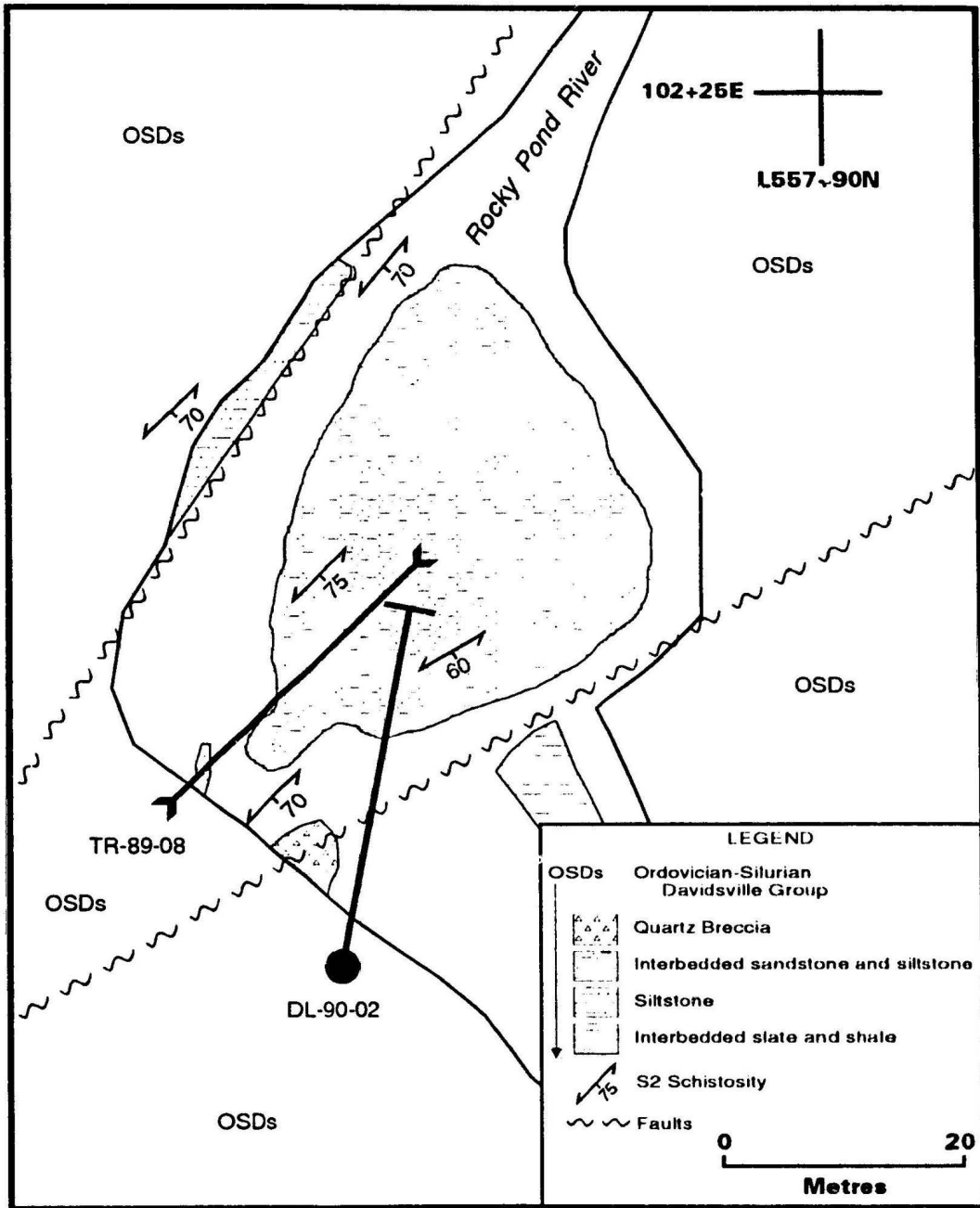


Figure 4.5: Geology of the Stinger Prospect with grid reference and location of drill hole DL-90-02 and trench TR-89-08.



Plate 4.4: Site of the Stinger Prospect. The mineralized zone extends across the river from the left hand river bank to the mid-stream island (right centre of photo).

mineralization is thought to be genetically related to that of the other zones. The shear which controls the mineralization at Stinger has a NE orientation and appears to be a second order splay from the main shear that transects the area of ground separating Rocky Pond from Duder Lake (Figure MA-1).

To test the subsurface extent of the Stinger mineralization, a diamond drill hole (DL-90-02) was completed and a mineralized zone 4m wide (12.25m to 16.3m) was encountered (Appendix V). Assay returns for this drill hole can be observed in Figure 4.6 with peak gold values in excess of 3000ppb coinciding with the start of the mineralized zone and a 2.04g/t Au/4.25m interval as the best drill hole section (Tallman, 1990).

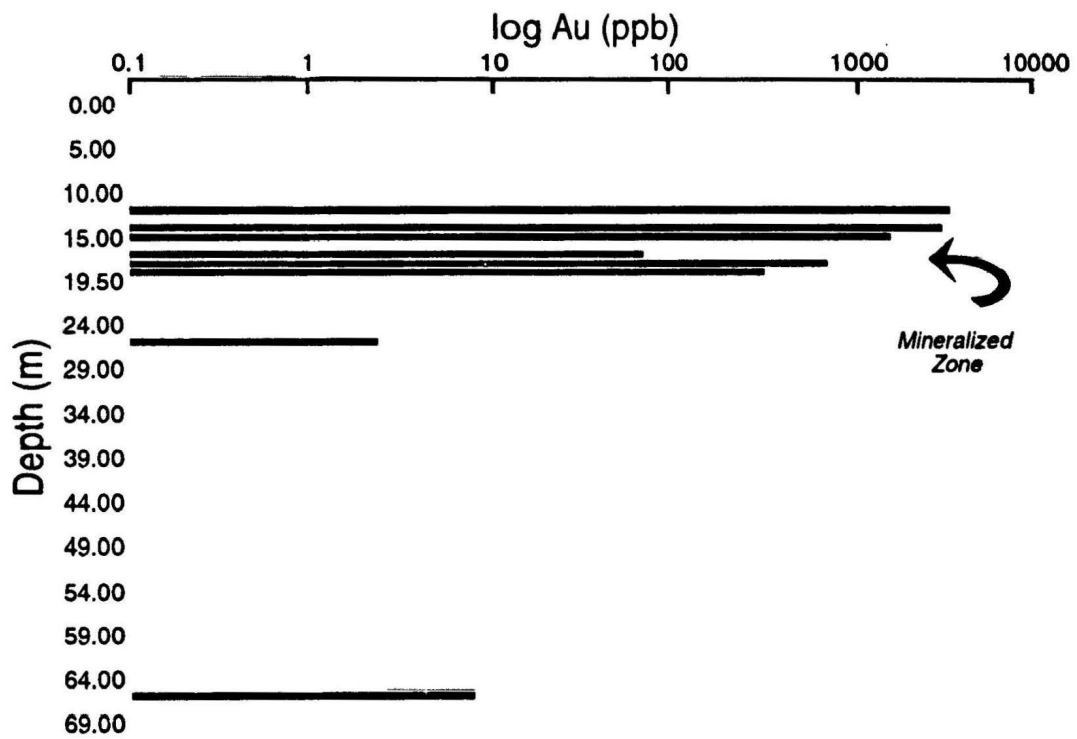


Figure 4.6: Log Au (ppb) assay values for diamond drill hole DL-90-02 from the Stinger Prospect. Note large increase in gold values from 12.50-19.40m coincides with visible arsenopyrite and pyrite mineralization in drill core. Refer to Appendix V for schematic visual drill logs and brief descriptive notes on the drill core.

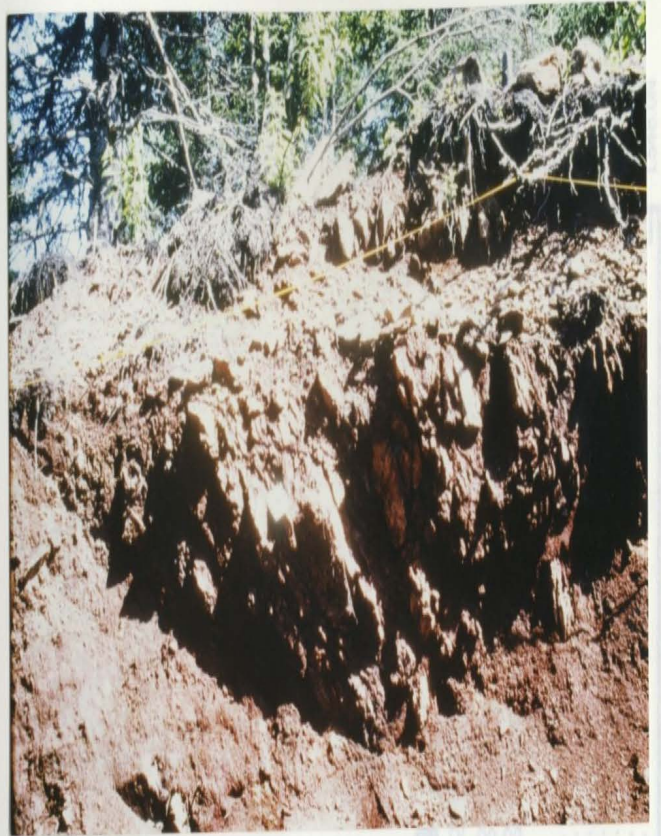
4.3.3 The Corvette Prospect

The Corvette Prospect is the most southerly of the four zones and is classified as a Type Ib mineralization (ie. gabbro-hosted, wall-rock replacement). This zone is hosted by a sliver of gabbro which appears to have been faulted away from a larger gabbro body (Figure 4.7). The geology of the Corvette Prospect is similar to that of the Stinger Prospect as the predominant lithology is dark grey to black siltstones and slates into which the gabbro intruded. Cleavage is moderate to strong and trends northeasterly with a steep southeast dip. Bedding measurements are not recorded for slates of the Corvette (actually for most of the Davidsville Group) since the fine-grained nature of the rocks as well as the strong cleavage completely obscure any bedding that may be present.

Mineralization at Corvette is readily visible in trenches as illustrated in Plate 4.5. The mineralized zones are manifested as gossanous and recessive zones in the trenches which also have a joint/fracture pattern best described as "blocky". This feature is very pronounced since the area proximal to the joint/fracture is much more heavily weathered and altered than are the blocks which they bound (Plate 4.6).

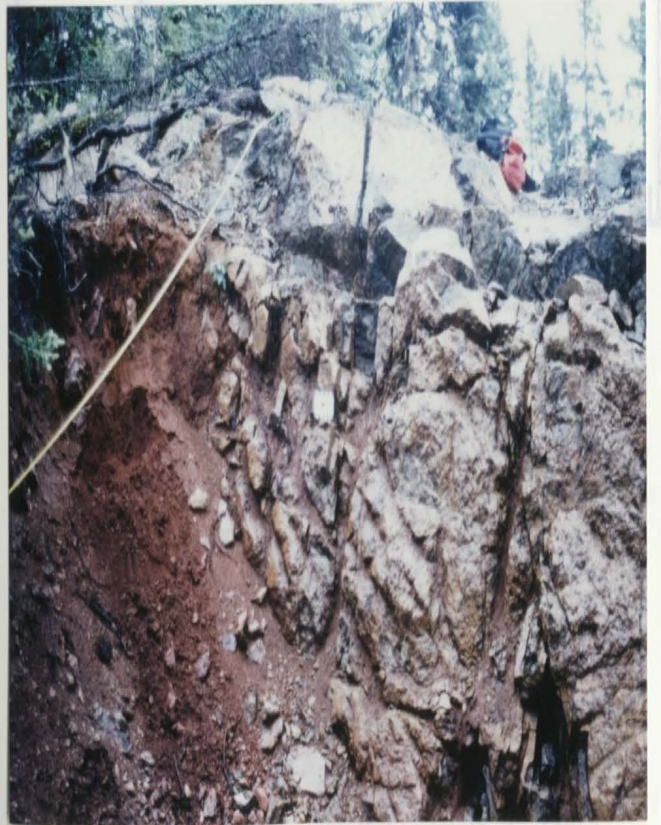
One diamond drill hole (DL-90-03) was completed at the Corvette Prospect where visible mineralization was delineated from 31.6-32.0m. The resulting gold assays for this hole shows large increases in gold concentrations between 26m and 32m with smaller increases at 41m, 62m, 66m and 70m depth (Figure 4.8). Peak gold values in this drill hole were only as high as 1000ppb. Tallman (1990) reports the best intersection in DL-90-03 as 1.48g/t Au/0.5m. Mineralization at Corvette is located approximately 600m

Plate 4.5: Recessively weathered, gossanous and mineralized section in trench TR-89-06 at the Corvette Prospect. Scale at left of centre measures 10cm in length.

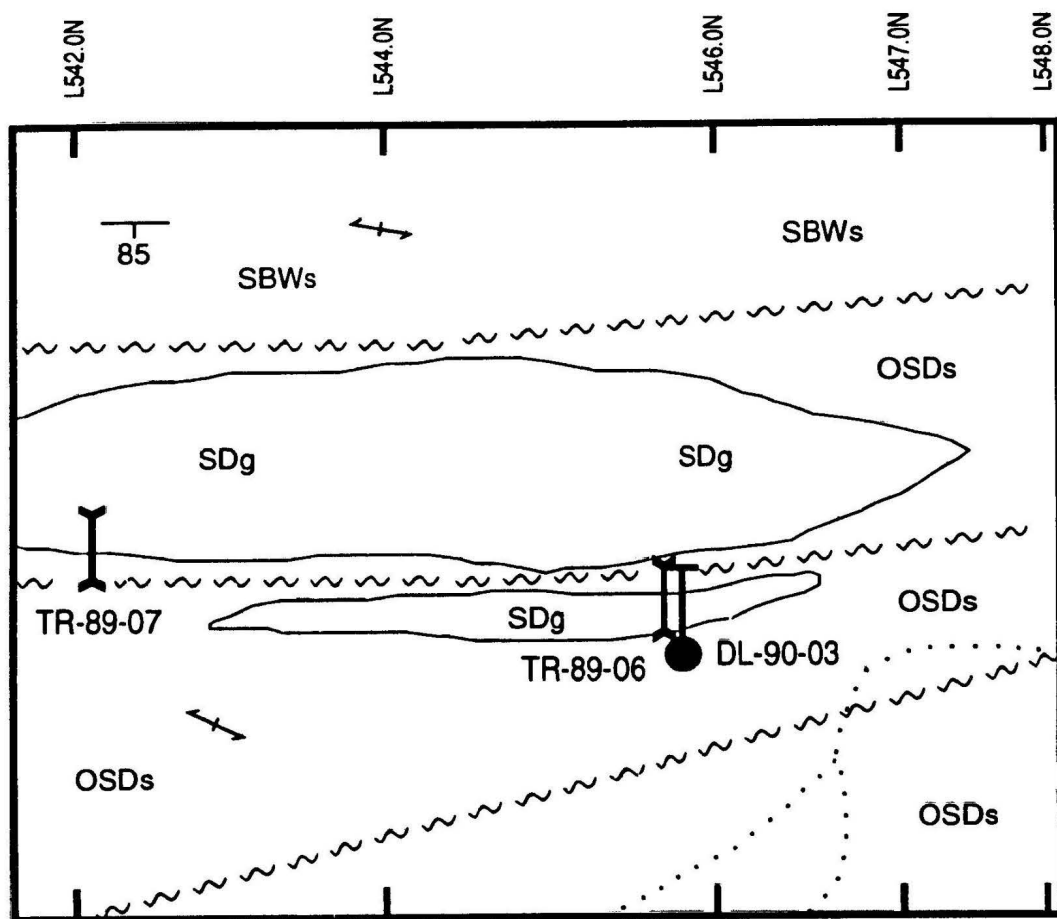


The Corvette Prospect is located approximately 600m north of the Goldstash Prospect. The geology of the Corvette Prospect is similar to that of the Goldstash Prospect as the predominant lithology is dark grey to black shales and slates into which the gabbro intruded. Cleavage is moderate to strong and trends northwesterly with a steep southeast dip. Bedding measurements are not recorded for slates of the Corvette (actually for most of the Davidsonville Group) since the fine-grained nature of the rocks as well as the strong cleavage completely obscures any bedding that may be present.

Plate 4.6: "Blocky" joint/fracture pattern as seen in trench wall (TR-89-05) at the Goldstash Prospect. Scale at centre of photo measures 10cm in length.



The mineralized zones are manifested as gossanous and recessive zones in the trenches which also have a "blocky" joint/fracture pattern. The joint/fracture is much more heavily weathered and altered than are the blocks which they bound (Plate 4.6). One diamond drill hole (DL-90-03) was completed at the Corvette Prospect where visible mineralization was delineated from 31.6-33.0m. The resulting gold assays for this hole shows large increases in gold concentrations between 30m and 32m with smaller increases at 41m, 62m, 66m and 70m depth (Figure 4.8). Peak gold values in this drill hole were only as high as 1000ppm. Tallman (1991) reports the best intersection in DL-90-03 as 1.48g/t Au@3.0m. Mineralization at Corvette is located approximately 600m



SILURIAN TO DEVONIAN

SDg Medium to coarse-grained gabbroic, dioritic, and diabasic sills and dykes..

SILURIAN

Botwood Group
Wigwam Formation

SBWs Siliceous and micaceous red to green, massive to laminated shallow water sandstone and minor siltstone.

ORDOVICIAN TO SILURIAN

Davidsville Group

OSDs Dark-grey, green, and black slate with minor argillaceous siltstone and fine-grained graphitic sandstone.

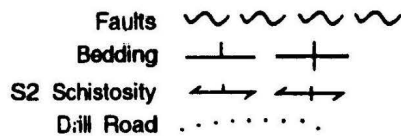


Figure 4.7: Géology of the Corvette Prospect with grid references and location of drill hole DL-90-03 and trenches TR-89-06 and TR-89-07. Line spacings are 100m, otherwise as labelled.

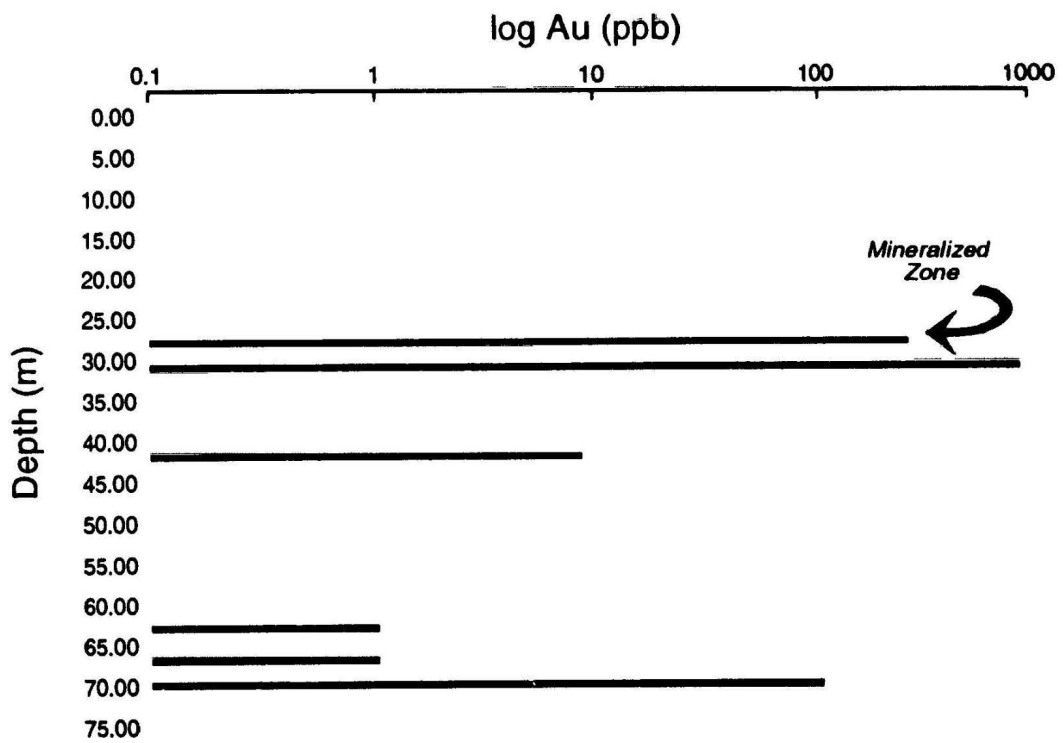


Figure 4.8: Log Au (ppb) assay values for diamond drill hole DL-90-03 from the Corvette Prospect. Note the increase in gold values coincides with visible arsenopyrite and pyrite mineralization associated with shearing observed in drill core. Refer to Appendix V for schematic visual drill logs and brief descriptive notes on the drill core.

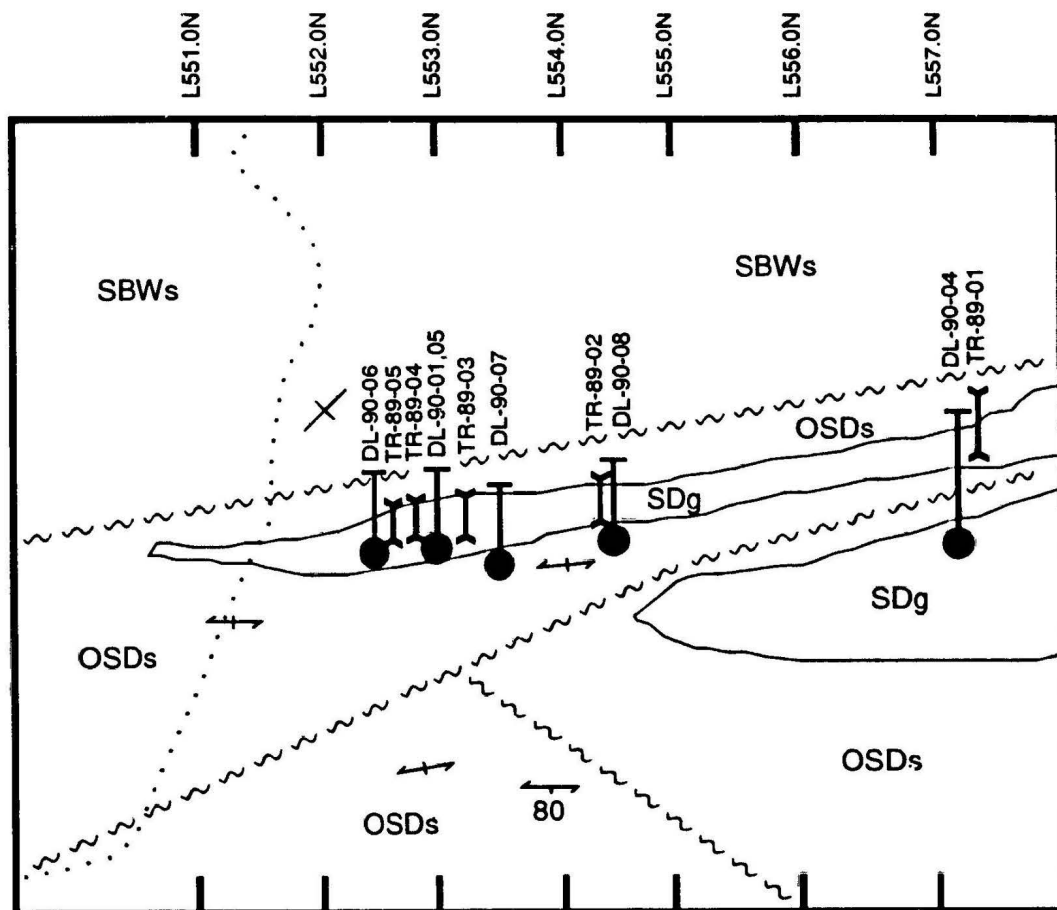
south of the main gold play at Duder Lake, the Goldstash Prospect - both of which lie along the same fault/shear system as the Flirt showing.

4.3.4 The Goldstash Prospect

The Goldstash Prospect is the main zone of gold mineralization at Duder Lake. This zone has been traced at surface and in drill core for a distance of 600m and is still open along strike and widening at depth. A total of six diamond drill holes and five trenches were completed on the Goldstash all of which had impressive gold intersections. Unfortunately most of the work completed on the Goldstash was concentrated on the southern end of the zone whereas more northern areas were under explored or not explored to their full capacity (Figure 4.9). As a result, little is known of the gabbro host between the southern end of the prospect to the location of DL-90-04 and north.

The geological setting of the Goldstash is similar to that of the Corvette in that Type Ib mineralization is hosted by gabbro which has intruded Davidsville Group siltstones, shales and slates close to the fault contact with sandstones and siltstones of the Wigwam Formation, Botwood Group (Figure 4.9). Once again a fault sliver of gabbro displaced from a larger body (southern intrusion in Figure 4.9) hosts the mineralization.

Cleavage trajectories are towards the northeast with vertical to steep southeast dips. Observation of cleavage trends disposed about the gabbro at Goldstash as well as all others in the Duder Lake area shows that they are very resistant to deformation and fabric development. As a result, the cleavage distribution in the lithologies bounding the



SILURIAN TO DEVONIAN

SDg Medium to coarse-grained gabbroic, dioritic, and diabasic sills and dykes..

SILURIAN

Botwood Group
Wigwam Formation

SBWs Siliceous and micaceous red to green, massive to laminated shallow water sandstone and minor siltstone.

ORDOVICIAN TO SILURIAN

Davidsville Group

OSDs Dark-grey, green, and black slate with minor argillaceous siltstone and fine-grained graphitic sandstone.





Faults 
 Bedding 
 S2 Schistosity 
 Drill Road 

Figure 4.9: Geology of the Goldstach Prospect with grid references and location of drill holes and trenches. Line spacings are 100m.

gabbros take on a lozenge shape with the central region having weak to no cleavage. On a larger scale, the lozenge shape appearance of many of the gabbros may also reflect the resistance to deformation and which will be discussed in the following section. Bedding is seen only in the sandstones of the Wigwam Formation and it also has a northeast trend and vertical orientation. The fault system hosting the Goldstash splays in the vicinity of L553.0N and hosts the Stinger 400m south.

The subsurface orientation of the mineralized zone and other geological units can be observed in Figure 4.10 which is a cross-section oriented at 023° (parallel to the baseline of the grid). For illustrative purposes, the visual drill logs have been rotated to vertical (from their dip of 45°) and unit thicknesses adjusted accordingly.

Alteration and mineralization at this prospect is similar in style and outcrop pattern to that seen at Corvette. However, gold concentrations and modal abundances of sulphides are somewhat higher at the Goldstash than at other localities. Tallman (1990) reported assays for Goldstash at 3.86g/t Au/9.8m or 7.01g/t Au/2.8m from DL-90-01. Grab samples from trench TR-89-04 obtained for this study have analyzed in excess of 30 000ppb (30g/t). Compilations of gold assays for all six drill holes can be observed in Figures 4.11 a,b with the zones of visible mineralization in core delineated and correlating with highest gold concentrations from assay which in many instances are in excess of 10 000ppb (10g/t).

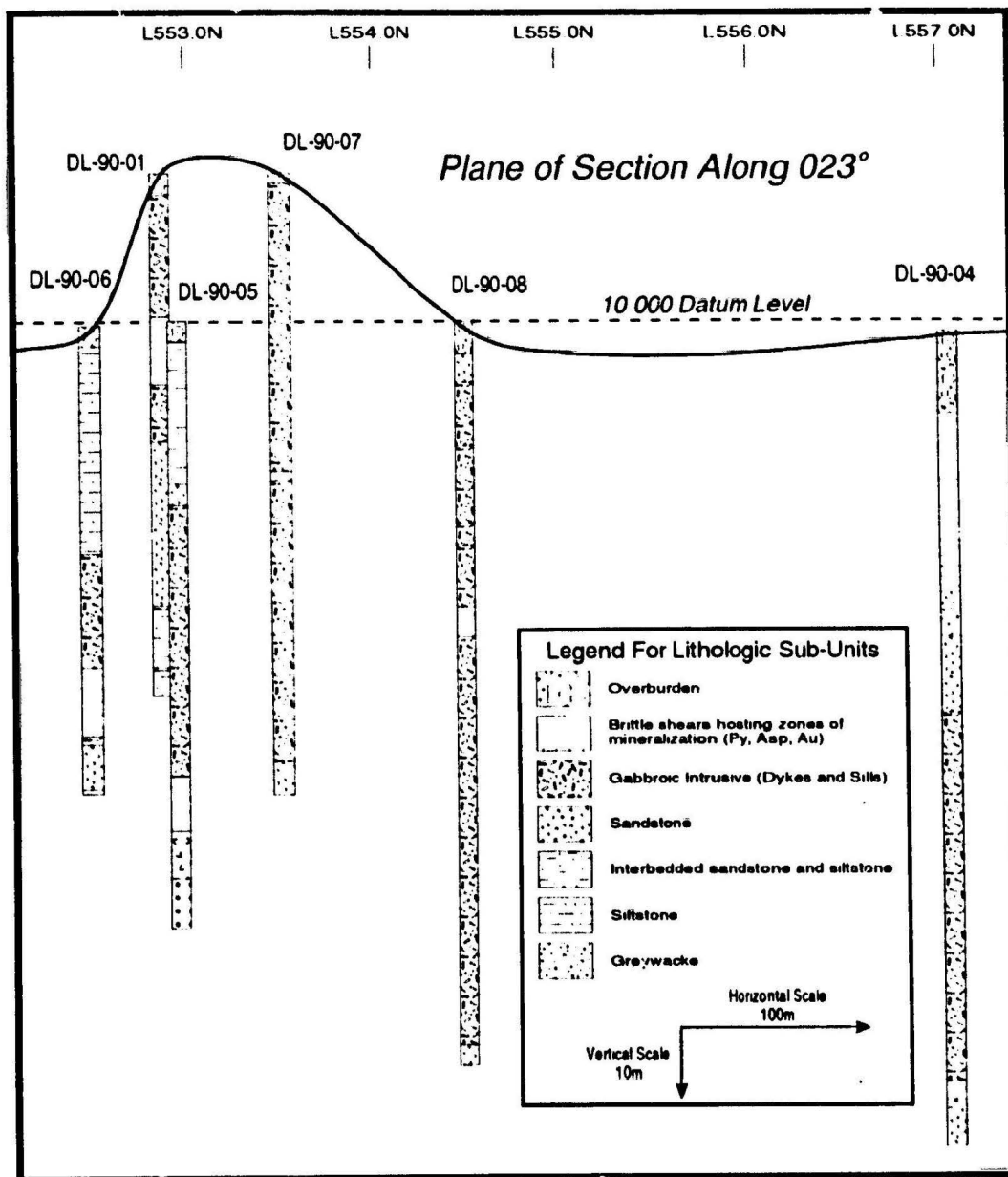


Figure 4.10: NE-SW oriented cross-section through the Goldstash Prospect showing topographic relief and lithological sub-units. Numbers at top of figure correspond to grid lines.

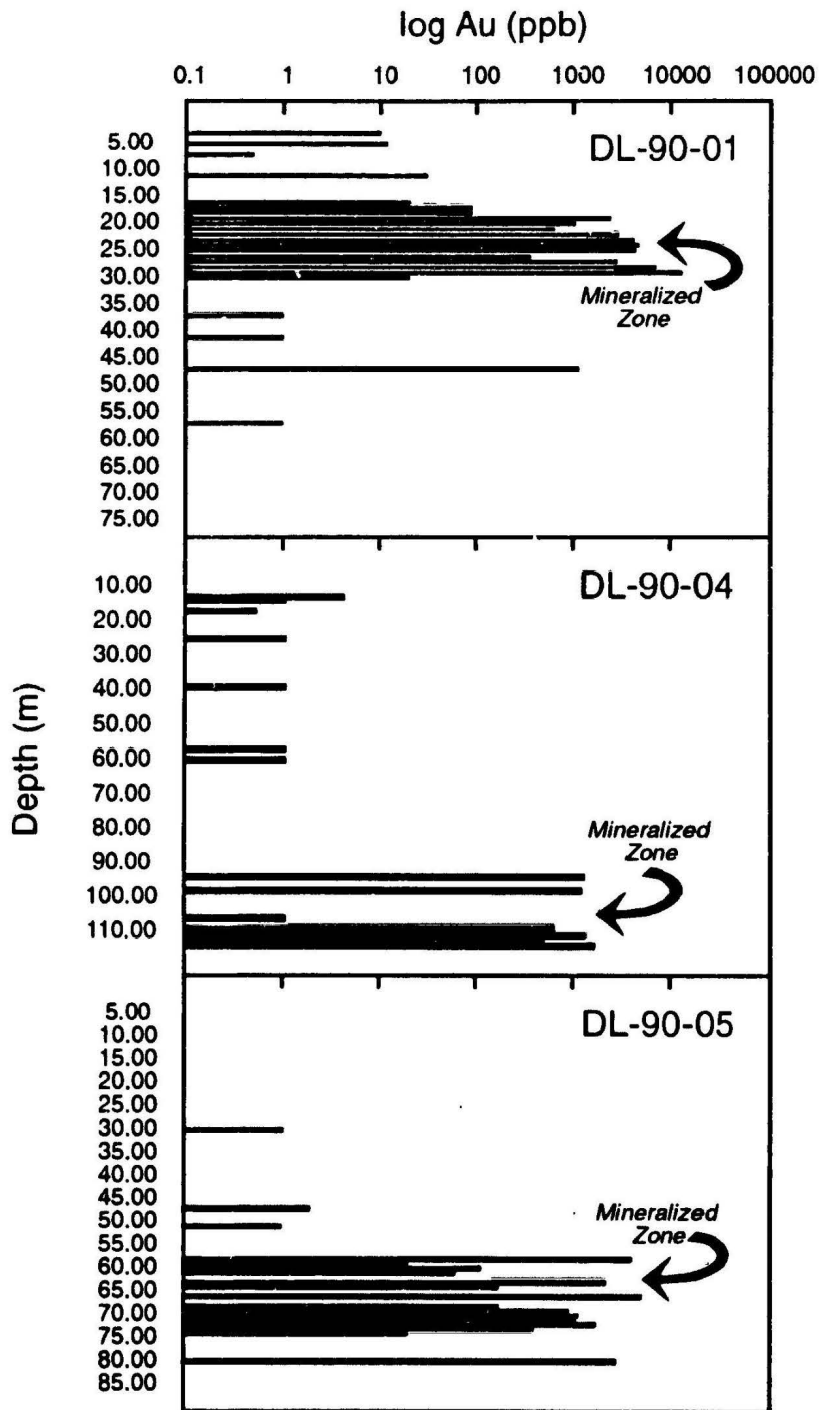


Figure 4.11a: Log Au (ppb) assay values for diamond drill holes DL-90-01, DL-90-04 and DL-90-05 from the Goldstash Prospect with zones of economic mineralization delineated that coincides with visible pyrite and arsenopyrite mineralization observed in drill core. Refer to Appendix V for schematic visual drill logs with brief descriptive notes.

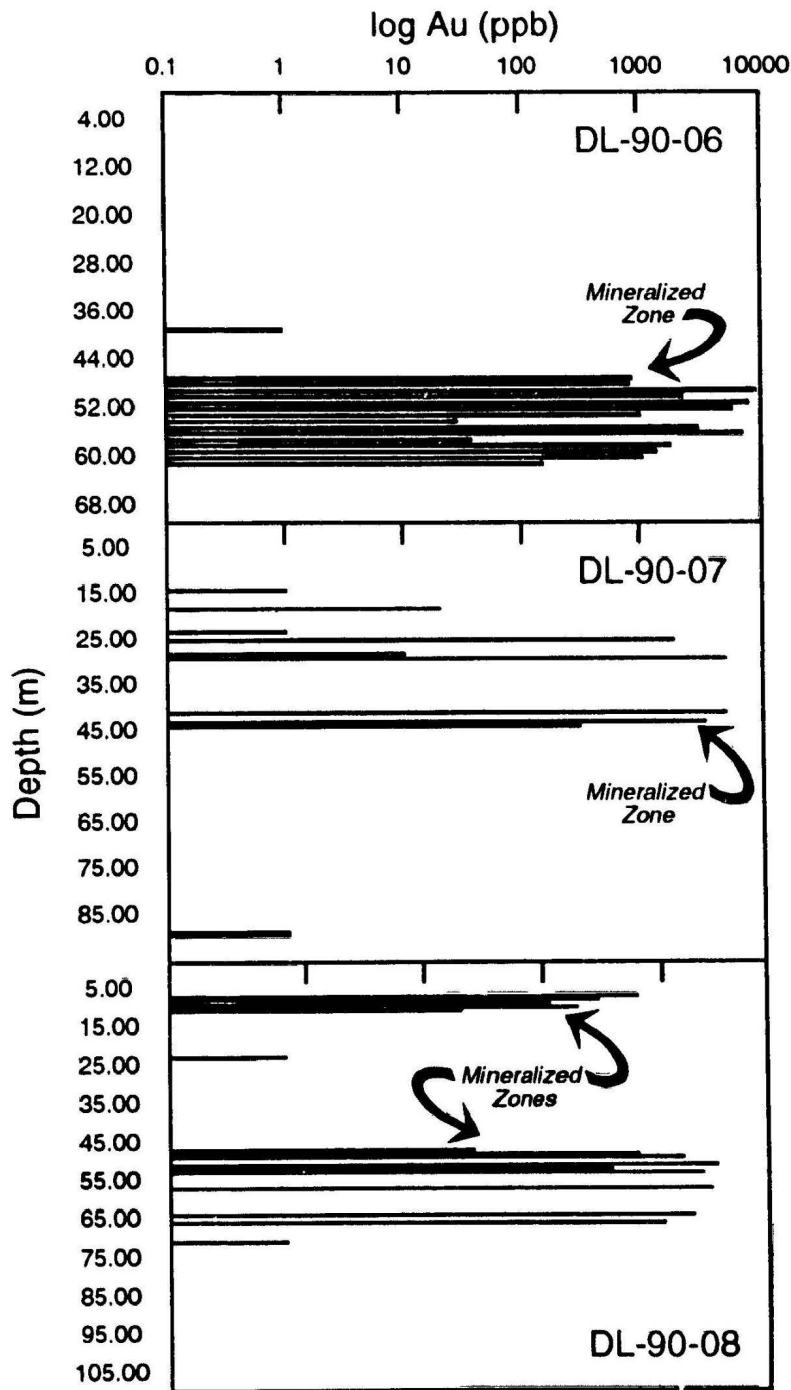


Figure 4.11b: Log Au (ppb) assay values for diamond drill holes DL-90-06, DL-90-07 and DL-90-08 from the Goldstash Prospect with zones of economic mineralization delineated that coincides with visible pyrite and arsenopyrite mineralization observed in drill core. Refer to Appendix V for schematic visual drill logs with brief descriptive notes.

4.4 Structural Control on Mineralization

All mineralization at Duder Lake appears to be late syn-deformational and as such constraints on mineralization are structurally controlled. Recent structural studies in the area of Duder Lake have shown that the area is transected by several northeast trending strike-slip faults, the largest of which is known as the Dog Bay Line (Williams, 1993). The Dog Bay Line is located approximately 1 km east of the gold prospects and in part forms a topographic low occupied by Rocky Pond. This southeast-dipping structure can be traced from Indian Islands 40 km northeast of Duder Lake southwest to the Trans-Canada Highway in the vicinity of Glenwood. The fault/shear system in the study areas measures up to 1000m in width and is composed of numerous faults with variable orientations (Figure MA-1).

Detailed kinematic studies of the Dog Bay Line indicate that it has been active from the Ordovician to Silurian with several episodes and style of movement and activation (Piasecki, 1993). According to Piasecki (1993), an early phase of ductile transpression was followed by dip-slip movement due to extensional relaxation. The third and final event was dextral transcurrent shearing. The long lived, and complex, nature of this structure and its subsidiary fault and shear system probably allowed for the formation of several generations of higher order (ie. smaller) structures which became inherent to an inferred late Silurian-early Devonian mineralizing event.

The aforementioned subsidiary structures, which may be secondary or even tertiary systems to the Dog Bay Line, are the hosts to mineralization, with the best

mineralization superimposed upon low angle, brittle-ductile, Riedel shears (Green, 1989; Churchill and Evans, 1992; Churchill *et al.*, 1993a). The Riedel shears are typically less than 3m in width, recessively weathered, gossanous, highly altered and of course mineralized (Plates 4.7 and 4.8). Oddly, the shears contain few quartz veins and those present can best be described as thin dilational tension veins formed in response to either P or S-shears.

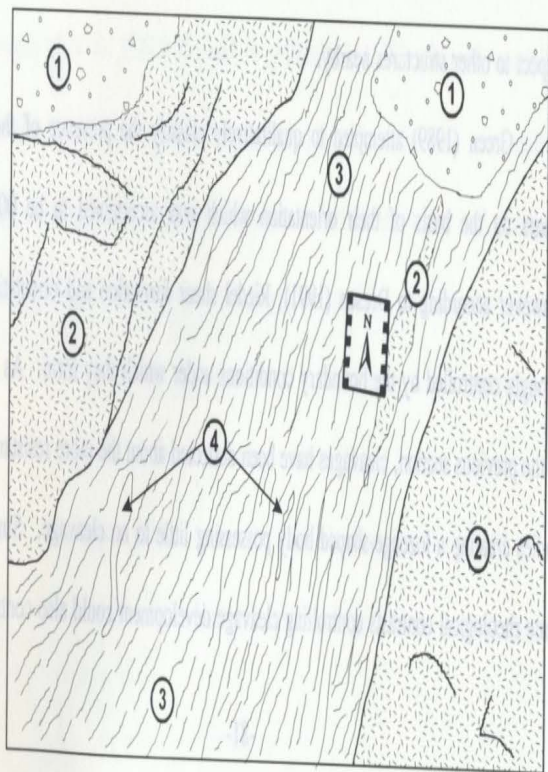
The Riedel shears are found at all scales ranging from metres in length, to others that are second order to the Dog Bay Line and which may be in excess of hundreds of metres in length. Since Riedel shears are subsidiaries of a larger shear, the orientations of those observed at Duder Lake are quite variable due to the fact that there are numerous shear zones transecting the area all with differing orientation. As such, no precise orientation can be given that would delineate the Riedel shears from another set of shear. This is accomplished by looking at the geometry of the Riedel shear with respect to other structures nearby.

Green (1989) attempted to qualitatively classify the presence of these Riedel shears on the basis of their orientation which was ascertained to be 000° - 010° . However according to Dresen (1991), Riedel shear formation and orientation can be strongly controlled by the boundary conditions under which they form. As mentioned in the previous section, cleavages have been deflected about the more resistant gabbroic bodies creating a lozenge-shaped body possessing little to no cleavage. Similarly, the same rheological contrasts controlling cleavage development could also control the

Plate 4.7: View of Riedel shear in trench TR-89-04 at the Goldstash Prospect (center of photo). Note the recessive nature and gossan developed in host gabbro. Dale Phillip's feet for scale.



Plate 4.8: Close-up of Riedel shear depicted in Plate 4.7. Note the thin dilational veins bottom centre of photo which formed in response to P or S-shears. Scale measures 9cm. Interpretative sketch of same photograph below. (1) talus, (2) weakly altered and deformed gabbro some of which are found within the plane of shear; (3) strongly sheared gabbro having shear fabric orientation 202/52 and (4) dilational quartz-carbonate veins formed at angles to main shear fabric.



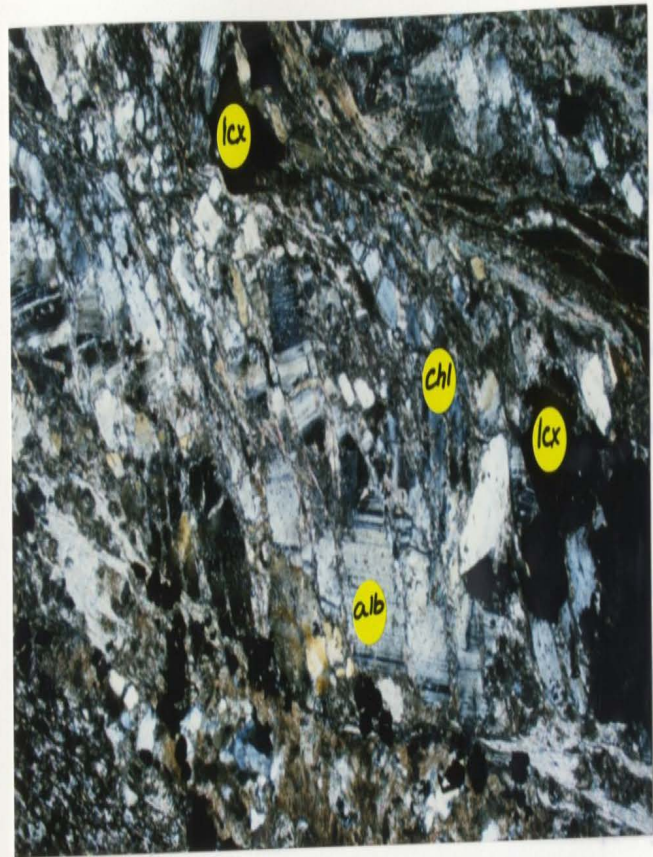
development and orientation of both the synthetic and antithetic sets of Riedel shears. Field observations suggest that not all of the Riedel shears at Duder Lake fall into the categorization of Green (1989).

Examination of the mineralized shear zones yield that they exhibit characteristics of both brittle and ductile deformation implying that they may have formed close to the brittle-ductile transition zone of Sibson (1977, 1989) where quasi-plastic (ductile) deformation is punctuated by brittle failure episodes. This can be observed both in silicate and sulphide minerals found within the shear zones where two modes of occurrence can be observed: (1) brecciated clasts/crystals reminiscent of brittle-style deformation (Plate 4.9) and (2) recrystallized, fine-grained phases in narrow bands defining a brittle recrystallization within the shear fabric (Plate 4.10). Both illustrate the brittle nature of the rocks found in an otherwise ductilely deformed shear zone.

In general, the association of mineralization with Riedel shears is a common occurrence in brittle-ductile shear systems which formed contemporaneously with regional metamorphism. Murphy (1989) stated that fluctuating $P_{(fluid)}/P_{(total)}$ due to metamorphic dehydration reactions may cause metal precipitation spatially and temporally associated with Riedel shears that act as conduits for the released fluids.

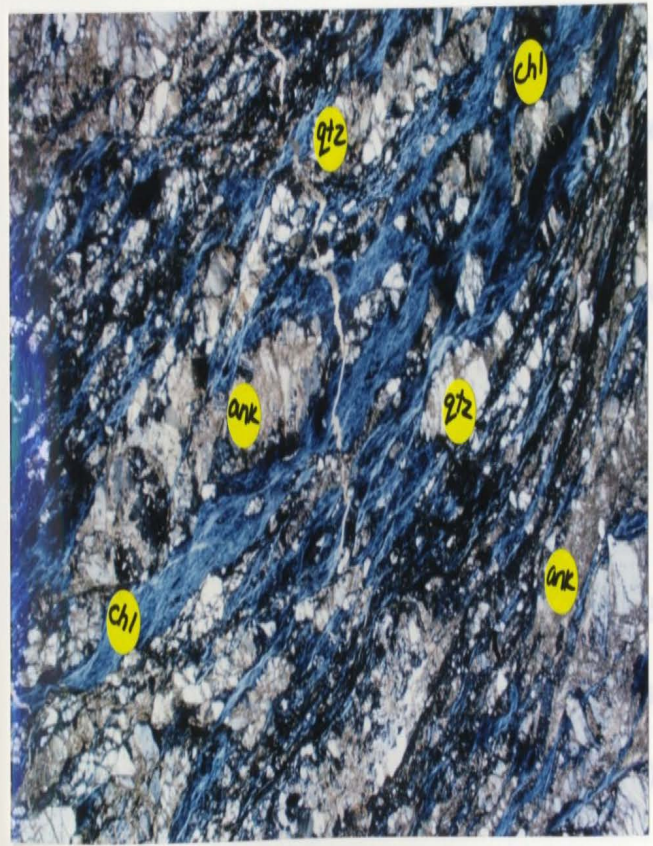
At Duder Lake, formation of these Riedel shears probably coincided with the ductile dextral transpressional event envisioned by Piasecki (1993). According to Tchalenko (1970), Riedel shears and conjugate Riedel shears begin to form just before the peak shear stress is reached. Since the early ductile event was the first shear event

Plate 4.9: Deformation effects observed in albite having a "domino" appearance resulting from brittle fracturing and rigid rotation. Abbreviations used; Alb (albite), Chl (chlorite) and Lcx (leucoxene). [10X magnification, XP]



upon the local stress fields which were active during their inception. Figure 4.11

Plate 4.10: Photomicrograph of fine-grained recrystallized quartz in narrow bands reminiscent of a ductile shear fabric. Abbreviations as follows: Ank (ankerite), Chl (chlorite) and Qtz (quartz). [10X magnification, XP].



along the Dog Bay Line, it is most likely that the formation of Riedel shears was a result of this early ductile event and is therefore Silurian in age associated with the Salinic (Silurian) Orogenic event (Dunning *et al.*, 1990).

Based on the Riedel shear depicted in Plates 4.7 and 4.8, as well as the shear and fault system orientations in the study area, a geomechanical model can be produced which describes the probable local stress field orientation as well as the genetic relationships observed for differing generations of faulting (Figure 4.12). It should be noted that the shears present in the Duder Lake area can range from structures measuring hundreds if not thousands of metres in length to structures that may measure only tens of metres in length. Thus, synthetic Riedel shears occur at several scales depending upon the local stress fields which were active during their inception. Figure 4.12 attempts to illustrate the relationships of the faults at Duder Lake in terms of P-, D-, or R-shears as determined by Tchalenko (1968) as well as showing the finite strain ellipse and the conditions required for the formation of Riedel shears. Of interest is the coincidence of synthetic Riedel shears with zones of known gold mineralization (Figure 4.12).

4.5 Geophysical Expression of Structures Inherent to Mineralization

As part of their exploration program, Noranda Exploration Company Limited geologists conducted both magnetometer and VLF surveys over the cut-grid. The results of both surveys are represented in Figure 4.13. The magnetometer survey (Figure 4.13a)

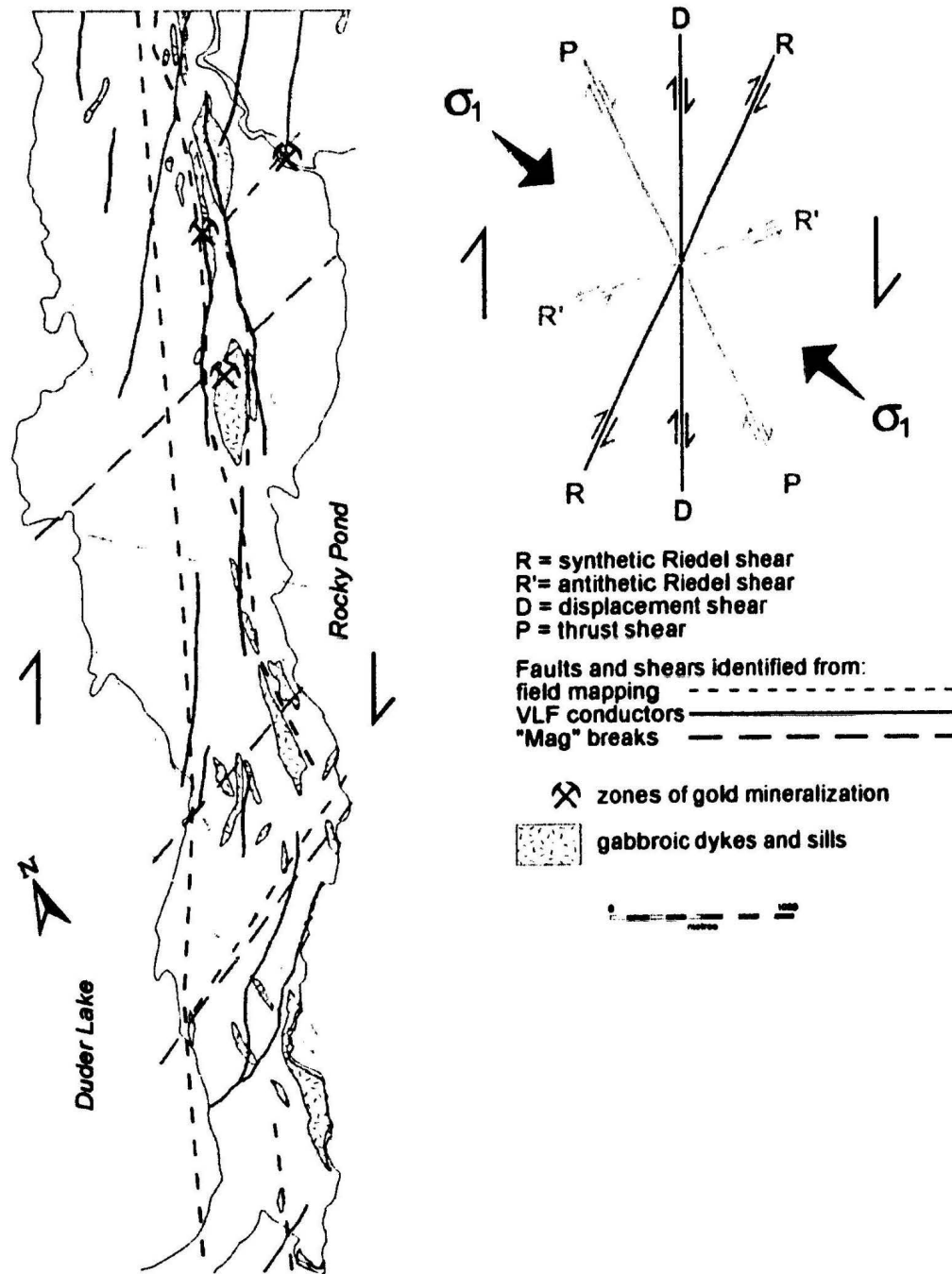


Figure 4.12: Geomechanical representation of megascopic, second order faults/shears associated with the Dog Bay Line. Dextral sense of shear as proposed by Plasecki (1993). Line type depicts how the structures were delineated: field mapping (short dashes), VLF conductors (solid) and "mag breaks" (long dashing). The line color states the nature of the shear: synthetic Riedel (red), antithetic Riedel (purple), thrust (green) and displacement (blue). Note coincidence of synthetic Riedel shears with mineralized zones.

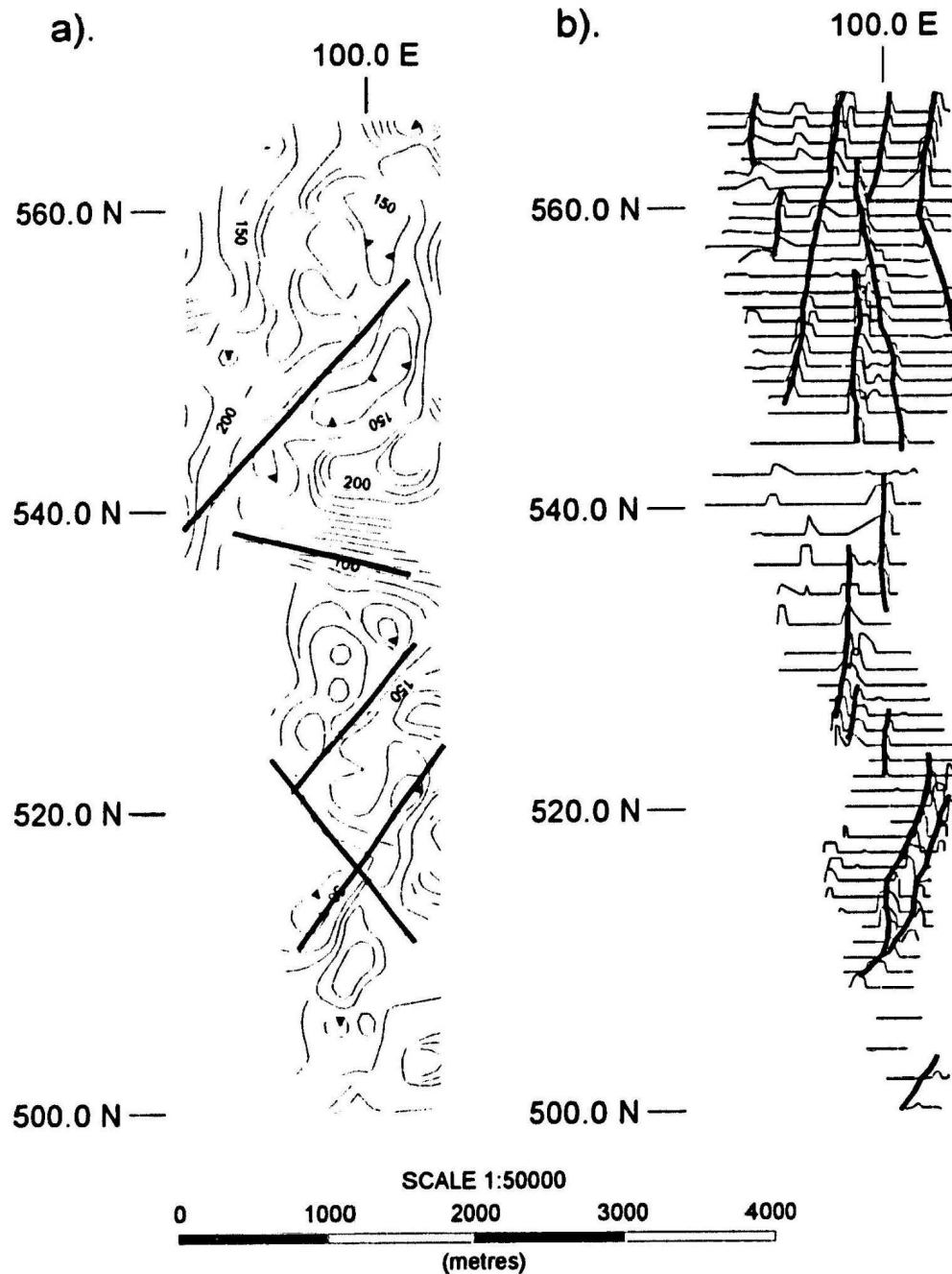


Figure 4.13: Geophysical expression of geological elements at Duder Lake. (a) Magnetometer data in nT and contour interval of 10nT. Mag highs correlate with gabbroic bodies (see Figure MA-1). Heavy black lines delineate "mag breaks" that correlate with known faults. (b) Fraser filtered VLF as line profiles. Dark lines are VLF conductors that correlate with faults and shears. Baseline 100.0E oriented at 023. Refer to text for further discussion. Figures modified from Churchill et al., 1993b.

indicates that most of the magnetic highs correlate with gabbros. One point of interest is that the magnetic signature for the gabbro hosting the Goldstash Prospect (in the vicinity of L550.0N to L560.0N) has very pronounced magnetic highs in excess of 200nT. The resultant magnetic high suggests that the gabbro body is much larger than what has been delineated by outcrop mapping and drilling. This implies that there is significant potential for more gold mineralization which is as yet untested. Further geophysical work such as induced polarization (IP) is needed to test this inference.

The other geophysical survey, VLF, better depicts the structural complexity of the Duder Lake area. Figure 4.13b illustrates Fraser filtered VLF profiles for each line for which data were collected. The VLF data are represented as peaks with variable amplitudes corresponding to the relative size of the VLF anomaly after Fraser filtering.

As can be seen from the arrangement of profile peaks in the survey, those which form linear arrays can be inferred to represent conductive structures (in this instance most likely faults and shears). Comparison of the VLF plot with the fault trace map (Figure 4.12) or the grid geology map (MA-1) shows that the VLF profiles correlate with several of the mapped faults. However, several other faults present in the mapping do not appear in the VLF patterns and this may be due to different conditions in the fault plane such as little to no hydration or graphite (ie. little to no conductivity).

Churchill *et al.* (1993b) endeavoured to correlate structures ascertained from the grid geophysical survey with other structures identifiable on a regional scale. The conclusions reached were that most of the structures present at grid scale are actually

secondary or even tertiary structures which are affiliated with a regional-scale north-northeast trending series of structures which are probably part of the Dog Bay Line system (Williams, 1993; Piasecki, 1993).

Comparison of the two geophysical surveys indicates that the magnetic highs are bounded by faults inferred from the VLF. This "lozengeing" of the gabbros has also been observed in both lithological mapping as well as from cleavage trajectories described in the previous section.

4.6 Summary

Gold mineralization was discovered at Duder Lake during the gold exploration boom of the mid- to late-1980's by Noranda Exploration Company Limited geologists and was subsequently classified as a mesothermal style of gold mineralization. Three kinds of gold mineralization occur at Duder Lake viz. Type Ia (vein hosted), Type Ib (wall-rock replacement) and Type II (graphitic sedimentary host with dilational space), with the most economically significant being the Type Ib.

The zones of mineralization occur within gabbros intruding rocks of the Davidsville Group (Corvette, Goldstash, Flirt) or in shears that cut graphitic siltstones of the Davidsville Group (Stinger). In all instances, the mineralization is controlled by the presence of brittle-ductile shears which have been classified as R and R' or synthetic and antithetic Riedel shears. Field observations and geophysics suggest that the Riedel shears are late structures associated with regional faulting that occurred in the Silurian.

CHAPTER 5

PETROGRAPHIC AND GEOCHEMICAL STUDIES OF ALTERATION AND MINERALIZATION

5.1 Introduction

This chapter will describe the character of the hydrothermal alteration that accompanied gold mineralization at Duder Lake. The approach of all discussion in subsequent sections will include description and data for fresh rocks through to altered and mineralized rocks. Such an approach will emphasize the continuity of the mechanisms of alteration and of mineralogical and geochemical changes which resulted from the hydrothermal event.

Since three of the four gold mineralized zones are hosted by gabbroic bodies, the discussion will be biased towards alteration and mineralization within the gabbros. Sampling in the Duder Lake area was also biased towards gabbros with a total of 62 fresh, altered and mineralized gabbro samples obtained from drill core and trench exposures. In addition, 7 samples of mineralized quartz veins intruding gabbro were also collected. Table 5.1 gives specific information on elements analyzed from both the gabbros and the mineralized quartz veins. Major oxides were analyzed using ICP-OES techniques at the NDME laboratories and REE were analyzed via the ICP-MS techniques at MUN. Trace element contents were determined by one of three analytical techniques including atomic absorption (AA) at the NDME labs, neutron activation analysis (NAA)

at Becquerel Labs in Ontario under contract to the NDME, and X-Ray Fluorescence (XRF) at MUN. Mineralized quartz veins were assayed for TiO₂, Al₂O₃, Fe₂O₃, MgO, CaO, Na₂O, K₂O, P₂O₅, Cr, Ni, Co, V, Cu, Pb, Zn, Cd, W, Mo, As, Sb, Au, Rb, Ba, Sr, La, Ce and Be by Eastern Analytical Laboratories of Springdale, Newfoundland. In addition to whole rock geochemical determinations, microthermometric measurements were obtained using the Fluid Inclusion Facility at MUN, and analyses of $\delta^{13}\text{C}$ and $\delta^{18}\text{O}$ from carbonate separates and $\delta^{34}\text{S}$ from pyrite and arsenopyrite were performed at the Stable Isotope Research Facility at MUN. Laser Ablation Microprobe -Inductively Coupled Plasma - Mass Spectrometry (LAM-ICP-MS) was performed on auriferous arsenopyrites at MUN. Other analyses such as SEM and XRD was also performed at

Table 5.1: Elements analyzed and numbers of samples per lithological type studied. Note that numbers in parentheses refers to the number of samples analyzed for the given analytical technique.

Mineralized Quartz Veins:

Total Number of Samples Collected = 7

Major Oxides (7): TiO₂, Al₂O₃, Fe₂O₃, MgO, CaO, Na₂O, K₂O, P₂O₅

Trace Elements (7): Cr, Ni, Co, V, Cu, Pb, Zn, Cd, W, Mo, As, Sb, Au, Rb, Ba, Sr, La, Ce, Be

Plutonic Rocks:

Total Number of Samples Collected = 62

Major Oxides (62): SiO₂, TiO₂, Al₂O₃, Fe₂O₃, MnO, MgO, CaO, Na₂O, K₂O, P₂O₅, H₂O, CO₂, LOI

Trace Elements (62): Cr, Ni, Co, Sc, V, Cu, Pb, Zn, Cd, W, Mo, S, As, Se, Sb, Au, Rb, Cs, Ba, Sr, Ga, Li, Ta, Nb, Hf, Zr, Y, Th, U, La, Ce, Sm, Eu, Tb, Dy, Yb, Lu, Cl, Br, Be

REE (17): Ba, Ta, Nb, Hf, Zr, Y, Th, La, Ce, Pr, Nd, Sm, Eu, Gd, Tb, Dy, Ho, Er, Tm, Yb, Lu

MUN. Detailed information about all of these methods can be found in Appendix I.

Nomenclature used in this discussion will include the terms fresh, altered and mineralized to describe the gabbro bodies. These terms are purely descriptive and in no way do they definitively describe the lithotypes. For example the term fresh is used to describe those rocks which illustrate no noticeable effects of hydrothermal alteration. These samples have been changed, however, from their original state by low- to mid-greenschist facies metamorphism, and the term is used to imply that they exhibit the least intensity of alteration effects of samples in the study area. Similarly, the distinction between altered rocks and mineralized rocks is also not definitive since some altered rocks contain mineralization, but not in significant concentrations. Problems in classification arise because there is a continuum between "fresh", "altered" and "mineralized" rocks. On this basis, no simple set of parameters can be used to subdivide the samples and as such comparisons of geochemistry, mineralogy and field relationships have to be used.

Chemical analyses of the gabbros and of the quartz veins can be found within this chapter as well as in Appendix II.

5.2 Petrography and Zonation of Alteration

As noted previously, numerous small mafic (gabbroic) dykes and sills of Silurian to Devonian age are present proximal to, and oriented parallel to the Dog Bay Fault. Initial field observations indicated that the gabbros were mineralogically varied due both

to a variety of primary igneous mineral compositions as well as to variations in the superimposed lower to mid-greenschist metamorphic facies mineral assemblages. Follow-up microscope study indicated that these variations are attributable to the degree of hydrothermal alteration and albitization of the gabbros, thus accounting for the variation in colour of the gabbros from apparent melano- to leucocratic varieties. In some instances, especially in larger intrusions, relict phaneritic textures and primary igneous clinopyroxene-orthopyroxene-plagioclase mineralogy can be observed.

To better define the geochemical systematics associated with metamorphism and localized zones of intense alteration, petrographical investigations were performed on both polished and covered thin sections using a combined transmitting/reflecting binocular microscope. In addition, semi-quantitative analyses of carbonates and chlorites were performed using a Hitachi SEM equipped with a Tracor Northern 5500 energy dispersive X-Ray analyser.

These combined investigations have resulted in definition of hydrothermally induced halos surrounding low-angle brittle-ductile, Riedel shears that can be qualitatively classified into the following zones:

1). GMA- (Greenschist Metamorphic Assemblage) Zone: This zone lacks any discernible minerals or geochemical concentrations associated with the gold mineralization event. These rocks preserve a mineral assemblage produced during prograde low- to mid-greenschist facies metamorphism and are the least altered of the three groups. This lithotype is found distal to the Riedel shears.

2). A- (Alteration) Zone: Rocks of this zone exhibit hydrothermal alteration which grades into fresh rocks distal to shearing and become progressively more intensely altered with proximity to the shear zone. The zone can be further subdivided into the A1- and A2-Zones which are classified on the basis of chemical changes in carbonates and chlorites as well as sulphide and sericite abundances. The A2-Zone grades into the M-Zone.

3). M- (Mineralized) Zone: The M-Zone is the zone of economic mineralization which contains the highest gold values and is proximal to the shear zone which it straddles. Alteration in this zone is so intense that primary igneous minerals as well as minerals produced during the early stages of metamorphism are almost completely destroyed.

Subsequent discussion will document each of the zones both mineralogically and geochemically as well as presenting the chemical reactions which took place which ultimately controlled the bulk geochemical changes between the zones. It will be shown from mineral associations that all mineralogical changes observed in each of the different zones is attributable to changing CO₂/H₂O abundances (*cf.* Dubé *et al.*, 1987; Harte and Graham, 1975; Billings and White, 1950). The changing CO₂/H₂O ratios are reflected in the alteration patterns observed and are partly responsible for gold mineralization.

5.2.1 The GMA-Zone

In most instances some relict igneous minerals such as pyroxene are preserved in gabbros in the GMA-Zone but other phases such as plagioclase and primary Fe-Ti oxide have been metamorphosed to albite-epidote-calcite (Reaction 1; Table 5.2) and Fe-Ti

oxide (Reaction 2; Table 5.2) respectively. In all subsequent discussion, the rutile-anatase-leucoxene intergrowths will be referred to as leucoxene for the sake of brevity.

The freshest (least altered) gabbros exhibit euhedral, locally uralitized clinopyroxene (Plate 5.1); abundant albitized and saussuritized plagioclase; calcitic veinlets and patches; and Fe-rich chlorite (clinocllore). Leucoxene, is also common to this alteration zone and microtextural evidence suggests it was formed from the breakdown of primary Fe-Ti oxides (Plate 5.2).

Epidote and/or actinolite are present as extremely fine-grained constituents of the groundmass and are locally observed as clots associated with chlorite. The presence of the epidote and/or actinolite may have been the result of uralitization of the pyroxenes during prograde metamorphism (Deer *et al.*, 1985). Based on numerous petrographic observations, those gabbros in the GMA-Zone which are classified as "fresh" have the following modal composition: chlorite (20%), actinolite-epidote (6%), albite (25%), pyroxene (8%), quartz (5%), uralitized pyroxene (10%), calcite (15%), leucoxene (6%) and other opaque minerals including oxides and sulphides (5%). Mean grain size is variable, ranging from micron scale for components of the groundmass to in excess of 1cm for the coarse pyroxene and albite. With the exception of the pyroxenes and albite, the other phases present are typically anhedral, locally exhibiting complex intergrowths as is the case for leucoxene-oxide and epidote-actinolite pairs.

Plate 5.1: Photomicrograph of "fresh" gabbro from the GMA-Zone exhibiting large euhedral pyroxene (Pyx) phenocrysts, albitized plagioclase (Alb) and minor chlorite (Chl). Fine grained calcite and epidote as pinkish specks in large albite grain. [Field of view approximately 6mm, XP].

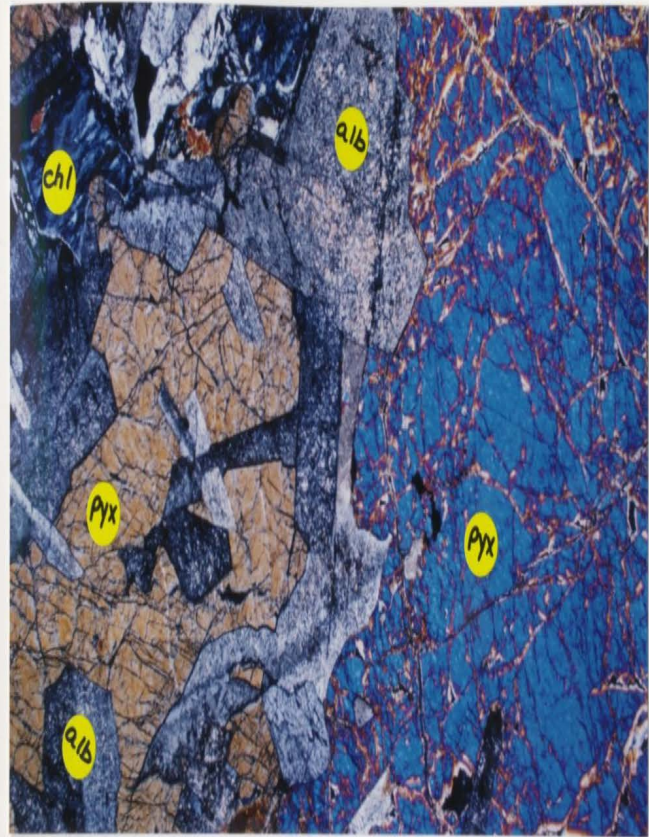
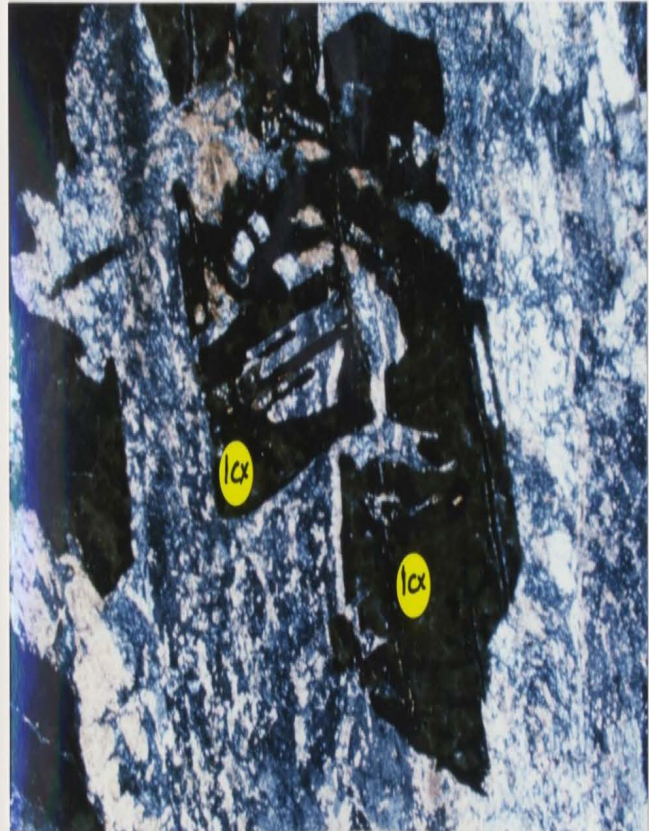


Plate 5.2: Skeletal leucoxene (Lcx) pseudomorphing Fe-Ti oxides in a fresh gabbro from the GMA-Zone. [Field of view approximately 6mm, XP].



5.2.2 The A-Zone

Lithologies in the A-Zone contain an assemblage of minerals which were produced under high water/rock conditions adjacent to the shears, and they grade transitionally into those rocks which preserve a low- to mid-greenschist facies metamorphic assemblage. Since alteration intensity in this zone increases proximal to the shear zone with concomitant changes in mineralogy, the A-Zone can be subdivided into the chlorite-ankerite (A1) Zone and the ankerite-sericite (A2) Zone.

5.2.2.1 The A1-Zone

The A1-Zone preserves the initial changes which were effected by hydrothermal alteration and is characterized by a mineralogy somewhat similar to that of the GMA-Zone but in addition the association chlorite-ankerite. Chlorite chemistry changes in this zone from the Fe-rich chlorite (clinochlore) associated with regional metamorphism to more Mg-rich compositions.

Other noticeable changes include the appearance of sericite, attributed to the breakdown of calcite and chlorite (Reaction 3, Table 5.2). Mineral associations in this zone, generally indicate that a_{H_2O} fluid and a_{CO_2} fluid were not reached, since minerals produced during regional metamorphism are present together with those that formed during the breakdown of these phases. For example, with respect to Reaction 3, Table 5.2 some rocks contain an assemblage including chlorite-calcite - sericite-ankerite which is interpreted to represent incomplete reaction since chlorite and calcite in the presence

of CO₂ will react to give sericite and ankerite. These "mixed" assemblages disappear with increasing alteration intensity. Another important change is that relict igneous minerals such as pyroxene are almost completely destroyed. The presence of uralitized pyroxene is most dramatic in the advanced stages of hydrothermal alteration in this zone. In the case of the pyroxenes, they have been almost completely uralitized (Plate 5.3), resulting in an obvious colour shift in rock samples from the dark greens and browns of the fresh gabbros to a colour that can be best described as lavender (Plate 5.4). This coloration may in part be attributable to mobilization of Ti from the pyroxenes and/or the Fe-Ti oxides during alteration.

Gabbros from this zone have the following modal abundances: chlorite (12%), actinolite-epidote (3%), albite (25%), pyroxene (5%), quartz (3%), uralitized pyroxene (20%), calcite (2%), leucoxene (7%), sericite (10%), ankerite (8%) and other opaque minerals including oxides and sulphides (5%). Mean grain size for these rocks is similar to that for rocks of the GMA-Zone. The new minerals such as the sericite and ankerite are usually present as fine-grained (<<1mm) clots and aggregates associated with anhedral chlorite and/or calcite.

The mineral assemblage in this zone grades into the A2-Zone which is more proximal to the shear zone and which better reflects the stronger CO₂ control on mineralogy.

Plate 5.3: Photomicrograph of gabbro from the A1-Zone showing uralitic (Ur) bounding relict pyroxenes (Pyx). Other phases such as albite (Alb) and quartz-carbonate veinlets (V) also present. [Field of view 6mm wide; XP].

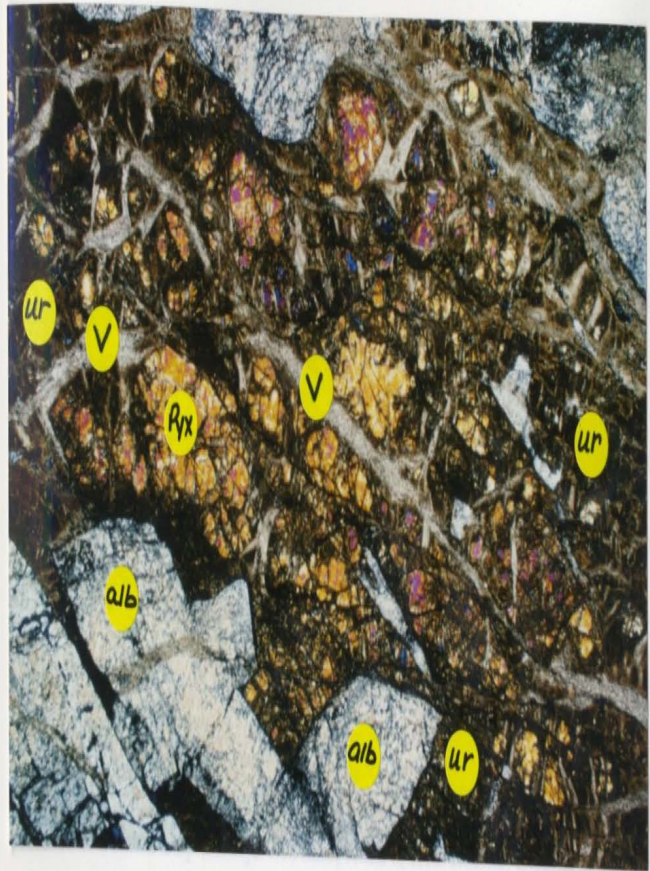
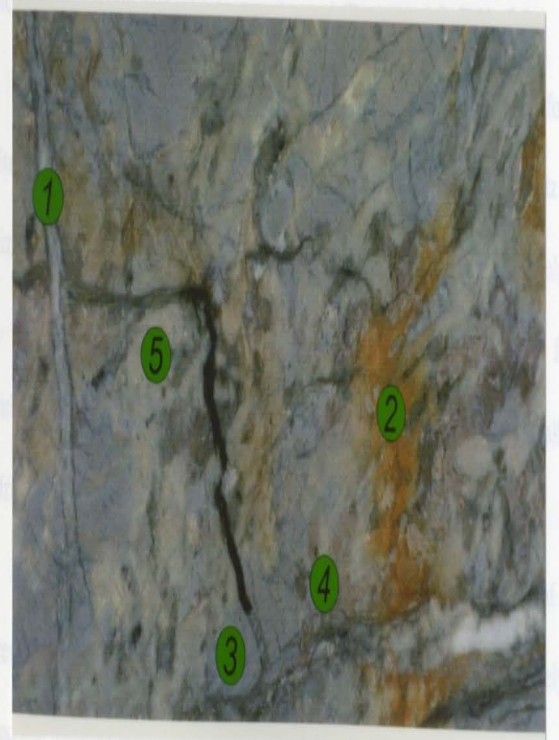


Plate 5.4: Computer enhanced image of altered gabbro from the A1-Zone. Numbers correspond to the following: (1) quartz-carbonate veinlet, (2) gossan patch associated with sulphide mineralization, (3) lavender coloration of uralitized pyroxene, (4) skeletal leucoxene and (5) albite-ankerite-sericite-quartz groundmass. Field of view measures 7.5cm across.



5.2.2.2 The A2-Zone

The A2-Zone is characterized by a secondary ankerite-sericite mineral assemblage superimposed on the system due to hydrothermal alteration. Other changes have also been documented including the diminishing abundance of chlorite which is now become increasingly Mg-rich as reflected by a very diagnostic berlin-blue birefringence (Reaction 4; Table 5.2/Plate 5.5). Calcite is almost been completely replaced as the carbonate species present by ankerite (Reactions 3,5,6,7; Table 5.2) and a common feature of this zone is the association of the Mg-chlorite with ankerite. This relationship may be explained by reaction 6 (Table 5.2) which shows that actinolite and epidote, in the presence of a mixed CO₂- and H₂O-rich fluid, reacts to form chlorite, ankerite and quartz (Plate 5.5). In addition to these observations, the first appreciable concentrations of sulphides, most notably arsenopyrite, are observed (Reactions 4,8; Table 5.2).

A representative modal composition for gabbros from this zone is as follows: chlorite (10%), actinolite-epidote (< 1%), albite (25%), pyroxene (< 1%), quartz (5%), uralitized pyroxene (10%), leucoxene (8%), other opaques including oxides and sulphides (8%), sericite (14%) and ankerite (20%). With the exception of the newly formed sulphides and sericite which have a euhedral habit, the remaining phases all have anhedral to subhedral habits due to progressive breakdown during alteration.

Grain size is variable with the largest sizes in excess of 1mm in the case of albite. The remaining phases, especially sericite and the sulphides, are typically extremely fine-grained and found as aggregates and/or isolated crystals (Plate 5.6). Other minerals such

as ankerite, quartz and uraltized pyroxene are of variable size which may be a reflection of the grain size of precursor minerals which were destroyed and ultimately led to their formation.

5.2.3 The M-Zone

The M-Zones are the zones of economic mineralization as well as being the sites of intense carbonatization and sulphidation, and they occur immediately adjacent to antithetic and synthetic Riedel shears. The M-Zones possesses variable widths about the shear zones, with the width being correlatable with the water/rock ratio as well as the CO₂/H₂O ratio, both of which are assumed to be highest closest to the shear zone (*cf.* Dubé *et al.*, 1987).

The M-Zone, due to its transitional nature with the A2-Zone, shares many of the mineralogical relationships observed in advanced sections of the A2-Zone. The petrography of the M-Zone is characterized by the mineral association ankerite-sericite-pyrite-arsenopyrite and will be discussed on the basis of non-metallic and metallic mineral content.

The major mineralogical changes observed in this zone is that sericite and ankerite are now the dominant mineralogies and there is an abundance of sulphides, in some instances exceeding 20% modal. Chlorite, where present, is Mg-rich and usually associated with both sulphides as well as ankerite/ferroan dolomite. The chlorite is most commonly found associated with shear planes within the shear zone (refer to Plate 4.10

Plate 5.5: Photomicrograph of altered gabbro from the A2-Zone. Alteration phases present include the spatial association of Mg-chlorite (Chl) with ankerite (pinkish speckles within chlorite). Other phases present include albite (Alb), quartz (Qtz) and uralitized pyroxene (Ur). Note chlorite-ankerite association at centre. [10X magnification, XP].

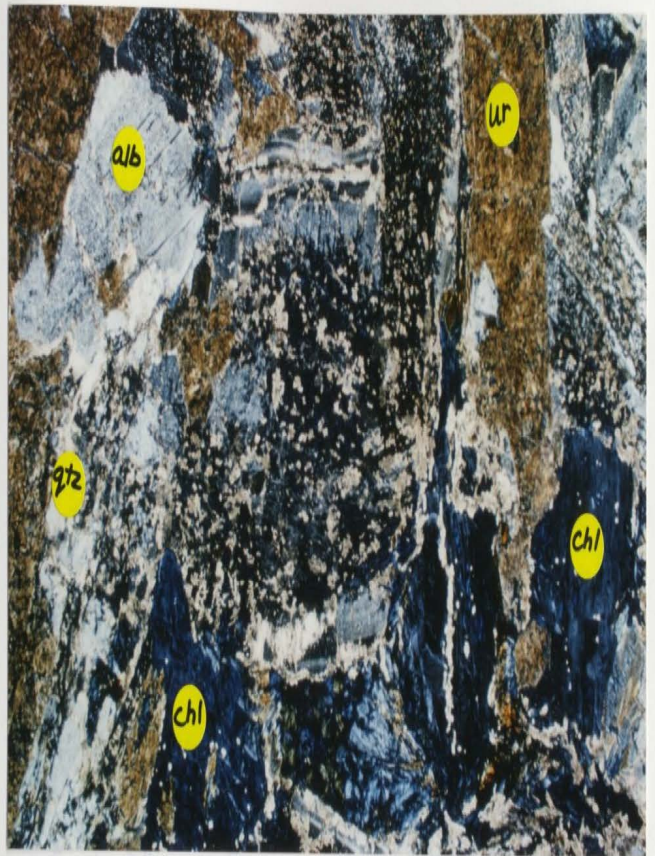
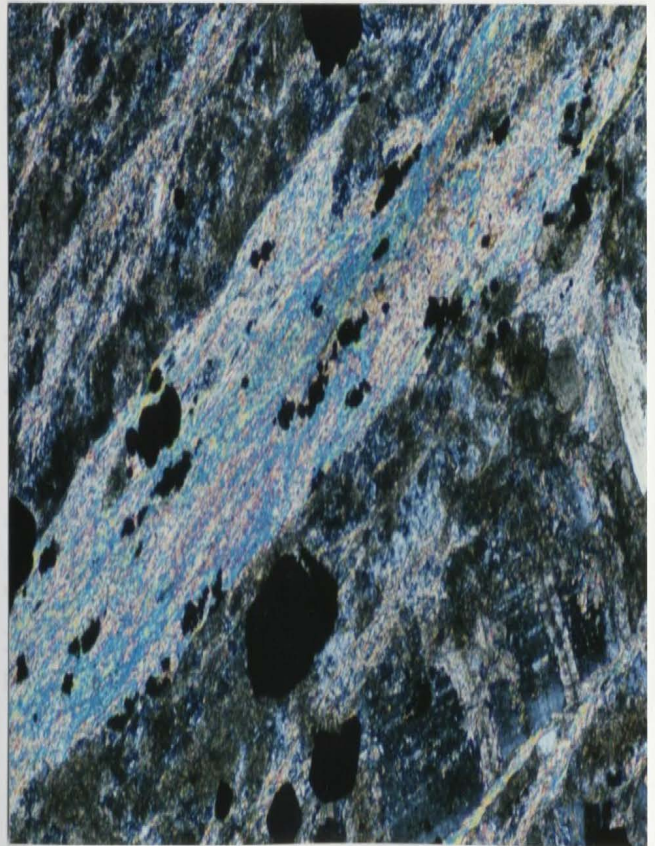


Plate 5.6: Photomicrograph of altered gabbro from the A2-Zone exhibiting fine-grained fibrous aggregates of sericite (blue) concentrated in millimetre wide bands. [10X magnification, XP].



of the previous chapter). Albites where present are extremely sericitized and usually have an anhedral appearance. Abundant quartz veinlets and stringers are associated with ankerite patches and the two are sometimes locally intergrown. Ankerite is more Fe,Mg-rich than that of the A2-Zone, so much so that ferroan dolomite may also form (refer to Table 5.4a for carbonate chemical data). Relict phases such as pyroxene, magnetite and ilmenite as well as early phases such as epidote and actinolite are now absent replaced by uralite, leucoxene-anatase-rutile (Plate 5.7) and ankerite respectively (refer to Table 5.2 for mineral reactions related to mineral formation in the M-Zone).

All non-sulphide phases have strongly anhedral to subhedral crystal habits and are usually closely intergrown and fine-grained (eg. Plate 5.5). The modal abundances of minerals in the M-Zone is as follows: chlorite (5%), albite (15%), quartz (8%), uralite (10%), leucoxene (4%), other opaques (15%), sericite (18%) and ankerite/ferroan dolomite (25%). Plate 5.8 is a photomicrograph representative of the alteration assemblage (non-metallic) from the M-Zone.

To compare and contrast the variations in modal abundances, as well as the major minerals present in each of the zones, Table 5.3 contains a compiled list of mineral proportions in each zone. In addition Figure 5.1 is a graphical representation of mineral proportions in each of the four zones.

5.2.3.1 Ore Mineralogy

There is a limited range of sulphide minerals associated with gold mineralization

Table 5.3: Compilation of minerals and mineral abundances of each of the four alteration zones based on optical observations.

Mineral	GMA-Zone	A1-Zone	A2-Zone	M-Zone
chlorite	20	12	10	5
actinolite-epidote	6	3	1	0
albite	25	25	23	15
pyroxene	8	5	1	0
quartz	5	3	5	8
uralitized pyroxene	10	20	10	10
calcite	15	2	0	0
leucoxene	6	7	8	4
opaques	5	5	8	15
sericite	0	10	14	18
ankerite	0	8	20	25

at Duder Lake. A pyrite and arsenopyrite assemblage is ubiquitous in the M-Zone and common in the A2-Zones. Other sulphides such as chalcopyrite, pyrrhotite (Plate 5.9) and minor sulphosalts are rare. As a result, the discussion which follows will pertain only to pyrite and arsenopyrite.

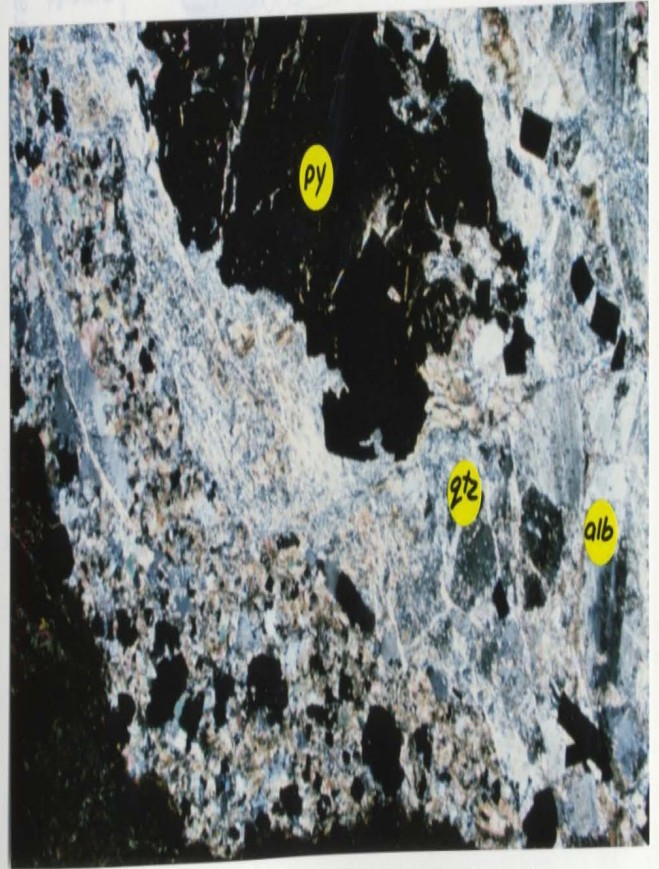
The textural relationships between both sulphide species are simple with the most complex being inclusions of arsenopyrite in pyrite and vice versa (Plate 5.10). Otherwise, the sulphides are present as subhedral to euhedral crystals which locally are concentrated into bands which are almost entirely mono-minerallic (Plate 5.11).

The inclusion of one sulphide species in another may give evidence for a changing fluid chemistry with ongoing sulphide precipitation. In one instance, a single grain of euhedral arsenopyrite was observed to be rimmed by pyrite with no noticeable grain

Plate 5.7: Photomicrograph of replacement features observed in leucoxene-anatase-rutile (brown) after titanomagnetite (yellow) as preserved in rocks of the M-Zone. [20X magnification, reflected light].



Plate 5.8: Photomicrograph of a representative mineral assemblage from the M-Zone. Minerals present include pyrite (Py), albite (alb), quartz (qtz), ankerite as fine-grained pink speckles, sericite as bright fine-grained aggregates right centre of photo. [2.5X magnification, XP].



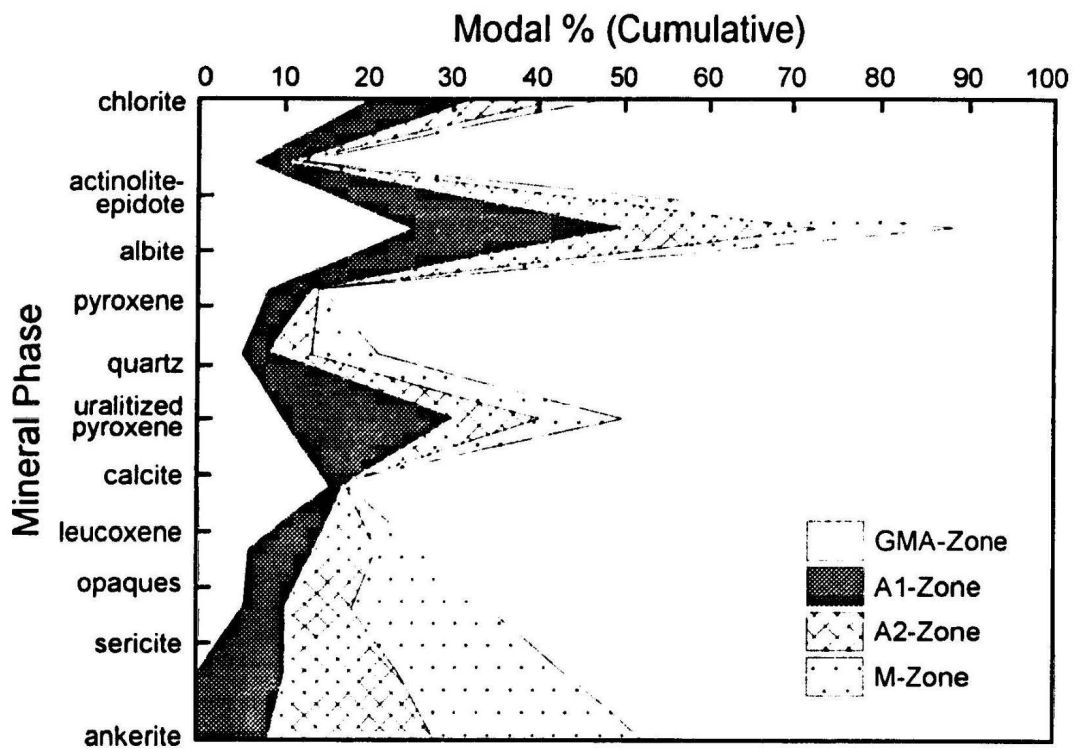


Figure 5.1: Cumulative modal percentage plot for each of the alteration zonations defined for the Duder Lake gold showings. Percentages used are based on visual observations (also refer to Table 5.3). Note important mineral changes such as ankerite and sericite which increase and chlorite and calcite which decrease with intensifying alteration (ie. from the GMA-Zone to

boundary delineating the change of sulphide species. The optical properties of the sulphides suggest a transition from Fe-rich arsenopyrite to As-rich pyrite. The concentration of sulphides into layers, however, suggests contemporaneity of sulphide precipitation with deformation (*viz.* shearing).

In addition to these textures, the morphology of single, and/or clusters of sulphide crystals is indicative of fracturing (brecciation) of megacrysts and annealing. These textures in combination with sulphide layers give evidence of a deformation coinciding with, and probably directly responsible for, mineralization.

According to Craig (1990), fracturing and brecciation of sulphides in massive sulphide deposits is a common phenomenon when these minerals have been subjected to regional stress. Similar features are observed in sulphide megacrysts from Duder Lake (Plate 5.12). As seen in the photograph, a large grain of pyrite has been fractured and broken apart to form numerous smaller grains but it still reflects the overall shape of the original pyrite grain. The only explanation for the apparent brecciation texture is that the sulphide was deformed either syn- or early post-precipitation. Another constraint on timing of mineralization with respect to deformation can be observed in Plate 5.13. In the centre of the photo, well developed curved cleavage can be observed in a grain of unaltered pyroxene. Along the cleavage traces small opaque grains of sulphides can be observed which are indicative of precipitation during deformation and cleavage development associated with the regional metamorphism.

Other features indicative of metamorphic sulphide mineralization include

Plate 5.9: Photomicrograph of pyrrhotite (brown) intergrown with pyrite (light brown).
 [10X magnification, reflected light].

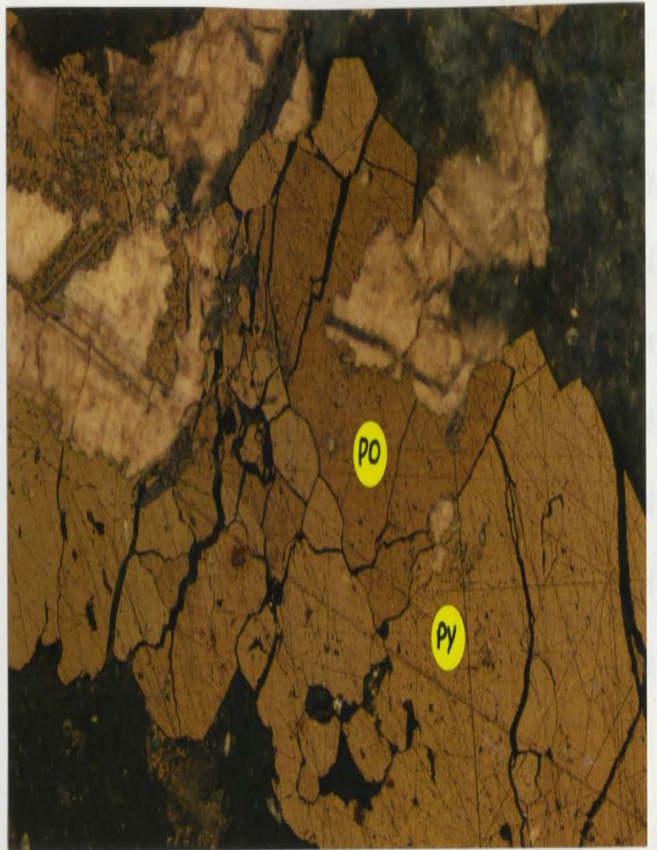
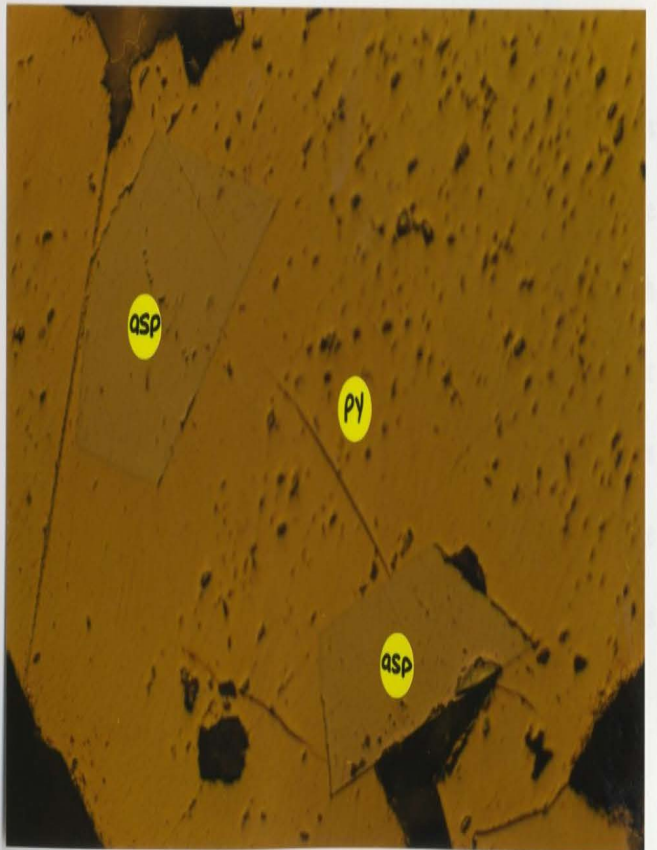


Plate 5.10: Photomicrograph of simple intergrowth relationships between pyrite and arsenopyrite. Euhedral arsenopyrite inclusions (pale grey-brown) within large pyrite grain (golden brown).
 [50X magnification, reflected light].



annealing of sulphide grains. Studies by Templeman-Kluit (1970) suggest that metamorphic temperatures allow for coarsening of sulphides, resulting in grains that may coalesce and/or become more euhedral. In addition, Stanton (1972) has shown that temperatures exerted on sulphide minerals cause them to become more equant and possess interfacial angles with other grains approaching 120° . Similar features can be observed in the sulphide phases at Duder Lake (Plate 5.14). In this photograph, a cluster of arsenopyrite crystals on the right hand side of the photo gives evidence of recrystallization and annealing due to the coalescence of the sulphide grains into one another. In addition, close inspection of the grains yield interfacial angles that appear to be on the order of 120° .

The final piece of evidence for contemporaneous sulphide precipitation and deformation lies with sulphide-silicate textural relationships. As stated in Section 4.4, there is evidence of both brittle and ductile deformation. The ductile shear fabric is readily recognizable by the presence of berlin blue chlorite along the shear planes (Plate 4.10). In more intensely altered rocks, this chlorite is intimately associated with sulphides such as in Plate 5.15, in which, approximately 20% modal sulphides occur concentrated in layers also occupied by pleochroic green chlorite. The chlorite delineates the ductile shear fabric with the anhedral sulphide grains. The relationship between the sulphides and the chlorite can be explained by Reactions 4 and 8 (Table 5.2) where it is inferred that Fe-chlorite in the presence of a reducing fluid breakdown to form Mg-chlorite and sulphide (pyrite).

Plate 5.11: Photomicrograph of bands of sulphide mineralization which parallel the shear foliation. Arsenopyrite whitish and pyrite yellowish. [10X magnification, reflected light].

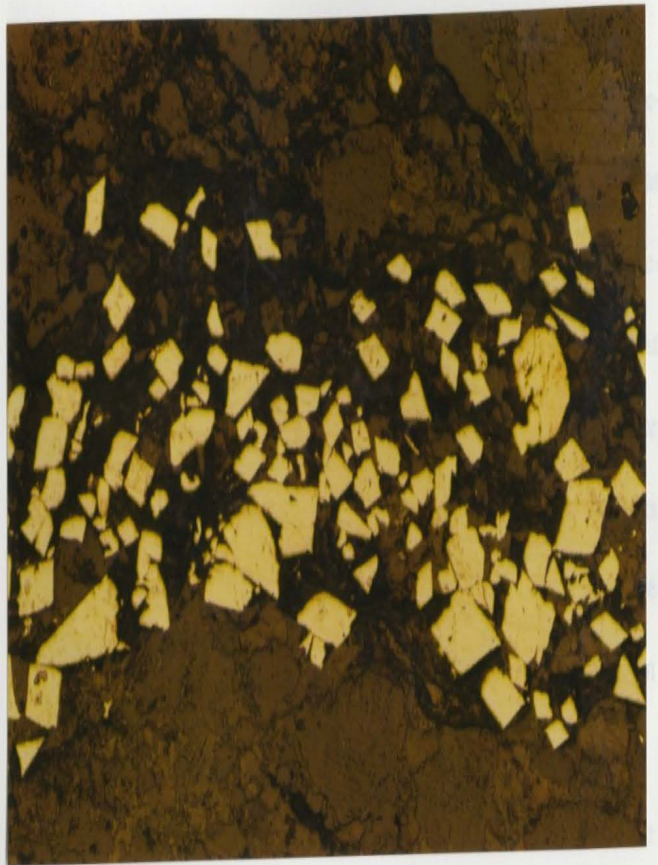


Plate 5.12: Photomicrograph of pyrite megaclast (light brown, centre of photo) having an appearance best described as brecciated. [2.5X magnification, reflected light].



Another common mineral assemblage of the M-Zone is pyrite-arsenopyrite-leucoxene-Fe,Ti oxides. The Fe-Ti oxides present may comprise both relict as well as newly created phases. Dubé *et al.* (1987) have shown that the magnetite-ilmenite-leucoxene-sulphide association is the result of a reducing fluid containing H₂ which was derived from H₂O dissociation (Reaction 9, Table 5.2). The reducing fluid can reduce titanomagnetite to the pseudomorphous leucoxene/anatase/pseudobrookite assemblage as per Reaction 2 (Table 5.2). In addition to amorphous titanium-bearing phases, sulphide phases can also result due to the excess S which was derived from H₂S dissociation (Reaction 10, Table 5.2).

These oxide assemblages mentioned above are common in natural systems. The FeO-Fe₂O₃-TiO₂ system (Figure 5.2a) contains three solid-solution series, one of which is the ulvöspinel-magnetite series. According to Lindsley (1976), if members of the ulvöspinel-magnetite series undergo oxidation during cooling, exsolution lamellae of ilmenite form in magnetite parallel to the (111) crystallographic plane (Plate 5.16).

The magnetite-ilmenite-sulphide assemblage is also stable at low temperatures as shown in Figure 5.2b. The Fe-O-S system illustrates how pyrite-pyrrhotite (Plate 5.9) and pyrite(arsenopyrite)-magnetite(ilmenite) (Plates 5.16, 5.17 and 5.18) can coexist. The coexistence of these phases has implications for the physico-chemical conditions of the mineralizing fluid(s) and which will be discussed in a later section.

Plate 5.13: Photomicrograph of large wulffite grain of pyroxene with visible cleavage traces occupied by sulphide grains. [2.5X magnification, XP].



Plate 5.14: Annealed arsenopyrite grains (right of centre) exhibiting coalescence as well as the indicative 120° grain boundaries. [10X magnification, reflected light].



5.2.4 Mineral Chemistry

To reaffirm the deductions inferred from the petrographical investigation, a series of samples containing coexisting chlorite and carbonate were analyzed to ascertain the overall geochemical compositions of these minerals (ie. Fe,Mg-rich versus Ca-rich for carbonates and Mg-rich versus Fe-rich for chlorites).

Major oxides including SiO₂, TiO₂, Al₂O₃, FeO, MnO, MgO, CaO and K₂O were analyzed by SEM in 32 carbonate and 39 chlorite grains from the various alteration zonations to ascertain the geochemical character of these minerals. Table 5.4 lists a summary of the analyses for samples from each of the three zones. It should be noted that the SEM analyses are semi-quantitative.

Ternary plots of the SEM data show interesting trends for both the carbonate and chlorite analysed. The carbonates (Figure 5.3a) show a gradual shift in composition from Ca-rich carbonate (calcite) in the least altered gabbroic rocks, attributed to a regional lower greenschist facies assemblage, to those carbonates which have a dominant Fe,Mg component (ferroan dolomite, magnesian ankerite) correlated with increased alteration and proximity to the shear zones. Complimenting the shift in Ca composition is an increase in Mg composition with increasing alteration. These shifts are interpreted to be the result of the CO₂/H₂O ratio, a measure of alteration intensity, approaching infinity (Dubé *et al.*, 1987) where actinolite and calcite in the presence of CO₂ react to give an ankerite-quartz assemblage (Reaction 7, Table 5.2).

Similar features can be seen in the ternary plot for chlorites (Figure 5.3b).

Plate 5.15: Photomicrograph of chlorite (green) concentrated along shear bands with sulphides (black). [10X magnification, PPL].

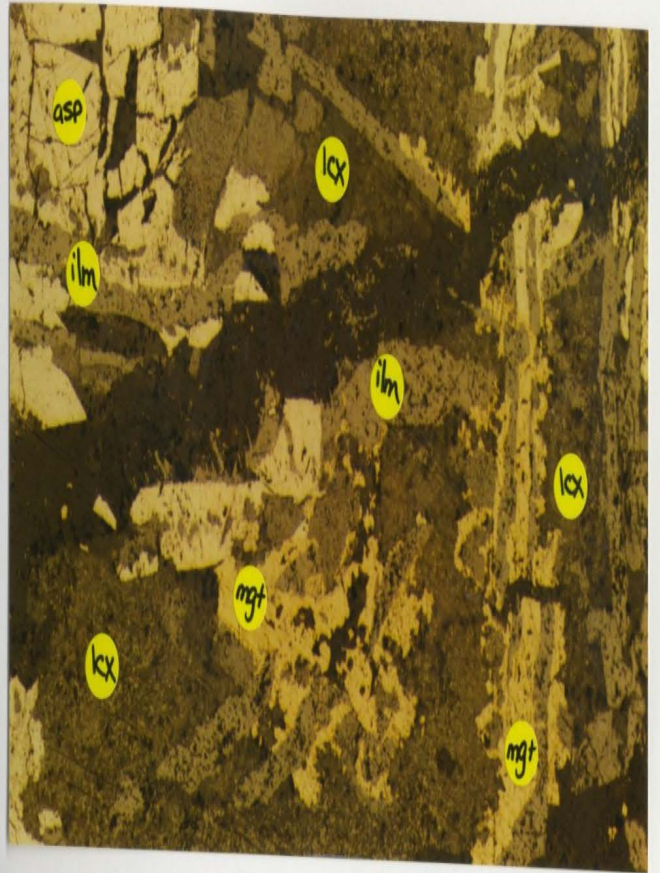


Plate 5.16: Photomicrograph of thin lamellae of exsolved ilmenite in a matrix of leucoxene (dark brown) and magnetite (Mgt). Also present is arsenopyrite (Asp) and pyrite (Py). [20X magnification, reflected light].



5.15

Plate 5.17: Photomicrograph of relict magnetite (mgt), ilmenite (ilm), leucoxene (lcx) and arsenopyrite (asp). [10X magnification, reflected light].



5.16

Plate 5.18: Intimate association of arsenopyrite (yellow-brown) with skeletal leucoxene-magnetite-ilmenite intergrowth (dark brown). [10X magnification, reflected light].



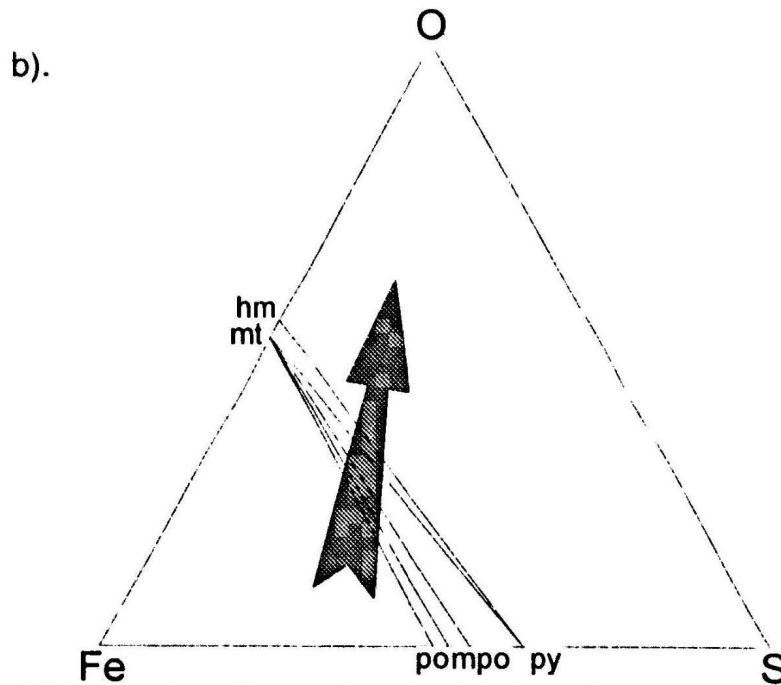
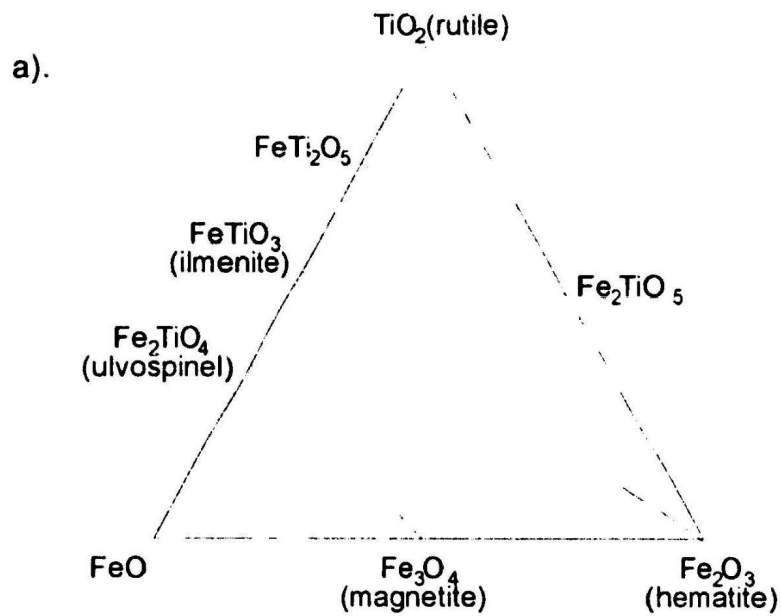


Figure 5.2: Ternary phase diagrams for (a) the FeO-Fe₂O₃-TiO₂ system showing three solid solution series including ulvospinel-magnetite and (b) the Fe-S-O system for low temperature assemblages. Arrow denotes trend of increasing oxidation. Labels include hematite (hm), magnetite (mt), pyrrhotite (po), monoclinic pyrrhotite (mpo) and pyrite (py). Diagrams after Craig (1990).

Table 5.4: Mean oxide concentrations from SEM mineral analyses. Note that numbers in parentheses refer to number of samples analyzed.

a). Carbonates

	GMA-Zone (n=14)	A-Zone (n=12)	M-Zone (n=6)
SiO ₂	1.15	0.77	2.46
TiO ₂	0.04	0.12	0.06
Al ₂ O ₃	0.68	0.45	1.90
FeO	2.24	23.68	16.31
MnO	1.63	1.04	0.75
MgO	0.49	12.92	23.24
CaO	93.51	60.74	54.95
K ₂ O	0.22	0.22	0.27

b). Chlorites

	GMA-Zone (n=6)	A-Zone (n=23)	M-Zone (n=10)
SiO ₂	34.75	29.99	35.71
TiO ₂	0.00	0.02	0.01
Al ₂ O ₃	16.35	21.78	20.62
FeO	39.74	37.06	23.30
MnO	0.07	0.18	0.13
MgO	8.79	10.35	18.89
CaO	0.32	0.27	1.40
K ₂ O	0.04	0.39	0.04

Chlorites from rocks which show little alteration have Fe-rich compositions but with increasing alteration intensity (ie. increasing carbonate alteration), the chlorites shift to a Mg-rich chemistry. This shift in chemistry, similarly for the Mg-enrichment observed in the carbonates, is probably the result of a sulphidation reaction in which Fe is

mobilized from the chlorite and ankerite and complexed with S to form sulphide minerals (Reactions 4,8; Table 5.2). The loss of Fe from both the chlorite and carbonate would result in an apparent Mg-enrichment as can be seen in Figure 5.3 where both the carbonate and chlorite show enrichment in Mg with increasing alteration intensity.

These mineralogical changes were most likely synchronous as illustrated in Reaction 6 where actinolite and epidote are replaced by ankerite and chlorite. This transition from Ca-rich carbonates and Fe-rich chlorite to more Mg-rich compositions also has implications for sulphide and gold mineralization (Reactions 4 and 8, Table 5.2) which are discussed in a later section.

5.2.5 Alteration Paragenesis and Model for Alteration Systematics

Based on the preceding lines of evidence, a paragenetic sequence can be suggested for the alteration event. Figure 5.4a is a diagrammatic representation of stability ranges for both alteration and relict phases for each of the three alteration zonations. As illustrated, phases such as Fe-chlorite, calcite, epidote, actinolite are destroyed with progressive alteration, while other minerals such as quartz, albite and pyrite are stable in all zones. Elements derived from the destruction, or partial breakdown, of these minerals may have been consumed during the formation of newly formed phases such as ankerite, ferroan dolomite, arsenopyrite-pyrite and Mg-chlorite.

A genetic model for the spatial distribution of the alteration zonations and the minerals contained therein is illustrated in Figure 5.4b. A similar model has been used

by Dubé *et al.* (1987) to illustrate the alteration patterns observed in the Bourbeau Sill in the Chibougamau region of Quebec. Briefly, the model states that decreasing $\text{CO}_2/\text{H}_2\text{O}$ and $\text{H}_2\text{O}/\text{rock}$ ratios are the mechanisms by which there are varied alteration mineral assemblages with increasing distance from the shear zone thus creating the alteration halo observed around the shears.

The alteration zonation observed at Duder Lake depicts a typical decrease in the water/rock and $\text{CO}_2/\text{H}_2\text{O}$ ratios away from the shear zone. This is evidenced primarily by the presence of iron and magnesian carbonate mineralogies proximal to the shear zones where the $\text{CO}_2/\text{H}_2\text{O}$ ratios would approach infinity where they would be stable (metastable) while hydrous mineralogies such as Ca, Fe and/or Mg silicates would breakdown contributing cations to the ankeritization. As the fluid equilibrates/evolves with the host rock, the $\text{CO}_2/\text{H}_2\text{O}$ ratio decreases since most of the CO_2 has been consumed.

The consumption of CO_2 is also coincident with the generation of H_2O which is produced during ankeritization of hydrous phases such as actinolite (Reaction 7; Table 5.2) which also in effect decreases the ratio.

Changing temperatures (which is a direct result of changing water/rock interaction) also dictates the alteration paragenesis. At high temperatures and high water/rock ratios, the H_2O dissociates and causes the breakdown of Fe-Mg oxides which locally go into the formation of pyrite and relict leucoxene. As the fluid evolves and becomes "buffered" by the host rock, the temperature decreases as does the water/rock

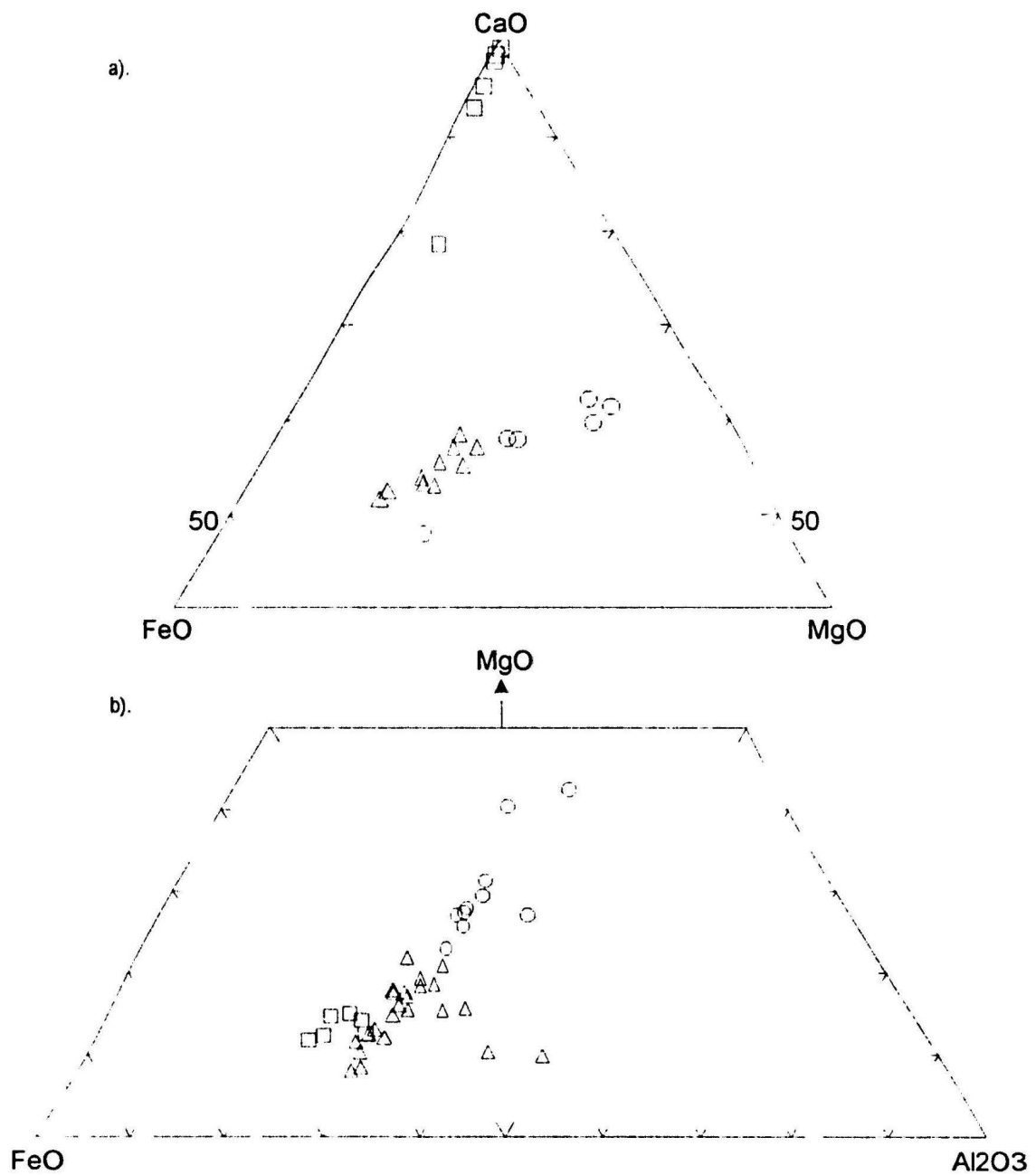


Figure 5.3: Semi-quantitative SEM analyses for (a) carbonates and (b) chlorites from the GMA-Zone (squares), A-Zone (triangles) and M-Zone (circles). Note the increases in MgO for both the carbonates and chlorites with increasing alteration intensity (ie. from the GMA- to the M-Zones).

ratio. This results in decreased dissociation of H₂O that causes a decrease in the CO₂/H₂O ratio that dictates the alteration assemblage that will be stable.

This alteration zonation is not only spatially arranged but also temporally arranged due to the time it would take for fluid infiltration and evolution during fluid-host rock reaction.

5.2.6 Summary

A distribution of alteration zones occurring in association with gold mineralization has been documented at Duder Lake. The alteration assemblages and relationships between the different zones has been ascertained from petrographical and mineral chemistry work to yield three different zones, namely the GMA-, A- and M-Zones. It has also been demonstrated how changing CO₂/H₂O ratios over time provides the mechanism by which the alteration distribution was formed. Relationships mentioned in the preceding sections will be used in the discussion of metallogenesis of the deposits in Chapter 6.

Although the alteration model, and to a certain extent the mineralization model, has been ascertained from standard petrographic observations and limited mineral chemistry, it still requires refinement with respect to geochemical characteristics which accompany the alteration and mineralization. The geochemical implications of the alteration and mineralization systematics will be discussed in the following sections.

a).

	GMA-Zone	A-Zone	M-Zone	
Fe-chlorite	—————	- - - -		Fe-chlorite
calcite	—————	- - - -		calcite
quartz	—————			quartz
albite	—————			albite
epidote-actinolite	— · · · ·			epidote-actinolite
magnetite-ilmenite	—————	- - - -	· · · · ·	magnetite-ilmenite
leucoxene				leucoxene
sericite	· · · · ·	- - - -		sericite
ankerite	·	- - - -	—————	ankerite
pyrite	· · · · ·	- - - -	—————	pyrite
Mg-chlorite		- - - -	—————	Mg-chlorite
arsenopyrite		- - - -	—————	arsenopyrite
gold			- - - -	gold
replacement	—————			replacement
deformation	—————			deformation

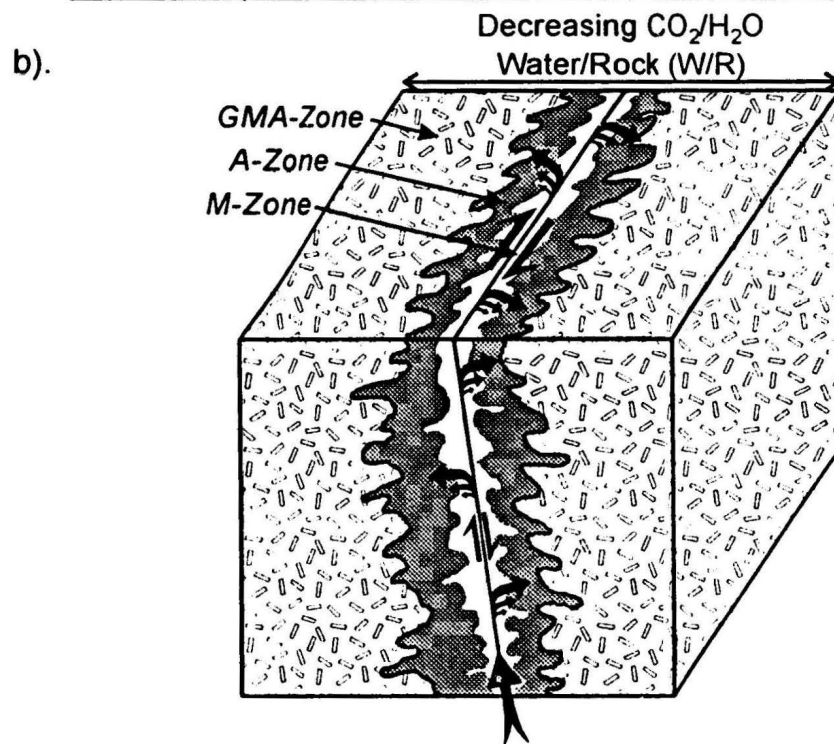


Figure 5.4: Alteration history and genetic model. (a) Paragenetic table depicting minerals important in the alteration zonations. Solid lines represent stable phases, dashed lines represent phases which are either being created or destroyed and dotted lines are metastable minerals. (b) Genetic model for the alteration zonations modelled for a dextral fault/shear system with a component of dip-slip motion. Arrows representative of CO₂-rich fluid flow along the shear plane extending into the host rock. The three alteration zones are labelled. Also shown is the decreasing nature of the CO₂/H₂O and W/R ratios important in the fluid evolution and which drives the alteration progression. Diagram modified from Dubé et al. (1987).

5.3 Geochemistry of Alteration and Mineralization

5.3.1 Introduction

As outlined previously, the gabbro samples collected from the Duder Lake gold showings were subdivided into three petrographic groups which also serve to illustrate the geochemical systematics inherent in the alteration and mineralization. A total of 13 samples representative of the GMA-Zone, 17 samples from the A-Zone and 32 samples representative of the M-Zone were collected and then analyzed by a number of whole rock geochemical techniques, and in addition, fluid inclusion and stable isotope analyses was performed on several of the samples. Tables 5.5 and 5.6 list the average geochemical abundances of all elements analyzed for each of the three lithotypes (alteration zonations). There are several obvious changes in the chemistry from rocks of the GMA- to those of the M-Zones. Most notable are increases in Au, As and CO₂ and decreases in SiO₂ and Al₂O₃. The changes in elemental content between each of the different zones will be discussed fully in the section pertaining to relative elemental gain and loss with comments on volume loss due to alteration.

In the following sections, discussion of the geochemical systematics pertains to large ion lithophile elements (LILE), stable isotopes, rare earth elements (REE), trace elements and fluid inclusions. The aim of the geochemical analysis is to better characterize: likely fluid sources and source regions, the model for mineralization, and illustrate the geochemical changes which accompany the alteration and mineralization.

Table 5.5: Average major oxide and trace element compositions for mafic plutonic rocks from the (a) GMA-Zone, (b) A-Zone and (c) M-Zones. Oxides in wt. %, Fe₂O₃ is total Fe, trace elements in ppm except gold (ppb). Max and min are the highest and lowest values respectively, mean is the average concentration and S.D. is standard deviation.

a). GMA-Zone (n = 13)

	Max	Min	Mean	S.D.
%				
Mg#	66.26	27.66	52.51	11.67
SiO ₂	56.10	43.00	49.34	4.08
TiO ₂	2.27	0.63	1.30	0.46
Al ₂ O ₃	17.70	13.85	15.83	1.02
Fe ₂ O ₃	13.21	2.68	9.42	2.86
MnO	0.26	0.07	0.20	0.06
MgO	9.85	1.20	5.86	2.82
CaO	12.47	3.78	7.26	2.73
Na ₂ O	8.81	3.09	4.47	1.95
K ₂ O	2.51	0.03	0.57	0.60
P ₂ O ₆	0.33	0.06	0.12	0.07
H ₂ O	5.55	0.98	3.92	1.44
CO ₂	7.46	0.44	3.18	2.12
LOI	10.44	3.48	6.63	2.15
ppm				
Cr	592	0	200	189
Ni	174	0	57	54
Co	62	27	47	13
Sc	63	0	36	18
V	445	19	219	120
Cu	154	3	61	43
Pb	56	0	7	15
Zn	171	19	71	38
Cd	1.00	1.00	1.00	0.00
W	119.00	17.00	57.46	31.84
Mo	2.50	2.50	2.50	0.00
S	1203.54	102.95	707.78	316.67
As	42.00	0.20	9.92	11.03
Se	1.00	1.00	1.00	0.00
Sb	135.00	0.17	16.91	37.54
Au(ppb)	4.6	1.0	1.3	1.0
K	20836	249	4770	5020
Rb	111	0	22	27
Cs	6.20	0.20	3.35	1.83
Sr	541	74	218	111
Ga	33	13	19	6
Li	127.10	2.60	53.07	37.68
Ti	13609	3777	7780	2736
U	2.90	0.10	0.70	0.96
Cl	151.82	22.24	56.38	34.48
Br	3.00	1.00	1.18	0.53
Be	3.70	0.50	1.38	0.88

b). A-Zone (n = 17)

	Max	Min	Mean	S.D.
<i>%</i>				
Mg#	65.70	16.44	44.35	19.10
SiO ₂	59.80	36.08	45.56	12.30
TiO ₂	3.11	0.74	1.46	0.99
Al ₂ O ₃	17.30	7.86	14.35	3.96
Fe ₂ O ₃	16.67	5.70	10.90	3.89
MnO	0.34	0.08	0.21	0.09
MgO	10.85	0.73	4.98	4.89
CaO	10.70	2.06	6.72	2.92
Na ₂ O	7.66	1.77	4.07	1.97
K ₂ O	2.04	0.04	0.77	0.48
P ₂ O ₆	0.56	0.03	0.18	0.16
H ₂ O	7.32	0.00	3.13	1.63
CO ₂	16.23	0.00	7.15	6.15
LOI	18.11	0.00	10.17	6.58
<i>ppm</i>				
Cr	500	0	123	670
Ni	328	0	60	240
Co	73	0	42	27
Sc	71	17	39	19
V	546	0	224	178
Cu	158	0	56	35
Pb	12	0	3	4
Zn	140	49	75	44
Cd	1.00	0.00	0.88	0.36
W	222.00	0.00	48.24	90.00
Mo	2.50	0.00	2.21	1.86
S	26886.82	173.05	2979.91	10105.61
As	14800.00	0.00	1389.92	11775.91
Se	1.00	0.00	0.88	0.36
Sb	85.80	0.00	24.51	46.82
Au(ppb)	3830.0	0.0	365.7	6538.9
K	16935	332	6368	3997
Rb	118	1	33	22
Cs	16.00	0.00	3.51	3.50
Sr	360	78	168	72
Ga	29	12	19	10
Li	158.80	0.00	52.38	34.59
Ti	18644	4436	8767	5929
U	2.60	0.00	0.48	0.41
Cl	123.72	22.74	47.94	24.86
Br	20.00	0.00	2.64	7.56
Be	2.55	0.00	1.21	0.69

c). M-Zone (n = 32)

	Max	Min	Mean	S.D.
%				
Mg#	79.89	16.12	39.23	17.75
SiO ₂	64.93	27.33	41.45	7.94
TiO ₂	3.86	0.10	1.67	0.94
Al ₂ O ₃	15.84	4.27	11.93	2.74
Fe ₂ O ₃	18.12	3.77	11.61	2.84
MnO	0.43	0.14	0.25	0.07
MgO	22.25	1.01	4.91	4.98
CaO	12.89	3.64	7.32	2.39
Na ₂ O	6.88	0.03	3.85	1.76
K ₂ O	1.51	0.02	0.82	0.41
P ₂ O ₆	0.51	0.01	0.17	0.15
H ₂ O	6.16	0.00	2.50	1.29
CO ₂	26.63	0.00	11.24	5.43
LOI	29.21	0.00	12.72	5.66
ppm				
Cr	2871	0	281	723
Ni	1002	0	95	256
Co	100	0	51	24
Sc	72	10	36	17
V	684	9	210	174
Cu	128	6	45	27
Pb	20	0	4	4
Zn	179	20	90	41
Cd	1.00	0.00	0.94	0.24
W	400.00	0.00	113.95	87.39
Mo	7.30	0.00	3.13	1.73
S	33200.18	403.71	14112.05	9494.61
As	54400.00	2.00	13189.71	11906.02
Se	1.00	0.00	0.94	0.24
Sb	218.00	0.00	70.29	44.63
Au(ppb)	36600.0	0.0	4465.9	6940.0
K	12576	166	6789	3413
Rb	67	1	29	16
Cs	10.00	0.00	3.55	2.85
Sr	288	71	154	51
Ga	38	5	21	9
Li	121.25	0.00	25.81	27.66
Ti	23111	600	10012	5650
U	0.30	0.00	0.10	0.04
Cl	114.43	18.70	35.47	19.95
Br	21.00	0.00	7.44	7.47
Be	2.10	0.00	1.21	0.58

Table 5.6: Average REE abundances for mafic plutonic rocks from each of the three zones. All elements as ppm. "Max" and "min" represent the highest and lowest values respectively, "mean" is the average concentration and "S.D." is standard deviation.

	GMA-Zone (n = 6)				A-Zone (n = 5)				M-Zone (n = 6)			
	Max	Min	Mean	S.D.	Max	Min	Mean	S.D.	Max	Min	Mean	S.D.
Ba	253	78	154	57	177	47	105	48	146	91	121	20
Ta	0.45	0.15	0.29	0.11	1.41	0.28	0.58	0.43	1.15	0.35	0.78	0.25
Nb	5.4	2.2	3.2	1.1	7.1	5.5	6.1	0.5	16.7	7.5	11.1	3.6
Hf	2.61	1.48	2.00	0.43	6.26	3.36	4.97	1.06	12.48	6.41	8.24	2.05
Zr	121	56	88	24	255	92	180	57	470	229	316	76
Y	32	18	26	5	59	34	48	8	109	63	81	14
Th	1.61	0.57	1.11	0.43	3.39	1.26	2.34	0.72	6.06	3.42	4.29	0.85
La	7.30	3.82	5.50	1.24	13.41	7.93	11.25	2.06	27.16	14.36	20.34	4.31
Ce	18.15	10.43	13.97	2.85	33.03	20.60	28.04	4.59	62.03	36.40	50.29	9.00
Pr	2.53	1.57	1.98	0.37	4.70	2.94	3.99	0.66	8.41	5.21	7.12	1.17
Nd	12.35	7.62	9.57	1.96	22.46	14.15	19.05	2.96	38.90	24.82	33.70	5.02
Sm	3.92	2.19	3.01	0.61	6.73	4.37	5.66	0.80	11.27	7.14	9.68	1.37
Eu	1.46	0.81	1.09	0.22	2.14	1.73	1.96	0.16	4.44	2.44	3.23	0.64
Gd	5.19	2.87	3.93	0.83	9.25	5.72	7.71	1.21	14.60	9.71	12.30	1.57
Tb	0.78	0.42	0.61	0.13	1.46	0.88	1.19	0.19	2.48	1.53	1.99	0.30
Dy	5.77	3.07	4.46	1.03	10.93	6.40	8.86	1.52	18.99	11.55	14.62	2.37
Ho	1.28	0.72	0.98	0.21	2.34	1.38	1.89	0.32	4.12	2.43	3.08	0.54
Er	3.90	2.22	3.02	0.67	7.11	4.25	5.75	0.97	12.88	7.61	9.45	1.71
Tm	0.56	0.29	0.44	0.10	1.02	0.61	0.84	0.15	1.89	1.12	1.39	0.25
Yb	3.74	1.94	2.79	0.65	6.93	3.72	5.55	1.12	12.62	7.50	9.13	1.71
Lu	0.55	0.29	0.43	0.10	1.03	0.57	0.81	0.16	1.93	1.13	1.39	0.27

5.3.2 Lithophile Element Systematics

Lithophile element systematics within potassic alteration domains of hydrothermal ore deposits, in particular lode gold deposits (*cf.* Kerrich, 1988a, 1988b, 1988c; Kerrich and Fryer, 1988; Burrows and Jemielita, 1989; Kerrich, 1989a, 1989b; Kerrich and Fryer, 1989; Kerrich *et al.*, 1990), can give indications of pertinent fluid sources and composition (*ie.* magmatic versus metamorphic), source processes and discrimination of chemical changes due to hydrothermal alteration versus variations in original

composition. Lithophile element characterization of host rock and the alteration effects have also been extensively studied by Armbrust and Gannicott (1980), Munha *et al.* (1980), and Ellis and Mahon (1964, 1967). These studies were focused on alteration in volcanogenic massive sulphide deposits, felsic spilites, and high temperature hydrothermal alteration by meteoric waters respectively. The conclusions drawn from this research were that K-metasomatism was controlled by partitioning of the lithophile elements that occurred during magmatic fractionation. The processes envisaged for this type of deposit however contrast with those of lode gold deposits, as discussed in the next chapter.

Figure 5.5 is a series of bivariate discriminant plots for selected elements including K, Rb, Ba, Cs, Li, Sr, Ce, Th, U, V, Ti, Ga and Al. These plots indicate two sub-groupings of elements - those which reflect hydrothermal alteration controls (K, Rb, Ba, Li and Cs) and those which appear to have behaved isochemically (Al, Ga, Th, U, Ti and V).

Within the first subgroup, the best correlations observed are those of K and Rb and to a lesser degree between K and Ba. The strong correlation between K and Rb suggests that both elements behaved similarly and as such may have substituted into newly forming potassic alteration phases as a coupled substitution. The strong positive correlation between K and Rb also has inferences for fluid source reservoirs which will be discussed later.

Other plots such as K versus Ba, K versus Cs and Ba versus Rb (Figure 5.5a) all

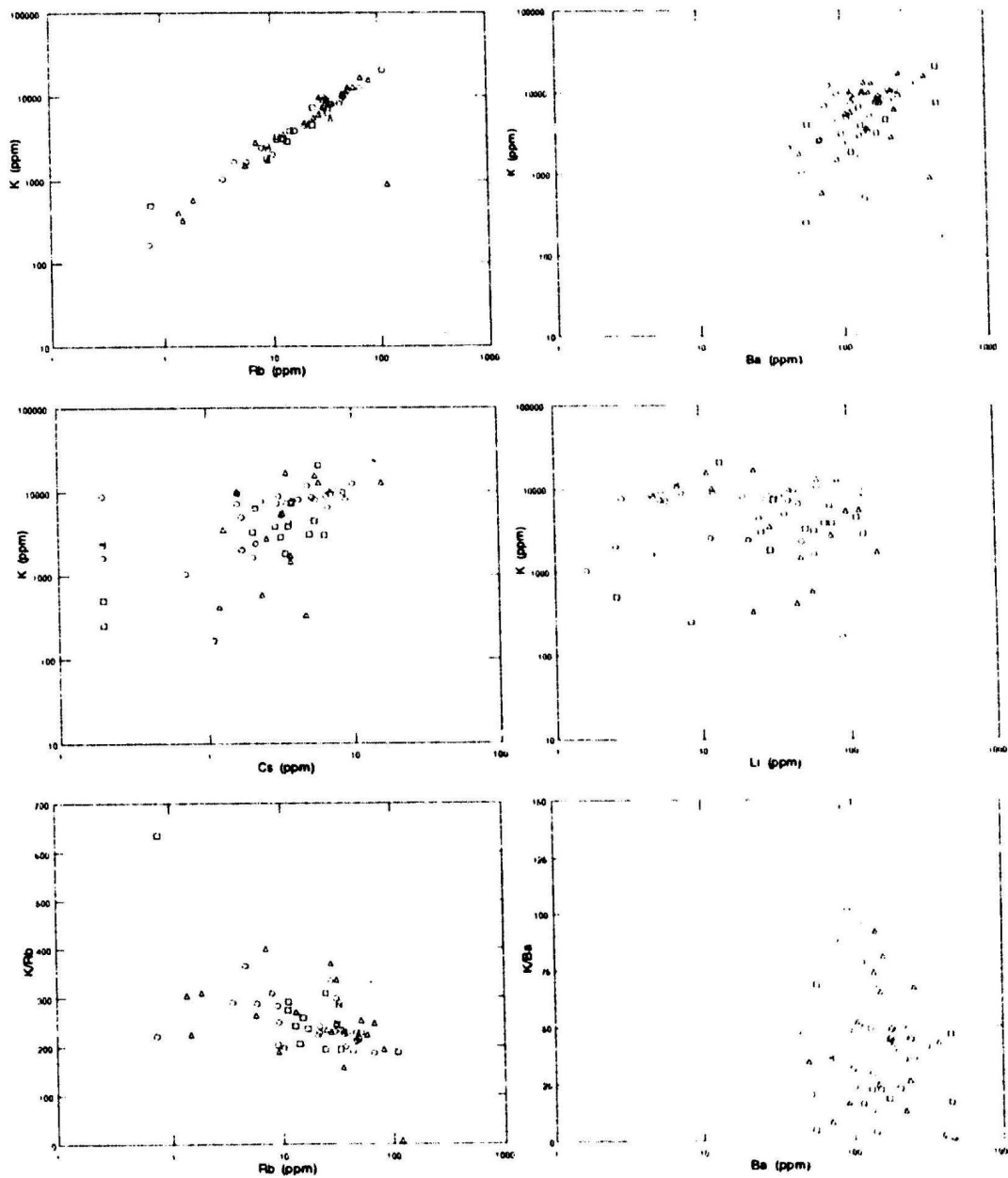


Figure 5.5a: Covariant plots of K vs. Rb; K vs. Ba; K vs. Cs; K vs. Li; K/Rb vs. Rb and K/Ba vs. Ba for samples representative of the GMA-Zone (squares), A-Zone (triangles) and the M-Zone (circles).

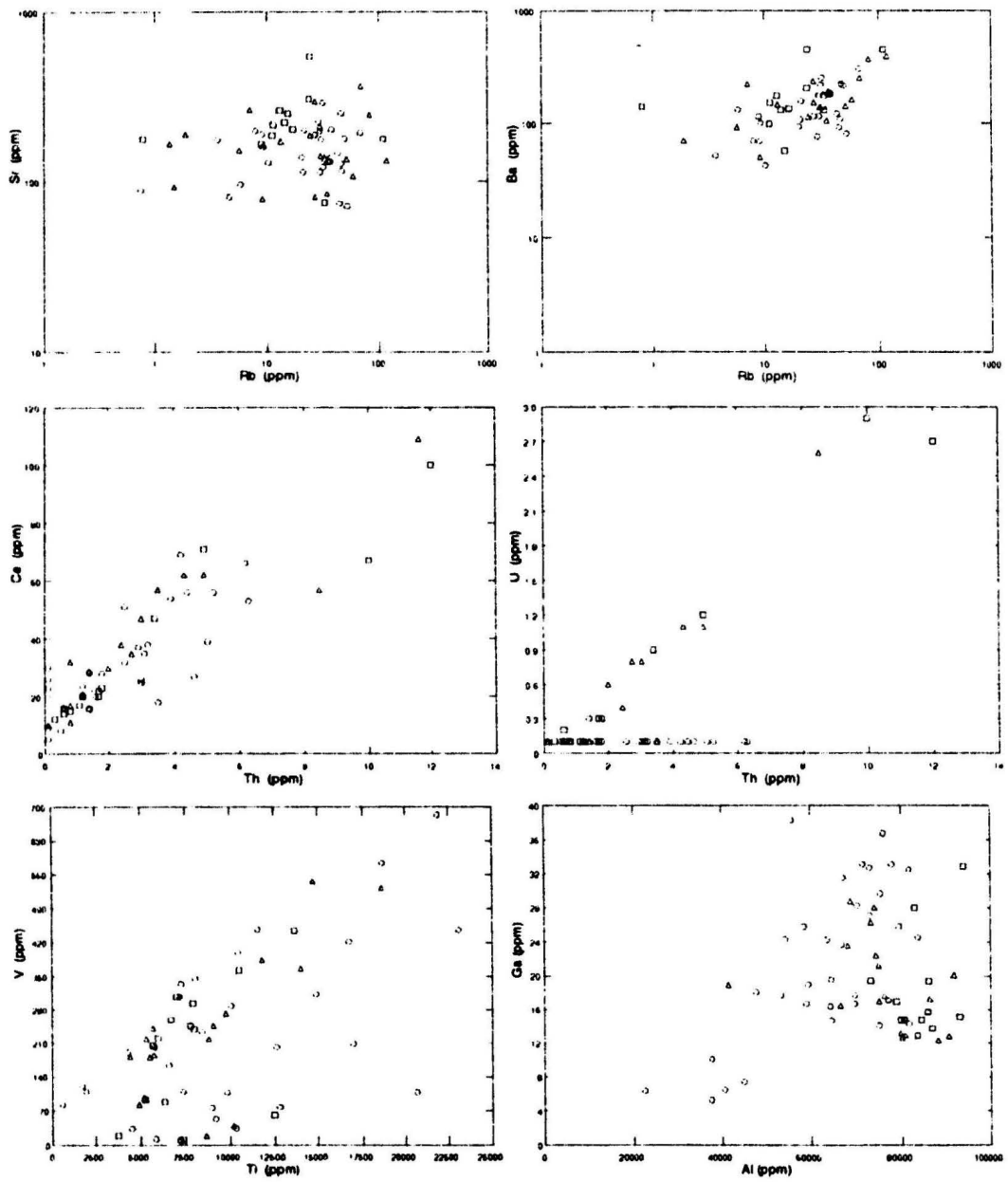


Figure 5.5b: Covariant plots of Sr vs. Rb; Ba vs. Rb; Ce vs. Th; U vs. Th; V vs. Ti and Ga vs. Al for samples from the three zones. Symbols as per Figure 5.5a.

exhibit weak positive correlations, implying that they may have had similar chemical controls as K and Rb during alteration and mineralization. Discriminant plots of K/Rb versus Rb and K/Ba versus Ba demonstrate possible local lithological controls (ie. heterogeneity of samples) since the correlations are much weaker than that of the bivariate analyses.

It should be noted that the variations observed in these bivariate plots are not only sensitive to the degree of alteration, but also to the volume and original composition, such that samples that had little to no K and Rb initially but which underwent intense alteration and volume loss may plot in the same field as a sample originally enriched in K and Rb and which had no volume change.

The systematics of Sr and Ba suggests that Sr was neither enriched or depleted with respect to Ba during alteration and mineralization. Kerrich (1989a) stated that the variability of K/Li, Rb/Sr and uniform K/Rb and K/Ba ratios suggest that the fluid into which these elements were partitioned was derived by dehydration reactions in lithologically complex source regions. That similar relations occur in the Duder Lake rocks has implications for the gold mineralization model.

The second subgroup of elements, those that are interpreted to have behaved isochemically, is plotted on bivariate plots in Figure 5.5b. The Ce versus Th and U versus Th plots show strong positive linear correlations which suggest isochemical behaviour (assuming these elements were positively correlated in the host rock prior to alteration). In addition, the total range of Ce, Th and U are well within the average

chemical concentrations set forth for mafic rocks (Kerrick, 1988a; Turekian and Wedepohl, 1961) suggesting that the compositions of these elements are little changed from their original compositions even though they have experienced alteration. According to Nesbitt *et al.* (1979) and Jahn *et al.* (1980) elements such as Ti, V and REE are immobile under conditions of low to mid-greenschist facies metamorphism and as such will behave isochemically.

It appears that K, Rb, Ba, Li and Cs were decoupled from Al, Ga, Th, U, Ti and V during alteration and mineralization processes. These preliminary findings are further substantiated in the section pertaining to mass balance.

5.3.3 CO₂ and Rare Metal Content as Indicators of Alteration Intensity

The Duder Lake gold deposits stand out from other deposits in the eastern Dunnage Zone in that the mineralization occurs in the wall rocks instead of veins. In addition, mineralized zones are anomalously As-rich, with grab samples assaying in excess of 7% arsenic. Enrichment of As in the wall rocks adjacent to the veins, coupled with intense carbonatization and alkali alteration are common themes in most gold systems (Boyle, 1979). Similarly, Sb, S and Au shows a close correlation with As in that all three are enriched well above background levels (Table 5.7). S is included in the discussion on ore metals since it is a measure of the sulphidation that is manifested in the form of pyrite and arsenopyrite. Figure 5.6 is a bar graph illustrating the degree of enrichment of As, S, Sb and Au which, for "normal" gabbro would have values of 2,

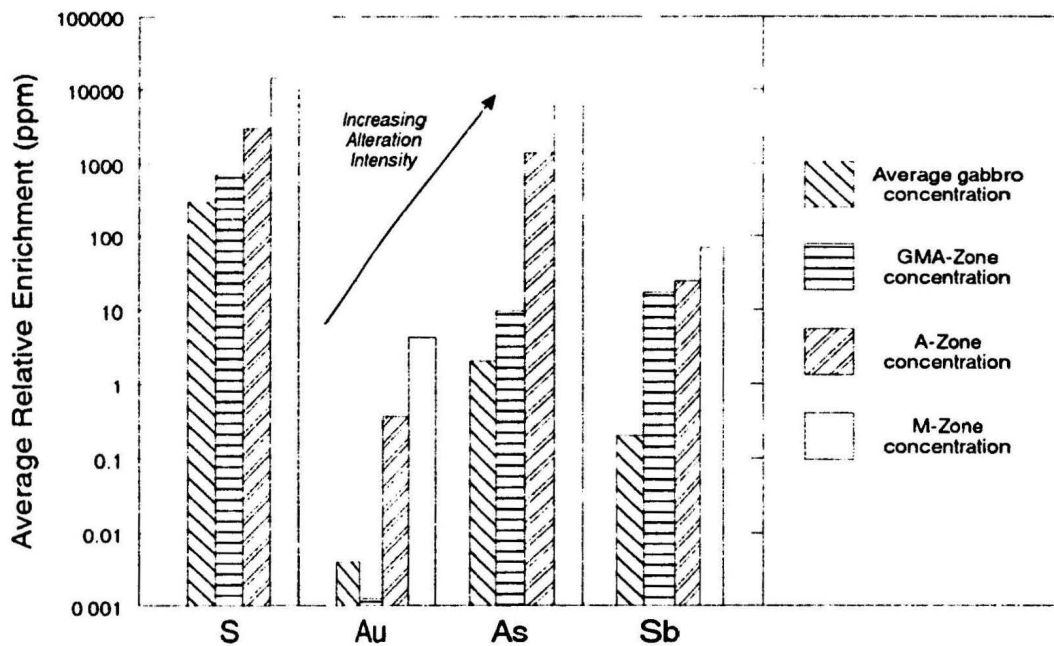


Figure 5.6: Enrichment diagram for As, Au, S and Sb from each of the alteration zonations in the Duder Lake gold occurrences. Average gabbro values are from Turekian and Wedepohl (1961). Note the correlation between increasing alteration intensity and element enrichment.

Table 5.7: Element concentrations used in Figure 5.7. Note that all concentrations are reported as ppm. Average gabbro values from Turekian and Wedepohl (1961). Numbers in brackets represent the number of samples used in calculating the mean element concentration in each zone.

	Average Gabbro	GMA-Zone (13)	A-Zone (17)	M-Zone (32)
S	300	707.78	2979.91	14112.05
As	2	9.92	1389.92	13189.71
Sb	0.2	16.91	24.51	70.29
Au	0.004	0.0013	0.3657	4.4569

300, 0.2 and 0.004 ppm respectively (Turekian and Wedepohl, 1961). The plot exhibits the enrichment trends of the Duder Lake occurrences with increasing degree of alteration intensity. Metal concentrations increase towards the shear zones and can be correlated with other geochemical trends such as CO₂, K₂O, W and CaO.

The relationships between the metals are examined before a discussion of the close association of the metals with CO₂ content and the use of both as indicators of alteration intensity.

5.3.3.1 As, Au, Sb and S Systematics

Whole rock analyses have indicated that anomalous concentrations (relative to gabbro values from Turekian and Wedepohl, 1961) of As, Au, Sb and S are >7 wt.%, 30g/t, 200ppm and >4 wt.% respectively. Although the assays are quite spectacular, the regional geochemical background for As, Au and Sb is also elevated in northeastern Newfoundland (Davenport and Nolan, 1988; Evans, 1992, p.240). Except for Au, the average mafic igneous values of Turekian and Wedepohl (1961) are much less than those for even the freshest rocks (GMA-Zone) attesting to the relatively enriched nature of bedrock in this region (Figure 5.6). Figure 5.7 further delineates the degree of enrichment through the use of frequency distribution diagrams. The diagrams for As and Au show a bimodal distribution indicative of two populations. The first populations have means of 56 ppm and 1.7 ppb for As and Au, respectively, and represent background values for the Duder Lake area. The second populations have means of 17782 ppm and

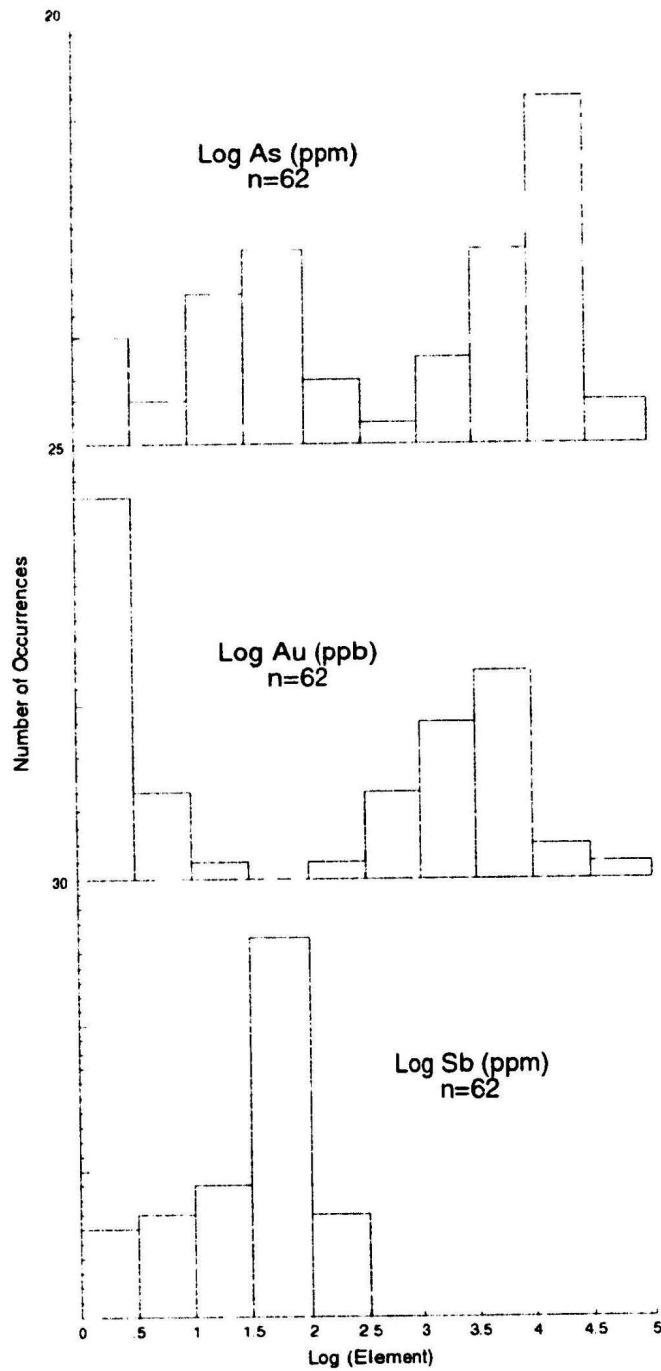


Figure 5.7: Log frequency distribution diagrams for As, Au and Sb. Note the presence of two populations for Au and As indicative of regional background (low log values) and metal enrichment during mineralization (high log values). Refer to text for further discussion.

5623 ppb for As and Au, respectively, and represent the mineralized zones. The frequency distribution diagram for Sb indicates only one population with a mean of 18 ppm, suggesting that enrichment of Sb during the alteration and mineralizing event was not great.

Regardless of the regional geochemical anomalies, concentrations of these metals coincide with the most intensely altered sections at Duder Lake. Inter-element relationships for As, S, Au and Sb suggest that they must have been mobilized from a common source and precipitated simultaneously. A series of bivariate plots for the metals is illustrated on Figure 5.8. The plots of S/As, S/Au and S/Sb all illustrate increasing S contents with increasing As, Sb and Au values suggesting that the formation of sulphides closely coincided with the alteration event - more precisely, to those rocks most intensely altered proximal to the shears.

Strong positive correlations between As/Au, Sb/Au and Sb/As indicate that all three elements were mobilized together. Kerrich and Fryer (1991) stated that low water to rock ratios, indicative of weakly to non-saline fluids in which base metals are insoluble, suppress the partitioning of base metals into the fluid phase and as such the fluids become relatively enriched in rare metals such as Au, Hg, B, W, As and Sb. This suggested inter-element relationship is somewhat problematic at Duder Lake since no visible Au or Sb-bearing minerals are observed in the ore mineral assemblages, but both the Sb and Au were incorporated into the arsenopyrite and pyrite crystals. The As-Au relationship is discussed later, but the Sb relationship remains problematic.

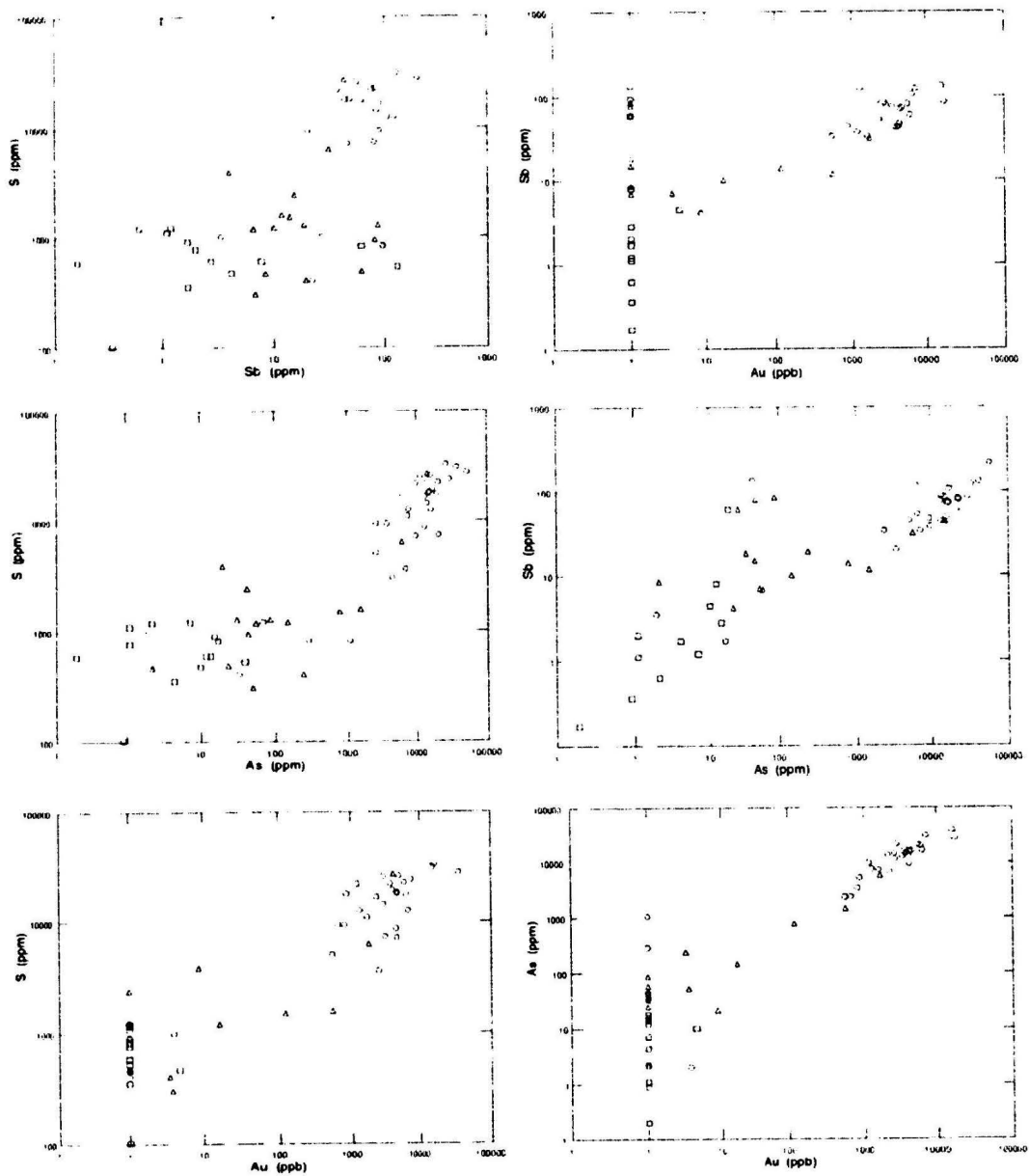


Figure 5.8: Bivariate plots of S/Sb, S/As, S/Au, As/Au, Sb/Au and As/Au which illustrate the interelement relationships for As, Sb and Au. Note the coenrichment trends of these elements with increasing alteration intensity. Symbols as per Figure 5.5.

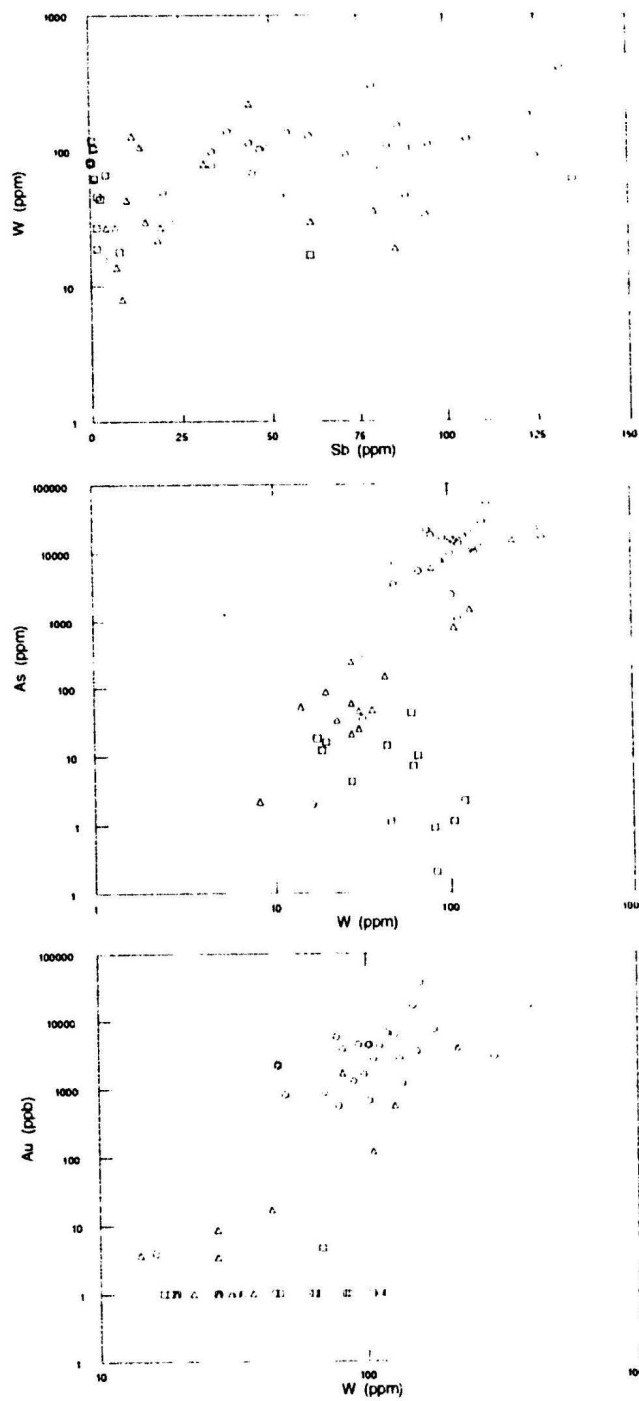


Figure 5.9: Plots of W versus Au, As and Sb showing correlation between increasing W contents and ore metal concentrations. Symbols as per Figure 5.5.

Other metals such as W also illustrate similar interelement ratios (Figure 5.9). Plots of W/Au, W/Sb and As/W show colinear relationships with increasing W content coinciding with increasing Au, As and Sb contents. The Au-W relationship is common to lode gold deposits (Kerrich and Fryer, 1991) and Higgins (1980) has shown that W may be complexed and transported by CO_3^{2-} in solution. The ubiquitous presence of carbonates in lode gold systems, which undoubtedly formed from CO_2 , CO_3^{2-} and/or CO-rich fluids, together with the Au-W and W- CO_2 relationships imply that gold was also complexed by a similar anionic species.

5.3.3.2 CO_2 , Molar Ratios and Alteration

The presence of intense carbonatization associated with gold mineralization, as well as the relationships between Au-W and W- CO_2 , suggests that the mineralizing fluids may have contained carbon-oxygen compounds such as CO_2 , CO_3^{2-} and/or CO as the complexing agent. The presence of CO_2 in the ore-forming hydrothermal fluid has been previously recognized by gold researchers who have documented carbonate alteration related to gold mineralization (Boyle, 1961, 1976, 1979; Meyer and Hemley, 1967; Rose and Burt, 1979) and spatially associated with faulting (Pyke, 1976, 1980; Jensen, 1980). Studies by Dubé *et al.* (1987) and Davies *et al.* (1982) of carbonate alteration have made use of whole rock CO_2 concentrations in an effort to explain the genesis, paragenesis, alteration characterization and zonation of the deposits. Davies *et al.* (1982) used CO_2 in combination with CaO and K_2O to yield molar ratios that were then used to measure

the intensity of the carbonate alteration. Combining the results of the molar ratio analysis with data on As abundances, target Au anomalies were generated. These anomalies usually coincided with the most intensely altered rocks in structurally complex areas.

These techniques were applied to samples from Duder Lake resulting in clarification of the metal-alteration relationships. Figure 5.10 consists of plots of CO_2 vs. W, CO_2 vs. As, CO_2 vs. Au and CO_2 vs. Sb which illustrate interesting inter-element relationships. There is a tendency for an increase in metal abundances with increasing CO_2 content, keeping in mind that CO_2 is a measure of the alteration intensity and the higher the CO_2 value, the more intense the alteration. Lithophile elements such as K and Rb show the greatest amounts of mobilization within the carbonate alteration domain (Davies *et al.*, 1982) suggesting a link between the increasing alteration intensity and the mobility of these elements. Lithophile element studies of the Duder Lake samples suggests isochemical behaviour of these elements but having considerable redistribution.

The degree of carbonate alteration accompanying gold mineralization can be further quantified on the basis of carbonate mineralogy which is deduced from the molar ratios of CO_2/CaO (Davies *et al.*, 1982). Values of 1 correspond to calcite mineralogies, ratios of 2 correlate with ankerite, and ratios higher than 2 are associated with mixtures of ankerite, ferroan dolomite, magnesite and/or siderite. To summarize, $\text{CO}_2/\text{CaO} > 1$ represents CO_2 supersaturation with respect to CaO. This CO_2 supersaturation probably corresponds to Dubé *et al.*'s (1987, and references therein) $\text{CO}_2/\text{H}_2\text{O}$ ratios equal to

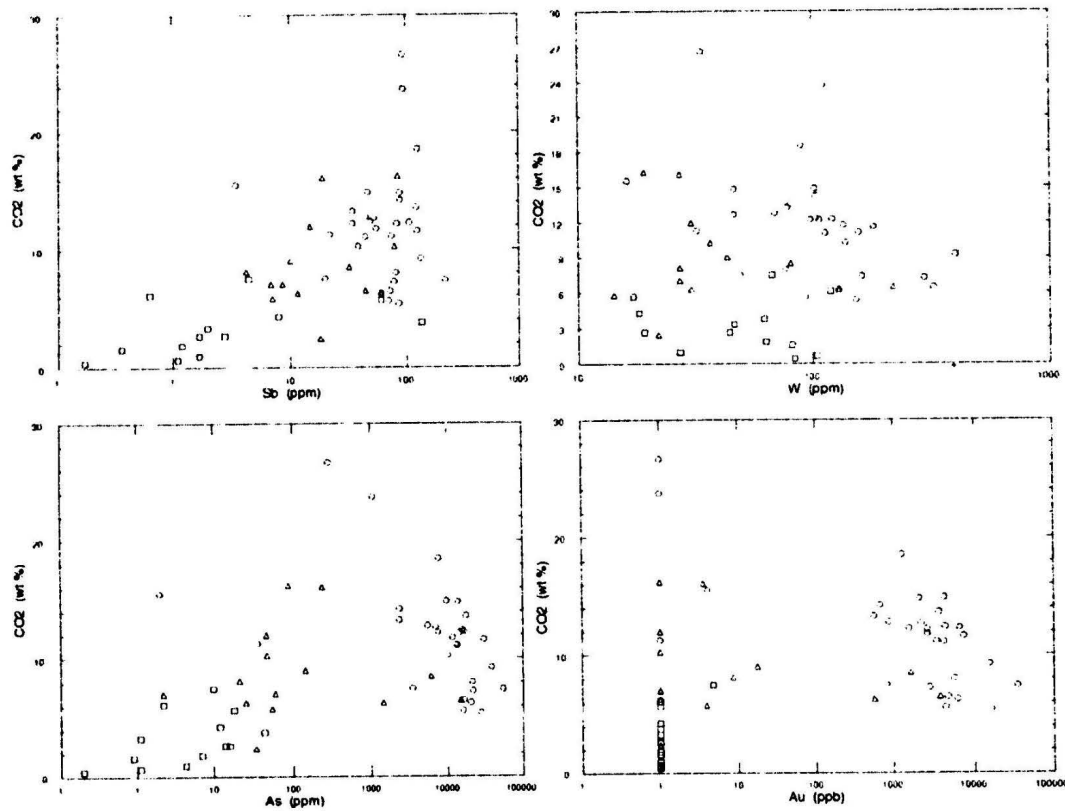


Figure 5.10: Bivariate plots of CO₂ versus Au, As, Sb and W. Note the correlation between CO₂ increase (alteration intensity indicator) and increasing metal contents. Symbols as per Figure 5.5.

infinity, which are in part responsible for the mineral reactions leading to the alteration zonations. Further refinement of the alteration zonation has been suggested by Davies *et al.* (1982) who stated that the gradual change in carbonate species from siderite to ankerite to calcite results from changing f_{CO_2} which is probably the result of the $\text{CO}_2/\text{H}_2\text{O}$ ratios approaching 1 due to fluid evolution through fluid-wall rock interaction.

To illustrate the molar ratio - alteration - mineralization relationships and to confirm petrographic observations for rocks from Duder Lake, Figure 5.11 contains plots of Au versus CO_2/CaO , CO_2 versus CO_2/CaO and K_2O versus CO_2/CaO . The plot of Au versus the molar ratio of CO_2/CaO summarizes the relationship between gold mineralization and carbonate alteration. The first appreciable concentrations of gold coincide with the transition from the calcite and Ca,Mg,Fe-bearing silicate domain ($\text{CO}_2/\text{CaO}=1$) to the calcite and ankerite domain ($\text{CO}_2/\text{CaO}=2$). This transition between the two carbonate species coincides with carbonatization reactions which breakdown the Ca,Mg,Fe-silicates and form Fe,Mg-rich varieties of carbonate (Reactions 3,5,6,7; Table 5.2). Associated with these carbonatization reactions are reactions which allow Fe from the Ca,Mg,Fe-silicates to complex with S thus forming sulphide (Reactions 4,8,10; Table 5.2). These reactions thereby allow for the formation of the carbonate alteration as well as for gold coprecipitation with sulphides. The other two plots further characterize the alteration by quantifying the changes in the molar ratio and correlation with other observed mineralogical changes.

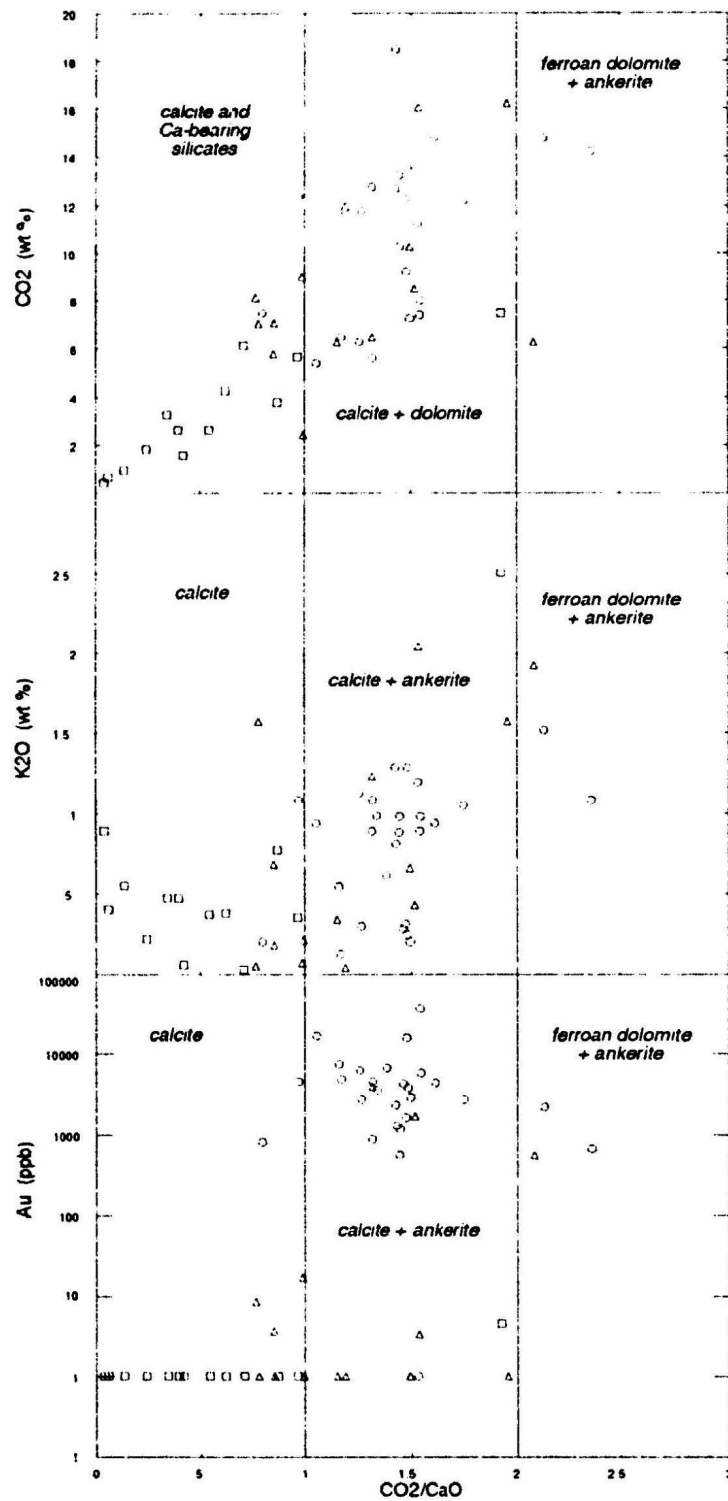


Figure 5.11: Plots of the molar ratio (CO_2/CaO) plotted against CO_2 (alteration index), K_2O (measure of potassic metasomatism) and Au (measure of mineralization). Positive correlations are observed in all plots suggesting coenrichment of all species during progressive alteration. Symbols as per Figure 5.5.

The final geochemical characterization of the alteration comes from $\text{CO}_2/\text{H}_2\text{O}$ ratios which complement the CO_2/CaO molar ratio diagrams. According to Dubé *et al.* (1987), the $\text{CO}_2/\text{H}_2\text{O}$ ratios represent the evolution of the fluid with increased and/or prolonged water/rock interaction. Nonetheless, the ratios are still a measure of CO_2 saturation in the alteration system and are similar to CO_2/CaO molar ratios in the information that they provide. Figure 5.12 consists of plots of $\text{CO}_2/\text{H}_2\text{O}$ versus Au, As and Sb, all of which show the same trend - increasing $\text{CO}_2/\text{H}_2\text{O}$ correlating with increasing metal contents. Elevated $\text{CO}_2/\text{H}_2\text{O}$ ratios are comparable to the CO_2 oversaturation scenario where Fe,Mg-carbonates precipitate and which are associated with gold mineralization.

The CO_2 techniques to analyze and interpret the alteration systematics accompanying hydrothermal metasomatism are quite useful, especially when used in combination with the ore metals. The discussion has illustrated how CO_2 has been an important agent in the alteration as well as possible mobilization of elements such as Sb, As, Au, CaO, K_2O and W. The following section, which pertains to a discussion of REE geochemistry, sheds more insight into the role CO_2 plays into these auriferous systems.

5.3.4 Rare Earth Element (REE) Geochemistry

A total of 17 samples were analyzed for their rare earth contents, which include

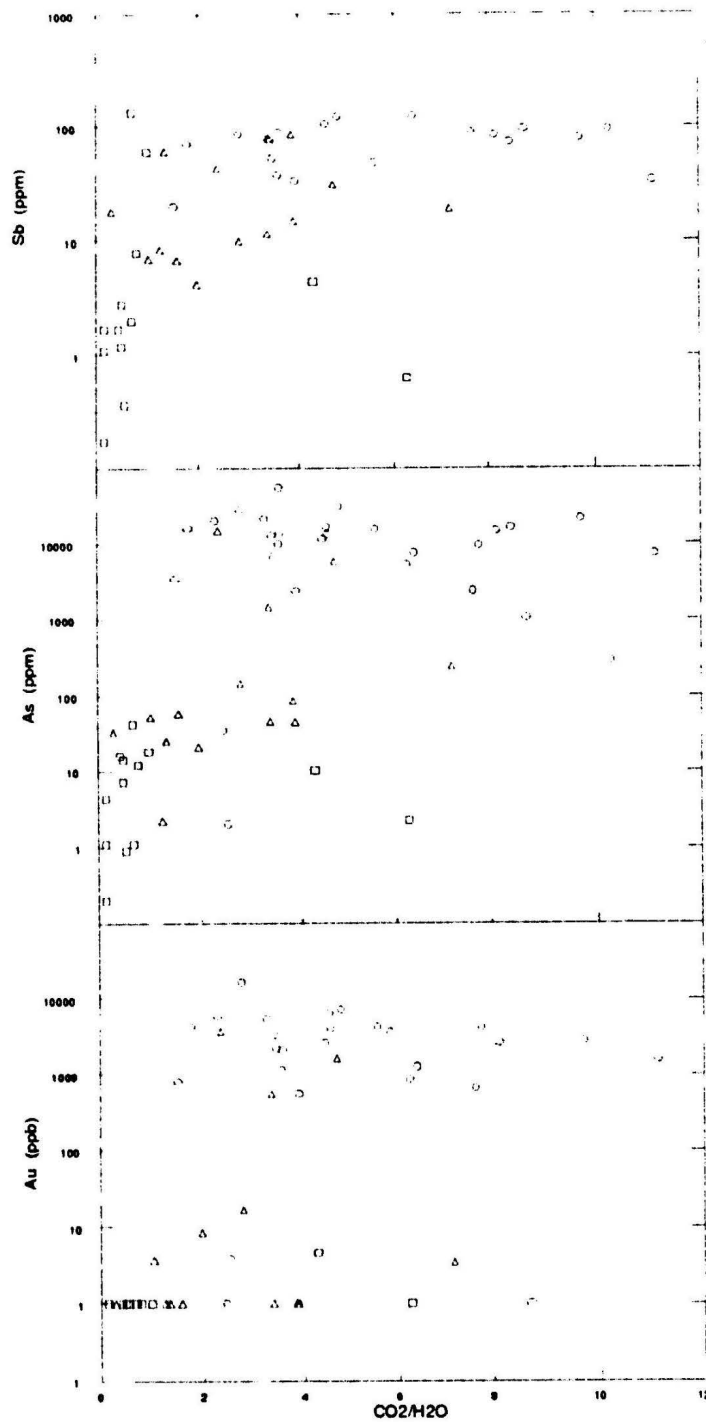


Figure 5.12: Plots of the CO₂/H₂O alteration index plotted against the ore metals. Refer to text for discussion. Symbols as per Figure 5.5.

the elements Ta, Nb, Hf, Zr, Y, Th, La, Ce, Pr, Nd, Sm, Eu, Gd, Tb, Dy, Ho, Er, Tm, Yb, Lu as well as Ba. These samples were carefully selected so as to represent each of the three lithotypes defined in this study. The analyses assist in determining a possible origin (setting and source) of these rocks as well as being an aid in characterizing the alteration and mineralization.

5.3.4.1 Petrogenesis and Tectonic Setting

Field relationships of these gabbros suggest that they are melts (of unknown affinity) and that they were not a source for the volcanic rocks in the area. The source of the gabbros is, however, still somewhat of a mystery, but the rare earth data provide some hints as to the origin of these rocks.

Although only the freshest gabbros were used for this petrogenetic investigation, the other gabbro lithotypes have similar REE patterns and abundances with the exception that both altered and mineralized show higher degrees of enrichment due to volume loss effects (see section pertaining to Rare Earth Element Behaviour During Alteration and Mineralization as well as the section on Geochemical Gains and Losses). Due to this volume effect, those samples considered to be altered and/or mineralized will be omitted from this discussion.

A total of six samples representative of fresh gabbros were plotted on numerous diagrams including tectonic discrimination plots and normalized rare earth element plots to illustrate some of the features exhibited by the chemistry.

The REE data for the fresh gabbros were normalized to normal mid-ocean ridge basalt (N-MORB; normalization values after Sun and McDonough (1989); See Table 5.8). The resulting REE plot (Figure 5.13) is characterized by negative Nb, enriched Th (5-10x N-MORB) and 1-3x enrichment of the light rare earth elements (LREE, La to Sm). The heavy rare earth elements (HREE, Gd to Lu) have a very flat pattern ranging from 0.6-1x N-MORB. The shape of the profiles as well as the elemental abundances suggest that these gabbros have been derived from a MORB-like mantle source which has been enriched in Th and LREE.

Epsilon Nd studies of the Loon Bay Granodiorite indicated an $\epsilon_{Nd} = +2$ suggesting mixing of arc material with a juvenile mantle source (Burke, 1992). Based on these findings, as well as geochemical and isotopic evidence of other Silurian intrusions west of the Red Indian Line, lower crustal material appears to have had an arc affinity (Burke, 1992; Fryer *et al.*, 1992). Since the Duder Lake gabbros are inferred to have a Silurian age of emplacement and to be spatially related to the Loon Bay granodiorite, it is postulated that the gabbros may be coeval with the granodiorite. If this inference is correct, the Duder Lake gabbros would have had the same heterogeneous mantle source. Comparison of REE data for an aplitic dyke cutting the Loon Bay granodiorite (Table 5.9) with averaged REE content of the gabbros at Duder Lake suggest a common origin on the basis of similarities observed in the REE patterns (Figure 5.14). Even though the aplite is enriched in elements such as Th, La and Lu it is probably a reflection of late-stage crystallization where these elements could be

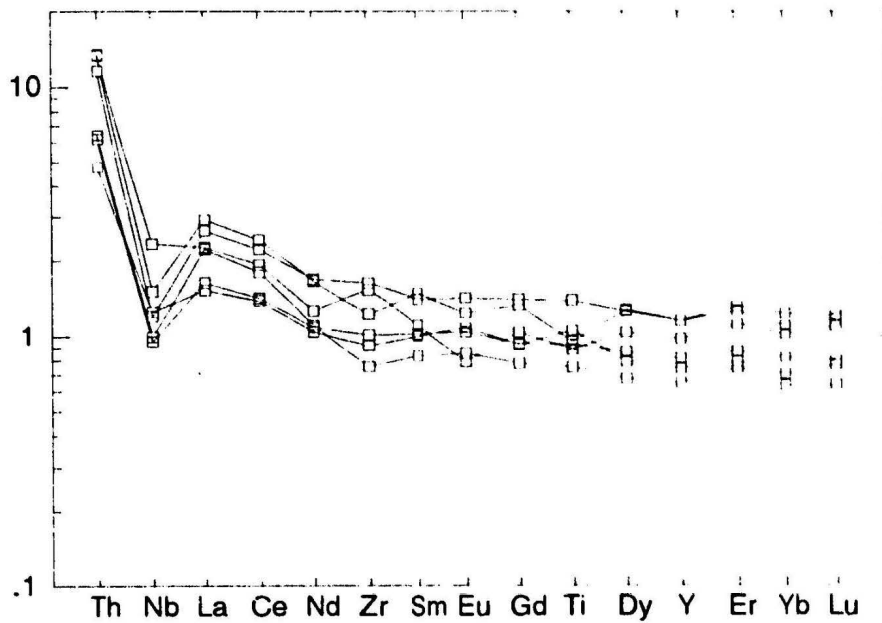


Figure 5.13: N-MORB normalized REE plot for fresh gabbros from the Duder Lake gold occurrences. Note the high Th, negative Nb and LREE enrichment indicative of an arc component and the flat LREE suggesting a "MORB-like" component.

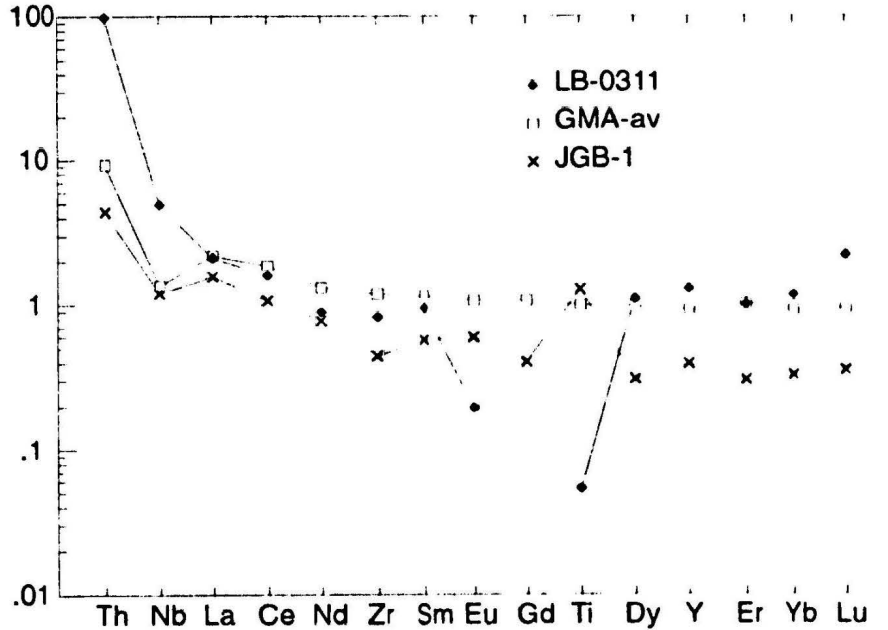


Figure 5.14: N-MORB normalized REE plots for Loon Bay granodiorite (LB-0311), island arc gabbro (JGB-1) and the average REE content for unaltered Duder Lake gabbros (GMA-av). See text for discussion.

concentrated. In addition, the large Eu anomaly is a reflection of feldspar formation in which Eu^{+2} will preferentially substitute for Sr^{+2} (Schnetzler and Philpotts, 1970). The depletion of Ti in the aplite may be a reflection of the lack of accessory minerals such as titanite, ilmenite or other titaniferous phases compared to the gabbro. Also included on the REE plot is the profile for the Geological Survey of Japan geostandard JGB-1 (Table 5.9; values from Govindaraju, 1987) which is calc-alkaline in chemistry. All

Table 5.8: Normalization values for N-MORB (after Sun and McDonough, 1989) and primitive (adapted from Hofmann, 1988). Hyphens (-) signify the element was not used in the normalization.

Element	N-MORB	Primitive
Th	0.12	-
Nb	2.33	-
La	2.5	0.63
Ce	7.5	1.59
Pr	-	0.251
Nd	7.3	1.21
Zr	74	-
Sm	2.63	0.399
Eu	1.02	0.15
Gd	3.68	0.533
Ti	7600	-
Tb	-	0.0974
Dy	4.55	0.661
Ho	-	0.1480
Y	28	-
Er	2.97	0.432
Tm	-	0.0676
Yb	3.05	0.4420
Lu	0.455	0.066

three patterns share some similarities, permitting the inference that there may be a genetic link between the Duder Lake and Loon Bay samples to a source with a component of arc chemistry.

Discrimination plots also give insight into the gabbro origin. Although the samples appear to have a tholeiitic chemistry associated with an ocean floor tectonic setting (Figure 5.15), other discrimination plots suggest a component of island arc material (Figure 5.16). This component of island arc material is manifested in the geochemistry and as such reflected on the discrimination diagrams by: (1) geochemistry suggests destructive plate margin basalt fields (Figure 5.16a); (2) plotting as andesitic to basaltic compositions suggesting a calc-alkaline component (Figure 5.16b); (3) shift from the tholeiitic field and primordial mantle compositions into the calc-alkaline field due to recycling of subducted material (Figure 5.16c); (4) forming a data array between volcanic arc basalts and N-MORBs (Figure 5.16d). Combining the information obtained from the discrimination diagrams with that of the REE data and the $\epsilon_{Nd} = +2$ for the Loon Bay granodiorite, a possible conclusion which could be drawn is that the magma forming the gabbros originated from a mixed mantle source comprising primordial mantle material with some component of arc material which may have also been the source for the Loon Bay intrusive rocks.

The REE data for the gabbros from Duder Lake have also been compared to data for host gabbros at the Clutha and Big Pond gold showings (Evans, 1991) as well as to the gabbros of the Gander River Complex (O'Neill, 1991). Normalized REE plots

(Figure 5.17) show that the gabbros of Duder Lake are distinct from gabbros of the Gander River Complex which has MORB affinities and different from the Big Pond and Clutha gabbros which have rare earth patterns suggestive of either a great deal of crustal contamination or of Ordovician-aged island arc, calc-alkaline affinities (G. Jenner, pers.

Table 5.9: Rare earth contents of aplite dyke sample (LB-0311) from Loon Bay (values from Burke, 1992) and for GSJ standard JGB-1 (values from Govindaraju, 1987).

	LB-0311 (aplite)	JGB-1 (gabbro)
Ba	189	63
Ta	2.27	0.17
Nb	11.4	2.8
Hf	2.20	0.84
Zr	61	33
Ti	406	9712
Y	36	11
Th	11.8	0.5
La	5.3	4.0
Ce	12	8
Pr	1.6	1.1
Nd	6.5	5.7
Sm	2.5	1.5
Eu	0.2	0.6
Gd	-	1.5
Tb	1	-
Dy	5	1
Ho	0.96	0.32
Er	3	1
Tm	1	-
Yb	3.53	1.00
Lu	1	-

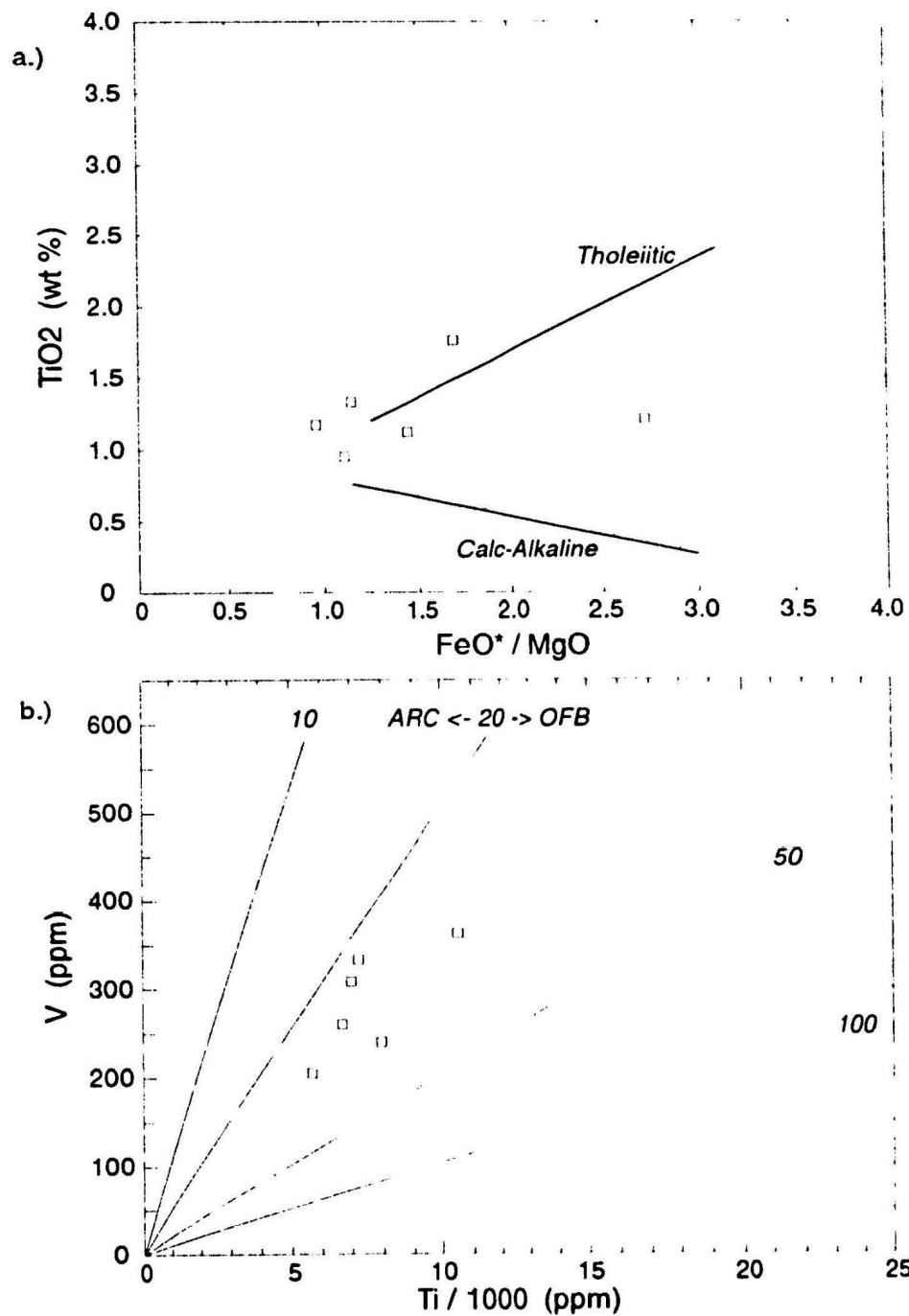


Figure 5.15: Discrimination plots that illustrate the chemical affinity of the gabbros. (a) Discrimination plot of Miyashiro (1974) depicting the tholeiitic nature of the gabbros and (b) Shervais (1982) plot showing an ocean floor ("MORB-like") affinity.

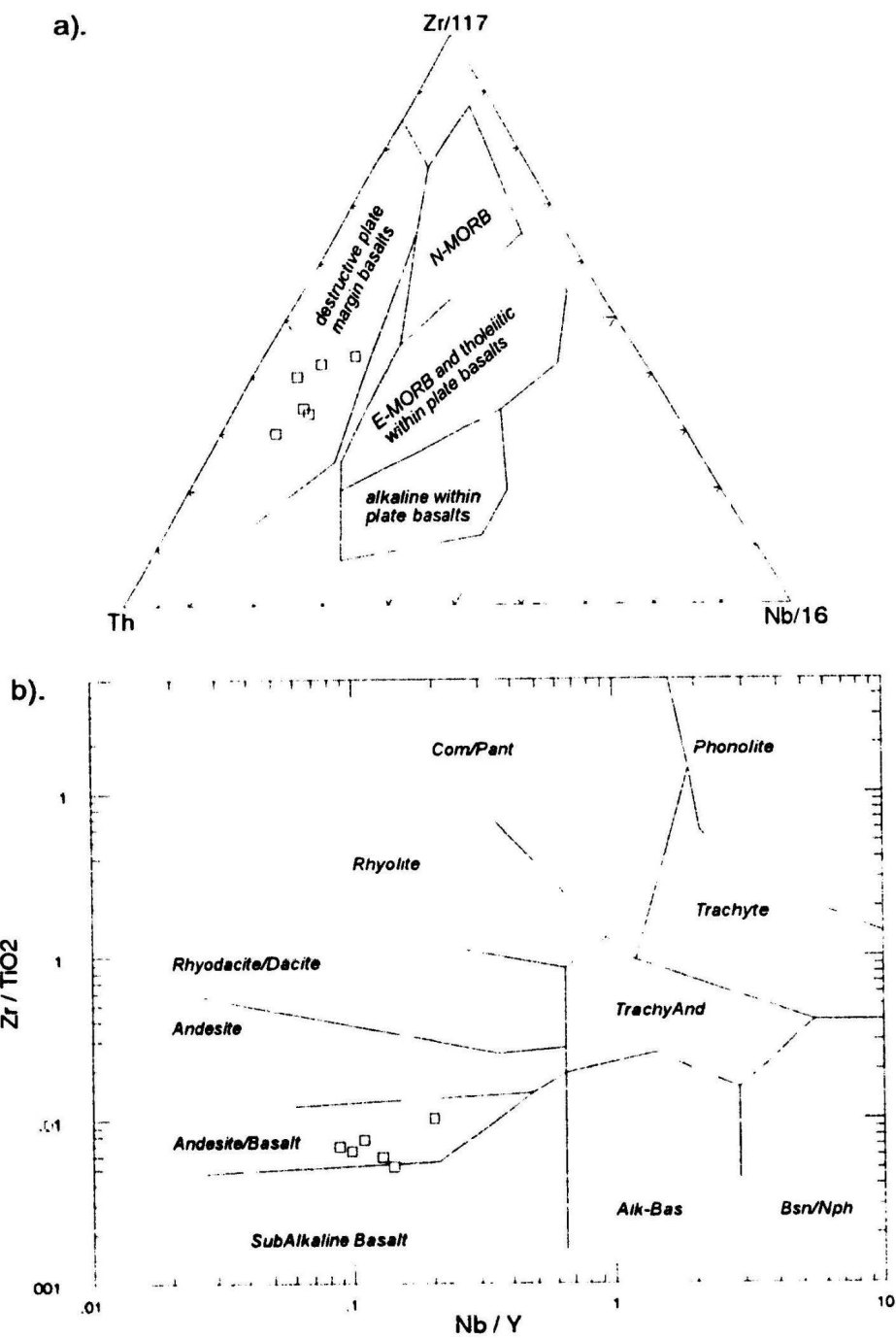


Figure 5.16: Discrimination plots that support the concept of an arc component in the gabbros. (a) Zr-Nb-Th plot of Wood (1980) and (b) Winchester and Floyd (1977) Zr/TiO₂ versus Nb/Y discrimination diagram. Refer to text for discussion.

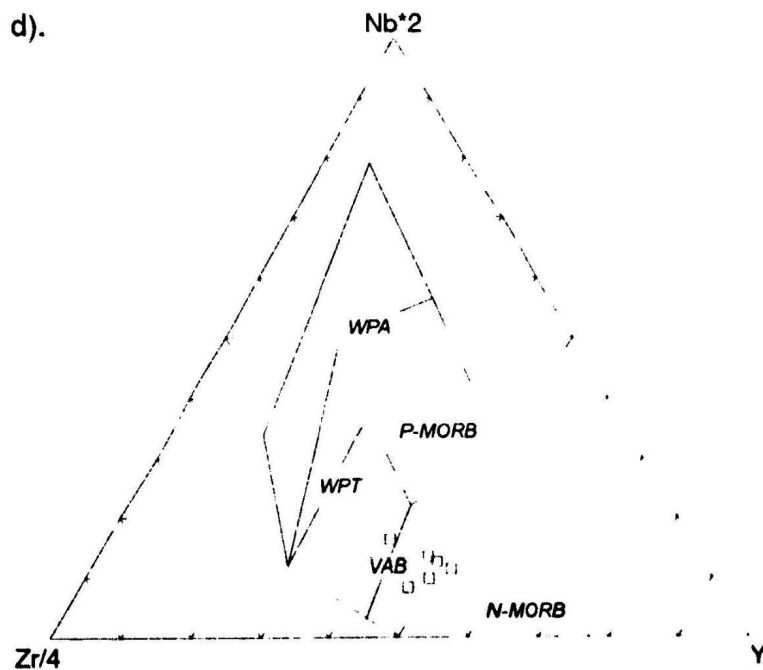
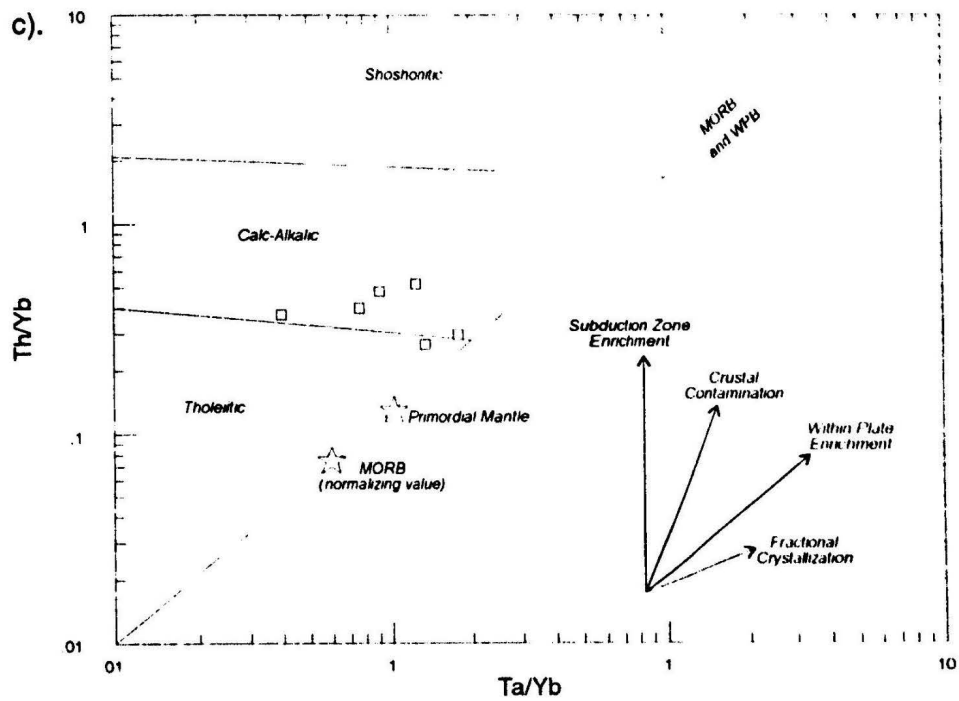


Figure 5.16 (continued): (c) Pearce (1983) Th/Yb versus Ta/Yb plot suggesting chemical shift in gabbros due to subduction zone enrichment, and (d) Nb-Y-Zr diagram of Meschede (1986). Refer to text for discussion.

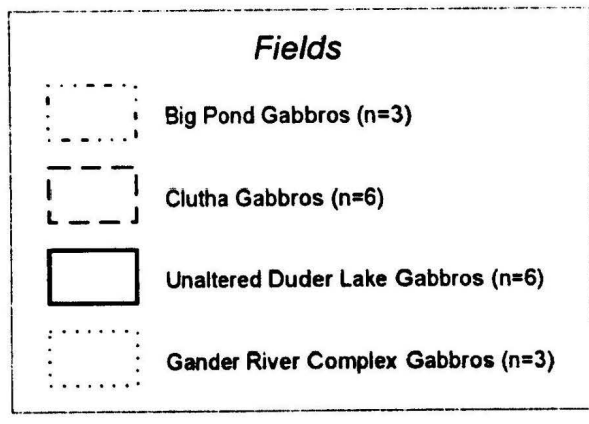
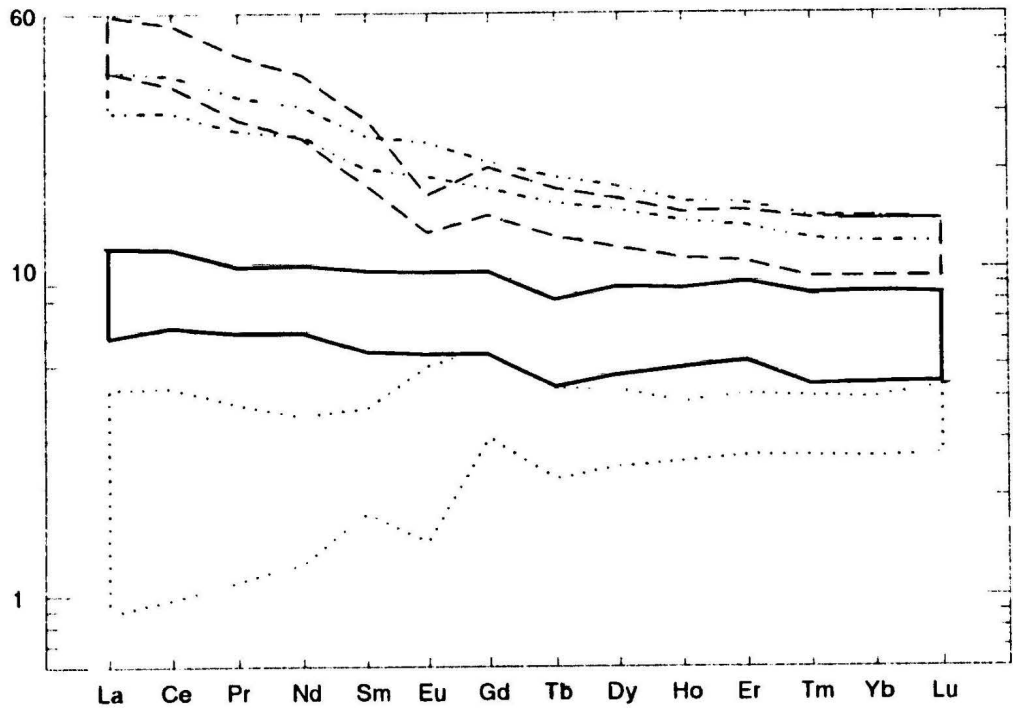


Figure 5.17: Compilation of REE data for gabbros from the Gander River Complex (O'Neill, 1991), Big Pond and Clutha gold occurrences (unpublished data, Newfoundland Department of Mines and Energy) and unaltered gabbros from Duder Lake (this study). All data normalized to primitive. Refer to text for discussion.

comm., 1993). Normalization values used for primitive are adapted from Hofmann, 1988 (also refer to Table 5.8).

The gabbros of Clutha and Big Pond have a similar geological setting, and lie along strike to those of Duder Lake. However, the geochemistry suggests that they may have a different source (genesis), and furthermore they may be of different age (?), suggesting that the plutonism responsible for the Duder Lake gabbros may have been a local, as opposed to regional, phenomenon possibly related to the formation and emplacement of the Loon Bay granodiorite. If the link between the two is valid, the 408 ± 2 Ma (Elliot *et al.*, 1991) obtained for the Loon Bay granodiorite may also reflect the age of the gabbros.

These findings are preliminary and still require detailed work before the complexities of gabbro relationships with Silurian-aged intrusive rocks can be ascertained.

5.3.4.2 Rare Earth Behaviour During Alteration and Mineralization

Studies of rare earth element behaviour in hydrothermal systems (Lottermoser, 1990; Wilton, 1985; Wyman and Kerrich, 1987; Kerrich and Fryer, 1979; Taylor and Fryer, 1980, 1982, 1983) have shown that REE mobility and abundance are a reflection of water to rock ratios during alteration and mineralization, and variations in these parameters give rise to a variety of REE patterns.

Primitive normalized (adapted from Hofmann, 1988) REE patterns for fresh,

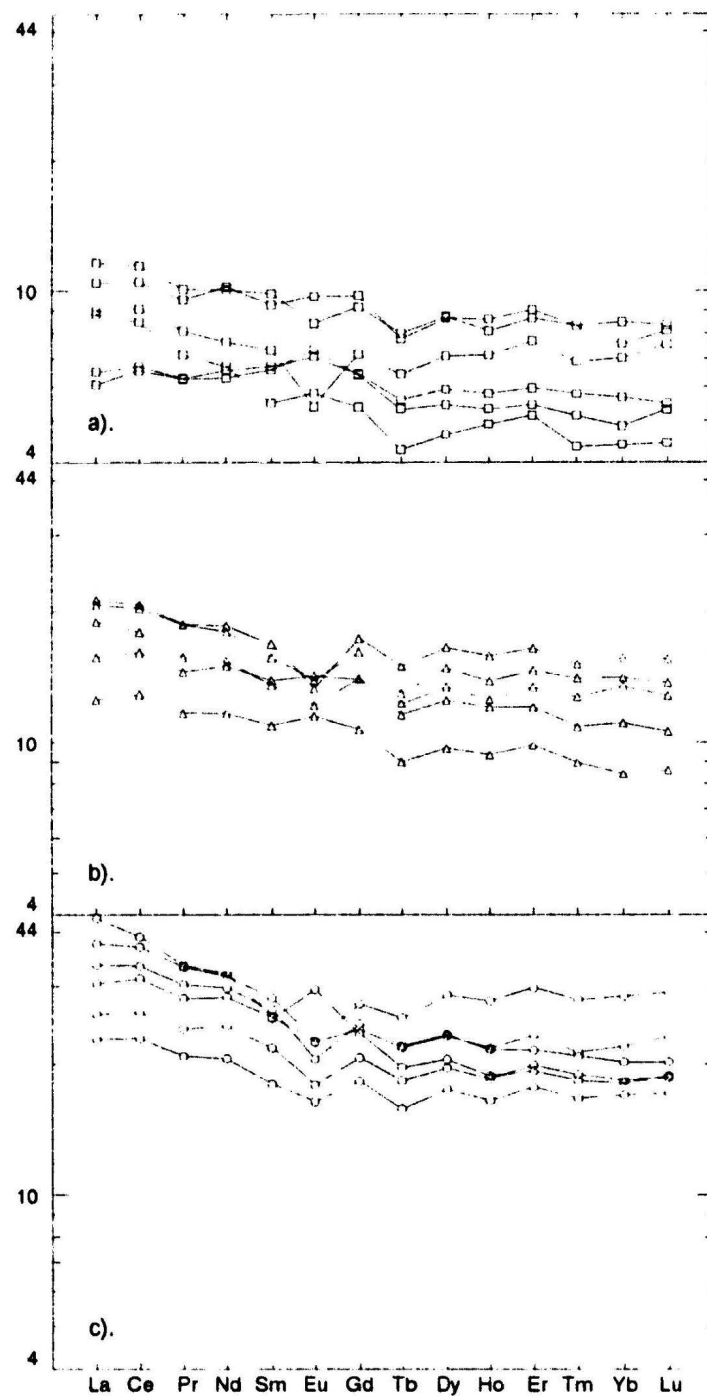


Figure 5.18: Primitive normalized REE plots for gabbros from the (a) GMA-Zone, (b) A-Zone and (c) M-Zone. Note the increase in total REE concentration with increasing alteration intensity.

altered and mineralized samples are remarkably similar, the only difference being the increase in relative abundance with increasing alteration intensity (Figure 5.18). The similar shapes of the patterns suggest that volume loss from the host rock, and not addition of REE, was the dominant cause of this shift. The REE are inferred to have behaved isochemically for the most part with only minor addition of LREE with progressive alteration (Figure 5.19). Comparison of the slopes of the LREE (La to Sm) profiles indicate that slope steepens with increasing alteration indicative of LREE addition and not HREE depletion since slopes of the HREE (Gd to Lu) have equal slopes suggesting no loss. Analysis of the mean profiles for all three lithotypes yields slopes of 0.24, 0.73 and 1.61 for gabbros of the GMA-, A- and M-Zones respectively which translates to a 7x increase in the amount of LREE occurring in the M-Zone relative to the GMA-Zone.

5.3.5 Quantification of Geochemical Losses and Gains

Lithophile element and REE data suggest that a major component of elemental concentration increase may be the result of volume loss as opposed to addition of lithophile elements and REE from the fluid phase. Numerous approaches has been used to characterize the apparent gains and losses for a hydrothermal system (eg. Gresens, 1967; Grant, 1986) taking into consideration the relative immobility of some elements, volume and mass considerations, and initial and final chemical concentrations. Grant (1986) simplified the technique of Gresens (1967) and by observing that if the

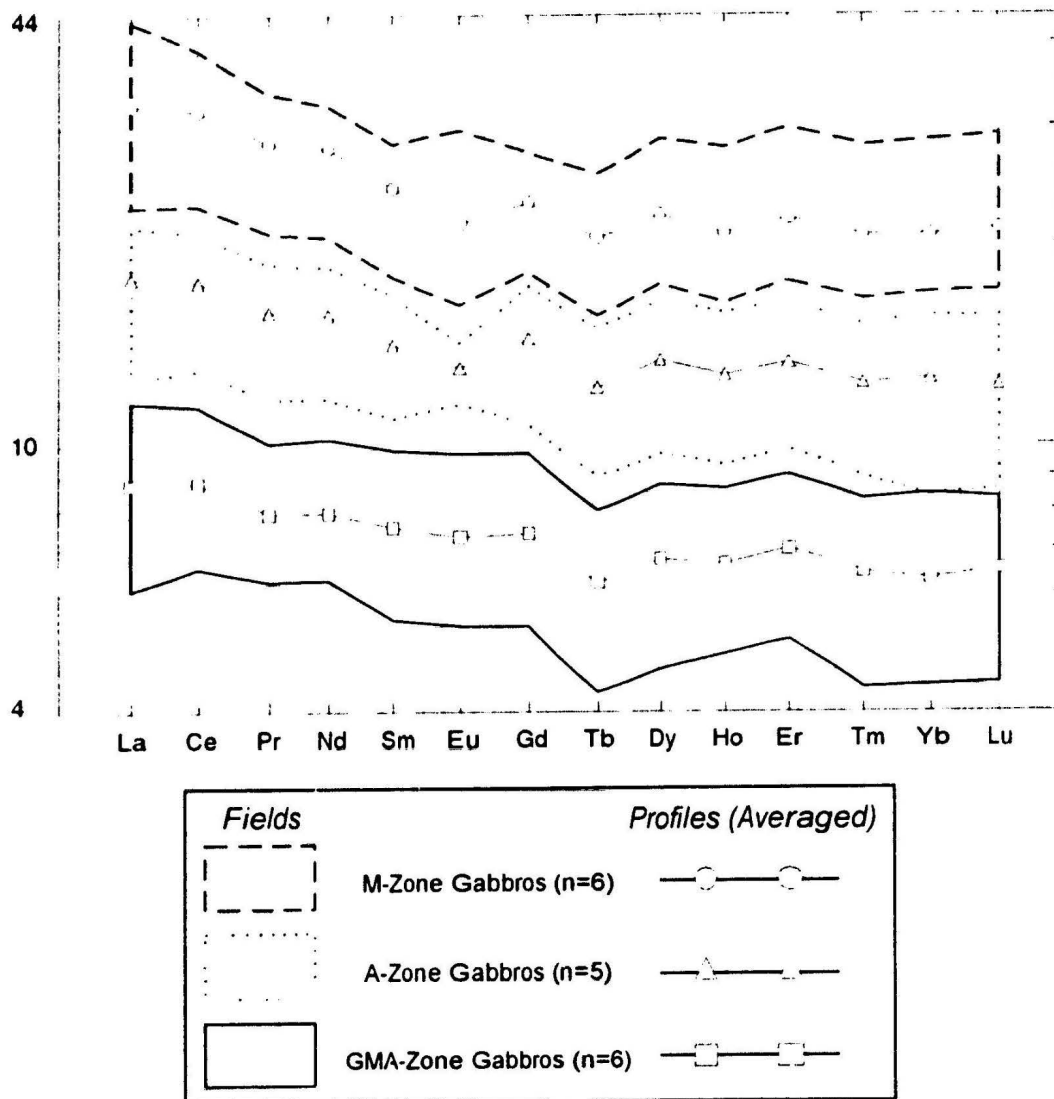


Figure 5.19: Compilation of primitive normalized REE data for each of the three lithotypes from the Duder Lake gold occurrences. Fields represent the range in concentrations of the normalized REE data. REE profiles represent the the mean normalization values for each lithotype.

compositions of representative fresh (unaltered) samples are plotted against their altered counterparts, any elements (or oxides) which are unchanged in concentration would plot along a line of equal concentration, or *isocon*, which may or may not also be the line of equal mass or equal volume. Lines not parallel to the isocon would represent mass or volume increases (if slope > than slope of isocon) or losses (slope < isocon slope).

Application of this technique depicts some interesting points about the geochemistry of the Duder Lake occurrences as well as reaffirming some of the inferences on the REE and lithophile element data.

A comparison between fresh (unaltered) and mineralized (altered) gabbros was performed in an effort to quantify relative losses and gains as well as to crudely estimate the amount of volume loss associated with mineralization and alteration. The data sets for 12 fresh and 32 mineralized gabbros were compiled and then averaged to give mean concentrations for the oxides and trace elements. The mean REE concentrations were deduced from 6 analyses for fresh gabbro and 6 analyses for mineralized gabbro.

The data sets used for the construction of the isocon diagrams are listed in Table 5.10. Also listed are the calculated losses and gains relative to fresh gabbro concentration. The calculation for the relative losses and gains is as follows:

$$\text{Relative Gains}\backslash\text{Losses} = \Delta C_i / C_i^o = (C_i^a - C_i^o) / C_i^o$$

where, C_i^a = concentration (wt. %, ppm, or ppb) of element 'i' in the altered rock
and, C_i^o = concentration (wt. %, ppm, or ppb) of element 'i' in the unaltered rock

Table 5.10: Average geochemical concentrations of fresh gabbros from the GMA-Zone (C^o) and mineralized gabbros of the M-Zone (C^a). Also listed are calculated losses ("-") values) and gains ("+" values) graphically represented in Figure 5.21.

		C ^o	C ^a	$\Delta C_i/C_i^o$
MAJORS (%)	P ₂ O ₅	0.12	0.18	+0.5
	MnO	0.20	0.25	+0.3
	K ₂ O	0.64	0.80	+0.2
	TiO ₂	1.29	1.68	+0.3
	H ₂ O	3.93	2.44	-0.4
	CO ₂	4.01	10.91	+1.7
	Na ₂ O	4.37	3.97	-0.1
	MgO	5.79	4.74	-0.2
	CaO	7.24	7.21	+0.0
	LOI	7.37	12.39	+0.7
	Fe ₂ O ₃	9.80	11.50	+0.2
	Al ₂ O ₃	15.83	11.90	-0.2
	SiO ₂ /10	4.81	4.23	-0.1
	Mg#/10	5.16	3.85	-0.3
TRACES (ppm) Au (pph)	Au/1000	0.16	4.43	+26.7
	Ta	0.83	0.45	-0.5
	As/1000	0.98	13.00	+12.3
	S/1000	1.85	14.17	+6.7
	Cs	3.82	3.22	-0.2
	K/1000	5.33	6.62	+0.2
	Hf	5.36	2.41	-0.6
	Nb	6.07	5.11	-0.2
	Ph	6.65	3.86	-0.4
	Ti/1000	7.74	10.06	+0.3
	Ba/10	18.60	14.70	-0.2
	Ga	19.20	21.64	+0.1
	Cr/10	20.70	26.40	+0.3
	Sr/10	21.60	15.30	-0.3
	Sb	22.05	67.75	+2.1
	V/10	22.70	19.50	-0.1
	Rb	24.99	27.39	+0.1
	Sc	37.01	35.06	-0.1
	Y	41.55	51.41	+0.2
	Co	47.07	50.89	+0.1
	Li	51.66	25.29	-0.5
Cl	54.24	36.46	-0.3	
W	56.64	118.26	+1.1	
Cu	61.15	43.08	-0.3	
Zn	71.45	90.40	+0.3	
REES (ppm)	Lu	0.43	1.39	+2.2
	Tm	0.44	1.39	+2.2
	Tb	0.61	1.99	+2.3
	Ho	0.98	3.08	+2.1
	Eu	1.09	3.23	+2.0
	Pr	1.98	7.12	+2.6
	Yb	2.79	9.13	+2.3
	Sm	3.01	9.68	+2.2
	Er	3.02	9.45	+2.1
	Gd	3.93	12.30	+2.1
	Dy	4.46	14.62	+2.3
	La	5.50	20.34	+2.7
	Nd	9.57	33.70	+2.5
	Ce	13.97	50.29	+2.6

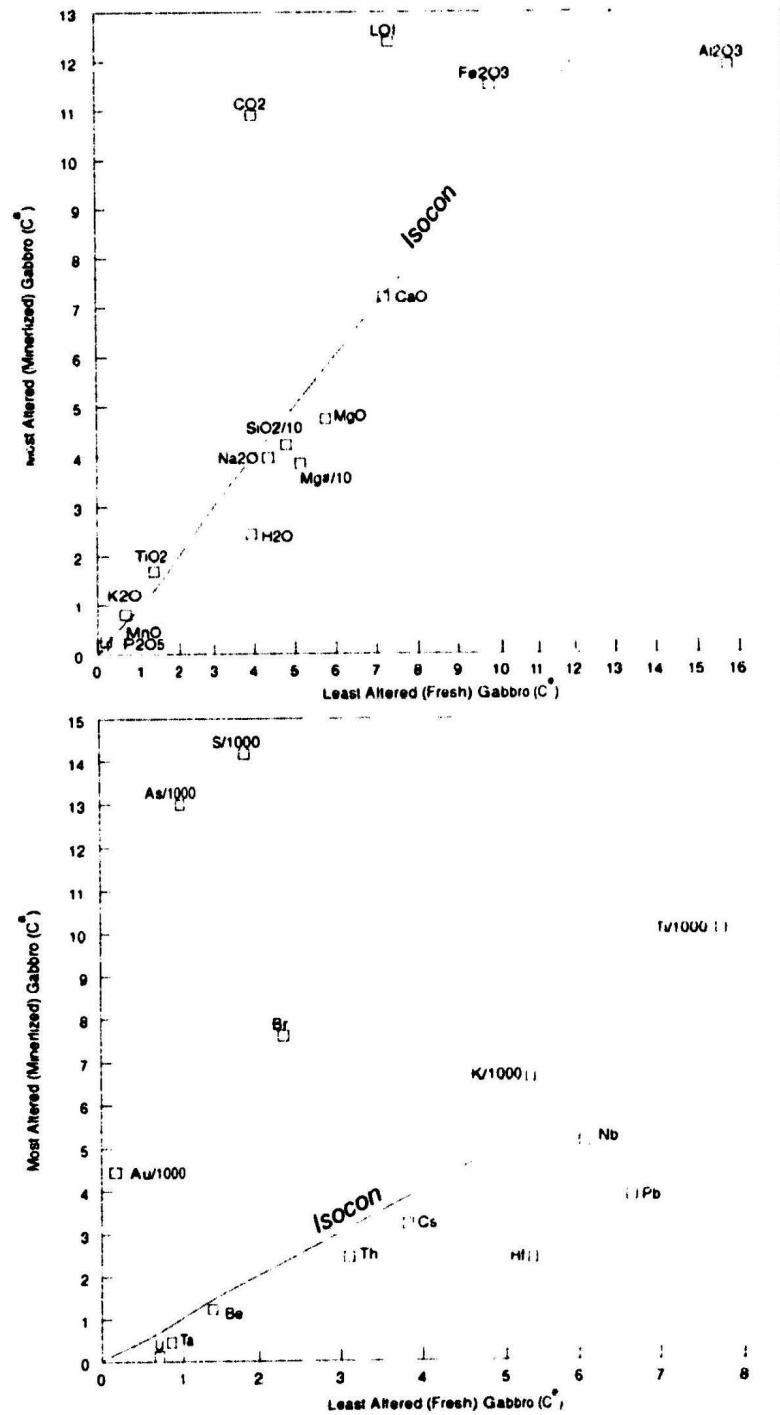


Figure 5.20: Isocon diagrams for average analyses of unaltered gabbro and mineralized gabbro. Oxides plotted as weight percent, trace elements as ppm, Au as ppb. Also plotted are lines of constant volume (isocon - refer to text for discussion).

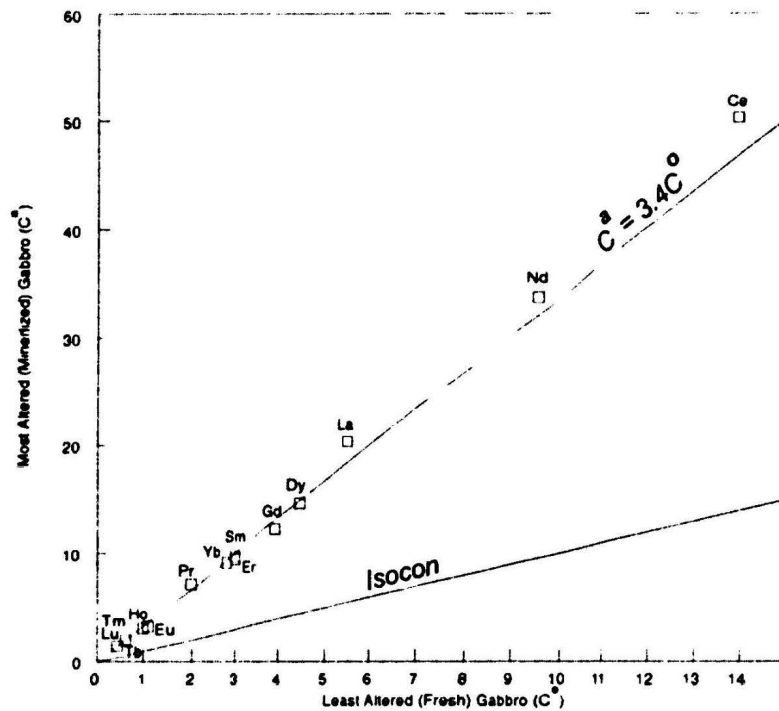
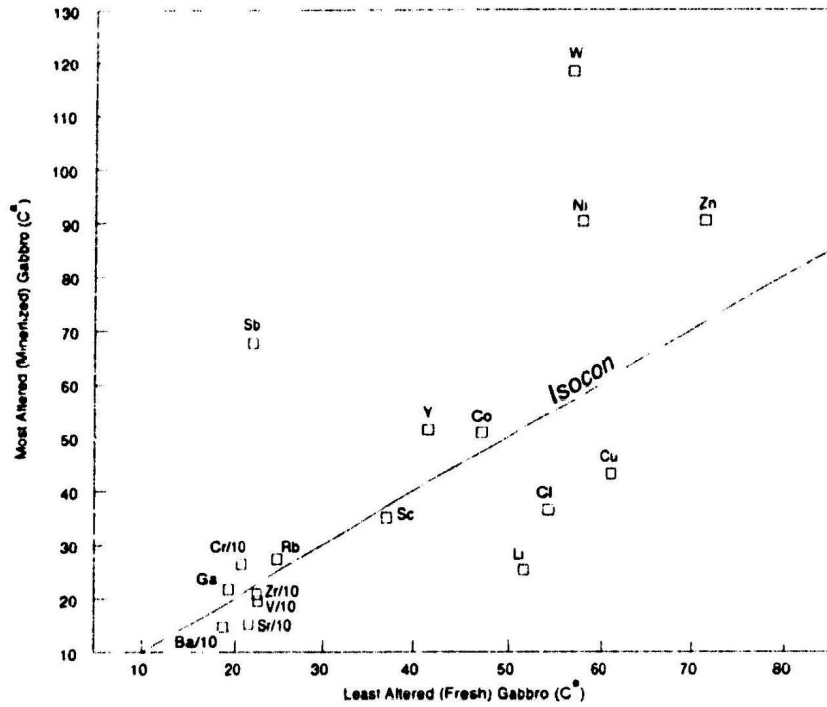


Figure 5.20 (continued): Note that the isocon diagram for the REE (lower diagram) suggests that there has been a 3.4x increase in relative concentration between unaltered and mineralized rocks corresponding to a volume decrease of -71%.

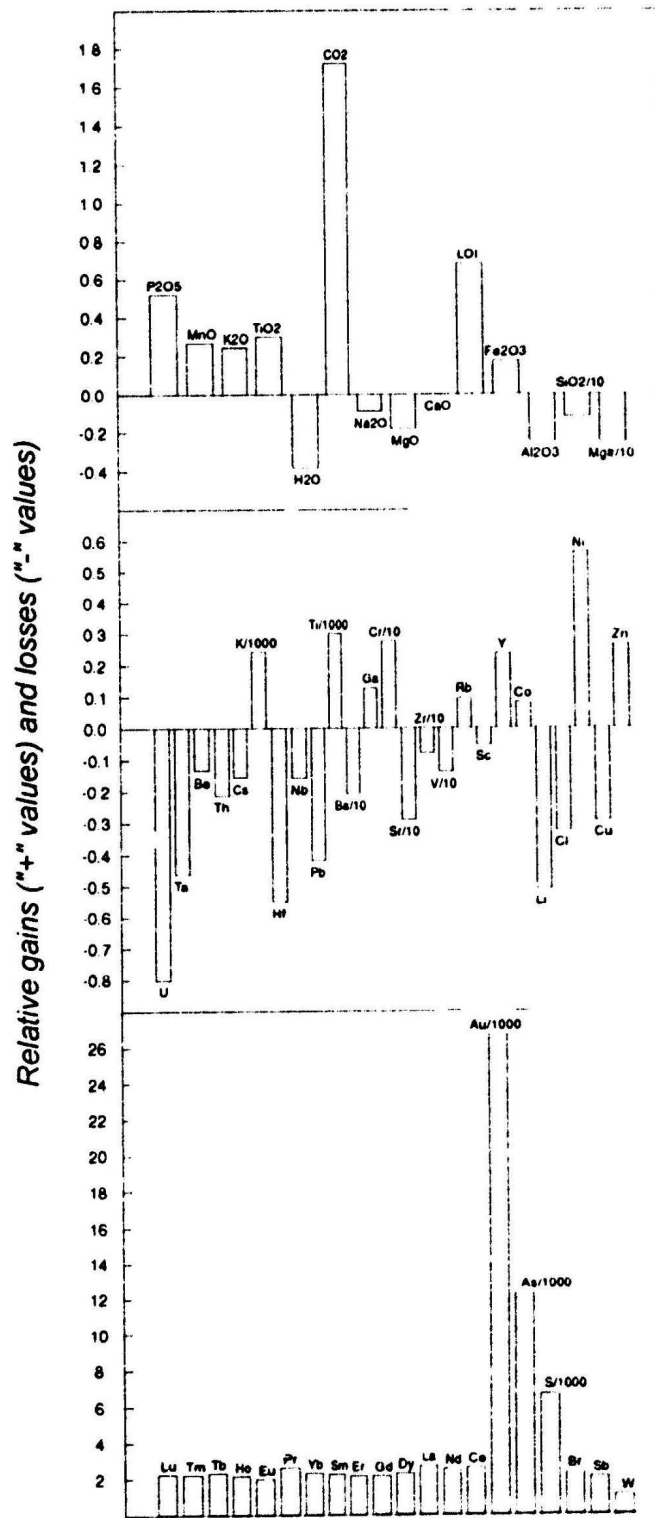


Figure 5.21: Relative gains ("+" values) and losses ("- values) calculated using the technique of Grant (1986) for changes observed between gabbros of the GMA- and M-Zones. Refer to text for discussion.

Figure 5.20 depicts the isocon diagrams constructed for the averaged data sets. The first diagram is that for the major oxides which illustrates little variation in relative concentration with the exception of CO_2 and Fe_2O_3 which exhibit apparent gains and Al_2O_3 and MgO exhibit apparent losses. The apparent loss of Al_2O_3 , generally assumed to be an immobile element, is a little baffling since elements easily mobilized such as CaO remain constant, but the result can be explained on the basis of mineralogical changes observed in the M-Zone. The M-Zone is characterized by the breakdown of Ca,Mg-silicates and the concomitant formation of Ca,Mg-carbonates which dominate the mineralogy in the zone. It is feasible that Al is "flushed" out of the mineralized zone explaining the loss since the amount of aluminous phases forming contemporaneously with the carbonate minerals is limited.

The second isocon diagram depicts some of the trace element variations between altered and unaltered gabbros. Large gains can be observed in Au, As, S, Br, K and Ti. These increases are expected since they define the potassic alteration domains of the mineralizing system as well as the ore metals themselves. Losses can be observed in U, Ta, Be, Th, Ca, Hf, Nb and Pb.

The third diagram is for trace elements. Major increases in Sb, W, Ni and Zn are observed while losses of Li, Cl, Cu, Ba, Sr, V and Zr are present. These gains and losses support the mineralizing character of the system as well as the lithophile element behaviour during alteration.

The fourth isocon diagram is that for the REE. As can be seen, the REE lie

along a best fit line which is approximately 3.4x the unaltered compositions. Since the REE patterns for rocks of the GMA- and M-Zones show that there was no major fractionation of REE with alteration, it is inferred that the 3.4x isocon defines the amount of volume loss in the mineralized zone. The volume loss calculation is as follows:

$$\begin{aligned} \text{Volume Loss} &= [(m_c/m_v)-m_c]*100 \\ &= [(1/3.4)-m_c]*100 \\ &= -71\% \end{aligned}$$

where, m_c is the slope of the constant volume isocon:
and, m_v is the slope of the volume decrease isocon.

This estimate for volume loss seems a little excessive and may be partially explained by the high water to rock ratios at the loci of the alteration zones, which may have been large enough to facilitate extreme volume loss.

Although valid, this is still not an acceptable explanation for the -71% volume decrease. The term "volume" insinuates a three dimensional area, but in the case of alteration studies, volume increase/decrease does not necessitate a physical change in dimensions of the rock undergoing alteration. Gresens (1967) and Grant (1986) stated that a relationship exists between volume and mass as given below:

$$\frac{M^a}{M^o} = \frac{V^o}{V^a} \times \frac{\rho^a}{\rho^o}$$

where,

M^a = mass of altered sample

M^o = mass of unaltered (original) sample

V^a = volume of altered sample

V^o = volume of unaltered (original) sample

ρ^a = density of altered sample

ρ^o = density of unaltered (original) sample

On this premise it is feasible that the volume loss calculated above may be more a reflection of a density and mass loss whereby denser Ca,Mg-silicates such as pyroxene, chlorite and epidote, as well as magnetite, were destroyed and replaced by much less dense carbonates and K-silicates such as sericite. Density measurements performed on representative samples from each zone shows that there are density differences. Average density values of 2.59 g/cm³ for GMA-Zone samples (n=6) , 2.56 g/cm³ for A-Zone samples (n=5) and 2.50 g/cm³ for M-Zone samples (n=6) reaffirm the supposition stated above.

This combination of mass-density change as well as physical dimensional changes in the host rock may explain the large calculated volume decreases.

5.3.6 Microthermometry

A total of 26 microthermometric measurements were performed on a set of 14 representative samples to (1) assess the physico-chemical parameters of the mineralizing fluid such as temperature and composition, including salinity and dissolved gas content, and (2) to characterize fluid evolution through the increasing water to rock ratios as observed in the transition from the GMA-Zone to M-Zone. The defined temperature constraints are then used in conjunction with isotopic analyses to calculate the probable isotopic composition of the fluid.

Three petrographic types were examined for the presence of primary fluid inclusions, including (1) alteration minerals such as carbonate and quartz that are either

Plate 5.19: Reflected light photomicrograph of understaturated two phase $H_2O(l)-H_2O(v)$ (Type I) inclusions associated with A-Zone alteration phases. This type has lower T_h 's and salinities than Type IV inclusions. Inclusions measure 8μ across.

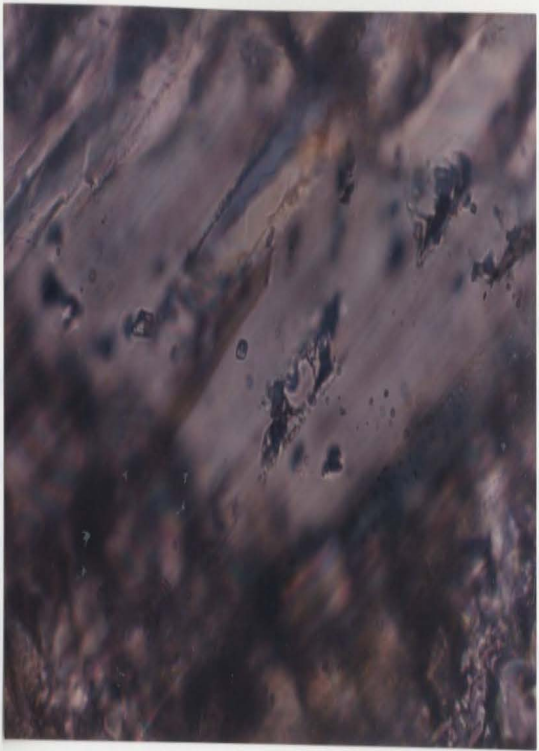
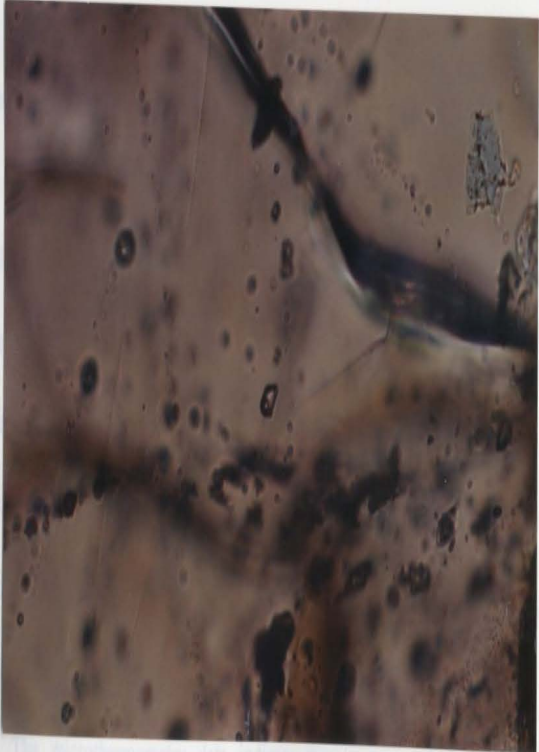


Plate 5.20: Reflected light photomicrograph of three phase $CO_2(l)-CO_2(v)-H_2O(l)$ (Type IV) inclusions associated with M-Zone alteration phases and mineralized quartz veins. Inclusion measures 10μ across.



Tables 5.11 to 5.13 list the data obtained from the fluid inclusions. Table 5.11 has brief descriptions of the samples from which fluid inclusion data were obtained.

The microthermometry data indicate some groups which are presented in

discreet minerals or intergrowths in M-Zone gabbros (MZ), (2) mineralized quartz-carbonate veins cutting M-Zone gabbros (MQV), and (3) patches of quartz and carbonate in A-Zone gabbros (AZ).

Two different inclusion types were documented in the samples which could be described as Types I and IV following the nomenclature of Dunne (1992), Reynolds (1990) and Nash (1976). Type I inclusions are undersaturated two phase ($H_2O(l)$ - $H_2O(v)$) inclusions (Plate 5.19) whereas Type IV inclusions are CO_2 -bearing containing $CO_2(l)$ - $CO_2(v)$ - $H_2O(l)$ (Plate 5.20) that are associated with the most intensely altered rocks.

Tables 5.11 to 5.13 list the data obtained from the fluid inclusions. Table 5.11 has brief descriptions of the samples from which fluid inclusion data were obtained. Table 5.12 lists the microthermometric data and Table 5.13 contains the calculated volumetric, density and molar compositional data for the inclusions.

Primary inclusions of both types are rare and are usually present in large isolated crystals. The inclusions have negative crystal morphology and occur, in growth rings within quartz, or along grain edges in carbonates. Secondary and pseudosecondary inclusions are much more abundant, extremely small ($<4\mu$), and occur along fracture planes and healed fracture planes. cursory observations indicate that some of these inclusions are younger and record a fluid(s) event different from the alteration and mineralization event.

The microthermometry data indicate three groups which are presented in

histogram form on Figure 5.22. Homogenization temperatures (T_h) in AZ (A-Zone) inclusions are lower than those of MZ (M-Zone) samples and the MQV (mineralized quartz vein) inclusions record intermediate T_h 's. The changes in T_h correlate with changes in the alteration assemblages as well as with the decreasing water/rock ratios envisioned for the alteration zonation. T_h is not a true representation of the formation trapping temperature (T_f) which must be calculated from T_h after correcting for pressure effects (Reynolds, 1990; Roedder, 1984). The calculated trapping temperatures (Table 5.12) indicate that the ore fluids range from 314-346°C while mineralized quartz veins formed in the temperature range 272-281°C and the temperature of wall rock alteration, distal to the shear zones, was in the range of 193-250°C. This shift in T_f is to be expected since the zones distal to the shear zones developed later and as a result the fluid probably would have cooled before reaching these areas.

The T_f closely approximates the T_h since T_f was calculated on the basis that the fluid was trapped at 2.0 kbar. This estimate of pressure was chosen since it correlates with peak metamorphic conditions of 2.5-3.5 kbar that was exerted upon rocks of the Mount Cormack Subzone (Deveau, 1992) southwest of the Duder Lake area. This area appears to have had a slightly higher grade of metamorphism than rocks at Duder Lake, thus the conservative pressure estimate of 2.0 kbar. Since mineralization is coincident with metamorphism, the pressure estimate of 2.0 kbars should be appropriate to reflect the conditions during the mineralizing event.

The fluid salinity also changes with increasing distance from the shear zone.

Table 5.11: Fluid inclusion sample descriptions. Abbreviations: MZ = M-Zone gabbro, MQV = mineralized quartz veins and AZ = A-Zone gabbro.

Sample	Litho	Description
DL3-91-08	AZ	Several Type I primary inclusions ranging in size from 1-2 μ up to 6 μ in coarse-grained carbonate vein cutting gabbro. Vein appears to post-date foliation. Numerous secondary inclusions present <2 μ in size are also present.
DL3-91-09	AZ	Type I primary inclusions hosted by calcite veins cross-cutting mineralized gabbro. Largest inclusions measure 8 μ .
DL5-91-06	AZ	Primary Type I inclusions from silicified zone in strongly altered gabbro. Primary inclusions are few and have sizes ranging from 6-8 μ .
DL5-91-09	MZ	One large (8 μ) Type IV inclusion from silicified area of mineralized gabbro. Three-phases observed indicating inclusion is CO ₂ -rich.
DL6-91-05	MZ	Coarse-grained, quartz-carbonate vein cutting gabbro and associated with sulphides. Vein contains several generations of small secondary inclusions and few good primary inclusions.
DL6-91-01	AZ	Several primary Type I inclusions up to 8 μ in size in calcite vein cutting gabbro.
DL7-91-01	AZ	Calcite vein cutting gabbro and which hosts abundant small primary and secondary Type I inclusions. Some larger primary inclusions (up to 8 μ) also present.
DL7-91-07	MZ	Syn-mineralization quartz-carbonate vein in gabbro with small (4 μ) Type IV inclusions occurring in growth rings in a euhedral quartz grain.
DL8-91-08	MZ	Small Type IV primary inclusions (4 μ) in silicified patch associated with sulphides in gabbro.
DL8-91-09	MZ	Large (8-10 μ) primary Type IV inclusions from silicified zone in mineralized gabbro. Silicified patch also contains abundant sulphides.
DL8-91-12	AZ	Quartz vein in gabbro containing abundant secondary inclusions along fracture planes as well as a couple of 8 μ Type I inclusions.
RC-91-31B	MZ	Gossanous quartz vein in mineralized gabbro containing several generations of secondary inclusions. Large subhedral quartz grain in vein hosts primary Type IV inclusions up to 6 μ in size.
RC-91-56	AZ	Barren quartz vein in altered siltstone with abundant 8 μ Type I inclusions.
DW-90-60	MQV	Mineralized, shear-controlled, quartz-carbonate vein containing numerous primary Type IV inclusions ranging in size from 4-10 μ . The best inclusions are associated with growth rings in euhedral quartz grains.

Table 5.12: Microthermometry data from fluid inclusions in quartz, calcite, and ankerite from variably altered gabbros and from quartz veins.

Sample	Litho ¹	Type ²	Host ¹	Size μ	T _{mCO₂} (°C)	T _{mice} (°C)	T _{mchl} (°C)	T _{hCO₂} (°C)	T _h (°C)	T _i ³ (°C)	wt. % NaCl ⁴
DL5-91-09	MZ	IV	qtz	8	-55.1	-2.9	8.4	25.5	315.7	322	3.6
DL6-91-05	MZ	IV	ank	10	-55.9	-3.4	8.2	23.3	320.3	327	3.9
DL7-91-07	MZ	IV	qtz	4	-55.6	-4.5	6.8	28.2	329.3	336	6.7
DL8-91-08	MZ	IV	qtz	6	-54.2	-3.8	7.6	26.6	335.7	343	5.3
DL8-91-09	MZ	IV	qtz	10	-53.7	-3.4	7.2	26.6	316.1	324	5.8
	MZ	IV	qtz	10	-51.2	-2.8	7.8	26.4	305.7	314	4.9
	MZ	IV	qtz	10	-53.8	-3.4	8.3	26.2	313.2	320	3.8
	MZ	IV	qtz	8	-50.8	-2.6	6.8	26.4	315.3	321	6.7
RC-91-31B	MZ	IV	qtz	6	-56.4	-3.7	8.2	26.2	340.8	346	3.9
	MZ	IV	qtz	6	-56.1	-2.4	7.9	26.1	339.3	345	5.0
DW-90-60	MQV	IV	qtz	10	-52.1	-3.0	7.6	25.8	274.3	281	5.3
	MQV	IV	qtz	8	-53.4	-4.8	8.6	25.3	266.8	272	3.2
	MQV	IV	qtz	6	-54.4	-4.2	8.4	25.6	268.3	273	3.6
	MQV	IV	qtz	8	-55.6	-3.4	7.1	25.2	270.1	276	5.7
	MQV	IV	qtz	4	-53.2	-4.4	6.9	27.6	272.2	276	6.6
	MQV	IV	qtz	6	-51.9	-4.9	6.5	25.4	270.9	275	6.3
DL3-91-08	AZ	I	cal	6	-	-0.4	-	-	210.0	213	0.7
	AZ	I	cal	6	-	-0.2	-	-	195.6	201	0.4
DL3-91-09	AZ	I	cal	8	-	-0.2	-	-	217.4	220	0.4
	AZ	I	cal	8	-	-0.4	-	-	217.7	220	0.7
DL5-91-06	AZ	I	qtz	8	-	-0.3	-	-	246.2	250	0.5
	AZ	I	qtz	6	-	-0.5	-	-	237.8	242	0.9
DL6-91-01	AZ	I	qtz	8	-	-0.2	-	-	225.3	229	0.4
DL7-91-01	AZ	I	cal	8	-	-0.8	-	-	188.8	193	1.4
DL8-91-12	AZ	I	qtz	8	-	-0.4	-	-	205.3	210	0.7
RC-91-56	AZ	I	qtz	8	-	-0.6	-	-	195.8	200	1.1

NOTES

Abbreviations: T_{mCO₂} = melting temperature of CO₂(s); T_{mice} = melting temperature of H₂O(s); T_{mchl} = melting temperature of clathrate (CO₂ · 5.75H₂O(s)); T_{hCO₂} = homogenization temperature of CO₂(g); T_h = homogenization temperature of CO₂(l) to CO₂(g) or H₂O(g) to H₂O(l); T_i = trapping temperature; wt. % NaCl = weight percent of all dissolved brines expressed as weight percent NaCl equivalent.

¹Refers to host rock lithology: MZ = M-Zone gabbro, MQV = mineralized quartz vein, AZ = A-Zone gabbro. Host is the mineral (or alteration mineral in the case of gabbros) containing the fluid inclusion which was analyzed.

²Classification of fluid inclusions based on observed phases at room temperature after Dunne (1992), Reynolds (1990) and Nash (1976).

³Pressure corrected temperature of formation and fluid entrapment (after Reynolds, 1990) assuming pressure of formation of 2 kbars (refer to text for discussion).

⁴Fluid salinity calculated using Reynolds' (1990) techniques for Type I inclusions and Collins' (1979) methodology for Type IV inclusions.

Table 5.13: Volumetric, density and molar compositional data for fluid inclusions.

Sample	Litho ¹	Type ²	Volumetric Proportions (%) ³				ρ^4 (g/cm ³)	Molar Composition ⁵		
			CO ₂ (l)	CO ₂ (g)	H ₂ O (l)	H ₂ O (g)		X _{CO2}	X _{H2O}	X _{NaCl}
DL5-91-09	MZ	IV	50	10	40	-	0.83	0.589	0.239	0.172
DL6-91-05	MZ	IV	50	10	40	-	0.83	0.586	0.238	0.176
DL7-91-07	MZ	IV	50	10	40	-	0.83	0.574	0.233	0.193
DL8-91-08	MZ	IV	50	10	40	-	0.83	0.579	0.235	0.186
DL8-91-09	MZ	IV	50	10	40	-	0.83	0.577	0.234	0.189
	MZ	IV	55	10	35	-	0.85	0.605	0.221	0.174
	MZ	IV	50	10	40	-	0.83	0.587	0.238	0.175
	MZ	IV	40	10	50	-	0.80	0.537	0.256	0.208
RC-91-31B	MZ	IV	50	10	40	-	0.83	0.586	0.238	0.176
	MZ	IV	50	10	40	-	0.83	0.580	0.235	0.185
DW-90-60	MQV	IV	30	10	60	-	0.75	0.512	0.278	0.210
	MQV	IV	30	10	60	-	0.75	0.528	0.286	0.186
	MQV	IV	35	10	55	-	0.78	0.536	0.274	0.189
	MQV	IV	40	10	50	-	0.80	0.543	0.259	0.199
	MQV	IV	30	10	60	-	0.75	0.507	0.275	0.219
	MQV	IV	40	10	50	-	0.80	0.538	0.257	0.206
DL3-91-08	AZ	I	-	-	80	20	0.86	-	0.682	0.318
	AZ	I	-	-	85	15	0.87	-	0.758	0.242
DL3-91-09	AZ	I	-	-	85	15	0.85	-	0.758	0.242
	AZ	I	-	-	85	15	0.85	-	0.689	0.311
DL5-91-06	AZ	I	-	-	85	15	0.80	-	0.730	0.271
	AZ	I	-	-	80	20	0.83	-	0.654	0.346
DL6-91-01	AZ	I	-	-	85	15	0.84	-	0.758	0.242
DL7-91-01	AZ	I	-	-	90	10	0.89	-	0.622	0.378
DL8-91-12	AZ	I	-	-	85	15	0.86	-	0.689	0.311
RC-91-56	AZ	I	-	-	85	15	0.87	-	0.639	0.361

NOTES

¹Refers to host rock lithologies: MZ = M-Zone gabbro, MQV = mineralized quartz vein, AZ = A-Zone gabbro.

²Inclusion classification: Type I(H₂O-NaCl), Type IV(CO₂-H₂O-NaCl).

³Volumetric proportions based on observed phases contained within inclusions at 25°C.

⁴Density (g/cm³) graphically estimated for Type I inclusions and calculated from volumetric proportions for Type IV inclusions.

⁵Molar compositions for CO₂, H₂O and NaCl calculated from volumetric proportions.

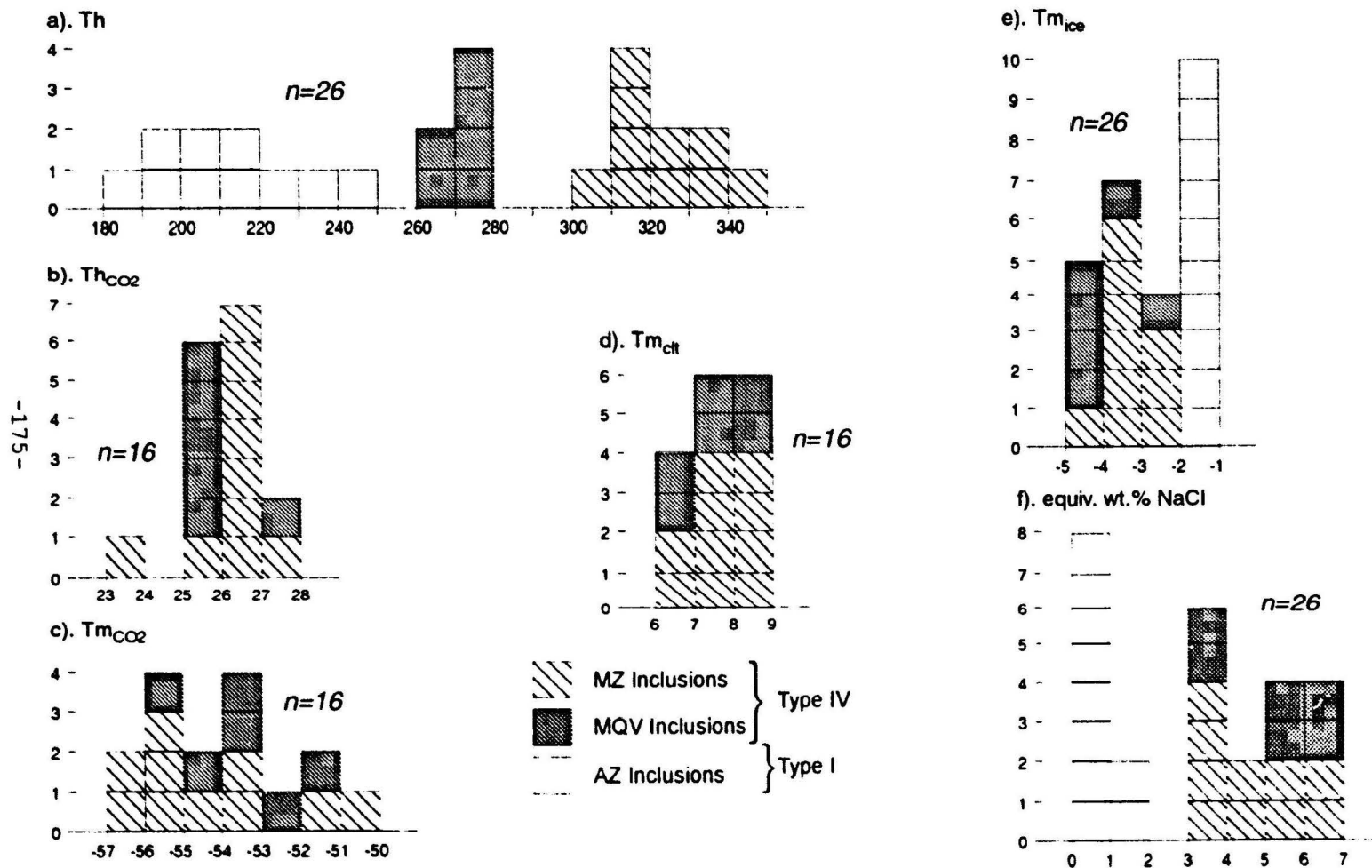


Figure 5.22: Histograms of thermometric data collected from $H_2O(l)-H_2O(v)$ (Type I) and $CO_2(l)-CO_2(v)-H_2O(l)$ (Type IV) inclusions using heating and freezing experiments. All temperatures are in degrees celsius. Refer to text for discussion.

Inclusions from veins and alteration phases of the M-Zone have salinities from 3.2 to 6.7 equivalent wt. % NaCl. In contrast, salinities for the AZ inclusions are in the range from 0.4 to 1.4 equivalent wt. % NaCl. The salinity shift is a reflection of fluid evolution due to wall rock interaction.

The presence of three phases in Type IV inclusions at room temperature, attests to the presence high CO₂ concentrations in the inclusions. According to Roedder (1984), two component inclusions (ie. Type IV, CO₂-H₂O), if excess CO₂ is present, should solidify at -56.6°C. However, the T_{mCO₂} data for the Duder Lake inclusions fall in the range -50.8 to -56.4°C, suggesting that either there may not be supersaturation of CO₂ or that dissolved gases such as CH₄ and N₂ are present which would depress the freezing temperatures of the CO₂ fluid (Zhang *et al.*, 1989). The presence of these gases is common in many mesothermal deposits especially when high concentrations of CO₂ is present in the inclusions (Dunne, 1992).

Estimates of fluid composition have been calculated for each inclusion studied and are tabulated in Table 5.13. Type IV inclusions molar concentrations of 50% molar CO₂, 30% H₂O and 20% NaCl. This contrasts with the compositional data for Type I inclusions which have calculated molar concentrations in the range of 70% H₂O and 30% NaCl. The loss of CO₂ from the fluid phase was the result of intense carbonatization of the wall rock proximal to the shear zones. Since no CO₂ is present in the Type I inclusions, the salinity calculated is much higher than that calculated for Type IV inclusions implying the presence of a second fluid. Similarly, the large variation in CO₂

and NaCl contents between the MZ and AZ inclusion types (Figure 5.23) would suggest that there may have been unmixing of a homogeneous CO₂-H₂O fluid to produce two fluids (one rich in CO₂ and the other rich in H₂O), a common feature of lode gold deposits (Robert and Kelly, 1987; Wood *et al.*, 1986; Walsh *et al.*, 1984; Ho *et al.*, 1985). However, fluid inclusion relationships and microthermometry data from the Duder Lake samples refute the notion that unmixing produced two fluids. Since coeval primary Type I and Type IV primary inclusions reflecting the mineralizing event never occurred together, it supports the notion of a homogeneous fluid. In addition, constant liquid to vapour ratios of both Type I and IV inclusions suggest trapping of a homogeneous fluid (Roedder, 1984) as does consistent CO₂ contents (Zhang *et al.*, 1989).

The data derived from the study of fluid inclusions in Duder Lake are compatible with data collected for mesothermal lode gold deposits elsewhere, namely studies by Robert and Kelly (1987); Wood *et al.* (1986); Walsh *et al.* (1984); Walsh *et al.* (1988); Ho *et al.* (1985); Coveney (1981); Goldfarb *et al.* (1986); Goldfarb *et al.* (1988); Smith and Kessler (1985); Lattanzi *et al.* (1989); Lattanzi (1991); Weir and Kerrick (1987). Dunne (1992) compiled the most recent fluid inclusion data for several deposit types and delineated fields for these deposit types on the basis of homogenization temperatures and equivalent wt.% salinity. The resulting diagram with Duder Lake data comprises Figure 5.24; MZ and MQV inclusions plot within the mesothermal gold field whereas the AZ inclusion data define an array spreading away from the mesothermal box towards lower homogenization temperatures.

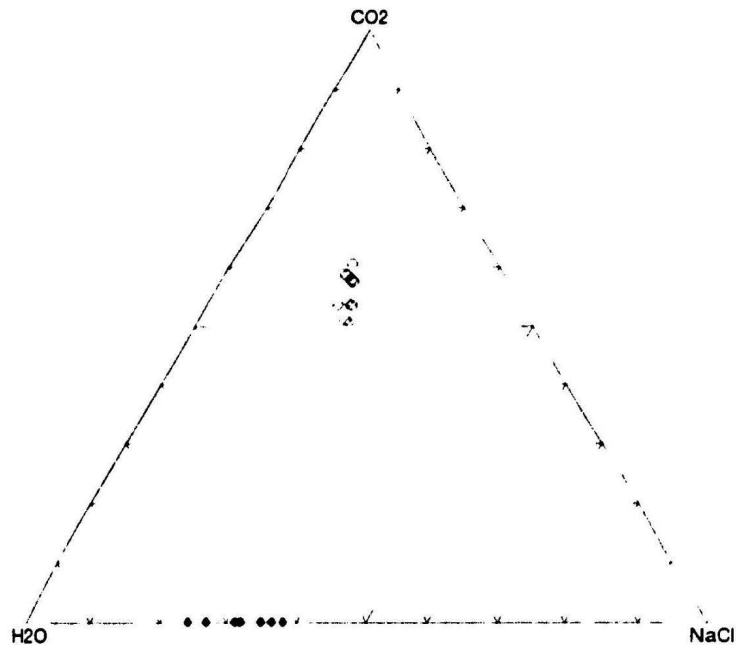


Figure 5.23: H₂O-CO₂-NaCl ternary diagram for calculated molar compositions for fluid inclusions. Symbols signify fluid inclusions from M-Zone gabbros (hollow circles), mineralized quartz veins associated with M-Zone gabbros (hollow diamonds) and unmineralized veins associated with distal alteration (solid diamonds).

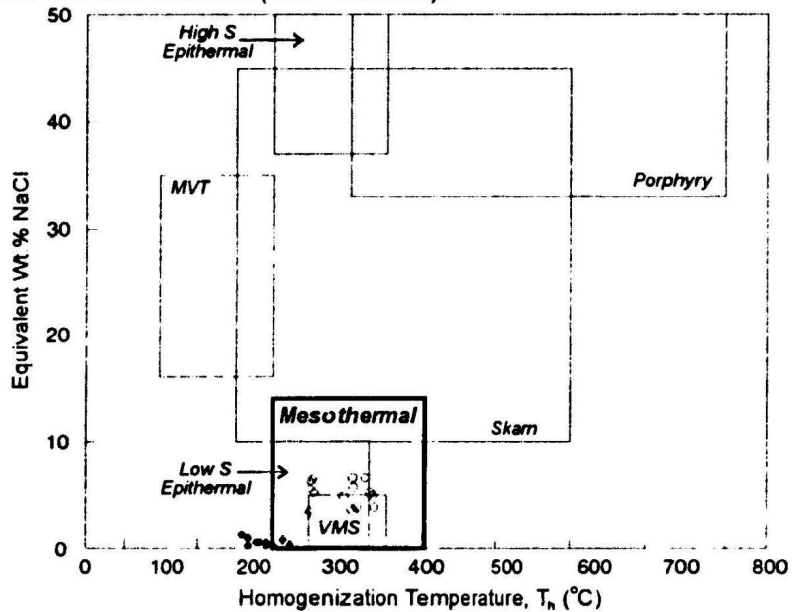


Figure 5.24: Equivalent Wt.% NaCl versus homogenization temperature plot for microthermometric data from the Duder Lake gold occurrences. Fields represent ranges in microthermometry data for Mississippi Valley type (MVT) deposits, volcanogenic massive sulphides (VMS), high and low sulphidation epithermal systems, skarn deposits, porphyry style mineralization and mesothermal gold deposits. Symbols as per Figure 5.23. Diagram modified from Dunne (1992).

To summarize, inclusions from three different alteration domains were collected from Duder Lake to ascertain fluid compositions as well as to characterize fluid evolution due to progressive host rock - hydrothermal fluid interaction. In decreasing order of homogenization temperatures and CO₂ contents are the MZ, MQV and AZ inclusions. This progression also signifies spatial and temporal change with respect to the loci of the alteration and mineralization system. Mineralization appears to have been related to a CO₂-rich fluid of moderate salinity at temperatures between 300-350°C while mineralized quartz veins formed at slightly lower temperatures between 250-300°C. More distal areas altered during the same event record temperatures between 200-250°C by a fluid having low CO₂-content and salinity. These findings are analogous to those for numerous mesothermal lode gold deposits worldwide.

5.3.7 Stable Isotope Studies

Samples were selected for stable isotope analyses to help ascertain probable fluid source and composition. A total of 9 samples known to contain abundant carbonate minerals (ie. ankerite or calcite) were analyzed for $\delta^{13}\text{C}$ (reported relative to PDB). In addition, these samples were also analyzed for their $\delta^{18}\text{O}$ content (reported relative to SMOW). One sample of quartz syngenetic with the ankerite was analyzed for its $\delta^{18}\text{O}$ content to ascertain if the carbonates equilibrated with the ore fluids. Eleven sulphur isotope determinations were performed on pyrite and arsenopyrite separates to obtain $\delta^{34}\text{S}$ (reported relative to CDT).

The isotopic data are reported as delta (δ) values in units of per mil (‰) relative to the isotopic standard using the following equation:

$$\delta_{\text{sample}} = \frac{(\text{HI/LI})_{\text{sample}} - (\text{HI/LI})_{\text{standard}}}{(\text{HI/LI})_{\text{standard}}} \times 10^3$$

where, δ_{sample} is the isotopic composition of the sample relative to the isotopic standard and, $(\text{HI/LI})_{\text{sample}}$ is the ratio of the heavy to light isotope of the sample and, $(\text{HI/LI})_{\text{standard}}$ is the ratio of the heavy to light isotope of the standard

5.3.7.1 Carbon and Oxygen Isotopes

Carbon and oxygen isotopes were performed in an effort to characterize the mineralizing fluids. To this end, several lithotypes were collected to ascertain if there were any appreciable shifts in the isotopic signature of the fluid resulting from prolonged water/rock interaction. These sample types include mineralized gabbros of the M-Zone, altered and non-mineralized gabbros of the A-Zone, a sample of fresh gabbro from the GMA-Zone and a quartz-carbonate vein cutting M-Zone gabbro. In all instances, carbonate minerals associated with the particular alteration style were analyzed and the results listed in Table 5.14. The range in $\delta^{13}\text{C}$ is -8.13‰ to -12.55‰ (\bar{x} = -11.07‰, median = -10.34‰, n=9) and the $\delta^{18}\text{O}$ range from 14.57‰ to 16.43‰ (\bar{x} = 15.71‰, median = 15.50‰, n=9). Comparison of $\delta^{18}\text{O}$ and $\delta^{13}\text{C}$ isotopic data in Table 5.14 for ankerite associated with mineralization and calcite developed due to regional metamorphism indicates no appreciable differences in the isotopic signatures, thus

reaffirming the supposition that gold mineralization coincided with the metamorphic event.

Since carbonate minerals such as calcite and ankerite are susceptible to resetting of isotopic ratios, the integrity of the $\delta^{18}\text{O}$ values was checked by obtaining the $\delta^{18}\text{O}$ composition of a syngenetic quartz sample (DL6-91-06). The "heavy" isotopic signature of this quartz, +15.01‰, is in agreement within error with the median $\delta^{18}\text{O}$ value of 15.50‰ for the carbonate minerals and indicates that the carbonates were in equilibrium with the hydrothermal fluid. Since the oxygen isotopic systematics appear to be representative of the hydrothermal event, by way of association, the $\delta^{13}\text{C}$ are also considered to be representative.

On the basis of carbon and oxygen isotope systematics, similar theories on the timing of gold mineralization coinciding with metamorphism and derivation of the fluids during these metamorphic events have been envisioned for gold mineralization in the Juneau Gold Belt/Cordillera (Nesbitt *et al.*, 1989; Goldfarb *et al.*, 1991); Superior Province/Abitibi Belt (Kerrick *et al.*, 1987; Kerrich, 1990); Western Australia (Golding *et al.*, 1988); Meguma Terrane, Nova Scotia (Kontak *et al.*, 1988; Sangster, 1992). Figure 5.25 is a comparison of $\delta^{18}\text{O}$ and $\delta^{13}\text{C}$ data respectively for several lode gold deposits having similarities with the Duder Lake occurrences as well as common isotopic reservoirs. The sources of data for the $\delta^{18}\text{O}$, $\delta^{13}\text{C}$ and $\delta^{34}\text{S}$ values are listed in Table 5.15.

The range in $\delta^{18}\text{O}$ values from 14.57‰ to 16.43‰ for quartz veins, M-Zone

Table 5.14: Stable isotope data from mineralized and non-mineralized samples.¹

<i>Sample</i>	<i>Zone²</i>	<i>Mineral³</i>	<i>Type⁴</i>	$\delta^{13}\text{C}$	$\delta^{18}\text{O}$	$\delta^{34}\text{S}$
DL4-91-19	M	Ank	WR	-11.65	+15.84	-
DL5-91-08	M	Ank	WR	-10.89	+15.68	-
DL6-91-03	M	Ank	WR	-10.98	+16.15	-
DL6-91-09	M	Ank	WR	-12.55	+16.43	-
DL7-91-04	M	Ank	WR	-10.71	+15.57	-
DL3-91-09	A1	Cal	WR	-12.47	+14.57	-
DL7-91-01	GMA	Cal	WR	-11.46	+15.83	-
DL7-91-04	V(M)	Cal	WR	-10.82	+16.19	-
W-90-59B	A1	Cal	MS	-8.13	+15.16	-
DL6-91-06	M	Qtz	MS	-	+15.01	-
DL1-91-10	M	Asp	MS	-	-	-0.01
	M	Py	MS	-	-	+0.72
DL2-91-01	A	Py \pm Asp	MS	-	-	+0.09
DL5-91-05	M	Asp	MS	-	-	+0.66
	M	Py	MS	-	-	+1.04
DL6-91-06	M	Py	MS	-	-	+5.51
DL8-91-12	A	Py	MS	-	-	+1.25
RC-91-31B	MQV	Py	MS	-	-	+0.99
	MQV	Asp	MS	-	-	+0.94
RC-91-61	M	Asp \pm Py	MS	-	-	+0.63
W-90-60	MQV	Py \pm Asp	MS	-	-	+0.37

NOTES:

¹Isotopic data (‰) recorded relative to PDB (carbon), SMOW (oxygen), CDT (sulphur). Oxygen isotopes for ankerite and calcite calculated from fractionation factors.

²Alteration Zonation as follows: M-Zone (M); A-Zone (A,A1); GMA-Zone (GMA); Mineralized quartz vein contemporaneous with M-Zone (MQV); Non-mineralized quartz veins cutting M-Zone gabbros, V(M).

³Mineral used for isotopic analysis: ankerite (ank); calcite (cal); quartz (qtz); arsenopyrite (asp); pyrite (py). Some sulphide samples may not be mono-minerallic due to the presence of fine-grained intergrowths.

⁴Type pertains to the form in which the sample was analyzed: whole rock (WR) sample where carbonates could not be separated from host. Acid digestion liberated gas from carbonates only; mineral separate (MS) in which mineral samples were hand picked.

gabbro samples and A-Zone samples is sufficiently narrow to imply that all three were the product of the same fluid (*c.f.* Nesbitt and Muehlenbachs, 1989). The range of isotopic composition for the Duder Lake samples can be explained on the basis of temperature decrease where a change in 2‰ can be caused by a temperature difference of approximately 100°C. This appears to be a valid explanation since the lightest isotopic composition (14.57‰) corresponds to unmineralized altered gabbro distal to the shear zone while the heaviest value (16.43‰) is that of an mineralized sample taken from the shear zone. A similar explanation can be made for the range in $\delta^{13}\text{C}$ compositions. The mineralized quartz vein possesses an intermediate composition.

Since each lithotype is spatially and temporally linked to the shear zone (which was the fluid conduit), it should follow that the isotopic signatures of both the rock and the calculated signature of the fluid should be different for each zone.

Fluid inclusion evidence shows that the total temperature variation from M-Zone alteration to A-Zone alteration spans a range of 100°C which in itself would effect a change of 2‰. This variation superimposed on diminishing water to rock ratios results in $\delta^{18}\text{O}$ signatures which are different for each zone and that emphasize the fluid evolution during progressive alteration. These results can be observed in Table 5.16.

The calculated compositions of the fluids corresponds with the range of $\delta^{18}\text{O}$ fluid compositions in metamorphic waters (Figure 5.26) and magmatic waters (Kerrick, 1989b). The lack of δD data did not permit the modelling of water/rock interactions which might have further highlighted the isotopic shifts in the system.

Table 5.15: Ranges of $\delta^{18}\text{O}$ and $\delta^{13}\text{C}$ isotopic compositions for selected lode gold deposits and isotopic reservoirs as well as the sources of data.

<i>a). Carbon Isotope Data</i>			
	Max(‰)	Min(‰)	Reference
Duder Lake	-8.13	-12.55	This Study
Cordillera	+2.00	-10.00	Nesbitt et al. (1989)
Abitibi	+0.50	-10.00	Kerrich et al. (1987)
Superior	-0.60	-9.00	Kerrich (1990)
Meguma	-13.50	-24.90	Kontak et al. (1988)
Western Australia	-1.50	-8.70	Golding et al. (1988)
Diamonds	-3.00	-7.00	Kerrich (1990)
Average Continental Crust 1	-7.10		Hoefs (1987)
Average Continental Crust 2	-5.40		Ohmoto and Rye (1979)
Reduced C in Sedimentary and Metamorphic Rocks	0.00	-30.00	Kerrich (1990)
Meteorites	+9.00	-12.00	Field and Fifarek (1985)
Marine Limestone	+4.00	-5.00	Field and Fifarek (1985)
Common Igneous Rocks	+3.00	-10.00	Field and Fifarek (1985)
Hydrothermal CaCO_3	+1.00	-10.00	Field and Fifarek (1985)
Mother Lode	-4.90	-6.60	Taylor (1990)
Mesothermal Gold	-0.50	-8.50	Kerrich (1990)
<i>b). Oxygen Isotope Data</i>			
	Max(‰)	Min(‰)	Reference
Duder Lake (carbonates)	+16.43	+14.57	This Study
Duder Lake (quartz)	+15.01		This Study
Cordillera	+18.00	+13.00	Nesbitt et al. (1989)
Abitibi	+17.80	+6.90	Kerrich et al. (1987)
Superior	+19.00	+10.00	Kerrich (1990)
Meguma	+18.00	+11.00	Sangster (1992)
Western Australia	+15.00	+9.00	Golding et al. (1988)
Juneau Gold Belt	+20.80	+15.20	Goldfarb et al. (1991)
Meteorites	+8.00	+2.00	Field and Fifarek (1985)
Common Igneous Rocks	+12.00	+4.00	Field and Fifarek (1985)
Sedimentary Carbonate	+38.00	+12.00	Field and Fifarek (1985)
Mother Lode	+22.00	+15.00	Taylor (1990)
Mesothermal Gold	+18.00	+10.00	Kerrich (1990)

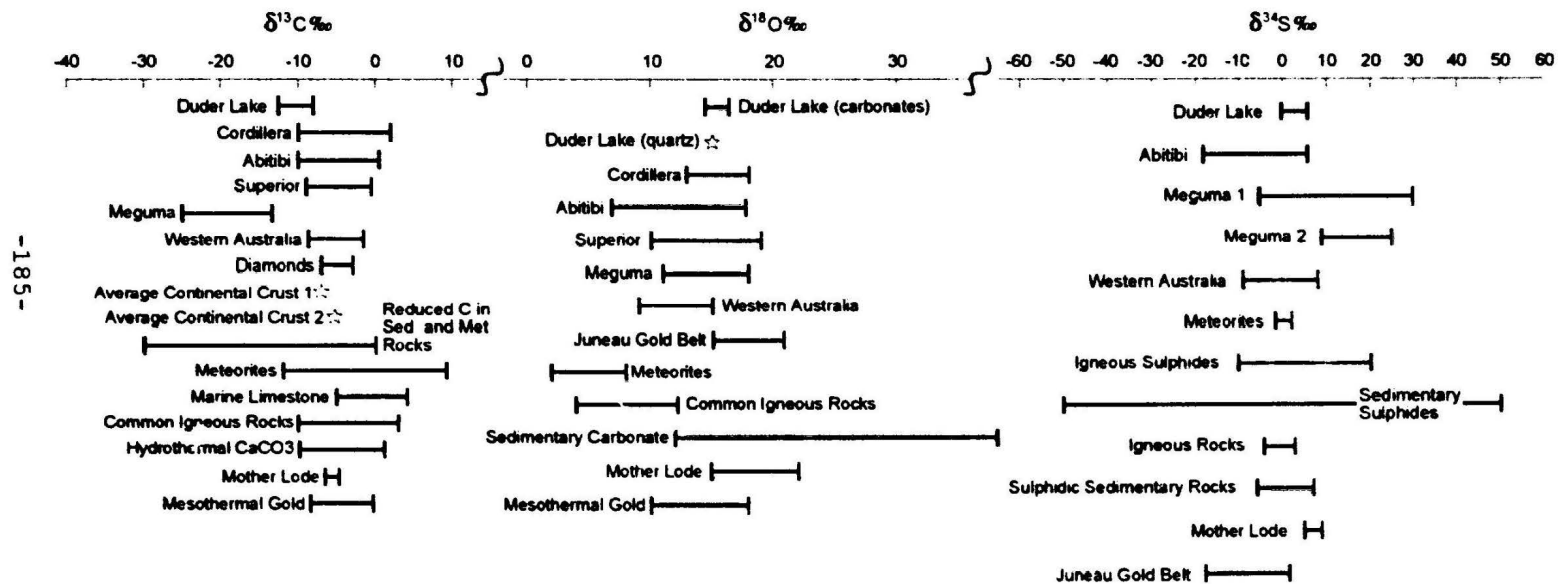


Figure 5.25: Carbon, oxygen and sulfur isotopic compositions for selected isotopic reservoirs as well as for numerous gold deposits which are similar in style to that of the Duder Lake occurrences. Refer to text for discussion and to Tables 5.15 and 5.17 for the isotopic data sources.

Table 5.16: Tabulated $\delta^{18}\text{O}_{\text{H}_2\text{O}}$ values for each of the three lithotypes analyzed, and information used in the calculation.

Lithotype	T(°C)	$1000\ln\alpha_{\text{cal-H}_2\text{O}}$	$\delta^{18}\text{O}_{\text{H}_2\text{O}}(\text{‰})$
M-Zone (MZ)	325	4.38	12.05
MQV	275	5.86	10.33
A-Zone (AZ)	225	7.81	6.76

The $\delta^{13}\text{C}$ systematics suggest that the carbon may have also had a metamorphic origin and the data plot within the fields of other Archean lode gold deposits (Figure 5.27). Patey and Wilton (1993) stated that the $\delta^{13}\text{C}$ compositions of carbonates from the Deer Cove gold deposit, Baie Verte Peninsula, Newfoundland, have a signature which could be either mantle or magmatic but which probably represent a heterogeneous crustal reservoir. Kerrich (1990) has documented similar compositions in the Archean deposits of Ontario and also attributed the light isotopic compositions to a heterogeneous crustal reservoir rather than a mantle/magmatic source, which has a composition of $6 \pm 2\text{‰}$. A similar source of the fluid is envisaged for the Duder Lake gold occurrences.

5.3.7.2 Sulphur Isotopes

A total of eleven sulphur $\delta^{34}\text{S}$ determinations were performed on pyrite and arsenopyrite phases from the main stage mineralization at the Duder Lake occurrences (Table 5.14). The spread of data is quite narrow except for one outlier value of

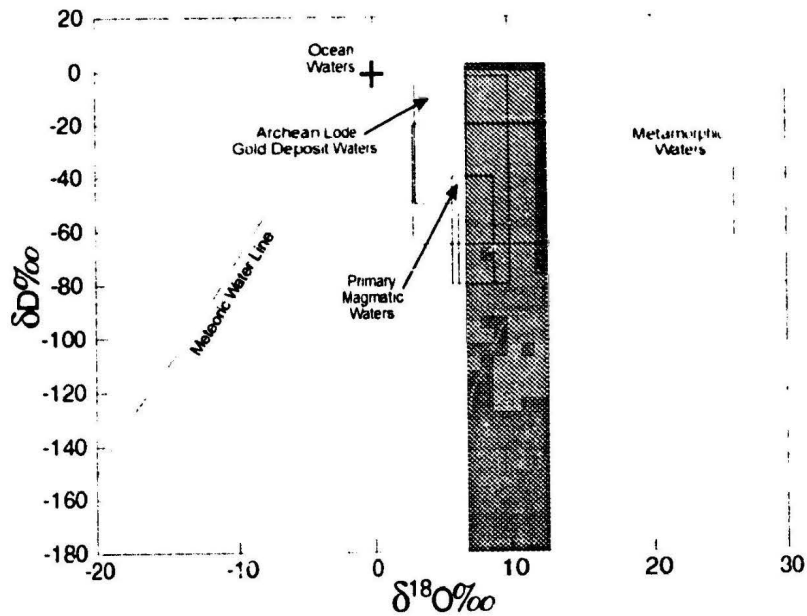


Figure 5.26: Deuterium versus oxygen isotope diagram illustrating the range of ^{18}O data for calculated ore fluids (shaded region). Fields are from Kerrich (1989b).

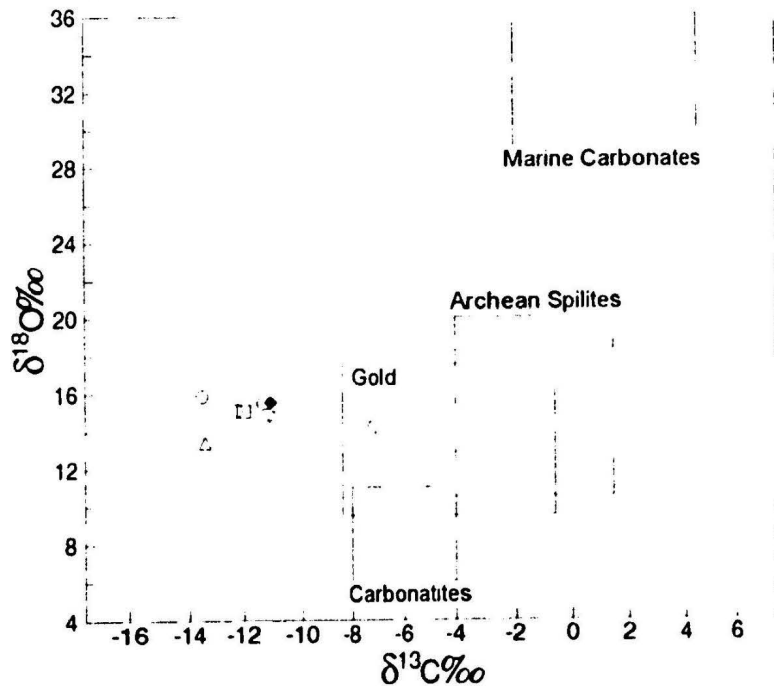


Figure 5.27: Oxygen versus carbon isotope diagram illustrating the range of ^{18}O and ^{13}C values for carbonate minerals. Fields are from Kerrich (1989b). Symbols signify alteration phases analyzed from M-Zone gabbros (open circles), A-Zone gabbros (open triangles), carbonate from the GMA-Zone (open square) and mineralized quartz veins belonging to the M-Zone alteration domain (filled diamond).

+5.51‰. The remaining 10 samples have a range in $\delta^{34}\text{S}$ composition from -0.01 to 1.25‰ (\bar{x} = 0.67‰; median = 0.63‰; n = 10). There are no noticeable differences in the isotopic signatures of those samples dominated either by pyrite or arsenopyrite suggesting that they formed from the same fluid, and any fractionation effects between the two minerals must have been negligible. Comparison of the $\delta^{34}\text{S}$ values from the Duder Lake occurrences with numerous gold deposits and possible sulphur isotope reservoirs is given in Figure 5.25.

Once again samples of different lithotypes were collected and analyzed to elucidate changing fluid composition with progressive alteration. Analyses of the $\delta^{34}\text{S}$ isotopic compositions for the different lithotypes shows that there are minor isotopic differences between samples from the M-Zone (median = 0.52‰), A-Zone (median = 0.67‰) and from mineralized quartz veins (median = 0.68‰). This progression shows that the isotopic signature is becoming heavier with increasing distance from the shear zone with samples from the A-Zone and mineralized quartz veins having similar compositions. The variation is undoubtedly a reflection on increasing ^{34}S fractionation with decreasing temperature. Taking into consideration the changing temperatures in each of the lithotypes, calculations of the isotopic composition of the fluid phase, $\delta^{34}\text{S}_{\text{H}_2\text{S}}$, (using equations from Field and Ficarek, 1985) shows an isotopic zonation as did the $\delta^{18}\text{O}$ calculated fluids and which can be observed in Table 5.18.

The isotopic zonation is a combined water to rock interaction and temperature phenomenon where it can be seen that the isotopes become lighter with decreasing

temperature and water/rock ratio which is a reflection on the temporal difference between distal and proximal alteration.

Table 5.17: Ranges of $\delta^{34}\text{S}$ isotopic compositions for selected lode gold deposits and isotopic reservoirs as well as the sources of data.

<i>Sulphur Isotope Data</i>			
	Max(‰)	Min(‰)	Reference
Duder Lake	+5.51	-0.01	This Study
Abitibi	+6.00	-18.00	Cameron and Hattori (1987)
Meguma 1	+30.00	-5.00	Sangster (1992)
Meguma 2	+25.00	+9.00	Kontak and Smith (1989)
Western Australia	+8.00	-9.00	Kerrick (1989)
Meteorites	+2.00	-1.00	Field and Fifarek (1985)
Igneous Sulphides	+20.00	-10.00	Field and Fifarek (1985)
Sedimentary Sulphides	+50.00	-50.00	Field and Fifarek (1985)
Igneous Rocks	+3.00	-4.00	Field and Fifarek (1985)
Sulphidic Sed. Rocks	+7.00	-6.00	Straus (1986)
Mother Lode	+5.00	+9.00	Taylor (1990)
Juneau Gold Belt	+1.20	-17.80	Goldfarb et al. (1991)

Table 5.18: Tabulated $\delta^{34}\text{S}_{\text{H}_2\text{S}}$ values for each of the three lithotypes analyzed as well as information used in the calculation of the value.

Lithotype	T(°C)	$1000\ln\alpha_{\text{py-H}_2\text{S}}$	$\delta^{34}\text{S}_{\text{H}_2\text{S}}$ (‰)
M-Zone (MZ)	325	1.12	+0.31
MQV	275	1.33	-0.56
A-Zone (AZ)	225	5.35	-4.06

Once again, the isotopic signature cannot be explained by one source (ie.

magmatic or sedimentary). A two end-member source is envisioned for the $\delta^{34}\text{S}$ comprising on the one hand igneous or magmatic sulphur with a dominant component of sedimentary sulphur producing the $\delta^{34}\text{S}$ values that hover about 0‰.

5.3.8 Au - Sulphide Relationships

Although gold has been assayed in high concentrations from both grab and channel samples, at no time could gold be observed using standard petrographical investigation techniques (ie. reflected light microscopy and scanning electron microscopy). This led to the problem of ascertaining the textural and paragenetic relationship of Au with the arsenopyrite and pyrite.

The conclusion reached on the mode of Au mineralization was that it was "invisible" and was more associated to arsenopyrite than pyrite. The lack of visible gold at the Duder Lake occurrences makes it unusual when compared with other gold mineralization of the eastern Dunnage Zone, where gold is usually present as spectacular, coarse clots such as at Big Pond, Knob and Bullet occurrences (*c.f.* Evans, 1991).

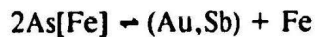
The gold contents of arsenopyrite were measured using the LAM-ICP-MS technique on unpolished sulphide grains in a slab of the host rock (refer to Appendix I, Section I.6 for information on the procedure). The data were recorded in counts per second and lacking a proper reference standard, the data could not be converted to concentrations. Nonetheless, the data show some interesting interelement relationships which are illustrated in Figure 5.28.

Figure 5.28 contains plots of counts per second versus time of ablation. As can be seen, there are positive correlations between Au, As, Sb, S and Fe. With the exception of crystal 1/site 1 the remaining LAM-ICP-MS analyses all show the arsenopyrites to have a homogeneous composition. The homogeneity of the sulphide minerals was reaffirmed from petrographic studies which yielded that the sulphides possessed no zoning.

Although not common to lode gold systems, the presence of invisible gold has been documented from numerous gold deposits in North America and Europe (Ayora *et al.* 1992; Boiron *et al.*, 1989; Cathelineau *et al.* 1988a, 1988b; Boiron, 1988; Korobushkin, 1969; El-Bouseily *et al.*, 1985; Silichev and Belozertseva, 1975; Mironov and Geletiy, 1979; Miser and Buseck, 1989; Wu and Delhove, 1989; Cabri *et al.*, 1989; Cook and Chryssoulis, 1990; Mao, 1991; and Springer, 1983).

In all instances, it has been found that arsenopyrite or extremely As-rich pyrite contains the greatest proportion of dissolved gold suggesting a link between As and Au substitution in the sulphide lattice. Cathelineau *et al.* (1988a) and Boiron *et al.* (1989) has suggested that Au and As may form bonds within the arsenopyrite lattice only when the As level reaches a critical concentration which coincides with a decrease in Sb and S. As a result, auriferous arsenopyrite should have lower Sb, S than would non-auriferous arsenopyrite. However, the reverse of this is observed for auriferous arsenopyrite from the Duder Lake occurrences, where both S and Sb show co-enrichment with Au suggesting that substitution may occur with another element such as Fe.

It has been noted in all mineralized zones that where there is an increase in arsenopyrite abundance there is also an increase in pyrite abundance and as well as the degree of carbonatization manifested as ankerite and ferroan dolomite increase, and all correlates with increased gold abundances. Mao (1991) has shown that when Fe^{2+} and As are present in a hydrothermal fluid, the stable complexes of Au (such as $\text{Au}(\text{HS})^{2-}$ and $\text{Au}_2\text{S}_2^{2-}$) can decompose resulting in the simultaneous deposition of Au and As with Fe being preferentially incorporated into pyrite as opposed to arsenopyrite. Similar findings have been made by Johan *et al.* (1989) who stated that auriferous arsenopyrite from the Chatelet and Villeranges deposits are the result of substitution of Au and Sb for As and Fe as per the following equation:



where the Fe would then be consumed in pyrite and the Au and Sb would go into the arsenopyrite lattice. This substitution could explain why analyses containing several hundred ppm of Sb have been obtained from the mineralized zones without ever documenting Sb-bearing minerals.

According to Cathlineau *et al.* (1988a,b), Boiron *et al.* (1989), Mao (1991) and Cabri *et al.* (1989), invisible gold most commonly occurs along zone planes, microcracks and grain boundaries. Since zoning is not present, and single non-fractured grains were analyzed from the Duder Lake occurrences, a possible explanation could be that the gold could form a bond with As at the lattice scale.

To summarize, all evidence supports the concept of invisible gold at the Duder

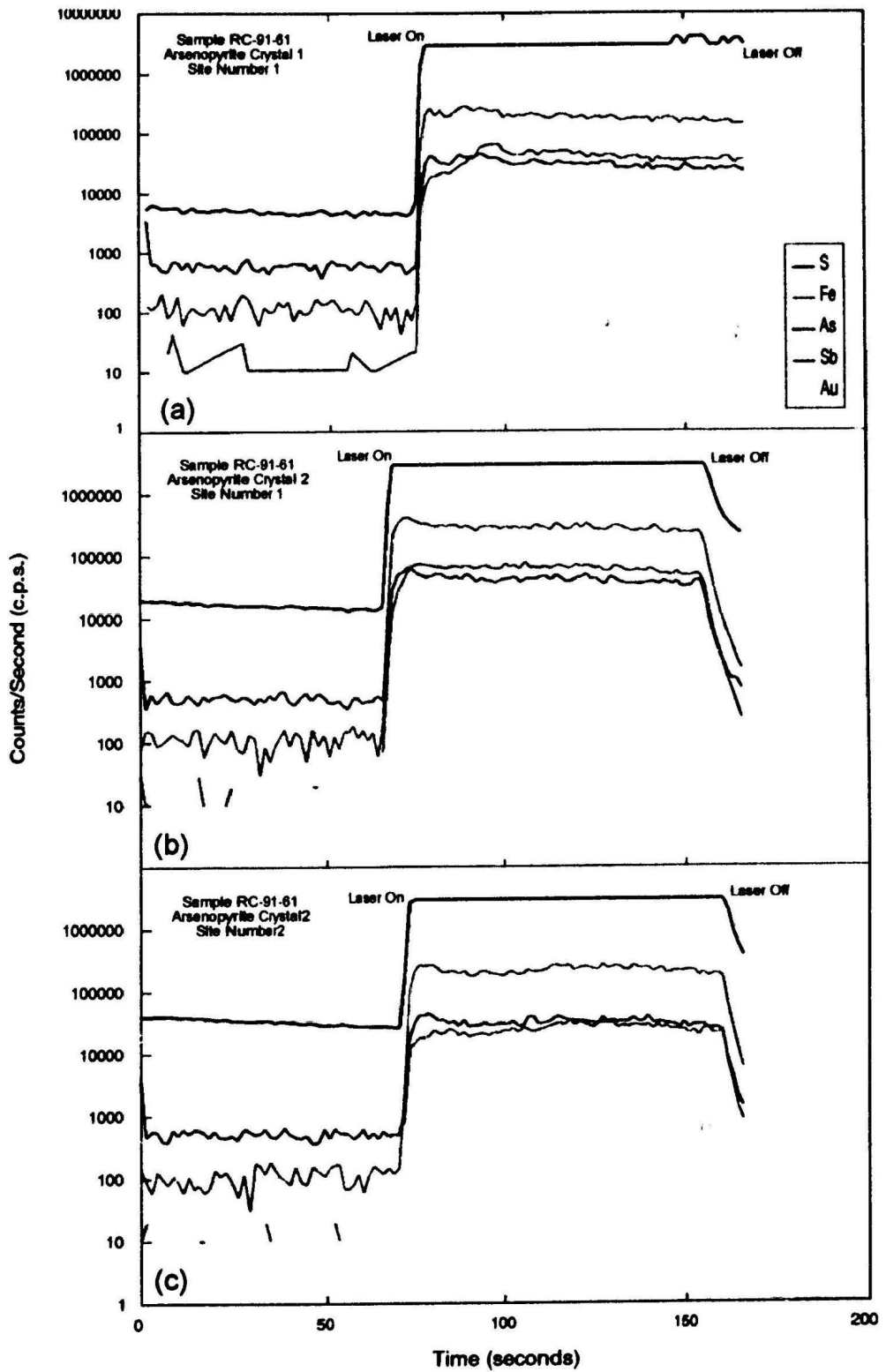


Figure 5.28: Plots of counts per second (c.p.s.) versus time for LAM-ICP-MS analyses of auriferous arsenopyrite representative of mineralization at Duder Lake. Note the increasing concentration of gold associated with increasing arsenic concentration.

Lake occurrences with arsenopyrite being the key sulphide phase associated with Au. Both Au and Sb appear to have substituted into the lattice replacing Fe and possibly As.

It should be added that any future developmental work on the Duder Lake should take into consideration the nature of the refractory gold ore which would not be liberated via standard cyanidation processes.

5.4 Summary

Numerous points have been presented in this chapter pertaining to the mechanisms of alteration and mineralization as well as on the geochemical and isotopic systematics and physico-chemical constraints. These points are briefly summarized below:

- 1). *Petrographic analysis indicates three different zones spatially related to the shear zones. Proximal is the M-Zone grading into the A-Zone and finally the GMA-Zone. The A-Zone is further subdivided into the A1- and A2-Zones on the basis of changes in chlorite and carbonate chemistry.*
- 2). *Alteration and mineralization were coincident with a low to mid-greenschist facies metamorphic event.*
- 3). *Alteration assemblages diagnostic of each of the alteration domains result from changing CO_2/H_2O and W/R ratios, which decrease away from the shear zones.*
- 4). *Sulphide grain morphology may substantiate time of formation coincident with metamorphism.*
- 5). *Sulphide formation was closely related to mineral reactions that formed chlorite and/or destroyed titanomagnetite.*
- 6). *Carbonate and chlorite become increasingly Mg-rich with increasing alteration, reflecting sulphidation.*
- 7). *K, Rb, Ba, Li and Cs are decoupled from Al, Ga, Th, U, Ti and V during alteration and mineralization such that the former group reflects changes during potassic metasomatism and the latter group were neither added nor removed and behaved quasi-isochemically.*
- 8). *As, S, Au and Sb may have been mobilized from a common source and precipitated simultaneously as evidenced by interelement co-enrichment.*
- 9). *Au, As, Sb and W are also correlated and the W-Au relationship suggests that carbon-oxygen anionic complexes responsible for W mobilization may have been important in Au mobilization as well.*

- 10). *CO₂ contents can be used as a measure of alteration intensity, with estimated CO₂/H₂O ratios defining carbonate chemistries inherent to the differing alteration domains.*
- 11). *REE geochemistry suggests that the gabbros at Duder Lake may be related to the Loom Bay granodiorite and could have been derived from a primordial mantle source having an arc component.*
- 12). *The gabbros hosting gold mineralization have contrasting REE chemistries with gabbros of other gold showings in the eastern Dunnage Zone.*
- 13). *Comparison of the LREE to HREE concentrations for rocks of the GMA-, A- and M-Zones translates to a 3.4X increase of the LREE in the M-Zone relative to the GMA-Zone.*
- 14). *Isocon analyses show that most of the element changes observed between the GMA- and M-Zones are the result of volume changes. However, major additions of Sb, Au, As, S, Br and K are noted.*
- 15). *Isochemical behaviour of the REE equate to a -71% volume decrease which is a reflection on the almost complete replacement of dense Ca,Mg silicates by less dense Ca,Mg carbonates and subsidiary silicates.*
- 16). *Microthermometry determinations from fluid inclusions show that the fluid evolved to lower temperatures, less saline and more H₂O-rich compositions with increasing distance from the shear zone. T_h's for the M-Zone, mineralized quartz veins of the M-Zone and for the A-Zone are 300-350°C, 250-300°C and 200-250°C respectively.*
- 17). *CO₂-rich fluids were important in mineralization but evolved to H₂O-rich fluids with progressive wall rock interaction.*
- 18). *δ³⁴S, δ¹⁸O, δ¹³C compositions of sulphides and carbonates respectively have strong comparisons with numerous lode-gold deposits. In addition, calculated fluid compositions indicate a possible mantle/magmatic component but which is swamped by a dominant heterogeneous crustal component.*
- 19). *Calculated δ¹⁸O for mineralizing fluids plots within the metamorphic waters field having some overlap with magmatic waters on a δD-δ¹⁸O diagram.*
- 20). *LAM-ICP-MS analysis proves that the arsenopyrite is Au-rich, supporting the notion that Au is invisible and with Sb probably forms bonds with As after displacing Fe from the Fe-sites in arsenopyrite.*

CHAPTER 6

DISCUSSION AND MODEL FOR GOLD MINERALIZATION

6.1 Introduction

The Corvette, Flirt, Goldstash and Stinger Prospects are all examples of mesothermal gold deposits similar in mode of occurrence and style of mineralization to other well known world class mesothermal gold deposits (MGDs) such as those of Western Australia, Superior and Slave Provinces of Canada and the Mother Lode District of California.

The processes leading to the formation of MGDs have long been debated, with a diverse set of genetic models proposed to explain their formation which invoke a wide variety of mechanisms and processes including:

A). Au derived from...

- Au-rich lamprophyres (Rock and Groves, 1988)
- tonalitic magmas (Burrows *et al.*, 1986; Spooner *et al.*, 1987)
- oxidized felsic magma (Cameron and Hattori, 1987; Hattori, 1987)

B). Au derivation processes...

- metamorphic dehydration (Fyfe and Henley, 1976; Kerrich and Fryer, 1979; Kerrich, 1986, 1987)
- metamorphic replacement (Groves and Phillips, 1987)
- lateral diffusion (Boyle, 1961, 1979)
- syngenetic exhalation (Hutchinson, 1976; Ridler, 1976)
- granulitization (Fyon *et al.*, 1984; Colvine *et al.*, 1984, 1988; Cameron, 1988)
- magmatism (Ferguson *et al.*, 1968; Griffis, 1968; Watson, 1975)
- meteoric water circulation (Nesbitt *et al.*, 1986; Henley, 1985)
- multistage processes

On the basis of the regional stratigraphic, structural and metamorphic constraints, the origin of the Duder Lake occurrences appears to be most analogous to that suggested

by the metamorphic dehydration model (as summarized by Nesbitt, 1988; Kerrich, 1989b). This supposition is based on the strong parallels between the salient features of this model and the characteristics of the Duder Lake gold occurrences as defined in this study, including:

- 1). *association of gold mineralization with metamorphic terranes or metamorphic events.*
- 2). *brittle/ductile features associated with metal precipitation.*
- 3). *hydrothermal fluids with low salinities (0-4 equivalent wt. % NaCl).*
- 4). *gold mineralization structurally controlled by third-order structures originating from major regional scale structures (such as the Dog Bay Line) that may have been active during the Silurian Orogenic event coinciding with timing of metamorphism.*
- 5). *$\delta^{18}\text{O}$, $\delta^{13}\text{C}$, $\delta^{34}\text{S}$ and LILE data which suggest that fluids were derived from a heterogeneous crustal source.*
- 6). *major ore and gangue minerals include quartz, carbonate, pyrite, arsenopyrite and muscovite (sericite).*
- 7). *hydrothermal alteration includes intense carbonatization, sulphidation, silicification and hydrothermal albitization - all of which are manifested at Duder Lake.*
- 8). *elements commonly associated with such deposits include As, Sb, Ag, Hg, B, W, Te, with As, Sb, B and W being in abundance at Duder Lake well above regional background levels*
- 9). *temperatures of formation between 250-350°C as determined from microthermometry measurements*
- 10). *CO₂ contents >4 mol %; at Duder Lake CO₂ contents of the fluid phase have been ascertained to have been as high as 60 mol %.*

Though these features indicate numerous similarities between the Duder Lake deposits and the metamorphic dehydration model, there are some inconsistencies between this model and the Duder Lake occurrences. The first is that MGDs are characterized by the huge quartz vein lodes. The only quartz veins observed at Duder Lake were centimetre wide, shear parallel veins that contained up to > 8600 ppb Au; whereas the host gabbro assayed up to 30 000 ppb Au thereby making the gabbro the ore-horizon. The second difference is that gold present in MGDs is usually coarse native gold, electrum and/or Au-Te alloys associated with sulphide grain boundaries and infillings in the sulphides. The gold at Duder Lake is, however, "invisible" in the truest sense of the word with the gold inferred to be bonded with As in the arsenopyrite lattice.

These two points suggest that the Duder Lake occurrences are somewhat unique compared to typical MGDs and also suggest that some exclusive physico-chemical controls were active during hydrothermal alteration and gold-sulphide mineralization. The data collected in the course of this study allow characterization of the ore fluids and may be used to substantiate a new subclass to the generic metamorphic dehydration model.

6.2 Discussion of Mechanisms of Alteration

The alteration model (Figure 5.4) for Duder Lake suggests that CO₂-rich fluids were probably derived from metamorphic devolatilization during the Silurian orogenic event which also produce the lower greenschist facies regional metamorphism. The CO₂-

bearing fluids ascended along conduits such as the Dog Bay Line fault/shear system and into higher order shears such as the low angle Reidel shears. The most intense alteration was situated at the focal point of shearing where reactions between the CO₂-bearing fluid and Fe-silicates was greatest forming abundant ankerite and ferroan dolomite. Similarly, chlorite which formed close to the shear was Mg-rich due to the excess CO₂ in the system that scavenged all the Fe for the production of the Fe carbonates as well as for sulphide formation. Rock-dominated buffering of the fluid effected a change in fluid composition since more and more CO₂ was consumed by the carbonatization reactions resulting in a diminished alteration intensity as can be seen by the transition from the M-Zone to the A-Zone. Subsequent reactions between the fluid and the host rock away from the shear also consumed CO₂ due to saussuritization of plagioclase in the GMA-Zone, the onset of sericitization in the A-Zone and the carbonatization of epidote and actinolite in the A-Zone. These mineralogical changes were caused by a fluid which was initially reducing, but with continued rock-dominated buffering of the fluid, the fluid may have acquired a more oxidizing chemistry, as can be inferred from diminishing CO₂/H₂O ratios, which would have allowed for the formation of secondary epidote and calcite (Dubé *et al.*, 1987).

Changes were also effected in the oxide mineralogy, as seen in the breakdown of titanomagnetite to form leucoxene as well as pyrite and arsenopyrite. Formation of leucoxene could be the result of hydrogen partitioned into the fluid phase due to the destabilization of water (Dubé *et al.*, 1987). Also if excess S is present in the fluid

phase, H₂S could form resulting in a strongly reducing fluid.

The alteration assemblages are spatially zoned, but it is inferred that they must also have been temporally zoned, reflecting changing CO₂/H₂O ratios and fluid evolution during reaction between the fluid and the wall rocks. As such, those rocks located proximal to the shear were altered first and those altered rocks at the fringes of the system were the last to experience any alteration.

6.3 Discussion of Mechanisms of Mineralization

The fluid-rock interactions which produced the alteration mineral zonation also controlled the formation of sulphide mineralization and the distribution of gold within the mineralizing system. These interactions were also influenced by local lithogeochemistry and rheology which controlled the localization of mineralization.

Lithology and rheology contrasts appear to have been important catalysts for mineralization. In all examples of sulphide (\pm gold) mineralization, the host rocks have strong lithological contrasts with bounding lithologies. For instance, argillaceous siltstones and shales surround Fe-rich gabbros at the Corvette and Goldstash Prospects, whereas the Stinger mineralization is developed within graphitic siltstone and shale which in turn is bounded by quartz and feldspar-rich siltstone and sandstone. Springer (1984, 1985) has shown that elevated Au values, relative to background, may occur in graphitic shear zones or in carbonaceous horizons which have been conditioned by shearing. These findings correspond to the physical features at the Stinger Prospect where graphitic

siltstone is cut by a splay from the north-northeast trending Dog Bay Line that transects the Duder Lake area and around which mineralization has been localized. Due to the shearing, the surface activity of carbon flakes comprising the graphite and/or coating other grains is enhanced and as a result Au fixation on C occurs in a process analogous to commercial gold fixation processes (Springer, 1984).

A different scenario is envisaged for gold mineralization within the gabbros which are Fe-rich, as evidenced by the abundance of primary titanomagnetite and Fe-chlorite in the least altered gabbro samples. Once the ore-fluids encountered the Fe-rich lithology, reactions occur between the fluid and rock, thus causing precipitation. While this statement is a somewhat simplistic model for the gold mineralization mechanism, it has been postulated as the cause of mineralization in Fe-rich lithologies of the Yilgarn Block, western Australia (Barley and Groves, 1990).

Petrographic support for this model of metal precipitation in the Duder Lake gabbros, is observed in an apparent link between primary Fe,Ti-oxides and Fe-chlorite and secondary Mg-chlorite and Fe-carbonates proximal to the shear zones. Breakdown of the Fe,Ti-oxides and the Fe-chlorite results in the liberation of ferric Fe which promotes dissociation of H_2O and creates a fluid that is strongly reducing. The Fe bonds with any free S that is in the fluid or that which is liberated by the destabilization of H_2S to form pyrite (and arsenopyrite if As is present). Excess Fe is also consumed during ankeritization and dolomitization of the host rocks which occur prior to sulphide precipitation. Since all the Fe is used in the carbonatization and sulphidation of the zones

proximal to the shear zones, secondary chlorite has a Mg-rich composition. Distal to the shear zones more and more CO₂ is consumed in reactions such as ankeritization of actinolite (Reaction 6; Table 5.2) causing the CO₂/H₂O ratio to decrease. Also affecting this ratio is the decreased dissociation of H₂O due to lower fluid temperatures. This rock dominated buffering of the fluid causes a shift in the redox state of the fluid from reducing to relatively oxidizing. The shift in redox is delineated by the destabilization of H₂S which liberates S that goes into the production of sulphides. This shift also dictates the timing and mode of occurrence of gold mineralization.

The precipitation of gold is commonly viewed to be the result of a temperature decrease or pressure reduction, an increase in oxygen fugacity, or even a change in the chemical speciation of the transporting fluid (Bowers, 1991). At Duder Lake, it appears that gold precipitation resulted from a change in the relative redox state of the fluid from reducing to relatively more oxidizing.

This change from reducing to more oxidizing fluid conditions is reflected by the mineralogical changes between the M- and A-Zones where the change from a sulphide-ankerite-leucoxene dominated assemblage (M-Zone) to a (Fe,Mg)chlorite-ankerite-(Fe,Ti) oxide assemblage (A-Zone) delineates a change to more oxidizing conditions.

The transition between the two alteration zonations also delineates the change in sulphide and gold contents from economic concentrations (M-Zone) to noneconomic concentrations which further supports the notion that the change in redox conditions was responsible for sulphide and gold precipitation.

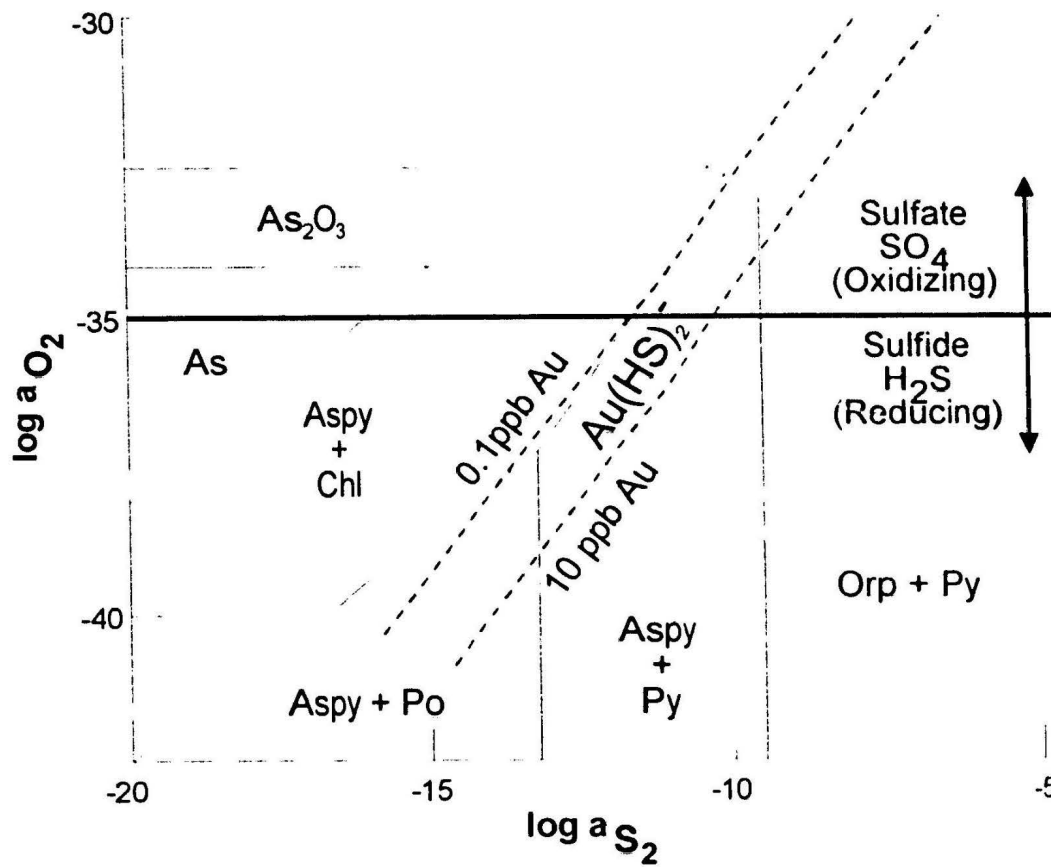


Figure 6.1: Calculated oxygen activity-sulphur activity diagram for the system Au-Fe-As-S-H₂O at 250°C and pH5. Stability fields for arsenopyrite, chlorite, pyrite, pyrrhotite, and orpiment (solid lines); gold-bisulphide solubility lines. Also depicted is the boundary between sulfate (oxidizing) and sulfide (reducing) species for this system. Diagram modified from Romberger (1985).

Romberger (1985) stated that pyrite, arsenopyrite, chlorite and gold are part of a common assemblage in many hydrothermal gold deposits which reflects a special set of circumstances constrained by a rather narrow range of a_{S_2} (-17 to -12) and a_{O_2} (-32 to -37; Figure 6.1). Figure 6.1 is a phase diagram for the system Au-Fe-As-NaCl-S-H₂O at 250°C and pH=5. Gold is least soluble as a bisulphide complex within the Chl-Aspy stability field suggesting that the reduction in a_{S_2} between the Aspy-Py and Chl-Aspy stability fields could cause precipitation of gold. Since reduction of a_{S_2} can be brought about by precipitation of sulphides, it destabilizes the bisulphide complexes and allow the gold to precipitate from solution.

The 0.1 ppb gold-bisulphide solubility line is subparallel to the boundary between the Aspy-Chl and Aspy-Py fields but the point at which it intersects this boundary almost perfectly coincides with the transition between the sulfide (reducing) and sulphate (oxidizing) fields of Romberger (1988). Values of $a_{O_2} > -35$ represent oxidizing conditions whilst $a_{O_2} < -35$ are reducing. The Aspy-Chl stability field represents the A-Zone and the Aspy-Py mineral assemblage correlate with the M-Zone. Since the gold is closely associated with the arsenopyrite, the change in the stability fields also dictates the deposition of gold. The change in the stability fields could be due to a decreased activity of reduced sulphur which could have been accomplished by having the redox state of the fluid changing from reducing to relatively more oxidizing (Seward, 1982).

The gold-sulphide assemblage at Duder Lake is a special case since the gold is contained within the arsenopyrite crystal structure as opposed to occurring in a free state.

Romberger (1985) attributed this phenomenon to coprecipitation of S and Au from the bisulphide complex where Au would enter the sulphide lattice in an interstitial substitution as precipitation proceeded.

6.4 Physico-Chemical Conditions of the Mineralizing Fluid and Postulations on Fluid Source Reservoirs

Based on the information presented in the discussions of geochemistry, fluid inclusion microthermometry, alteration paragenesis, stable isotope studies, and sulphide stabilities, a set of parameters can be defined which constrain the physico-chemical nature of the fluid associated with gold. These are:

- (1). *Given the great enrichments in As, Au and Sb in the mineralized zones relative to unaltered rocks spatially associated with the mineralized zones, it can be inferred that the fluids sampled a huge volume of rock (regional scale) to concentrate these elements in the fluid phase.*
- (2). *The pervasive ankeritization of the mineralized and advanced alteration (A2) zones as well as information obtained from fluid inclusions suggests that the fluid was enriched with respect to CO₂.*
- (3). *The relative lack of Cu, Pb, Zn enrichment relative to the background contents in unaltered rocks which suggests that chloride complexes were not important, and may have been absent, in the fluid phase.*
- (4). *LILE abundances suggest that the ore fluids had a signature analogous to an average crustal composition (K/Rb approximately 250; Kerrich, 1988c) suggestive of a metamorphic fluid sampling a lithologically diverse/complex area.*
- (5). *Both the isocon analysis of the REE and the similar REE patterns for different alteration domains, suggest that REE behaved isochemically in a closed system with no additions or losses.*

- (6). *The fluid/rock ratio was very high within the M-Zone since a -71% volume loss was calculated based on immobile REE behaviour.*
- (7). *Microthermometry data illustrate fluid evolution with time and continued host-rock interaction. Mineralization in the host-gabbro occurred at temperatures between 300-350°C, mineralized quartz-carbonate veins outboard from the shear zone at 250-300°C and finally distal alteration at 200-250°C. Not only is there a temperature decrease, but there is also a change in fluid composition from high CO₂ and 3-6wt. % NaCl in the M-Zone to aqueous fluids lacking any CO₂ and having salinities of 0.5-1.5wt. % NaCl. Freezing experiments suggest the presence of other dissolved gases such as CH₄ and N₂.*
- (8). *Fluid evolution is also reflected in the calculated isotopic compositions of the hydrothermal fluid in different zones and which are summarized below:*

Lithotype	$\delta^{18}O_f$	$\delta^{34}S_f$
M-Zone	12.05	0.31
MQV	10.33	-0.56
A-Zone	6.76	-4.06

The oxygen isotopic data are in accordance with the $\delta^{18}O$ compositions of metamorphic fluids, while the $\delta^{34}S$ data suggest a sedimentary sulphur source which could have been acquired as the result of fluid sampling of a regional sedimentary-dominated area. The carbon isotope data also suggest an average crustal signature, but one that may also have a mantle/magmatic component.

- (9). *Sulphide-Au-silicate stability diagrams show that gold precipitation occurred in within a narrow range of a_{S_2} (-17 to -12) and a_{O_2} (-32 to -37) during a change in redox state from reducing to oxidizing that coincided with silicate mineralogy changes.*
- (10). *The main Au complexing agents in the hydrothermal fluids were bisulphide. Destabilization of the complexes due to diminishing a_{S_2} was brought about by a relative redox change which in turn caused simultaneous precipitation of Au and As.*
- (11). *Strongly reducing fluids were derived via alteration of Fe,Ti oxides and/or silicates at relatively high temperatures where ferric Fe was liberated to the fluid phase and promoted the dissociation of H₂ from H₂O.*

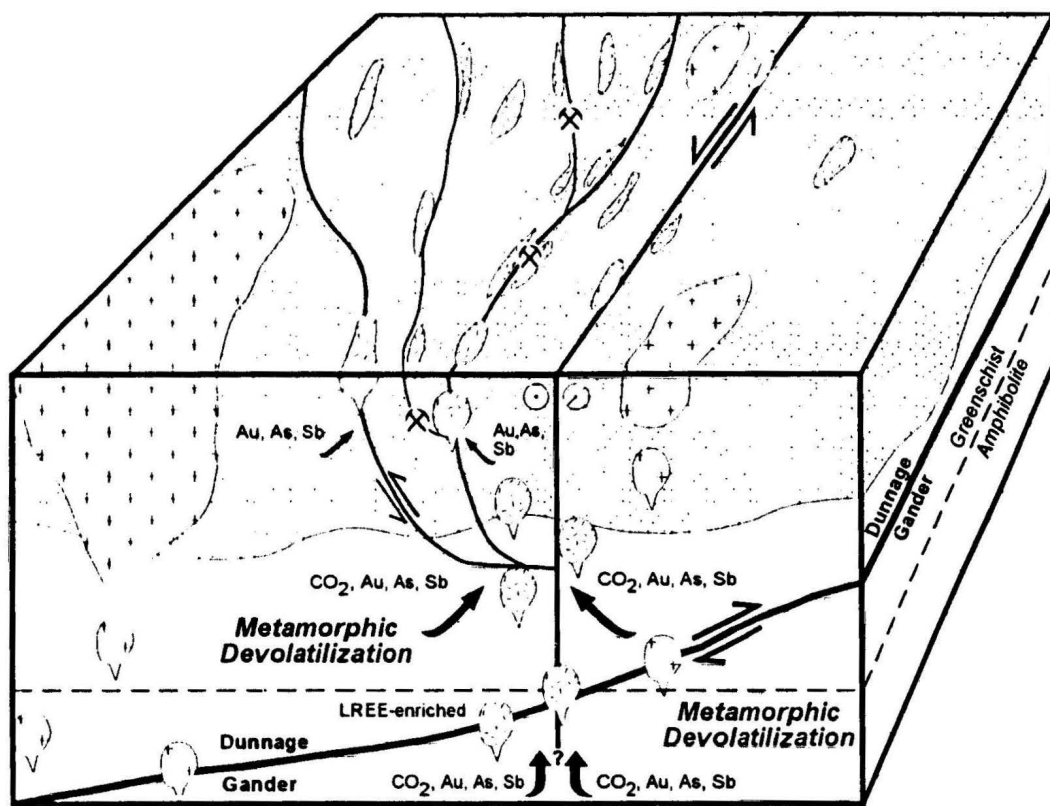
(13). *A high proportion of H₂ and dissolved S must have resided in the fluid phase.*

These details all suggest a fluid that was derived via metamorphic processes from a source that was probably deep seated (ie. amphibolite facies metamorphism of lower crustal material?). To summarize, the physico-chemical parameters inferred to be extant in the mineralizing fluid are:




<i>T°C</i>	mineralization 300-350°C decreasing to 200-250°C
<i>Dissolved Components</i>	CO ₂ (±CH ₄ , N ₂), As, Sb, Au, S, H ₂ O, H ₂ , H ₂ S
<i>Redox State</i>	initially strongly reducing changing to more oxidizing with alteration
<i>Complexing Agent</i>	bisulphide
<i>Isotopic Composition</i>	δ ¹⁸ O=12.05; δ ³⁴ S=0.31
<i>a_{S2}</i>	-17 to -12
<i>a_{O2}</i>	-32 to -37 (most likely -35)
<i>Salinity</i>	> 6 Equiv. Wt. % NaCl decreasing with alteration
<i>pH</i>	slightly acidic

6.5 Genetic Model for Mineralization



A genetic model for gold mineralization related to regional metamorphism is favoured for the Duder Lake occurrences (Figure 6.2). As have been illustrated, the timing of mineralization closely coincides with several other events including metamorphism, faulting and plutonism. Since all four events are temporally intertwined, the genetic model will have to take into account all factors to construct a model which is geologically sound.








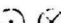
LITHOLOGIES

-  Siluro-Devonian gabbroic to dioritic dykes and sills
-  Siluro-Devonian granitic to granodioritic plutons
-  Ordovician-Silurian mixed sedimentary and volcanic succession. Diverse lithologies.

PLUTONISM

-  Gabbroic to dioritic melts derived from the lower crust(?). Possibly a coeval, mafic equivalent to the granitic-granodioritic plutonism of Siluro-Devonian age.
-  Granitic to granodioritic plutons arising from anatexis of Gander Zone as well as overlying Dunnage Zone rocks(?).

FAULTING

-  Late Ordovician thrust juxtaposing Dunnage and Gander Zones
-  Siluro-Devonian transpressional Dog Bay Line (DBL)
-  Secondary structures to the DBL
-  Tertiary structures to the DBL
-  Fault/shear movement in plane of page
-  Fault/shear movement into page


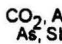

-  Fluid derivation due to metamorphic devolatilization of Gander Zone rocks
-  $\text{CO}_2, \text{Au}, \text{As}, \text{Sb}$ Major chemical components concentrated within the fluid phase
-  Gold mineralization

Figure 6.2: Schematic genetic model for gold mineralization in the Duder Lake area. Sketch also attempts to illustrate the spatial and temporal relationships between metamorphism, faulting, plutonism and mineralization. Refer to text for discussion.

For the sake of brevity, the sequence of events leading to gold mineralization will be listed in point form in chronological order.

- (1). *Development of Cambro-Ordovician pre-accretionary lithologies within the Dunnage Zone. These lithologies include rocks belonging to the Dunnage Mélange, Caradocian Shale, Davidsville Group, and so on.*
- (2). *During the late-Arenig Penobscot Orogeny, rocks of the Dunnage Zone were obducted onto the Gander Zone (Colman Sadd et al., 1992).*
- (3). *Post-accretionary sedimentary and volcanic lithologies such as the Wigwam and Laurenceton Formations respectively were developed upon the newly accreted zones.*
- (4). *Tectonism continued until the Silurian when a new orogenic pulse (Salinic Orogeny) resulted in widespread plutonism until Devonian times.*
- (5). *During the Silurian, anatexis of underthrust Gander Zone rocks and/or lowermost Dunnage Zone rocks resulted in melts of granitic to gabbroic composition which may or may not have been genetically related to a common source.*
- (6). *Development of major transpressional structures such as the Dog Bay Line coincided with plutonism and in some instances may have provided zones of relative permeability for the emplacement of gabbroic to dioritic dykes and sills.*
- (7). *Coincident with plutonism was active metamorphism of underthrust Gander Zone rocks as well as lowermost Dunnage Zone rocks which produced fluids rich in CO₂, H₂O, As, Au and Sb.*
- (8). *These fluids were focused along the transpressional fault and shear systems where they were probably seismically pumped due to seal-and-crack mechanics along the fault system (c.f. Sibson et al., 1988). Once fluid pressure exceeded the confining pressure, seismogenic fault failure created zones of rupture porosity allowing for draining of the hydrothermal reservoir.*
- (9). *The fluids infiltrated first the major structures and then higher order structures where the water/rock ratios were much higher and thus allowed for more intensive alteration of the host lithologies. The fluids not only carried chemical components derived from the metamorphic devolatilization but also leached elements such as Au from the host rocks through which it travelled. Evidence for*

the regional derivation of fluid comes from both stable isotope and LILE geochemistry.

- (10). *The interaction of the hydrothermal fluid with the host rock invariably resulted in numerous geochemical changes of both the fluid and host rock. Continued buffering of the fluid by the host rocks with increasing time and distance from the shear zones resulted in the distinctive alteration haloes observed.*
- a). Proximal to the shear zone where the temperature is highest, H₂O dissociation was greatest resulting in a fluid that was strongly reducing and containing abundant H₂S.*
- b). Due to decreasing temperature and relative changes in the redox state of the fluid, the aS₂ was decreased which caused instability in the bisulphide complexes that carried Au thus leading to gold precipitation.*
- c). Proximal to the shear zones, the degree of ankeritization was greatest since the breakdown of primary Fe, Ti oxides and silicates contributed Fe, first to the sulphidation of the host rocks and then to the carbonatization. This is the zone in which most of the CO₂ in the fluid is consumed.*
- d). Increasing distance from the shear zone sees lower temperatures, decreased H₂ from H₂O dissociation, and less CO₂. As a result, since the fluid is less reducing and has a lower CO₂/H₂O ratio (ie. higher H₂O content), minerals such as carbonate, epidote, actinolite and Fe, Ti oxides are stable.*
- e). Although the effects of hydrothermal alteration are pronounced in the gabbros, not all sections of the gabbro are equally affected. This may in part be due to differences in original composition/chemistry of the host rocks or a function of unequal fluid penetration into the host (ie. some zones more permeable than others).*
- (11). *Mechanisms of mineralization within the graphitic sedimentary rocks are somewhat different than those of the gabbros due to differences in chemistry and rheology between the two hosts. Alteration is not well developed in sedimentary hosts due to lower Fe contents which directly controls the degree of sulphidation and ankeritization.*
- (12). *Finally the precipitation of gold coincided with the precipitation of arsenopyrite from the fluid and resulted in gold being incorporated into the arsenopyrite lattice.*

Unfortunately, the conditions resulting in gold deposition at Duder Lake were such that the gold precipitated within the arsenopyrite crystal structure thus making the sulphide phases difficult to mill based on standard cyanidation processes. Consequently, any further work on the Duder Lake occurrences should take into account the nature of the ore and difficulties in refining that may arise.

The similarities between the Duder Lake gold mineralization and numerous other analogous sites of mineralization within the eastern Dunnage Zone of the Newfoundland Appalachians may suggest a common origin for all. The genetic model envisaged in this study may hold true not only for the Duder Lake and analogous Newfoundland gold mineralization examples but also similar deposits in the Dunnage Zone of the Appalachians (*e.g.* Rocky Brook - Millstream area mineralization, New Brunswick).

The characteristics of the Duder Lake occurrences make them unique in mesothermal gold deposit classification and this thesis represents the first documentation of such a deposit type in the Appalachian Orogen. On this basis, new gold exploration targets may perhaps be generated in the Appalachians utilizing the criteria presented in this study of "*Duder-Type*" gold mineralization.

REFERENCES

- Andrews, K.
1980 (compiler): Mineral occurrence map, Botwood, Newfoundland. Newfoundland Department of Mines and Energy, Mineral Development Division Map 80-4, Scale 1:250 000.
- Armbrust, G.A. and Gannicott, R.A.
1980: K/Rb ratios as source indicators for hydrothermal fluids of the Seneca volcanogenic massive sulphide deposit, British Columbia. *Economic Geology*, volume 75, pages 466-477.
- Armott, R.J., McKerrow, W.S., and Cocks, L.R.M.
1985: The tectonics and depositional history of the Ordovician and Silurian rocks of Notre Dame Bay, Newfoundland. *Canadian Journal of Earth Sciences*, volume 22, pages 607-618.

1985: The tectonics and depositional history of the Ordovician and Silurian rocks of Notre Dame Bay, Newfoundland: Reply. *Canadian Journal of Earth Sciences*, volume 23, pages 588-590.
- Ayora, C., Ribera, F. and Cardellach, E.
1992: The genesis of the arsenopyrite gold veins from the Vall de Ribes district, eastern Pyrenees, Spain. *Economic Geology*, volume 87, pages 1877-1896.
- Barley, M.E. and Groves, D.I.
1990: Mesothermal gold mineralization in the Yilgarn Craton, western Australia, the result of late Archean convergent tectonics? *Chronique de la Recherche Minière*, Number 498, pages 3-13.
- Billings, M.P. and White, W.S.
1950: Metamorphosed mafic dikes of the Woodsville Quadrangle, Vermont and New Hampshire. *American Mineralogist*, volume 35, pages 629-643.
- Blackwood, R.F.
1982: Geology of the Gander Lake (2D/15) and Gander River (2D/2) area. Newfoundland Department of Mines and Energy, Mineral Development Division, Report 82-4, 56 pages.
- Blewett, R.S.
1989: Mélange development along the Luke's Arm - Sop's Head Fault (Red Indian Line): a major lineament controlling deformation in Notre Dame Bay, north-central Newfoundland. *Geological Association of Canada, Program with Abstracts*, volume 14, page A10.
- Blewett, R.S. and Pickering, K.T.
1988: Sinistral shear during Acadian deformation in north-central Newfoundland, based on transecting cleavage. *Journal of Structural Geology*, volume 10, pages 125-127.
- Bouon, M.C.
1988: Gold-bearing arsenopyrite ores spatially associated to the Marche-Combrailles shear zone (Massif Central, France): geology and genesis. *In Bicentennial Gold '88. Extended Abstracts. Edited By A.D.T. Goode, E.L. Smyth, W.D. Birch and L.I. Bosma, Geological Society of Australia*, volume 23, pages 252-254.

- Boiron, M.C. Cathelineau, M. and Trescases, J.-J.
1989: Conditions of gold-bearing arsenopyrite crystallization in the Villeranges Basin, Marche-Combrailles shear zone, France: a mineralogical and fluid inclusion study. *Economic Geology*, volume 84, pages 1340-1362.
- Bowers, T.S.
1991: The deposition of gold and other precious metals: pressure-induced fluid immiscibility and associated stable isotope signatures. *Geochimica et Cosmochimica Acta*, volume 55, pages 2417-2434.
- Boyle, R.W.
1961: The geology, geochemistry, and origin of the gold deposits of the Yellowknife district. *Canadian Geological Survey Memoir* 310, 193 pages.

1976: Mineralisation processes in Archean greenstone and sedimentary belts. *Geological Survey of Canada Paper* 75-15.

1979: The geochemistry of gold and its deposits. *Geological Survey of Canada Bulletin* 280, 584 pages.
- Burke, B.
1992: Petrology and geochemistry of the Loon Bay Suite: tectonic implications. Unpublished B.Sc.(Hons) Thesis. Memorial University of Newfoundland, St. John's, Newfoundland, 70 pages.
- Burrows, D.R. and Jemielita, R.A.
1989: Lithophile-element systematics of Archean greenstone belt Au-Ag vein deposits: implications for source processes: Discussion. *Canadian Journal of Earth Sciences*, volume 26, pages 2741-2743.
- Burrows, D.R., Wood, P.C. and Spooner, E.T.C.
1986: Carbon isotope evidence for a magmatic origin for Archean gold-quartz vein ore deposits. *Nature*, volume 321, pages 851-854.
- Cabri, L.J., Chryssoulis, S.L., de Villiers, J.P.R., LaFlamme, J.H.G. and Buseck, P.R.
1989: The nature of invisible gold in arsenopyrite. *Canadian Mineralogist*, volume 27, pages 353-362.
- Calon, T.J. and Szybinski, Z.A.
1988: Lobster Cove Fault: dextral strike-slip fault system. *Geological Association of Canada, Program with Abstracts*, volume 13, page A17.
- Cameron, E.M.
1988: Archean gold: relation to granulite formation and redox zoning in the crust. *Geology*, volume 16, pages 109-112.
- Cameron, E.M. and Hattori, K.
1987: Archean gold mineralization and oxidized hydrothermal fluids. *Economic Geology*, volume 82, pages 1177-1191.

- Castaing, C., Cassard, D. Gros, Y. Moisy, M. and Chabod, J.C.
1993: Role of rheological heterogeneities in vein-ore localization. *Canadian Journal of Earth Sciences*, volume 30, pages 113-123.
- Cathelineau, M., Boiron, M.C., Hollinger, P. and Marion, P.
1988a: Gold-rich arsenopyrites: crystal chemistry, gold location and state, physical and chemical conditions of crystallization. *In Bicentennial Gold '88. Extended Abstracts. Edited By A.D.T. Goode, E.L. Smyth, W.D. Birch and L.I. Bosma, Geological Society of Australia, volume 23, pages 235-240.*
- Cathelineau, M., Hollinger, P., Marion, P. and Denis, M.
1988b: Gold in arsenopyrites: location and state, physical and chemical conditions of deposition. *In The Geology of Gold Deposits: The Perspective in 1988. Edited By R.R. Keays, W.R.H. Ramsay and D.I. Groves; Economic Geology Monograph 6, pages 328-341.*
- Churchill, R.A. and Evans, D.T.W.
1992: Geology and gold mineralization of the Duder Lake gold showings, eastern Notre Dame Bay, Newfoundland. *In Current Research. Newfoundland Department of Mines and Energy, Geological Survey Branch, Report 92-1, pages 211-220.*
- Churchill, R.A., Wilton, D.H.C. and Evans, D.T.W.
1993a: Geology, alteration assemblages and geochemistry of the Duder Lake gold showings, northeastern Newfoundland. *In Current Research. Newfoundland Department of Mines and Energy, Geological Survey Branch, Report 93-1, pages 317-334.*
- Churchill, R.A., Wilton, D.H.C. and Miller, H.G.
1993b: Second- and third-order structural control on lode gold mineralization, eastern margin of the Dunnage Zone, Newfoundland Appalachians: geochemical and geophysical evidence. *In CIM Geological Field Conference, Bathurst '93 Program with Abstracts, volume 3, page 71.*
- Collins, P.L.F.
1979: Gas hydrates in CO₂-bearing fluid inclusions and the use of freezing data for estimation of salinity. *Economic Geology*, volume 74, pages 1435-1444.
- Colman-Sadd, S. and Swinden, H.S.
1984: A tectonic window in Central Newfoundland? Geological evidence that the Appalachian Dunnage Zone may be allochthonous. *Canadian Journal of Earth Sciences*, volume 21, pages 1349-1367.
- Colman-Sadd, S., Dunning, G.R. and Dec, T.
1992: Dunnage-Gander relationships and Ordovician Orogeny in central Newfoundland: a sediment provenance and U/Ph study. *American Journal of Science*, volume 292, pages 317-355.
- Colvine, A.C. Fyon, J.A., Heather, K.B., Marmont, S., Smith, P.M. and Troop, D.G.
1988: Archean Lode Gold Deposits in Ontario. Mines and Minerals Division, Ontario Geological Survey, Miscellaneous Paper 139, 136 pages.

- Colvine, A.C., Andrews, A.J., Cherry, M.E., Durocher, M.E., Fyon, A.J., Lavigne, M.J., Macdonald, A.J., Marmont, S., Poulsen, K.H., Springer, J.S. and Troop, D.G.
1984: An integrated model for the origin of Archean lode gold deposits. Ontario Geological Survey, Open File Report 5524, 98 pages.
- Cook, N.J. and Chryssoulis, S.L.
1990: Concentrations of "invisible gold" in the common sulphides. *Canadian Mineralogist*, volume 28, pages 1-16.
- Coveney, R.M.
1981: Gold quartz veins and auriferous granite at the Oriental Mine, Alleghany District, California. *Economic Geology*, volume 76, pages 2176-2199.
- Coyle, M. and Strong, D.F.
1987: Geology of the Springdale Group: a newly recognized Silurian epicontinental-type caldera in Newfoundland. *Canadian Journal of Earth Sciences*, volume 24, pages 1135-1148.
- Cox, K.G., Bell, J.D. and Pankhurst, R.J.
1979: The interpretation of igneous rocks. Allan and Unwin, London, 450 pages.
- Craig, J.R.
1990: Textures of the ore minerals. *In* *Advanced Microscopic Studies of Ore Minerals. Edited By J.L. Jambor and D.J. Vaughan, Mineralogical Association of Canada Short Course Notes Volume 17, pages 213-262.*
- Currie, K.L.
1992: A new look at Gander-Dunnage relations in Carmanville map area, Newfoundland. *In* *Current Research, Part D; Geological Survey of Canada, Paper 92-1D, pages 27-33.*

1993: Ordovician-Silurian stratigraphy between Gander Bay and Birchy Bay, Newfoundland. *In* *Current Research, Part D; Geological Survey of Canada, Paper 93-1D, pages 11-18.*
- Currie, K.L., Pajari, G.E., and Pickerill, R.K.
1980: Comments on the boundaries of the Davidsville Group, northeastern Newfoundland. *In* *Current research, Part A, Geological Survey of Canada, Paper 80-1A, pages 115-118.*
- Currie, K.L., Pickerill, R.K. and Pajari, G.E.
1983: Structural interpretation of the eastern Notre Dame Bay area, Newfoundland: regional post-middle Silurian thrusting and asymmetrical folding: Discussion. *Canadian Journal of Earth Sciences*, volume 20, pages 1351-1352.
- Davenport, P.H. and Nolan, L.W.
1988: Gold and associated elements in lake-sediment from regional surveys in the Botwood map area (NTS 2E). Newfoundland Department of Mines, Mineral Development Division. Open File 2E/563.

- Davies, J.F., Whitehead, R.E.S., Cameron, R.A. and Duff, D.
1982: Regional and local patterns of CO₂-K-Rb-As alteration: a guide to gold in the Timmins area. *In* *Geology of Canadian Gold Deposits*. Edited By R.W. Hodder and W. Petruk, Canadian Institute of Mining and Metallurgy Special Volume 24, pages 130-143.
- Dean, P.L.
1977: A report on the geology and metallogeny of the Notre Dame Bay area, to accompany maps 12H/1,8,9, and 2E/3,4,5,6,7, 8,9,10,11 and 12. Newfoundland Department of Mines and Energy, Mineral Development Division, Report 77-10, 17 pages.

1978a: The volcanic stratigraphy and metallogeny of Notre Dame Bay, Newfoundland. Unpublished M.Sc. Thesis, Memorial University of Newfoundland, 205 pages.

1978b: Geological compilation map. Comfort Cove, Newfoundland. Newfoundland Department of Mines and Energy, Mineral Development Division Map 4462G. Scale 1:63 360.
- Dean, P.L. and Strong, D.F.
1977: Folded thrust faults in Notre Dame Bay, central Newfoundland. *American Journal of Science*, volume 277, pages 97-108.
- Deer, W.A., Howie, R.A. and Zussman, J.
1985: *An Introduction to the Rock-Forming Minerals (15th edition)*. Longman Group Limited, England, 528 pages.
- Deveau, S.W.
1992: A metamorphic, structural and geophysical investigation of the Mount Cormack Subzone, central Newfoundland. Unpublished M.Sc. Thesis, Memorial University of Newfoundland, 291 pages.
- Dresen, G.
1991: Stress distribution and the orientation of Riedel shears. *Tectonophysics*, volume 188, pages 239-247.
- Dubé, B.
1985: Géologie, pétrographie et métallogénie d'indices aurifères localisés dans le filon-couche de Bourbeau, Centre-Nord du canton de Barlow, Chibougamau, Québec. Thèse de Maîtrise, Université Laval Québec, 220 pages.
- Dubé, B., Guha, J. and Rocheleau, M.
1987: Alteration patterns related to gold mineralization and their relation to CO₂/H₂O ratios. *Mineralogy and Petrology*, volume 37, pages 267-291.
- Dunne, K.P.E.
1992: Application of fluid inclusion petrography to mineral exploration. University of British Columbia, Mineral Deposits Research Unit Technical Report MT-2, 27 pages.

- Dunning, G.R., O'Brien, S.J., Colman-Sadd, S.P., Blackwood, R.F., Dickson, W.L., O'Neill, P.P., and Krogh, T.E.
1990: Silurian orogeny in the Newfoundland Appalachians. *Journal of Geology*, volume 98, pages 895-913.
- El-Bouseily, A.M., El-Dahhar, M.A. and Arslan, A.I.
1985: Ore-microscopic and geochemical characteristics of gold-bearing sulphide minerals, El Si gold mine, Eastern Desert, Egypt. *Mineralium Deposita*, volume 20, pages 194-200.
- Elliot, C.G. and Williams, P.F.
1986: The tectonics and depositional history of the Ordovician and Silurian rocks of Notre Dame Bay, Newfoundland: Discussion. *Canadian Journal of Earth Sciences*, volume 23, pages 586-588.
- Elliot, C.G., Dunning, G.R. and Williams, P.F.
1991: New U/Pb zircon age constraints on the timing of deformation in north-central Newfoundland and implications for early Paleozoic Appalachian orogenesis. *Geological Society of America Bulletin*, volume 103, pages 125-135.
- Ellis, A.J. and Mahon, W.A.J.
1964: Natural hydrothermal systems and experimental hot water/rock interactions. *Geochimica et Cosmochimica Acta*, volume 28, pages 1323-1357.

1967: Natural hydrothermal systems and experimental hot water/rock interactions (part II). *Geochimica et Cosmochimica Acta*, volume 31, pages 519-538.
- Evans, D.T.W.
1991: Gold metallogeny, Eastern Dunnage Zone, Central Newfoundland. *In Current Research. Newfoundland Department of Mines and Energy, Geological Survey Branch, Report 91-1*, pages 310-318.

1992: Gold mineralization in the eastern Dunnage Zone, Central Newfoundland. *In Current Research. Newfoundland Department of Mines and Energy, Geological Survey Branch, Report 93-1*, pages 339-349.

1993: Gold metallogeny of the eastern Dunnage Zone, Central Newfoundland. *In Current Research. Newfoundland Department of Mines and Energy, Geological Survey Branch, Report 92-1*, pages 231-243.
- Evans, D.T.W., Kean, B.F., and Dunning, G.R.
1990: Geological studies, Victoria Lake Group, central Newfoundland. *In Current Research. Newfoundland Department of Mines and Energy, Geological Survey Branch, Report 90-1*, pages 131-144.
- Ferguson, S.A., Burrum, B.S.W., Carter, O.F., Griffiths, A.T., Holmes, T.C., Hurst, M.E., Jones, W.A., Lone, H.C. and Langley, C.S.
1968: Ontario Department of Mines, GR 58, 177 pages.

- Field, C.W. and Fifarek, R.H.
1985: Light stable-isotope systematics in the epithermal environment. *In* *Geology and Geochemistry of Epithermal Systems*. Edited By B.R. Berger and P.M. Bethke, Society of Economic Geologists, Reviews in Economic Geology, volume 2, pages 99-128.
- Fryer, B.J., Kerr, A., Jenner, G.A. and Longstaffe, F.J.
1992: Probing the crust with plutons: regional isotopic geochemistry of granitoid intrusions across insular Newfoundland. *In* *Current Research*. Newfoundland Department of Mines and Energy, Geological Survey Branch, Report 92-1, pages 119-139.
- Fyfe, W.S. and Henley, R.W.
1976: Some thoughts on chemical transport processes with particular reference to gold. *Minerals Science Engineering*, volume 5, pages 295-303.
- Fyon, J.A., Schwarcz, H.P. and Crockett, J.H.
1984: Carbonatization and gold mineralization in the Timmins area, Abitibi Greenstone Belt: genetic link with Archean mantle CO₂-degassing and lower crustal granulitization. *Geological Association Programs with Abstracts*, volume 9, page 65.
- Gibbons, R.V. and Papezik, V.S.
1970: Volcanic rocks and arsenopyrite veins of the Moreton's Harbour area, Notre Dame Bay, Newfoundland. *The Geological Association of Canada, Proceedings*, volume 22, pages 1-9.
- Goldfarb, R.L., Leach, D.L., Miller, M.L. and Pickthorn, W.J.
1986: Geology, metamorphic setting, and genetic constraints of epigenetic lode-gold mineralization within the Cretaceous Valdez Group, south-central Alaska. *In* *Turbidite Hosted Gold Deposits*. Edited By J.F. Keppie, R.W. Boyle and S.J. Haynes. Geological Association of Canada Special Paper 32, pages 87-105.
- Goldfarb, R.J., Leach, D.L., Pickthorn, W.J. and Paterson, C.J.
1988: Origin of lode-gold deposits of the Juneau gold belt, southeastern Alaska. *Geology*, volume 16, pages 440-443.
- Goldfarb, R.J., Newberry, R.J., Pickthorn, W.J. and Gent, C.A.
1991: Oxygen, hydrogen, and sulphur isotope studies in the Juneau Gold Belt, southeastern Alaska: constraints on the origin of hydrothermal fluids. *Economic Geology*, volume 86, pages 66-80.
- Golding, S.D., McNaughton, N.J., Turner, J.V., Barley, M.E., Groves, D.I., Ho, S.E. and Rock, N.S.
1988: Fluid sources and circulation paths for Archean gold deposits: constraints from carbon and oxygen isotope studies. *In* *Bicentennial Gold '88. Extended Abstracts*. Edited By A.D.T. Goode, E.L. Smyth, W.D. Birch and L.I. Bosma, Geological Society of Australia, volume 23, pages 217-224.
- Goodwin, L.B. and O'Neill, P.
1991: The structural evolution of the northern segment of the Dunnage Zone-Gander Zone boundary, Newfoundland. *In* *Current Research*. Newfoundland Department of Mines and Energy, Geological Survey Branch, Report 91-1, pages 97-107.

- Govindaraju, K.
1989: 1989 compilation of working values and sample descriptions for 272 geostandards. Geostandards Newsletter Special Issue, volume 13, 113 pages.
- Grant, J.A.
1986: The isocon diagram - a simple solution to Gresens' equation for metasomatic alteration. *Economic Geology*, volume 81, pages 1976-1982.
- Green, K.
1989: First year assessment report on Licenses 3411, 3429, 3449, 3453, 3493, 3494, 3502, 3503, and 3504. NTS 2D/15, 2E/2, 2E/7. Noranda Exploration Company Limited, Confidential report, 39 pages. [NFLD (1890)]
- Gresens, R.L.
1967: Composition-volume relationships of metasomatism. *Chemical Geology*, volume 2, pages 47-55.
- Griffis, A.T.
1968: McIntyre Porcupine Mines Limited. *In Geology and Ore Deposits of Tinsdale Township*. Ontario Department of Mines, Geological Report 58, pages 122-130.
- Groves, D.I. and Phillips, G.N.
1987: The genesis and tectonic control on Archean gold deposits of the western Australian Shield - a metamorphic replacement model. *Ore Geology Reviews*, volume 2, pages 287-322.
- Harte, B. and Graham, C.M.
1975: The graphical analysis of greenschist to amphibolite facies mineral assemblages in metabasites. *Journal of Petrology*, volume 16, pages 347-370.
- Hattori, K.
1987: Magnetic felsic intrusions associated with Canadian Archean gold deposits. *Geology*, volume 15, pages 1107-1111.
- Haworth, R.T. and Miller, H.G.
1982: The structure of Paleozoic oceanic rocks beneath Notre Dame Bay, Newfoundland. *In Major Structural Zones and Faults of the Northern Appalachians*. Edited By P. St-Julien and J. Béland, The Geological Association of Canada Special Paper 24, pages 149-173.
- Helwig, J.A.
1972: Structural sequence in eastern Notre Dame Bay, Newfoundland Appalachians. *Geological Society of America, Program with Abstracts*, volume 4, page 20.
- Henley, R.W.
1985: The geothermal framework for epithermal deposits. *In Geology and Geochemistry of Epithermal Systems*. Edited By B.R. Berger and P.M. Bethke, *Reviews in Economic Geology*, volume 2, Bookcrafters Incorporated, Michigan, pages 1-24.

- Hibbard, J.P., Stouge, S. and Skevington, D.
1977: Fossils from the Dunnage Mélange, north-central Newfoundland. *Canadian Journal of Earth Sciences*, volume 14, pages 1176-1178.
- Hibbard, J.P. and Williams, H.
1979: Regional setting of the Dunnage Mélange in the Newfoundland Appalachians. *American Journal of Science*, volume 279, pages 993-1021.
- Higgins, N.
1980: Fluid inclusion evidence for the transport of tungsten by carbonate complexes in hydrothermal solution. *Canadian Journal of Earth Sciences*, volume 17, pages 823-830.
- Ho, S.E., Groves, D.I. and Phillips, G.N.
1985: Fluid inclusions as indicators of the nature and source of ore fluids and ore depositional conditions for Archean gold deposits of the Yilgarn block, western Australia. *Geological Society of South Africa Transactions*, volume 88, pages 149-158.
- Hoefs, J.
1987: *Stable isotope geochemistry (3rd Edition)*. Springer-Verlag, New York.
- Hofmann, A.W.
1988: Chemical differentiation of the Earth: the relationship between mantle, continental crust and oceanic crust. *Earth and Planetary Science Letters*, volume 90, pages 297-314.
- Horne, G.S. and Helwig, J.
1967: Ordovician stratigraphy of Notre Dame Bay, Newfoundland. *Memoir 12. In North Atlantic Geology and Continental Drift. A Symposium. Edited By M. Kay, Proceedings of a conference held at Gander, Newfoundland, August, 1967.* pages 388-407.
- Hutchinson, R.W.
1976: Lode gold deposits: the case for volcanogenic derivation. *In Proceedings Volume, Pacific Northwest Mining and Metals Conference, Portland, Oregon, 1975, Oregon Department Geology Minerals Industry*, pages 64-105.
- Irvine, T.N. and Barager, W.R.A.
1971: A guide to the chemical classification of the common igneous rocks. *Canadian Journal of Earth Sciences*, volume 8, pages 523-548.
- Jahn, B.M., Auvray, B., Blais, S., Capdevila, R., Cornichet, J., Vidal, F. and Hameurt, J.
1980: Trace element geochemistry and petrology of Finnish greenstone belts. *Journal of Petrology*, volume 21, pages 210-244.
- Jensen, L.S.
1980: The relationship between volcanism and gold mineralization in the Kirkland Lake district. *In Genesis of Archean Volcanic-Hosted Gold Deposits. Edited By R.G. Roberts, Ontario Geological Survey Open File Report 5293*, pages 280-302.

- Johan, Z., Marcoux, E. and Bonnemaïson, M.
1989: Arsénopyrite aurifère: mode de substitution de Au dans la structure de FeAsS. C.R. Acad. Sci., volume 308, pages 185-191.
- Karlstrom, K.E., Van Der Pluijm, B.A. and Williams, P.F.
1982: Structural interpretation of the eastern Notre Dame Bay area, Newfoundland: Regional post-middle Silurian thrusting and asymmetrical folding. Canadian Journal of Earth Sciences, volume 19, pages 2325-2341.

1983: Structural interpretation of the eastern Notre Dame Bay area, Newfoundland: Regional post-middle Silurian thrusting and asymmetrical folding: Reply. Canadian Journal of Earth Sciences, volume 20, pages 1353-1354.
- Kay, E.A.
1982: A geochemical and fluid inclusion study of the arsenopyrite-stibnite-gold mineralization, Moreton's Harbour, Notre Dame Bay, Newfoundland. Unpublished M.Sc. Thesis. Memorial University of Newfoundland, St. John's, Newfoundland, 209 pages.
- Kay, E.A. and Strong, D.F.
1983: Geologic and fluid controls in As-Sb-Au mineralization in the Moreton's Harbour area, Newfoundland. Economic Geology, volume 78, pages 1590-1604.
- Kay, M.
1967: Stratigraphy and structure of northeastern Newfoundland bearing on drift in North Atlantic. American Association of Petroleum Geologists Bulletin, volume 51, pages 579-600.

1975: Campbellton sequence, manganiferous beds adjoining the Dunnage Mélange, northeastern Newfoundland. Geological Society of America Bulletin, volume 86, pages 105-108.
- Kay, M. and Williams, H.
1963: Ordovician - Silurian relations on New World Island, Notre Dame Bay, northeast Newfoundland (Abstract). Geological Society of America Bulletin, volume 74, page 807.
- Keen, C.E., Keen, M.J., Nichols, B., Reid, I., Stockmal, G.S., Colman-Sadd, S.P., O'Brien, S.J., Miller, H., Quinlan, G., Williams, H., and Wright, J.
1986: Deep seismic reflection profile across the northern Appalachians. Geology, volume 14, pages 141-145.
- Keen, C.E., Loncarevic, B.D., Reid, I., Woodside, J., Haworth, R.T., and Williams, H.
1990: Tectonic and geophysical overview; Chapter 2 *In* Geology of the Continental Margin of Eastern Canada. Edited By M.J. Keen and G.L. Williams; Geological Survey of Canada, Geology of Canada, No.2, pages 31-85.
- Kennedy, M.J. and McGonigal, M.H.
1972: The Gander Lake and Davidsville Groups of northeastern Newfoundland: new data and geotectonic implications. Canadian Journal of Earth Sciences, volume 9, pages 452-459.

Kerrich, R.

1986: Fluid infiltration into fault zones: chemical, isotopic and mechanical effects. *Journal of Pure and Applied Geophysics*, volume 124, pages 225-268.

1987: The stable isotope geochemistry of Au-Ag deposits in metamorphic rocks. *In Stable Isotope Geochemistry of Low Temperature Fluids. Edited By T.K. Kyser, Mineralogical Association of Canada Short Course Notes Volume 13*, pages 287-336.

1988a: Lithophile element systematics of Archean lode gold deposits: I. monitor of source processes. *In Bicentennial Gold '88. Extended Abstracts. Edited By A.D.T. Goode, E.L. Smyth, W.D. Birch and L.I. Bosma, Geological Society of Australia*, volume 23, pp602-603.

1988b: Lithophile element systematics of Archean lode gold deposits: II. discriminants of metamorphic versus magmatic processes. *In Bicentennial Gold '88. Extended Abstracts. Edited By A.D.T. Goode, E.L. Smyth, W.D. Birch and L.I. Bosma, Geological Society of Australia*, volume 23, pages 604-605.

1988c: Lithophile element systematics of gold vein deposits in Archean greenstone belts: implications for source processes. *In The Geology of Gold Deposits: The Perspective in 1988. Edited By R.R. Keays, W.R.H. Ramsay and D.I. Groves; Economic Geology Monograph 6*, pages 508-519.

1989a: Source processes for Archean Au-Ag deposits: evidence from lithophile-element systematics of the Hollinger-McIntyre and Buffalo Ankerite deposits, Timmins. *Canadian Journal of Earth Sciences*, volume 26, pages 755-781.

1989b: Geochemical evidence on the sources of fluids and solutes for shear zone hosted mesothermal Au deposits. *In Mineralization and Shear Zones. Edited By J.T. Bursnall, Geological Association of Canada Short Course Notes Volume 6*, pages 129-198.

1990: Carbon-isotope systematics of Archean Au-Ag vein deposits in the Superior Province. *Canadian Journal of Earth Sciences*, volume 27, pages 40-56.

Kerrich, R. and Fryer, B.J.

1979: Archean precious-metal hydrothermal systems, Dome Mine, Abitibi greenstone belt. II. REE and oxygen isotope relations. *Canadian Journal of Earth Sciences*, volume 16, pages 440-458.

1988: Lithophile-element systematics of Archean greenstone belt Au-Ag vein deposits: implications for source processes. *Canadian Journal of Earth Sciences*, volume 25, pages 945-953.

1989: Lithophile-element systematics of Archean greenstone belt Au-Ag vein deposits: implications for source processes: Reply. *Canadian Journal of Earth Sciences*, volume 26, pages 2744-2748.

1991: The separation of rare elements from abundant base metals in Archean lode gold deposits: implications of low water/rock source regions. *Economic Geology*, volume 76, pages 160-166.

- Kerrick, R. and Fryer, B.J. and Jemielita, R.A.
1990: Lithophile-element systematics of Archean greenstone belt Au-Ag vein deposits: implications for source processes: Reply. *Canadian Journal of Earth Sciences*, volume 27, pages 1788-1789.
- Kerrick, R., Fryer, B.J., King, R.W., Willmore, L.M. and van Hees, E.
1987: Crustal outgassing and LILE enrichment in major lithosphere structures. Archean Abitibi greenstone belt: evidence on the source reservoir from strontium and carbon isotope tracers. *Contributions to Mineralogy and Petrology*, volume 97, pages 156-168.
- Kontak, D.J., Smith, P.K., Kerrich, R. and King, R.W.
1988: Distribution of carbonate $\delta^{13}\text{C}$ and $^{87}\text{Sr}/^{86}\text{Sr}$ in gold deposits of the Meguma Terrane, Nova Scotia and Superior Province, Canada: implications for C and Sr source reservoirs. *In Bicentennial Gold '88. Extended Abstracts. Edited By A.D.T. Goode, E.L. Smyth, W.D. Birch and L.I. Bosma*, Geological Society of Australia, volume 23, pages 225-229.
- Korobushkin, I.M.
1970: Forms of occurrence of finely dispersed gold in pyrite and arsenopyrite. *Doklady Akademii Nauk USSR*, volume 192, pages 122-123.
- Kranck, E.H.
1952: Preliminary report on the geological survey in the Notre Dame Bay area in the Summer, 1952. Newfoundland Department of Mines and Resources, Unpublished Report, 14 pages.
- Lafrance, B. and Williams, P.F.
1989: Silurian-Devonian transcurrent movement deformation in the Canadian Appalachians (Abstract). *Atlantic Geology*, volume 25, page 163.

1992: Silurian deformation in eastern Notre Dame Bay, Newfoundland. *Canadian Journal of Earth Sciences*, volume 29, pages 1899-1914.
- Lattanzi, P.F.
1991: Applications of fluid inclusions in the study and exploration of mineral deposits. *European Journal of Mineralogy*, volume 3, pages 689-701.
- Lattanzi, P.F., Curti, E. and Bastogi, M.
1989: Fluid inclusion studies on the gold deposits of the Upper Anzascia Valley, northwestern Alps, Italy. *Economic Geology*, volume 84, pages 1382-1397.
- Lindsley, D.H.
1976: Experimental studies of oxide minerals. *In Oxide Minerals. Edited By D. Rumble*, Mineralogical Society of America Short Course Notes Volume 3, pages 61-68.
- Liverman, D. and Taylor, D.
1989: Surficial geology of Botwood (NTS 2E). Government of Newfoundland and Labrador, Department of Mines and Energy, Geological Survey open file NFLD (1904). Scale 1:250,000

- Lottermoser, B.G.
1990: Rare-earth element and heavy-metal behaviour associated with the epithermal gold deposit on Lihir Island, Papua, New Guinea. *Journal of Volcanology and Geothermal Research*, volume 40, pages 269-289.
- Mao, S.H.
1991: Occurrence and distribution of invisible gold in a Carlin-Type gold deposit in China. *American Mineralogist*, volume 76, pages 1964-1972.
- McCann, A.M. and Kennedy, M.J.
1974: A probable glacio-marine deposit of late Ordovician - early Silurian age from the north-central Newfoundland Appalachian belt. *Geological Magazine*, volume 111, pages 549-564.
- McKerrow, W.S. and Cocks, L.R.M.
1986: Oceans, island arcs and olistostromes: the use of fossils in distinguishing sutures, terranes and environments around the Iapetus Ocean. *Journal of the Geological Society of London*, volume 143, pages 185-191.
- Meschede, M.
1986: A method of discriminating between different types of mid-ocean ridge basalts and continental tholeiites with the Nb-Zr-Y diagram. *Chemical Geology*, volume 56, pages 207-218.
- Meyer, C. and Hemley, J.J.
1967: Wall rock alteration. *In Geochemistry of Hydrothermal Ore Deposits. Edited By H.L. Barnes*, Holt, Rinehart and Winston, New York, N.Y., pages 166-235.
- Miller, H.G. and Deutsch, E.R.
1970: Structural implications of gravity and magnetic anomalies over eastern Notre Dame Bay, Newfoundland (Abstract). *Maritime Sediments*, volume 6, page 142.
- Mironov, A.G. and Geletiy, V.F.
1979: Experimental study of gold distribution in sulphides. *Doklady Akademii Nauk, USSR*, volume 247, pages 218-222.
- Miser, D.E. and Buseck, P.R.
1989: Defect microstructures in a gold-bearing arsenopyrite. *Geological Association of America Program with Abstracts*, volume 21, pages A239-A240.
- Miyashiro, A.
1974: Volcanic rock series in island arcs and active continental margins. *American Journal of Science*, volume 274, pages 321-355.
- Muir, I.D.
1970: Differentiation and pyroxene relations in the Deccan Trap. *In West Commemoration Volume. Edited By T.V.V.G.R.K. Murthy and S.S. Rao*, University of Saugar, pages 394-404.

- Munha, J., Fyfe, W.S. and Kerrich, R.
1980: Adularia, the characteristic mineral of felsic spilites. *Contributions to Mineralogy and Petrology*, volume 75, pages 15-19.
- Murphy, J.B.
1989: Tectonic environment and metamorphic characteristics of shear zones. *In Mineralization and Shear Zones. Edited By J.T. Bursnall*, Geological Association of Canada Short Course Notes Volume 6, pages 29-50.
- Myers, K.E. and Bretkopf, J.H.
1989: Basalt geochemistry and tectonic settings: a new approach to relate tectonic and magmatic processes. *In Proterozoic Geochemistry. Edited By R. Gorbatshev*, *Lithos*, volume 23, pages 53-62.
- Najjarpour, H. and Upadhyay, H.D.
1987: The closing of the Iapetus Ocean in eastern Notre Dame Bay, Newfoundland: geochemical evidence. *Geological Society of America, Program with Abstracts*, volume 19, page 236.
- Nash, J.T.
1976: Fluid inclusion petrology - data from porphyry copper deposits and applications to exploration. *United States Geological Survey Professional Paper 907-D*, 16 pages.
- Nelson, K.D.
1981: Mélange development in the Boone's Point Complex, north-central Newfoundland. *Canadian Journal of Earth Sciences*, volume 18, pages 433-442.
- Nesbitt, B.E.
1988: Gold deposit continuum: a genetic model for lode Au mineralization in the continental crust. *Geology*, volume 16, pages 1044-1048.
- Nesbitt, B.E. and Muehlenbachs, K.
1989: Geology, geochemistry, and genesis of mesothermal lode gold deposits of the Canadian Cordillera: evidence from evolved meteoric water. *In The Geology of Gold Deposits: The Perspective in 1988. Edited By R.R. Keays, W.R.H. Ramsay and D.I. Groves*; *Economic Geology Monograph 6*, pages 508-519.
- Nesbitt, B.E., Murowchick, J.B. and Muehlenbachs, K.
1986: Dual origins of lode deposits in the Canadian Cordillera. *Geology*, volume 15, pages 472-473.
- Nesbitt, B.E., Muehlenbachs, K. and Murowchick, J.B.
1989: Genetic implications of stable isotope characteristics of mesothermal Au deposits and related Sb and Hg deposits in the Canadian Cordillera. *Economic Geology*, volume 84, pages 1489-1506.
- Nesbitt, R.W., Sun, S.-s and Pruvist, A.C.
1979: Komatiites: geochemistry and genesis. *The Canadian Mineralogist*, volume 17, pages 165-186.

- Ohmoto, H. and Rye, R.O.
1979: Isotopes of sulphur and carbon. *In* *Geochemistry of Hydrothermal Ore Deposits (2nd Edition)*. Edited By H.L. Barnes, John Wiley and Sons, New York, pages 509-567.
- O'Brien, B.H.
1991: Geological development of the Exploits and Notre Dame subzones in the New Bay area (Parts of NTS 2E/6, and 2E/11), amp area, Notre Dame Bay, Newfoundland. *In* *Current Research*. Newfoundland Department of Mines and Energy, Geological Survey Branch, Report 91-1, pages 155-166.

1993: A mapper's guide to Notre Dame Bay's folded thrust faults: Evolution and regional development. *In* *Current Research*. Newfoundland Department of Mines and Energy, Geological Survey Branch, Report 93-1, pages 279-291.
- O'Neill, P.P.
1991: Geology of the Weir's Pond area, Newfoundland (NTS 2E/1). Newfoundland Department of Mines and Energy, Geological Survey Branch, Report 91-3, 144 pages.
- Papezik, V.S.
1972: Late Precambrian ignimbrites in eastern Newfoundland and their tectonic significance. *In* *Proceedings of the 24th International Geological Congress, Montreal, Section 1*, pages 147-152.
- Patey, K. and Wilton, D.H.C.
1993: The Deer Cove deposit, Baie Verte Peninsula, Newfoundland, a Paleozoic mesothermal lode-gold occurrence in the northern Appalachians. *Canadian Journal of Earth Sciences*, volume 30, pages 1532-1546.
- Patrick, T.O.H.
1956: Comfort Cove, Newfoundland. Geological Survey of Canada, Paper 55-31 (geological map with marginal notes).
- Pearce, J.A.
1983: Role of the sub-continental lithosphere in magma genesis at active continental margins. *In* *Continental Basalts and Mantle Xenoliths*. Edited By C.J. Hawkesworth and M.J. Norry, Shiva Publishing Limited, pages 230-249.
- Pearce, J.A. and Cann, J.R.
1973: Tectonic setting of basic volcanic rocks determined using trace element analyses. *Earth and Planetary Science Letters*, volume 19, pages 290-300.
- Phillips, G.N. and Groves, D.I.
1982: Fluid access and fluid-wall rock interaction in the genesis of the Archean gold-quartz vein deposit at Hunt Mine, Kambalda, western Australia. *In* *Gold'82: The Geology, Geochemistry and Genesis of Gold Deposits*. Edited By R.P. Foster, Geological Society of Zimbabwe Special Publication Number 1, pages 390-416.

- Piasecki, M.A.J.
1993: Tectonics along the Dog Bay Line - a Silurian terrane boundary in northeastern Newfoundland. *In* Current Research, Part E; Geological Survey of Canada, Paper 93-1E, pages 291-298.
- Pyke, D.R.
1976: On the relationship between gold mineralization and ultramafic rocks in the Timmins area, northeastern Ontario. *Canadian Institute of Mining and Metallurgy Bulletin*, volume 69, pages 79-87.

1980: Relationship of gold mineralization to stratigraphy and structure in Timmins and surrounding area. *In* Genesis of Archean Volcanic-Hosted Gold Deposits. *Edited By* R.G. Roberts, Ontario Geological Survey Open File Report 5293, pages 359-387.
- Quinlan, G.M., Hall, J., Williams, H., Wright, J.A., Colman-Sadd, S.P., O'Brien, S.J., Stockmal, G.S., and Marillier, F.
1992: Lithoprobe onshore seismic reflection transects across the Newfoundland Appalachians. *Canadian Journal of Earth Sciences*, volume 29, pages 1865-1877.
- Rast, N., O'Brien, B.H., and Wardle, R.J.
1976: Relationships between Precambrian and lower Paleozoic rocks of the Avalon Platform in New Brunswick, the northeast Appalachians and the British Isles. *Tectonophysics*, volume 30, pages 315-338.
- Reynolds, T.J.
1990: Short Course on Fluid Inclusions: Workshop on Application of Fluid Inclusions to Minerals Exploration. Unpublished Course Notes, January 29 - February 2, Department of Earth Sciences, Memorial University of Newfoundland, St. John's, Newfoundland. 57 pages.
- Ricketts, M.J. and McGrath, B.
1990: Granular aggregate resource mapping of the Gander Lake (NTS 2D/15), Gander River (NTS 2E/2) and Comfort Cove-Newstead (NTS 2E/7) map areas. *In* Current Research. Newfoundland Department of Mines and Energy, Geological Survey Branch, Report 90-1, pages 65-75.
- Ridler, R.H.
1976: Stratigraphic keys to the gold metallogeny of the Abitibi Belt. *Canadian Mining Journal*, volume 97, pages 81-88.
- Robert, F. and Kelly, W.C.
1987: Ore-forming fluids in Archean gold-bearing quartz veins at the Sigma Mine, Abitibi greenstone belt, Quebec, Canada. *Economic Geology*, volume 82, pages 1464-1482.
- Rock, N.M.S. and Groves, D.I.
1988: Can lamprophyres resolve the genetic controversy over mesothermal gold deposits? *Geology*, volume 16, pages 538-541.

- Roedder, E.
1984. Fluid Inclusions, Mineralogical Society of America; Reviews in Mineralogy, volume 12, Edited By P.H. Ribbe, 644 pages.
- Romberger, S.B.
1985: The solution chemistry of gold applied to the origin of hydrothermal deposits. *In Gold in the Western Shield. Edited By L.A. Clark, Canadian Institute of Mining and Metallurgy, Special Volume 38, pages 168-186.*
- Rose, A.W. and Burt, D.M.
1979: Hydrothermal alteration. *In Geochemistry of Hydrothermal Ore Deposits (2nd Edition). Edited By H.L. Barnes, Wiley, New York, N.Y., pages 173-235.*
- Roser, B.P. and Korsch, R.J.
1986: Determination of tectonic setting of sandstone - mudstone suites using SiO₂ content and K₂O/Na₂O ratios. *Journal of Geology, volume 94, pages 635-650.*
- Sangster, A.L.
1992: Light stable isotope evidence for a metamorphogenic origin for bedding-parallel, gold bearing veins in Cambrian flysch, Meguma Group, Nova Scotia. *Exploration and Mining Geology, volume 1, pages 69-79.*
- Scheuing, D.F. and Jacobi, R.D.
1990: Geochemical variability in the lower Paleozoic sedimentary section of eastern Notre Dame Bay, Newfoundland: evidence for a change in depositional environment. *Geological Society of America, Program with Abstracts, volume 22, page 68.*
- Schnetzler, C.C. and Philpotts, J.A.
1970: Partition coefficients of rare-earth elements between igneous matrix material and rock-forming mineral phenocrysts - II. *Geochimica et Cosmochimica Acta, volume 34, pages 331-340*
- Seward, T.M.
1982: The transport and deposition of gold in hydrothermal systems. *In Gold'82: The Geology, Geochemistry and Genesis of Gold Deposits. Edited By R.P. Foster, Geological Society of Zimbabwe Special Publication Number 1, pages 165-181.*
- Shaw, D.M.
1968: A review of K-Rb fractionation trends by covariance analysis. *Geochimica et Cosmochimica Acta, volume 32, pages 573-601.*
- Shervais, J.W.
1982: Ti-V plots and the petrogenesis of modern and ophiolitic lavas. *Earth and Planetary Science Letters, volume 59, pages 101-118.*
- Sibson, R.H.
1977: Fault rocks and fault mechanisms. *Journal of the Geological Society of London, volume 133, pages 191-213.*

- 1989: Earthquake faulting as a structural process. *Journal of Structural Geology*, volume 11, pages 1-14.
- Sibson, R.H., Robert, F. and Poulsen K.H.
1988: High-angle reverse faults, fluid-pressure cycling, and mesothermal gold-quartz deposits. *Geology*, volume 16, pages 551-555.
- Silichev, M.K. and Belozertseva, B.V.
1975: Distribution of gold among sulphides and sulphosalts in a gold deposit. *Geochemistry International*, volume 12, pages 90-94.
- Smith, T.J. and Kessler, S.E.
1985: Relation of fluid inclusion geochemistry to wallrock alteration and lithochemical zonation at the Hollinger-McIntyre gold deposit, Timmins, Ontario, Canada. *Canadian Institute of Mining and Metallurgy Bulletin*, volume 78, pages 35-46.
- Snelgrove, A.K.
1935: Geology of gold deposits in Newfoundland. Newfoundland Department of Natural Resources, Geological Section, Bulletin No. 2, 46 pages.
- Spooner, E.T.C., Bray, C.J., Wood, P.C. Burrows, D.R. and Callan, N.J.
1987: Au-quartz vein and Cu-Au-Ag-Mo-anhydrite mineralization, Hollinger-McIntyre Mines, Timmins, Ontario: $\delta^{13}\text{C}$ values (McIntyre) fluid inclusion gas chemistry, pressure (depth) estimation, and $\text{H}_2\text{O}-\text{CO}_2$ phase separation as a precipitation and dilation mechanism. *Ontario Geological Survey Miscellaneous Paper*, volume 136, pages 35-56.
- Springer, J.
1983: Invisible gold. *In The Geology of Gold in Ontario. Edited By A.C. Colvine*, Ontario Geological Survey Miscellaneous Paper 110, pages 240-250.

1984: Gold in carbon-rich rocks: improbable protore. *In Gold in the Western Shield. Edited By L.A. Clark*, Canadian Institute of Mining and Metallurgy, Special Volume 38, pages 104-112.

1985: Carbon in Archean rocks of the Abitibi Belt (Ontario-Quebec) and its relation to gold distribution. *Canadian Journal of Earth Sciences*, volume 22, pages 1945-1951.
- St. Croix, L. and Taylor, D.
1991: Regional striation survey and deglacial history of the Notre Dame Bay area, Newfoundland. *In Current Research*, Newfoundland Department of Mines and Energy, Geological Survey Branch, Report 91-1, pages 61-68.
- Stanton, R.L.
1972: *Ore Petrology*. McGraw-Hill, New York, U.S.A.
- Strauss, H.
1986: Carbon and sulphur isotopes in Precambrian sediments from the Canadian Shield. *Geochimica et Cosmochimica Acta*, volume 50, pages 2653-2662.

- Strong, D.F.
1974: Mineral occurrences of the Moreton's Harbour area. *In* Plate Tectonic Setting of Newfoundland Mineral Occurrences. *Edited By* D.F. Strong, A Guidebook for the NATO Advanced Studies Institute on Metallogeny and Plate Tectonics, pages 62-71.
- Studemeister, P.A.
1983: The redox state of iron: a powerful indicator of hydrothermal alteration. *Geoscience Canada*, volume 10, pages 189-194.
- Sun, S.-s. and McDonough, W.F.
1989: Chemical and isotopic systematics of oceanic basalts: implications for mantle composition and processes. *In* Magmatism in the Ocean Basins. *Edited By* A.D. Saunders and M.J. Norry, Geological Society Special Publication Number 42, pages 313-345.
- Szybinski, Z.A., Swinden, H.S., O'Brien, F.H.C., Jenner, G.A., and Dunning, G.R.
1990: Correlation of Ordovician volcanic terranes in the Newfoundland Appalachians. Lithological, geochemical, and age constraints. Geological Association of Canada, Program with Abstracts, volume 15, page A128.
- Tallman, P.
1990: Second year assessment report on geological and diamond drilling exploration for the Noranda/Noront GRUB Line North Project for licence 3989 on claim blocks 6077, 6080-6081, 7184 and 7187-7188 in the Duder Lake area, Newfoundland (6721). NTS 2E/2 and 2E/7. Noranda Exploration Company Limited, Confidential report, 50 pages. [2E/02(0744)]
- Taylor, B.E.
1990: C-O-H-S fluids in the California Mother Lode - do they provide answers or just solutions? *In* Greenstone Gold and Crustal Evolution, NUNA Conference Volume. *Edited By* F. Robert, P.A. Sheahan and S.B. Green. Proceedings of a Workshop held at Val d'Or, Quebec, May 24-27, 1990. Mineralogical Association of Canada, pages 214-216.
- Taylor, R.P. and Fryer, B.J.
1980: Multiple-stage hydrothermal alteration in porphyry copper systems in northern Turkey. the temporal interplay of potassic, propylitic and phyllic fluids. *Canadian Journal of Earth Sciences*, volume 17, pages 901-926.
- 1982: Rare earth element geochemistry as an aid to interpreting hydrothermal ore deposits. *In* Metallization Associated with Acid Magmatism. *Edited By* A.M. Evans, John Wiley and Sons Limited, pages 357-365.
- 1983: Rare earth element lithochemistry of granitoid mineral deposits. *Canadian Institute of Mining and Metallurgy Bulletin*, volume 76, pages 74-84.
- Tchalenko, J.S.
1968: The evolution of kink bands and the development of compression textures in sheared clays. *Tectonophysics*, volume 6, pages 159-174.

- 1970: Similarities between shear zones of different magnitudes. *Geological Society of America Bulletin*, volume 81, pages 1625-1640.
- Templeman-Kluit, D.J.
1970: The relationship between sulphide grain size and metamorphic grade of host rocks in some stratabound pyritic ores. *Canadian Journal of Earth Sciences*, volume 7, pages 1339-1345.
- Thompson, R.N., Morrison, M.A., Dickin, A.P. and Hendry, G.L.
1983: Continental flood basalts...arachnids rule OK?. *In* *Continental Basalts and Mantle Xenoliths. Edited By C.J. Hawkesworth and M.J. Norry*, Shiva Publishing Company, Nantwick, UK., pages 158-185.
- Turekian, K.K. and Wedepohl, K.H.
1961: Distribution of the elements in some major units of the Earth's crust. *Bulletin of the Geological Society of America*, volume 7, pages 175-192.
- Twenhofel, W.H. and Shrock, R.R.
1937: Silurian strata of Notre Dame Bay and Exploits Valley, Newfoundland. *Geological Society of America Bulletin*, volume 48, pages 1743-1772.
- Van der Pluijm, B.A. and Williams, P.F.
1985: Fault controlled stratigraphic repetition in the Notre Dame Bay area, Newfoundland. *Geological Association of Canada, Program with Abstracts*, volume 10, page A65.
- Van der Pluijm, B.A., Karlstrom, K.E. and Williams, P.F.
1987: Fossil evidence for fault-derived stratigraphic repetition in the northeastern Newfoundland Appalachians. *Canadian Journal of Earth Sciences*, volume 24, pages 2337-2350.
- Walsh, J.F., Cloke, P.L., and Kesler, S.E.
1984: Fluid (H₂O-CO₂) immiscibility and *f*O₂ as factors in gold mineralization; Pamour No. 1 mine, Timmins, Ontario. *Geological Society of America, Program with Abstracts*, volume 16, page 686.
- Walsh, J.F., Kesler, S.E., Duff, D. and Cloke, P.L.
1988: Fluid inclusion geochemistry of high-grade, vein-hosted gold ore at the Pamour Mine, Porcupine Camp, Ontario. *Economic Geology*, volume 83, pages 1347-1367.
- Wasowski, J.J. and Jacobi, R.D.
1985: Geochemistry and tectonic significance of the mafic volcanic blocks in the Dunnage Mélange, north-central Newfoundland. *Canadian Journal of Earth Sciences*, volume 22, pages 1248-1256.

1986: The tectonics and depositional history of the Ordovician and Silurian rocks of Notre Dame Bay, Newfoundland: Discussion. *Canadian Journal of Earth Sciences*, volume 23, pages 583-585.
- Watson, J.
1975: Mineralization in Archean provinces. *In* *The Early History of the Earth. Edited By B.J. Windley*, John Wiley, London, pages 443-454.

- Weir, R.H. Jr. and Kerrick, D.M.
1987: Mineralogic, fluid inclusion, and stable isotope studies of several gold mines in the Mother Lode, Tuolumne and Mariposa Counties, California. *Economic Geology*, volume 82, pages 328-344.
- Williams, H.
1962: Botwood (west half) map area, Newfoundland. Geological Survey of Canada, Paper 62-9, 16 pages.
1964: Botwood, Newfoundland. Geological Survey of Canada, Map 60-1963 (geological map with marginal notes).
1967: Silurian rocks of Newfoundland. *In Geological Association of Canada Special Paper Number 4, Geology of the Atlantic Region*, pages 93-137.
1972: Stratigraphy of the Botwood map area, northeastern Newfoundland. Geological Survey of Canada, Open File 113, 103 pages.
1978a (compiler): Tectonic lithofacies map of the Appalachian Orogen. Memorial University of Newfoundland Map No. 1, Scale 1:1,000,000.
1978b: Geological development of the northern Appalachians: its bearing on the evolution of the British Isles. *In Crustal Evolution in Northwestern Britain and Adjacent Regions. Edited By D.R. Bowes and B.E. Leake, Geological Journal Special Issue Number 10*, pages 1-22.
1982: Geology of the Canadian Appalachians. *In Perspectives in Regional Geological Synthesis. Edited By A.R. Palmer, Decade of North American Geology Special Publication No.1*, pages 57-66.
1992: Mélanges and coticule occurrences in the northeast Exploits Subzone, Newfoundland. *In Current Research, Part D; Geological Survey of Canada, Paper 92-1D*, pages 121-127.
1993: Stratigraphy and structure of the Botwood Belt and definition of the Dog Bay Line in northeastern Newfoundland. *In Current Research, Part D; Geological Survey of Canada, Paper 93-1D*, pages 19-27.
- Williams, H., Dean, P.L. and Pickering, K.T.
(in press): Botwood Belt. *In Chapter 4 of Geology of the Appalachian-Caledonian Orogen in Canada and Greenland. Edited By H. Williams, Geological Survey of Canada, Geology of Canada, No. 6.*
- Williams, H. and Hatcher, R.D. Jr.
1982: Suspect terranes and accretionary history of the Appalachian Orogen. *Geology*, volume 10, pages 530-536.

- Williams, H. and St. Julien, P.
1982: The Baie Verte - Brompton Line: early Paleozoic continent ocean interface in the Canadian Appalachians. *In Major Structural Zones and Faults of the Northern Appalachians. Edited By P. St-Julien and J. Beland, The Geological Association of Canada Special Paper 24, pages 177-208.*
- Williams, H., Colman-Sadd, S.P., and Swinden, H.S.
1988: Tectonic-stratigraphic subdivisions of central Newfoundland. *In Current Research, Part B, Geological Survey of Canada, Paper 88-1B, pages 91-98.*
- Williams, P.F.
1984: Deformation in the New World Island area, Newfoundland: late stage transcurrent faulting. *Geological Society of America, Program with Abstracts, volume 16, page 71.*
- Wilton, D.H.C.
1985: REE and background Au/Ag evidence concerning the origin of hydrothermal fluids in the Cape Ray electrum deposits, southwestern Newfoundland. *Canadian Institute of Mining and Metallurgy Bulletin, volume 78, pages 48-59.*
- Wilton, D.H.C. and Evans, D.T.W.
1991: Comparison of gabbro hosted mesothermal gold mineralization from opposite margins of the Dunnage Zone. *Geological Association of Canada, Program with Abstracts, volume 16, page A133.*
- Winchester, J.A. and Floyd, P.A.
1977: Geochemical discrimination of different magma series and their differentiation products using immobile elements. *Chemical Geology, volume 20, pages 325-343.*
- Winkler, H.G.F.
1974: *Petrogenesis of Metamorphic Rocks (3rd Edition)*. Springer Verlag, New York, 320 pages.
- Wood, D.A.
1980: The application of a Th-Hf-Ta diagram to problems of tectonomagmatic classification and to establishing the nature of crustal contamination of basaltic lavas of the British Tertiary volcanic province. *Earth and Planetary Science Letters, volume 50, pages 11-30.*
- Wood, P.C., Burrows, D.R., Thomas, A.V. and Spooner, E.T.C.
1986: The Hollinger-McIntyre Au-quartz vein system, Timmins, Ontario, Canada; geologic characteristics, fluid properties and light stable isotope geochemistry. *In Gold '86. Edited By A.J. Macdonald, Willowdale, Ontario, Konsult International Incorporated, pages 56-80.*
- Wu, X. and Delbove, F.
1989: Hydrothermal synthesis of gold-bearing arsenopyrite. *Economic Geology, volume 84, pages 2029-2032.*
- Wyman, D.A. and Kerrich, R.
1987: REE distributions associated with Au-mineralization at the Archean Agnico-Eagle mine, Quebec. *Geological Society of America, Program with Abstracts, volume 19, page 900.*

Zhang, X. Nesbitt, B.E. and Muehlenbachs, K.
1989: Gold mineralization in the Okanagan Valley, southern British Columbia: fluid inclusion and stable isotope studies. *Economic Geology*, volume 84, pages 410-424.

APPENDIX I

ANALYTICAL METHODS

I.1. Sample Preparation

Individual rock samples (outcrop and drill core) for whole rock geochemical analyses were prepared by cutting a slab weighing approximately 100g from a larger sample making sure to remove and discard any weathering surfaces and/or veins which could result in erroneous data. Each 100g slab was then crushed in a steel jaw crusher to a particle size of about 1cm² and transferred to tungsten-carbide bowl-puck assembly and powdered to -100 mesh. Between samples the jaw crusher was cleaned with a wire brush to remove any solid residue, followed by cleaning with a pressurized air gun and finally methanol. The puck and bowl assembly was cleaned with a high purity quartz sand which was powdered in a similar manner as the samples and discarded, cleaned with the air gun, and washed by methanol.

Samples utilized for isotopic analyses (viz. sulphides, quartz, and carbonates) were visually separated from a coarse-grained (ie. >-100 mesh) whole rock powder using a binocular microscope, special tweezers and probes designed for picking small samples.

I.2. Scanning Electron Microscope (SEM) Determinations

Carbon coated polished thin sections were examined using the Hitachi S570 scanning electron microscope (SEM) located in the Biology Department, Memorial

University of Newfoundland. The SEM operated at a normal voltage of 15 kilovolts with backscatter (grey scale) images obtained with a GW Electronic Type 113 solid state Backscatter Electron Detector. Semi-quantitative X-ray analyses were procured with a Tracor Northern 5500 Energy Dispersive X-ray Analyser having a spectral resolution of 145 electron volts. The SEM was utilized to determine semi-quantitative major oxide data on chlorite and carbonate minerals. In addition it was also used in the examination of auriferous sulphides associated with gold mineralization.

I.3. X-Ray Diffractometer (XRD) Mineral Identification

A computer automated Rigaku X-ray diffractometer, located in the Department of Earth Sciences, MUN, was used in the determination of unknown mineral specimens as well as to ascertain purity/relative proportions of carbonate in whole rock powders. The samples were mounted on a standard glass thin section with the sample secured to the section by making an acetone or methanol smear with the sample powder.

Standard operating conditions were at 20 milliamps and 40 volts with a generator ramp-up and ramp-down time frame of approximately 5 minutes thus allowing for stable x-ray transmission. Unknown samples were analyzed from 5° to 120° 2θ with a sweep of 5° 2θ per minute whereas the carbonate scans were analyzed from 5° to 70° 2θ with a sweep of 2° 2θ per minute. The data were then stored to a computer file as well as printed on paper and compared with standard peaks for a wide range of elements in a search match routine. Output consisted of a list of possible minerals which could create

the same arrangement of peaks (ie. counts per second versus degrees 2Θ) obtained using the Search-Match subroutine in the Rigaku XRD support software.

I.4. Fluid Inclusion Techniques

Microthermometry data were collected from several samples representative of either ore-stage or post-mineralization fluid events to ascertain temperatures of formation as well as to give information about fluid composition. A total of 14 samples were studied with a total of 26 observations were performed at the Fluid Inclusion Facility, Department of Earth Sciences, MUN.

Fluid inclusion sections were prepared using the procedure of Higgins (1980) and examined using a standard petrographic microscope (under high magnification and illumination) with a universal stage assembly. The thermometric data were derived using a modified U.S.G.S. heating/freezing stage (*cf.* Reynolds, 1990). The heating/freezing stage was mounted on the microscope stage assembly and attached to a temperature control unit consisting of a rheostat (actual temperature controller) and LED temperature display which allowed the user to manually control cooling and/or heating of the stage. The temperature readings on the LED readout are resolved to $\pm 0.1^\circ\text{C}$.

The heating/freezing stage was calibrated using a series of synthetic fluid inclusions with known temperatures of homogenization and melting and it was discovered that the apparatus was within a few tenths of a degree to those listed.

Heating is facilitated by passing $\text{O}_2(\text{g})$ over the thermocouple which then heats the

air in the sample chamber which in turn heats the fluid inclusion sections. Freezing measurements are facilitated by using $N_2(g)$ which displaces liquid nitrogen from an insulated dewar and then to the sample chamber. Freezing measurements are more prone to error since temperature increase/decrease is harder to control and interpretation of ice and/or clathrate disappearance (especially small inclusions) can be very subjective.

For a comprehensive review of the apparatus and theory behind fluid inclusion study see Roedder (1984).

I.5. Stable Isotope Techniques

All stable isotope techniques were performed at the Stable Isotope Facility, Department of Earth Sciences, MUN on samples which were deemed to have important information as to mineralizing fluid composition and source region. The isotope systems utilized were $\delta^{13}C$ and $\delta^{18}O$ (from calcite and ankerite), $\delta^{18}O$ (from quartz) and $\delta^{34}S$ (from pyrite and arsenopyrite).

a. $\delta^{13}C$ and $\delta^{18}O$ Determinations from Carbonates

This section describes the sample preparation and extraction of CO_2 from carbonate samples for determinations of $\delta^{18}O$ and $\delta^{13}C$ according to the technique of McCrea (1950) with subsequent analysis via a MAT-252 mass spectrometer.

For the isotope analysis, a total of 9 whole rock samples were analyzed. Whole-rock carbonate samples were used since the physical separation of the carbonate minerals (ie. ankerite and calcite) proved to be too difficult due to the fine-grained nature in the

altered and mineralized rocks. To obtain estimates of carbonate content, the samples were first analyzed using the X-ray diffractometer, and based on the intensity of the carbonate peak(s), an appropriate amount of sample was used.

The carbonate samples were added to double-arm reaction vessels with the sample in the main arm and a 2-5 ml aliquot of anhydrous phosphoric acid in the sidearm. Once both sample and acid were loaded, the reaction vessel was placed on the vacuum line and any atmosphere was pumped from the vessels to minimize errors due to acid hydration and resulting $\text{CO}_2\text{-H}_2\text{O}$ fractionation. After ensuring that the reaction vessels were not outgassing, the vessels were removed from the line to the 25°C water bath for 30 minutes to allow both the sample and acid to reach the same temperature as the bath. After this period of time, the acid was spilled from the sidearm, causing reaction with the carbonate and release CO_2 . Depending on the nature of the carbonate(s) present, the equilibration was for the set period of time as outlined below:

1). For Pure Calcite Samples: Equilibration between acid and sample for a period of not less than four hours. However, overnight (twelve hour) equilibrations seemed to allow for the best gas yields.

2). For Pure Ankerite Samples: Equilibration between acid and sample for a period of 48 hours.

3). For Mixed Ankerite and Calcite Samples: Once the acid is spilled, equilibration takes place for 30 minutes and then a split of CO_2 gas was removed from the vessel representative of calcite dissolution only. The vessel was returned to the bath for 6 hours

after which time any remaining CO₂ from the calcite dissolution was pumped away on the vacuum line. After the removal of this gas aliquot, the vessel was once again returned to the bath where the ankerite was allowed to equilibrate with the acid for 48 hours thus producing CO₂ representative of the ankerite.

Once the samples had equilibrated for an appropriate period of time, they were removed from the bath, attached to the vacuum line and the gas released into a liquid nitrogen trap where it was frozen and the vessel pumped once again. Once this was done, the trap was bathed in a slush, a mixture of liquid nitrogen and ethanol which has a freezing temperature less than that of liquid nitrogen, thereby releasing the frozen CO₂. The gas was passed through a second slush trap to a liquid nitrogen cold-finger where it was once again frozen. The combination of nitrogen and slush traps are designed to remove water which may have formed in the reaction vessel. The gas in the nitrogen finger was gradually warmed (ie. melted) and the gas volume recorded (in centimetres of Hg). The gas was then passed through another slush trap where it was frozen into a sample vessel.

Once the sample vessel was sealed, it was then removed from the vacuum line and loaded into the Finnigan MAT-252 mass spectrometer where the δ¹³C was measured relative to PDB. In addition, the ¹⁸O/¹⁶O ratio was calculated after being ¹⁷O corrected and reported relative to PDB. The following calculations were then used to standardize the oxygen data in terms of V-SMOW.

For Calcite: $\delta^{18}\text{O}_{\text{Calculated}} = (1.02207 \times \delta^{18}\text{O}_{\text{Raw}}) + 22.07$

For Ankerite: $\delta^{18}\text{O}_{\text{calculated}} = \{[(1.03255 \times \delta^{18}\text{O}_{\text{Raw}}) + 1032.55] - 1000\alpha\} / \alpha$

where $\alpha = 1.0111$ (for ankerite at 25°C; Rosenbaum and Sheppard, 1986)

b. $\delta^{34}\text{S}$ Determinations from Sulphides

This section describes the sample preparation and extraction of SO_2 from sulphide samples for determination of $\delta^{34}\text{S}$ according to the technique of Rafter (1965) with analysis via the PRISM 903 mass spectrometer. A total of 11 pure pyrite and/or arsenopyrite sulphide separates were analyzed for their $\delta^{34}\text{S}$ content. In three of the samples, the pyrite and arsenopyrite were so finely intergrown that separation was not possible, so that the isotopic determination includes both minerals.

A sample of sulphide weighing 6mg was ground together with a 150mg amount of CuO pellets. The resulting powder was then loaded into a 1½ cm long piece of quartz glass tubing (a.k.a. "boat") with the open ends capped by quartz glass wool. The boat was then put into a reaction vessel, placed on the vacuum line and evacuated until vacuum was achieved in the vessel. The reaction vessel was then placed into an electric oven and baked for 20 minutes at a temperature of 1000°C such that any sulphate present would decompose and the sulphur from the sulphides reacted with oxygen to yield SO_2 . The gases produced during combustion were then trapped in a U-shaped liquid nitrogen trap and frozen. After the gases had been frozen, the excess oxygen produced by the combustion of the CuO was pumped away. The frozen gases may constitute a mixture of several oxides as opposed to pure SO_2 , so the nitrogen trap was interchanged with a liquid nitrogen-pentane slush trap (-128°C to -120°C) for a period of approximately 6

minutes and then the unwanted gases pumped away. The SO₂ was moved along the line where it was subsequently trapped in a nitrogen cold finger and the gas yield measured (in centimetres of Hg). Finally the gas was trapped in a sample vessel and removed to the mass spectrometer for analysis.

c. $\delta^{18}\text{O}$ Determinations from Quartz

In an effort to check the quality of, and ensure equilibrium conditions of the $\delta^{18}\text{O}$ and $\delta^{13}\text{C}$ data obtained from carbonates, one sample of quartz, syngenetic with respect to ore-stage carbonates, was analyzed for $\delta^{18}\text{O}$ content. The procedure used for oxygen gas extraction from quartz was that of Clayton and Mayeda (1963).

I.6. Laser Ablation Microprobe - Inductively Coupled Plasma - Mass Spectrometer (LAM-ICP-MS)

This procedure is a relatively new procedure performed at the Department of Earth Sciences, MUN and described in detail by Jackson *et al.* (1992) and Longerich *et al.* (1991). The LAM-ICP-MS system was utilized to ascertain gold contents in ore-stage arsenopyrite from rock-chip samples. Figure I.1 is a schematic diagram of the LAM-ICP-MS system.

The system consists of a Q-switched 1064nm Nd:YAG laser which is beamed down the optical tube of a standard petrographic microscope and focused onto the sample with the aid of three optical mirrors. Both site selection and the ablation procedure were monitored using a TV camera and monitor. The resultant plume of ablated material is

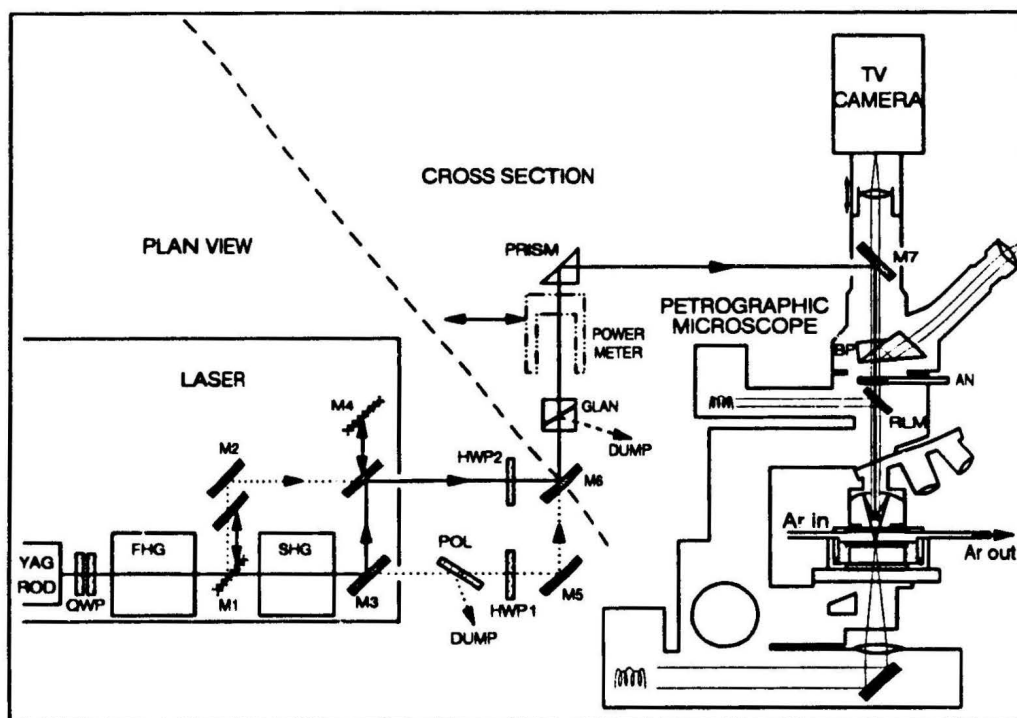


Figure 1.1: Plan and cross-sectional views of the LAM-ICP-MS (modified from Jackson et al., 1992). Abbreviations are as follows: QWP=quarter wave plates (1064nm); FHG, SHG=first, second harmonic generator; M=dielectric mirror (1,2=532nm; 3,4=266nm; 5=1064nm; 6,7=interchangeable); POL=dielectric polariser (1064nm); HWP=half wave plate (1=1064nm; 2=532/266nm); GLAN=glan laser calcite prism polariser; BP=binocular prism; AN=analyser; and RLM=reflected light mirror.

flushed from the sample chamber by a 1l/minute flow of argon gas and introduced into the ICP-MS torch where the ablated material was ionized and analyzed for the following isotopic masses: ^{33}S , ^{34}S , ^{57}Fe , ^{58}Fe , ^{65}Cu , ^{66}Zn , ^{67}Zn , ^{75}As , ^{121}Sb , ^{181}Ta , ^{197}Au and ^{208}Pb (refer to Table I.1 for information pertaining to the elements analyzed). The Ta was analyzed to monitor possible interference effects of TaO (isotopic mass 197) with gold. A narrow range of isotopes was selected for analysis to optimize the limits of detection - more isotopic masses require longer counting times (cps) and result in higher limits of detection. The data are reported as counts/second since a standard does not exist to standardize the laser data on sulphides, but but the data do reflect, semi-quantitatively, the compositions of the ablated materials. In addition, machine background and drift is ascertained by ablating NBS-610 (a synthetic glass standard spiked with 61 trace elements of known concentration - see Longerich *et al.*, 1991) several times before and after the arsenopyrite ablation.

1.7. Quartz Vein Assays

Assays on mineralized quartz veins (a total of 7) were performed by Eastern Analytical Limited in Springdale, Newfoundland. Two analytical packages were utilized to determine the abundances of the following elements: Au, Ce, Sr, Ba, Fe, P, Hg, Mg, As, V, Na, Mo, Al, Be, Ca, Zn, Cu, Sb, Ag, Pb, Bi, Ti, Cd, Co, Ni, W, La, K, Mn, Rb and Cr (see Table I.2 for limits of detection). Gold was analyzed using Fire Assay with an Atomic Absorption finish whereas the remainder were analyzed using aqua regia

digestion - inductively coupled plasma - mass spectrometry (AR-ICP).

Table 1.1: *Isotopic masses and natural abundances of isotopes used in LAM-ICP-MS determinations.*

Element	Mass	Abundance	Comments
S	33	0.75%	Both masses summed to give total S in analysis.
	34	4.20%	
Fe	57	2.14%	Both masses summed to give total Fe in analysis.
	58	0.31%	
Cu	65	30.9%	Both masses summed to give total Zn in analysis.
Zn	66	27.8%	
	67	4.1%	
As	75	100%	Analyzed due to possible interference effects on ¹⁹⁷ Au.
Sb	121	57.3%	
Ta	181	99.9%	
Au	197	100%	
Pb	208	52.4%	

a. Fire Assay/Atomic Absorption (AA) Finish

The sample is weighted at 1 assay ton and is then homogenized with a flux. After homogenization, a preset amount of silver is added to the mixture and then fused and cupelled. After cupellation, the beads are immersed in nitric acid thereby removing the silver after which the bead is then digested in hydrochloric acid. Once digested, the solution is brought up to volume, stirred, and allowed to settle. Finally, the sample is aspirated on the AA machine which has been calibrated to give the Au concentration in ppb with the limits of detection for gold at 0.03 ppb.

b. AR/ICP-30

A 0.500g sample is digested with 2ml of HNO₃ in a warm water bath (95°C) for a period of ½ hour, after which 1ml of HCL is added and the sample returned to the bath for an additional ½ hour. After the solution has sufficiently cooled, it is diluted

with 10ml of deionized water, stirred and let stand for a period of 1 hour to allow any precipitate to settle. Once this is accomplished, the solution is filtered and then analyzed by the ICP-MS. Table I.2. gives the limits of detection for the elements analyzed by this technique.

Table I.2: Limits of detection (LD) for elements analyzed by the AR-ICP technique.

Oxide	LD%	Trace	LD ppm
TiO ₂	0.01	Cr	1
Al ₂ O ₃	0.01	Ni	1
Fe ₂ O ₃	0.01	Co	1
MgO	0.01	V	1
CaO	0.01	Cu	1
Na ₂ O	0.01	Pb	2
K ₂ O	0.01	Zn	1
P ₂ O ₅	0.01	Cd	0.5
		W	10
		Mo	1
		As	5
		Sb	5
		Rb	20
		Ba	10
		Sr	1
		La	10
		Ce	10
		Be	0.5

I.8. Infra-red Determinations

These analyses were performed at the Newfoundland Department of Mines and Energy Labs in St. John's. The following procedure is taken from Wagenbauer *et al.* (1983) using the method first described by Bouvier and Abbey (1980). A 0.2g aliquot of sample is weighed into a nickel boat and mixed with 0.5g of vanadium pentoxide and

0.5g tungstic anhydride - all of which is then fused at 950°C. The evolved gases are carried by a nitrogen stream to an infrared analyzer which measures water content and then on to two other analyzers to ascertain CO₂ and S contents. Resultant readings are recorded as millivolts but converted to percent by comparison with known standards.

Table I.3 gives precision and accuracy using MRG-1 (gabbro, Canadian Certified Reference Materials Project standard) and SY-2 (syenite, Canadian Certified Reference Materials Project standard).

Table I.3: Precision and accuracy for infra-red analyses. Abbreviations include S.D. for standard deviation and Pub. for published values. Published values obtained from Govindaraju (1989).

	MRG-1			SY-2		
	Mean (n=2)	Pub.	S.D.	Mean (n=2)	Pub.	S.D.
H ₂ O%	1.175	1.13	0.0225	0.67	0.63	0.02
S%	0.055	-	0.035	0.015	-	0.005
CO ₂ %	1.05	1.07	0.01	0.52	0.5	0.01

1.9. Multi-Element Direct Neutron Activation Analysis (NAA)

This analytical technique was performed by Becquerel Laboratories Incorporated, Mississauga, Ontario who are contracted by the Newfoundland Department of Mines and Energy for the multi-element analyses. Elements analyzed by this technique include Au, Ag, As, Ba, Br, Cd, Ce, Co, Cr, Cs, Eu, Fe, Hf, Hg, Ir, La, Lu, Mo, Na, Ni, Rb, Sb, Sc, Se, Sm, Sn, Ta, Tb, Te, Th, U, W, Yb, Zn and Zr.

In this procedure 30g of sample is introduced to a nuclear reactor for a sufficient

period of time so as to irradiate the entire sample. The irradiated sample is then removed from the reactor and placed in a lead containment unit where it is allowed to cool. While the sample is cooling, the amount of gamma radiation given off is measured and quantified using scintillometers and then reduced by mini-computer to determine elements and concentrations present.

Table I.4 gives the precision and accuracy of standards MRG-1 (gabbro, United States Geological Survey standard) and SY-2 (syenite, Canadian Certified Reference Materials Project standard).

I.10. Atomic Absorption Spectroscopy (AAS) Trace Element Determinations

Trace element determinations using AAS were performed by the Newfoundland Department of Mines and Energy. The procedural technique is summarized from Wagenbauer *et al.* (1983). In a teflon beaker, 1g of sample is added to 15ml of concentrated HF, 5ml of concentrated HCL and 5ml of 50 vol.% HClO₄. The sample mixture sits overnight and then evaporated on a hot plate. The residue is then digested in 10 vol.% HCL facilitated by heating and once cool made up to a volume of 50ml with 10 vol.% HCL. The following elements are then directly determined using AAS: Rb, Cu, Pb, Zn, Ni, Cr, Co, V, Mo, Li and Be. For Ba and Sr, a 5ml aliquot of the solution is transferred to a 25ml volumetric flask containing 5ml of 5% La³⁺ solution and 6.5ml of concentrated HCL and then made up to volume with deionized water. This solution can then be analyzed by AAS to ascertain the Ba and Sr concentrations.

Table 1.4: Precision and accuracy for neutron activation analyses. Published values are from Govindaraju (1989). Abbreviations used: Det. = lab determination, Pub. = published value and S.D. = standard deviation.

	MRG-1			SY-2		
	Det.	Pub.	S.D.	Det.	Pub.	S.D.
Sb	0.58	0.86	0.14	0.27	0.25	0.01
As	0.9	0.73	0.085	17.00	.73	0.15
Ba	78.5	61	8.75	25.00	460	217.5
Br	1	-	-	1.00	-	-
Cd	1	168	83.5	1.00	0.208	0.396
Ce	20	26	3	120.00	175	27.5
Cs	0.4	0.57	0.085	2.60	2.4	0.1
Cr	410	430	10	69.00	9.5	29.75
Co	92.5	87	2.75	11.00	8.6	1.2
Eu	1.8	1.39	0.205	1.30	2.42	0.56
Au	10.6	5.4	2.6	1.00	0.52	0.24
Hf	4.25	3.76	0.245	7.00	7.7	0.35
La	7.5	9.8	1.15	48.00	75	13.5
Lu	0.02	0.12	0.05	1.90	2.7	0.4
Mo	2.5	0.87	0.815	2.50	1.8	0.35
Ni	215	193	11	5.00	9.9	2.45
Rb	10.05	8.5	0.775	250.00	217	16.5
Sm	6.3	4.5	0.9	0.10	16.1	8
Sc	49.8	55	2.6	4.40	7	1.3
Se	1	0.194	0.403	1.00	0.02	0.49
Ag	-2	110	56	-2.00	1100	551
Ta	1.15	0.8	0.175	2.40	2.01	0.195
Tb	0.445	0.51	0.0325	3.10	2.5	0.3
Th	0.8	0.93	0.065	404.00	379	12.5
W	1	0.3	0.35	1.00	0.76	0.12
U	0.1	0.24	0.07	275.00	284	4.5
Yb	1.15	0.6	0.275	0.20	17	8.4
Zn	240	191	24.5	190.00	248	29
Zr	100	108	4	100.00	280	90

The precision and accuracy of standards MRG-1 (gabbro, Canadian Certified Reference Materials Project standard) and SY-2 (syenite, Canadian Certified Reference Materials Project standard) can be observed in Table 1.5.

Table 1.5: Precision and Accuracy for AAS Trace-Element Analyses. Published values are from Govindaraju (1989). Abbreviations used are the same as those in Table 1.4.

	MRG-1			SY-2		
	Mean (n=2)	Pub.	S.D.	Mean (n=2)	Pub.	S.D.
Cu	129.5	134	2.25	3	5.2	1.1
Pb	11.5	10	0.75	92.5	85	3.75
Zn	185	191	3	251.5	280	14.25
Co	82	87	2.5	10.5	8.6	0.95
Ni	182	193	5.5	9.5	9.9	0.2
Ga	26	17	4.5	28.5	29	0.25
V	500.5	526	12.75	53.5	50	1.75
Nb	15	20	2.5	28	29	0.5
Zr	91.5	108	8.25	286	280	3
Th	2	0.93	0.535	329.5	379	24.75
Y	12.5	14	0.75	126.5	128	0.75
Sr	250	266	8	276	271	2.5
La	11.0	9.8	0.6	80.5	75	2.75
Ce	29	26	1.5	176.5	175	0.75
Ba	46.5	61	7.25	468	460	4
Sc	54.65	55	0.175	7	7	0
Dy	2.7	2.9	0.1	17.65	18	0.175
Be	0.8	0.61	0.095	22.25	22	0.125
Li	3.75	4.2	0.225	94.95	95	0.025

1.11. X-Ray Fluorescence (XRF) Trace Element Analyses

Trace element analyses were carried out on pressed whole rock powder pellets by x-ray fluorescence (XRF) techniques using an ARL 8420⁺ automatic x-ray fluorescence spectrometer with a rhodium tube located in the Department of Earth Sciences, MUN. Pressed pellets were made by combining 10g of whole rock powder with 1-1.5g of Union Carbide phenolic resin (TR-16933) binder. The mixture was then homogenized using ball bearings that were placed in the sample vial and then put on a roller for a period of not less than 4 minutes. The homogenized powder was pressed at 30 tons/inch² for approximately 10 seconds and then baked at 150°C for ten minutes. Data reduction was

performed on a Hewlett-Packard 9845B mini-computer. Trace elements analyzed include the following: S, Cl, Sc, V, Cr, Ni, Cu, Zn, Ga, As, Rb, Sr, Y, Zr, Nb, Ba, Ce, Pb, Th, U. Precision and accuracy of standards BCR-1 (basalt, United States Geological Survey standard); DNC-1 (diabase, United States Geological Survey standard); PACS-1 (marine sediment, National Research Council of Canada standard) and W-2 (diabase, United States Geological Survey of Canada standard) can be viewed in Table I.6.

I.12. Inductively Coupled Plasma - Emission Spectroscopy (ICP-ES) Major Oxide Determinations

Procedure used is that of Wagenbauer *et al.* (1983). A mixture of 0.1g of sample and 0.5g of lithium metaborate are fused in a graphite crucible at 1000°C. The melt is then transferred to a 250ml polycarbonate bottle containing 25ml of 4 vol. % HCL and 5ml of concentrated HF. Solution is then digested at 90°C for 1.5 hours and once cooled to room temperature, 50ml of 50g/l boric acid is added to complex excess HF and then allowed to digest at the same conditions as previous digestion. The solution is then transferred to a 100ml volumetric flask, made to volume and mixed. The following oxides are analyzed by ICP-ES using the procedures of Langhmyr and Paus (1968), Abbey (1968), and Buckley and Cranston (1971): SiO₂, Al₂O₃, Fe₂O₃^T, MgO, CaO, Na₂O, TiO₂ and MnO. Phosphorous oxide is analyzed spectro-photometrically following the procedure of Riley (1958) and Hounslow and Moore (1966). Loss on ignition (LOI)

*Table I.6: Precision and Accuracy for XRF analyses. Published values are from Govindaraju (1989).
Abbreviations used are the same as those listed in Table I.4.*

	BCR-1			DNC-1			PACS-1			W-2		
	Mean (n=17)	Pub.	S.D.	Mean (n=5)	Pub.	S.D.	Mean (n=12)	Pub.	S.D.	Mean (n=3)	Pub.	S.D.
S	846.50	410	218.25	1053.2	392	330.60	13200	11320	940	499.70	79	210.35
Cl	285.82	59	113.41	794.15	37	378.57	23900	23900	0	1123.7	190	466.82
Sc	29.87	32.6	1.36	30.89	31	0.06	15.43	-	-	37.29	35	1.14
V	411.72	407	2.36	145.12	148	1.44	152.08	127	12.54	260.73	262	0.64
Cr	11.55	16	2.23	288.73	285	1.86	120.74	113	3.87	88.73	93	2.13
Ni	24.50	13	5.75	246.78	247	0.11	43.53	44.1	0.28	67.54	70	1.23
Cu	24.37	19	2.69	89.05	96	3.47	376.54	452	37.73	103.09	103	0.05
Zn	154.45	129.5	12.47	70.05	66	2.03	701.85	824	61.07	84.15	77	3.58
Ga	22.39	22	0.19	14.41	15	0.30	15.33	-	-	18.45	20	0.77
As	1.27	650	324.36	-2.14	0.2	1.17	211.00	211	0.00	0.28	1.24	0.48
Rb	49.26	47.2	1.03	3.46	4.5	0.52	47.80	-	-	19.82	20	0.09
Sr	332.92	330	1.46	139.90	145	2.55	265.83	277	5.59	191.22	194	1.39
Y	34.81	38	1.59	16.36	18	0.82	15.38	-	-	19.83	24	2.09
Zr	190.25	190	0.12	34.46	41	3.27	123.86	-	-	89.31	94	2.35
Nb	12.66	14	0.67	1.54	3	0.73	8.78	-	-	7.04	7.9	0.43
Ba	706.78	681	12.89	109.21	114	2.39	653.56	-	-	175.33	182	3.34
Ce	46.30	53.7	3.70	-15.90	10.6	13.25	52.77	-	-	16.98	24	3.51
Pb	17.46	13.6	1.93	7.78	6.3	0.74	372.59	404	15.70	10.26	9.3	0.48
Th	6.89	5.98	0.45	0.20	0.2	0.00	-5.24	-	-	1.59	2.2	0.30
U	2.13	1.75	0.19	-0.55	0.1	0.32	-2.12	-	-	0.33	0.53	0.10

is determined at 1000°C using the procedure of Hillebrand *et al.* (1953). Table I.7 gives precision and accuracy for standards VS-N (glass, Association Nationale de la Recherche Technique (Paris) standard) and RGM-1 (rhyolite, United States Geological Survey standard).

Table I.7: Precision and accuracy for major-oxide ICP-ES analyses. Published values from Govindaraju (1989) and abbreviations as per Table I.4.

	VS-N			RGM-1		
	Det.	Pub.	S.D.	Det.	Pub.	S.D.
SiO ₂	56.00	55.57	0.215	73.15	73.45	0.15
Al ₂ O ₃	13.24	13.44	0.1	13.74	13.72	0.01
Fe ₂ O ₃ ¹	4.06	4.14	0.04	1.87	1.86	0.005
MgO	4.39	4.51	0.06	0.27	0.275	0.0025
CaO	4.40	5.53	0.565	1.20	1.15	0.025
Na ₂ O	6.17	5.95	0.11	4.13	4.07	0.03
K ₂ O	8.03	8.12	0.045	4.30	4.3	0
TiO ₂	1.07	1.08	0.005	0.27	0.267	0.0015
MnO	0.10	0.10	0.00	0.03	0.036	0.003
P ₂ O ₅	0.02	-	-	0.04	0.048	0.004

I.13. Inductively Coupled Plasma - Mass Spectrometry (ICP-MS) Techniques

The ICP-MS technique was used to determine the trace and rare earth elements Ba, Ta, Nb, Hf, Zr, Y, Th, La, Ce, Pr, Nd, Sm, Eu, Gd, Tb, Dy, Ho, Er, Tm, Yb, and Lu. The procedure was performed at the Department of Earth Sciences, MUN and makes use of the Na₂O₂ Sinter dissolution due to increased effectiveness of dissolving resistant minerals such as zircons, sulphides, and other insoluble phases. Preliminary XRF analyses of the samples to be analyzed by the ICP-MS technique indicated

anomalous S in excess of 3%. The high proportion of S would have reacted with the Ni crucibles upon firing, thus the S had to be oxidized before standard procedure could be followed. The samples were placed in a high-temperature oven for a period of 12 hours where temperature was increased in increments to 1000°C over a period of four hours. This temperature was then sustained for another four hours and then gradually decreased over a period of four hours. This firing sufficiently oxidized the S so as not to pose problems for the crucibles.

After the samples cooled, 0.2g of sample was accurately weighed into a 30ml Ni-crucible and 0.8g of Na_2O_2 added to the crucible. Both the peroxide and sample were well stirred and a thin layer of peroxide was sprinkled on top of the mixture. The crucibles were then placed in a muffle furnace at 480°C and sintered for 90 minutes. The crucibles were then removed from the oven, covered, cooled, and 10ml of water was added to each crucible drop-wise until the reaction ceased.

The mixture was then added to a 50ml teflon centrifuge tube, well rinsing both the crucible and its lid. A final volume of 30ml was made up in each tube using distilled water and then centrifuged for 15 minutes. The liquid was then poured off, and the residue rinsed with 25ml of distilled water and centrifuged. A final centrifuge was then completed using another 25ml of distilled water and following which the liquid was discarded.

To the residue was added 2.5ml of 8N HNO_3 and 1ml of oxalic acid. The crucible was washed with 0.2N HNO_3 and this was also added to the tube. The solutions

were then transferred to a clean teflon tube and made up to 50g with distilled water. A final dilution was then carried out on the samples before running on the ICP-MS. A 2g aliquot of sample was accurately weighed into a teflon test tube and added to it was 8g aliquot of 0.2N HNO₃, such that the final sample concentration was approximately 0.2N.

In addition to the samples analyzed, a blank, two sample duplicates, and three accepted standards including MRG-1 (gabbro; Canadian Certified Reference Materials Project standard), DNC-1 (diabase, United States Geological Survey standard) and BIR-1 (basalt, United States Geological Survey standard) were also analyzed so as to determine precision and accuracy (Table I.8.).

Table 1.8: Precision and accuracy for ICP-MS analyses. Published values (BIR-1) from Jenner et al. (1990) otherwise published values are from Govindaraju (1989). Abbreviations as per Table 1.4.

	BIR-1			DNC-1			MRG-1		
	Mean	Pub.	S.D.	Mean	Pub.	S.D.	Mean	Pub.	S.D.
Y	13.727	16.8	1.536	15.219	18	1.390	11.659	14	1.171
Zr	10.888	16	2.556	33.810	41	3.595	108.33	108	0.165
Nb	0.636	0.508	0.064	2.087	3	0.456	22.970	20	1.485
Ba	9.151	7.64	0.756	98.934	114	7.533	49.142	61	5.929
La	0.584	0.594	0.005	3.552	3.8	0.124	8.720	9.8	0.540
Ce	1.853	1.8	0.012	8.007	10.6	1.296	25.275	26	0.363
Pr	0.357	0.341	0.008	1.049	1.3	0.126	3.680	3.4	0.140
Nd	2.210	2.19	0.010	4.557	4.9	0.172	17.608	19.2	0.796
Sm	1.149	1.07	0.040	1.425	1.38	0.023	4.437	4.5	0.032
Eu	0.495	0.457	0.019	0.571	0.59	0.009	1.367	1.39	0.012
Gd	1.770	1.520	0.125	1.998	2	0.001	4.149	4	0.074
Tb	0.247	0.30	0.026	0.306	0.41	0.052	0.485	0.51	0.013
Dy	2.047	2.25	0.102	2.377	2.7	0.162	2.793	2.9	0.054
Ho	0.533	0.550	0.008	0.595	0.62	0.013	0.465	0.49	0.013
Er	1.557	1.50	0.029	1.793	1.8	0.003	1.104	1.12	0.008
Tm	0.227	0.227	0.000	0.271	0.1	0.086	0.129	0.11	0.010
Yb	1.617	1.36	0.128	1.816	2.01	0.097	0.831	0.6	0.116
Lu	0.223	0.227	0.002	0.285	0.32	0.018	0.112	0.12	0.004
Hf	0.477	0.58	0.051	1.056	1.01	0.023	3.699	3.76	0.030
Ta	0.027	0.062	0.017	0.080	0.098	0.009	0.805	0.8	0.003
Th	0.712	0.031	0.340	0.720	0.2	0.260	0.760	0.93	0.085

References Cited in Appendices

Abbey, S., 1968: Analysis of rocks and minerals by atomic absorption spectroscopy. Part 2: determination of total iron, magnesium, calcium, sodium and potassium. Geological Survey of Canada Paper 68-20, 21 pages.

Bouvier, J.L. and Abbey, S., 1980: Simultaneous determination of water, carbon dioxide and sulphur in rocks by volatilization and non-dispersive infrared absorptiometry. Canadian Journal of earth Sciences, volume 25, No. 5.

Buckley, D.E. and Cranston, R.E., 1971: Atomic absorption analysis of 18 elements from a single decomposition of aluminosilicates. Chemical Geology, volume 7, page 273.

Clayton, R.N. and Mayeda, T.K., 1963: The use of bromine pentafluoride in the extraction of oxygen from oxides and silicates for isotopic analysis. Geochimica et Cosmochimica Acta, volume 27, pages 43-52.

Govindaraju, K., 1989: 1989 compilation of working values and sample descriptions for 272 geostandards. Geostandards Newsletter Special Issue, volume 13, 113 pages.

Higgins, N.C., 1980: The genesis of the Grey River tungsten prospect: A fluid inclusion, geochemical and isotopic study. Unpublished Ph.D. Thesis. Memorial University of Newfoundland, St. John's, Newfoundland, 404 pages.

Hillebrand, W.F., Lundell, G.E.F., Bright, H.A. and Koffman, J.I., 1953: Applied inorganic analysis (Second Edition). John Wiley and Sons, Inc., New York.

Hounslow, A.W. and Moore, J.R., 1966: Preparation and analysis of silicate rocks and minerals. Geological Paper 66-1, Carleton University, Ottawa.

Jackson, S.E., Longerich, H.P., Dunning, G.R., and Fryer, B.J., 1992: The application of laser ablation microprobe - inductively coupled plasma - mass spectrometry (LAM-ICP-MS) to in situ trace-element determinations in minerals. Canadian Mineralogist, volume 30, pages 1049-1064.

Jenner, G.A., Longerich, H.P., Jackson, S.E., and Fryer, B.J., 1990: ICP-MS - A powerful tool for high precision trace-element analysis in earth sciences: Evidence from analysis of selected U.S.G.S. reference samples.

Langhmyr, F.J. and Paus, P.E., 1968: Analysis of silicate rocks. *Analytica Chimica Acta*, volume 43, pages 397-408.

Longerich, H.P., Jackson, S.E., Fryer, B.J., and Strong, D.F., 1991: The laser ablation microprobe - inductively coupled plasma - mass spectrometer (LAM-ICP-MS). *Geoscience Canada*, volume 20, pages 21-27.

McCrea, J.M., 1950: On the stable isotope chemistry of carbonates and a paleotemperature scale. *Journal of Chemistry and Physics*, volume 18, pages 849-857.

Rafter, T.A., 1965: Recent sulphur isotope measurements on a variety of specimens examined in New Zealand. *Bulletin of Volcanology*, volume 28, pages 3-20.

Reynolds, T.J., 1990: Workshop on application of fluid inclusions to minerals exploration. Short Course Notes. Memorial University of Newfoundland, St. John's, Newfoundland. 57 pages.

Riley, J.P., 1958: The rapid analysis of silicate rocks and minerals. *Analytica Chimica Acta*, volume 19, pages 413-428.

Roedder E., 1984: Fluid Inclusions, *Mineralogical Association of America Reviews in Mineralogy*, volume 12, 644 pages.

Rosenbaum, J. and Sheppard, S.M.F., 1986: An isotopic study of siderites, dolomites and ankerites at high temperatures. *Geochimica et Cosmochimica Acta*, volume 50, pages 1147-1150.

Wagenbauer, H.A., Riley, C.A. and Dawe, G., 1983: Report of the geochemical laboratory for 1983. *In Current Research*. Newfoundland Department of Mines and Energy, Minerals Development Division, Report 83-1, pages 133-137.

APPENDIX II

WHOLE ROCK GEOCHEMICAL ANALYSES

The following pages (Appendices IIa through IIg) contain listings of the geochemical data for samples from the Duder Lake area including Noranda Exploration Company Limited gold assays which were relevant to this study. With respect to the reported data, note:

- 1). All oxides are reported in wt. %, trace elements and rare earth elements as ppm and gold as ppb.
- 2). Fe_2O_3 is total Fe.
- 3). LOI is loss on ignition.
- 4). Mg# calculation: $(\text{MgO}/\text{MgO}_{\text{mw}})/[(\text{Fe}_2\text{O}_3/\text{Fe}_2\text{O}_{3\text{mw}}) + (\text{MgO}/\text{MgO}_{\text{mw}})]$
where "mw" is the molecular weight for the oxide.
- 5). "na" is not analyzed.
- 6). "-" is not detected.
- 7). Abbreviations used in header data: GMA-Zone (fresh gabbro), A-Zone (altered gabbro) and M-Zone (mineralized gabbro).
- 8). Since several of the analytical methods overlapped with respect to some elements, reported values were chosen from the analytical method which produced the best data quality for that element. Table II.1 is a compilation of the elements and oxides reported in the data tables as well as the analytical method inferred to have produced the best data quality for that element (oxide).
- 9). The analytical procedures for the whole rock determinations can be viewed in Appendix I.

Table II.1: Elements utilized from the different analytical techniques and which were used in all geochemical applications. Column headings as follows: emission spectroscopy (ES), atomic absorption (AA), neutron activation (NAA), x-ray fluorescence (XRF) and Na₂O₂ sinter (REE).

	ES	AA	NAA	XRF	REE		ES	AA	NAA	XRF	REE
SiO ₂						Rb					
TiO ₂						Cs					
Al ₂ O ₃						Ba					
Fe ₂ O ₃						Sr					
MnO						Ga					
MgO						Li					
CaO						Ta					
Na ₂ O						Nb					
K ₂ O						Hf					
P ₂ O ₅						Zr					
H ₂ O						Ti					
CO ₂						Y					
LOI						Th					
Cr						U					
Ni						La					
Co						Ce					
Sc						Pr					
V						Nd					
Cu						Sm					
Pb						Eu					
Zn						Gd					
Cd						Tb					
W						Dy					
Mo						Ho					
S						Er					
As						Tm					
Se						Yb					
Sb						Lu					
Ag						Cl					
Au						Br					
K						Be					

Appendix IIa: Major- and trace-element data for mafic volcanic rocks of the Lawrenceton Formation.

	RC-91-62	RC-92-04	JH-92-310	DE-90-51
%				
Mg#	51.76	25.62	44.63	54.90
SiO ₂	51.00	50.07	59.07	49.57
TiO ₂	1.78	3.28	0.93	1.30
Al ₂ O ₃	13.24	14.02	16.69	15.76
Fe ₂ O ₃	9.56	13.92	6.08	9.72
MnO	0.12	0.46	0.09	0.17
MgO	5.76	2.69	2.75	6.64
CaO	6.82	7.32	5.29	8.98
Na ₂ O	4.68	2.91	4.30	3.82
K ₂ O	0.06	0.24	0.58	0.39
P ₂ O ₅	0.30	0.74	0.19	0.13
H ₂ O	4.12	na	na	na
CO ₂	3.54	na	na	na
LOI	7.89	3.36	2.55	3.92
Total	101.20	99.01	98.52	100.41
ppm				
Cr	359	20	33	268
Ni	104	13	24	29
Sc	29	42	16	37
V	366	387	110	290
Cu	29	32	15	33
Pb	-	10	13	-
Zn	82	152	66	70
S	84.00	2475.00	32.00	394.00
As	-	-	-	-
K	457	1992	4815	3238
Rb	1	9	15	7
Ba	65.00	168.00	283.00	170.00
Sr	157.60	215.50	385.60	221.30
Ga	16	28	19	16
Nb	13.8	11.6	8.1	5.9
Zr	104	295	160	101
Ti	10671	19670	5575	7823
Y	21	67	23	28
Th	-	5.00	5.00	-
U	-	-	-	-
Ce	-	38.00	58.00	-
Cl	45.00	60.00	43.00	-

Appendix IIb: Rare earth element data (ppm) for mafic volcanic rocks of the Lawrenceton Formation.

	JH-92-310	DE-90-51	RC-91-62	RC-92-04
Ba	248	154	66	157
Ta	1.60	1.36	1.01	1.53
Nb	9.0	6.2	12.4	11.8
Hf	3.65	2.58	2.73	6.83
Zr	153	101	104	285
Y	22	26	21	63
Th	5.69	2.27	0.95	3.80
La	19.26	9.37	11.62	22.31
Ce	41.45	22.24	27.44	57.56
Pr	4.97	3.02	3.74	8.12
Nd	19.47	13.46	16.49	37.89
Sm	4.26	3.67	4.08	10.36
Eu	1.16	1.08	1.50	3.32
Gd	4.64	4.71	4.79	12.35
Tb	0.63	0.72	0.68	1.85
Dy	4.24	5.06	4.51	12.63
Ho	0.86	1.05	0.86	2.60
Er	2.37	3.15	2.17	7.42
Tm	0.34	0.42	0.29	1.02
Yb	2.26	2.76	1.93	6.40
Lu	0.34	0.41	0.28	0.97

Appendix IIc: Major- and trace element data for mafic plutonic rocks.

	DL191-01	DL191-02	DL191-05	DL191-06	DL191-07	DL191-09
%	A-Zone	GMA-Zone	M-Zone	M-Zone	M-Zone	M-Zone
Mg#	59.28	59.08	44.73	33.46	29.02	23.78
SiO ₂	43.00	45.40	36.58	40.92	33.85	50.40
TiO ₂	0.89	0.95	1.94	1.40	2.79	1.50
Al ₂ O ₃	16.68	15.97	12.19	13.81	12.72	12.15
Fe ₂ O ₃	9.88	11.32	11.58	11.66	13.60	9.31
MnO	0.17	0.22	0.31	0.25	0.35	0.28
MgO	8.07	9.17	5.26	3.29	3.12	1.63
CaO	6.83	6.72	9.19	6.94	9.14	5.57
Na ₂ O	3.59	3.32	4.07	5.08	3.64	6.88
K ₂ O	0.68	0.47	0.94	1.05	1.28	0.13
P ₂ O ₅	0.08	0.06	0.08	0.10	0.12	0.50
H ₂ O	5.26	5.46	1.91	1.50	2.33	0.77
CO ₂	5.78	2.64	14.84	12.18	13.58	6.46
LOI	10.98	7.53	14.35	12.66	13.97	8.91
Total	100.85	101.13	96.47	97.17	94.58	97.25
<i>ppm</i>						
Cr	266	171	195	12	21	7
Ni	124	92	17	4	8	9
Co	50	61	41	48	50	73
Sc	36	38	63	43	54	24
V	219	205	447	234	422	76
Cu	62	89	37	31	47	21
Pb	-	-	4	-	20	6
Zn	51	60	90	76	98	48
Cd	1.00	1.00	1.00	1.00	1.00	1.00
W	14.00	19.00	102.00	107.00	80.00	328.00
Mo	2.50	2.50	5.30	2.50	2.50	2.50
S	306.16	896.69	7193.35	14500.64	19476.37	26035.08
As	52.50	16.00	9555.00	14600.00	17600.00	16300.00
Se	1.00	1.00	1.00	1.00	1.00	1.00
Sb	7.00	1.70	46.70	83.70	121.00	73.40
Au	3.7	1.0	4305.0	2680.0	3720.0	4700.0
K	5645	3902	7762	8716	10667	1038
Rb	24	17	31	38	49	4
Cs	3.30	2.90	2.30	5.10	7.30	0.70
Ba	113.60	133.43	218.97	179.78	214.59	52.07
Sr	183.64	199.17	174.82	199.28	176.30	173.93
Ga	12	15	20	27	32	16
Li	119.30	77.90	26.80	4.50	6.90	1.60
Ta	0.10	0.10	0.10	0.82	0.75	1.40
Nb	1.3	1.2	3.3	4.6	5.6	5.1
Hf	2.40	1.30	0.20	4.80	4.90	3.60
Zr	53	56	131	258	217	179
Ti	5336	5695	11630	8423	16726	8963
Y	16	18	34	56	50	49
Th	0.60	0.60	1.20	2.90	2.50	1.80
U	0.10	0.20	0.10	0.10	0.10	0.10
La	3.60	3.50	4.45	9.30	9.40	16.00
Ce	16.00	14.00	23.50	37.00	32.00	28.00
Sm	2.60	2.90	4.70	6.90	7.90	8.00
Eu	0.25	1.80	2.33	1.60	3.60	2.50
Tb	0.63	0.58	0.20	1.60	1.80	1.60
Dy	2.30	2.70	3.30	3.40	4.10	3.60
Yb	2.80	2.80	21.50	0.20	0.20	0.20
Lu	0.42	0.38	1.55	1.10	1.10	0.94
Cl	50.65	63.78	61.00	64.32	59.24	32.94
Br	1.00	1.00	16.00	1.00	1.00	1.00
Be	0.80	0.70	1.35	1.30	1.50	0.80

Appendix IIc: (continued)

	DL191-10	DL191-11	DL291-01	DL291-02	DL391-03	DL391-04
%	M Zone	M Zone	A Zone	GMA-Zone	M-Zone	A-Zone
Mg#	15.39	57.72	39.97	36.17	39.52	46.24
SiO ₂	44.58	41.25	56.05	56.10	40.40	46.05
TiO ₂	1.73	0.96	0.87	0.88	1.68	1.63
Al ₂ O ₃	14.75	15.42	17.30	16.31	13.18	14.42
Fe ₂ O ₃	11.76	9.74	5.70	6.29	12.49	12.35
MnO	0.24	0.16	0.13	0.16	0.22	0.25
MgO	1.20	7.47	2.13	2.00	4.58	5.96
CaO	5.14	7.36	3.01	3.87	6.01	5.51
Na ₂ O	5.97	2.13	4.70	3.16	4.17	3.98
K ₂ O	0.94	1.20	1.92	2.51	1.08	0.34
P ₂ O ₅	0.50	0.07	0.18	0.18	0.08	0.15
H ₂ O	1.94	4.62	1.86	1.76	1.86	4.53
CO ₂	5.39	11.28	6.28	7.46	14.20	6.29
LOI	10.73	15.01	8.65	9.74	15.08	10.71
Total	97.52	100.77	100.64	101.20	98.97	101.35
ppm						
Cr	-	226	20	27	15	28
Ni	-	81	5	6	18	18
Co	52	48	37	27	56	48
Sc	25	43	23	19	48	61
V	34	202	98	93	288	272
Cu	25	60	9	12	77	43
Pb	9	-	5	8	-	-
Zn	167	57	62	55	78	81
Cd	1.00	1.00	1.00	1.00	1.00	1.00
W	152.00	31.50	129.00	66.00	103.00	30.00
Mo	2.50	2.50	2.50	2.50	2.50	2.50
S	33200.18	403.71	1565.34	471.03	9466.58	485.96
As	27700.00	35.00	1450.00	10.00	2380.00	25.00
Se	1.00	1.00	1.00	1.00	1.00	1.00
Sb	86.80	22.05	11.60	4.40	89.30	61.10
Au	16500.0	1.0	558.0	4.6	665.0	1.0
K	7762	9920	15938	20836	8965	2822
Rb	33	47	82	111	32	7
Cs	3.80	8.55	5.40	5.70	6.40	2.50
Ba	175.15	220.26	370.14	450.48	250.52	221.47
Sr	133.04	114.98	244.62	175.32	287.66	260.66
Ga	33	14	20	19	18	18
Li	2.90	121.25	11.20	13.90	12.40	76.70
Ta	1.20	0.10	1.20	1.30	0.10	0.10
Nb	8.6	1.8	9.6	9.7	3.3	3.3
Hf	7.10	0.20	0.20	4.80	0.20	0.20
Zr	331	77	165	166	118	116
Ti	10341	5785	5216	5276	10072	9772
Y	81	22	26	26	32	33
Th	3.90	1.20	8.50	10.00	0.10	0.80
U	0.10	0.10	2.60	2.90	0.10	0.10
La	15.00	4.55	22.00	26.00	6.60	6.90
Ce	54.00	20.50	57.00	67.00	30.00	32.00
Sm	12.90	3.45	6.70	7.90	5.30	5.60
Eu	3.70	1.10	0.25	1.30	0.25	2.20
Tb	2.80	0.45	0.20	1.10	0.62	1.10
Dy	6.30	2.80	3.90	4.20	3.00	4.30
Yb	0.20	3.05	4.70	3.20	8.60	6.00
Lu	1.70	0.38	0.61	0.54	0.61	0.66
Cl	63.35	114.43	35.31	89.11	30.11	49.53
Br	1.00	1.00	1.90	1.00	5.20	1.20
Be	1.50	0.55	1.90	1.80	1.20	0.90

Appendix IIc: (continued)

	DL391-05	DL391-06	DL391-09	DL391-11	DL491-01	DL491-02
%	<i>A-Zone</i>	<i>M-Zone</i>	<i>A-Zone</i>	<i>GMA Zone</i>	<i>M-Zone</i>	<i>M-Zone</i>
Mg#	46.06	46.21	41.54	58.26	78.14	78.12
SiO ₂	43.70	27.33	43.70	45.50	34.60	28.95
TiO ₂	1.51	1.75	1.98	1.33	0.33	0.29
Al ₂ O ₃	14.20	11.15	12.59	16.25	7.67	7.09
Fe ₂ O ₃	11.08	13.71	11.16	9.78	11.09	9.87
MnO	0.24	0.20	0.16	0.16	0.14	0.14
MgO	5.31	6.61	4.45	7.66	22.25	19.77
CaO	6.87	12.89	10.70	9.64	3.70	3.64
Na ₂ O	4.05	2.39	3.98	3.09	0.03	0.33
K ₂ O	0.66	0.81	0.05	0.47	0.02	1.13
P ₂ O ₅	0.13	0.06	0.30	0.06	0.03	0.02
H ₂ O	3.02	2.90	4.15	4.31	6.16	2.59
CO ₂	10.28	18.50	8.13	3.29	15.50	26.63
LOI	12.62	18.57	10.85	7.28	20.36	29.21
<i>Total</i>	100.37	95.47	99.92	101.22	100.22	100.44
<i>ppm</i>						
Cr	307	45	-	198	2391	2871
Ni	48	35	10	108	1002	838
Co	43	61	37	52	100	100
Sc	42	64	40	35	18	17
V	247	399	384	239	109	120
Cu	64	81	60	74	73	62
Pb	-	-	-	-	-	-
Zn	49	80	72	62	44	52
Cd	1.00	1.00	1.00	1.00	1.00	1.00
W	36.00	89.00	27.00	46.00	16.00	33.00
Mo	2.50	2.50	2.50	2.50	2.50	2.50
S	935.97	12633.66	3869.00	765.58	1001.21	819.22
As	46.00	7510.00	21.00	1.10	2.00	291.00
Se	1.00	1.00	1.00	1.00	1.00	1.00
Sb	79.60	125.00	4.20	2.00	3.50	94.40
Au	1.0	1280.0	8.6	1.0	3.9	1.0
K	5479	6683	415	3902	166	9380
Rb	35	29	1	15	1	45
Cs	3.20	6.60	1.20	3.60	1.10	7.00
Ba	105.04	76.21	-	57.18	466.09	92.01
Sr	84.13	222.41	164.65	248.11	88.01	73.86
Ga	17	17	16	16	6	5
Li	97.50	47.20	45.00	70.00	89.10	43.80
Ta	0.10	0.10	0.66	0.57	0.10	0.10
Nb	2.6	2.3	5.5	1.5	1.1	0.7
Hf	3.70	0.20	6.30	2.30	0.20	0.20
Zr	92	82	254	68	25	23
Ti	9052	10491	11870	7973	1978	1739
Y	27	24	56	20	7	6
Th	1.40	0.10	2.40	0.30	0.50	0.10
U	0.10	0.10	0.40	0.10	0.10	0.10
La	6.80	4.80	13.00	3.50	1.00	2.00
Ce	29.00	23.00	38.00	12.00	8.00	5.00
Sm	5.30	3.60	9.30	3.30	1.20	1.00
Eu	0.25	3.10	2.80	1.60	0.25	0.25
Tb	1.00	0.20	1.70	0.53	0.20	0.20
Dy	3.90	2.80	6.80	3.30	0.90	0.80
Yb	5.80	19.00	8.40	3.40	0.20	4.60
Lu	0.76	1.10	1.20	0.52	0.02	0.02
Cl	70.17	40.78	54.45	27.54	37.66	33.60
Br	1.10	13.00	1.00	1.00	1.00	2.50
Be	1.10	1.10	0.80	0.50	0.30	0.40

Appendix IIc: (continued)

	DL491-05	DL491-10	DL491-11	DL491-16	DL491-17	DL491-18
%	M Zone	GMA Zone	GMA Zone	A-Zone	M-Zone	GMA-Zone
Ag#	74.97	52.77	44.38	27.82	28.30	43.42
SiO ₂	34.70	50.35	55.30	48.30	40.45	50.20
TiO ₂	0.72	1.12	0.63	1.70	3.86	2.27
Al ₂ O ₃	8.53	15.11	15.69	13.87	11.22	13.85
Fe ₂ O ₃	9.36	10.27	2.68	10.91	17.72	12.17
MnO	0.15	0.24	0.07	0.29	0.34	0.24
MgO	15.73	6.44	1.20	2.36	3.92	5.24
CaO	3.71	4.38	8.70	5.60	9.44	7.69
Na ₂ O	0.54	3.29	8.81	6.24	2.18	4.76
K ₂ O	1.43	0.77	0.03	0.43	0.20	0.22
P ₂ O ₅	0.04	0.10	0.10	0.20	0.14	0.12
H ₂ O	2.74	4.99	0.98	1.84	4.82	3.36
CO ₂	23.69	3.79	6.13	8.50	7.47	1.83
LOI	26.01	8.22	6.88	9.06	10.39	5.14
Total	100.92	100.29	100.09	98.96	99.87	101.90
ppm						
Cr	2247	248	7	-	-	42
Ni	816	77	-	-	-	12
Co	100	53	28	30	53	50
Sc	24	42	10	24	37	56
V	190	260	19	39	446	445
Cu	66	154	3	25	53	47
Pb	-	56	5	6	4	-
Zn	67	171	19	84	130	84
Cd	1.00	1.00	1.00	1.00	1.00	1.00
W	111.00	61.00	119.00	80.00	49.00	62.00
Mo	2.50	2.50	2.50	2.50	2.50	2.50
S	820.59	527.18	1193.11	6367.49	9405.82	1203.54
As	1060.00	42.00	2.20	5840.00	3405.00	7.10
Se	1.00	1.00	1.00	1.00	1.00	1.00
Sb	95.40	135.00	0.63	31.60	20.20	1.20
Au	1.0	1.0	1.0	1670.0	809.5	1.0
K	11871	6392	249	3570	1660	1826
Rb	52	33	-	13	6	9
Cs	4.80	2.10	0.20	1.30	2.00	3.40
Ba	80.91	130.34	54.99	146.83	131.88	114.09
Sr	71.11	74.38	83.23	169.49	95.32	164.05
Ga	7	15	28	26	19	19
Li	6.80	75.90	8.40	29.80	59.30	30.10
Ta	0.10	0.10	1.60	0.56	0.31	0.71
Nb	2.1	3.2	12.8	9.2	5.0	3.4
Hf	0.20	0.20	19.00	6.50	0.20	4.20
Zr	54	114	772	470	147	148
Ti	4316	6714	3777	10192	23111	13609
Y	14	28	125	103	43	39
Th	0.10	1.70	12.00	4.90	1.40	1.70
U	0.10	0.10	2.70	1.10	0.30	0.30
La	2.70	5.20	30.00	20.00	8.10	6.60
Ce	9.00	20.00	100.00	62.00	28.50	22.00
Sm	1.80	3.50	15.70	13.40	6.45	6.10
Eu	0.25	0.25	2.60	4.70	2.08	1.80
Tb	0.20	0.60	3.10	2.40	0.86	1.30
Dy	1.40	3.70	16.80	8.20	7.05	5.70
Yb	6.10	7.20	20.00	23.00	8.85	5.80
Lu	0.36	0.54	3.10	2.50	0.85	0.82
Cl	28.56	28.87	58.21	29.82	21.47	48.83
Br	3.10	3.00	1.00	10.00	5.25	1.00
Be	0.40	0.90	3.70	1.90	1.50	0.90

Appendix IIc: (continued)

	DL491-19	DL591-01	DL591-02	DL591-03	DL591-04	DL591-05
%	<i>M-Zone</i>	<i>GMA-Zone</i>	<i>A-Zone</i>	<i>GMA Zone</i>	<i>A Zone</i>	<i>M Zone</i>
Mg#	51.30	55.81	56.31	48.64	30.52	30.32
SiO ₂	41.85	43.00	36.08	46.15	41.35	34.50
TiO ₂	1.20	1.32	0.95	1.76	3.11	3.12
Al ₂ O ₃	12.21	16.44	15.08	14.91	14.08	12.63
Fe ₂ O ₃	9.27	11.67	8.35	12.08	15.78	15.79
MnO	0.31	0.25	0.20	0.25	0.30	0.36
MgO	5.48	8.27	6.04	6.42	3.89	3.86
CaO	9.15	5.90	10.47	6.95	8.30	8.85
Na ₂ O	3.79	3.74	3.65	3.88	3.96	4.31
K ₂ O	0.88	0.35	2.04	0.38	0.18	0.61
P ₂ O ₅	0.06	0.12	0.03	0.10	0.15	0.12
H ₂ O	3.39	5.32	2.25	4.94	4.39	2.75
CO ₂	13.25	5.66	16.07	4.27	7.05	12.29
LOI	14.94	10.44	17.62	8.24	10.40	12.64
<i>Total</i>	99.14	101.50	100.51	101.12	101.50	96.78
<i>ppm</i>						
Cr	151	299	244	182	60	63
Ni	26	126	109	31	14	15
Co	48	52	49	50	52	54
Sc	72	50	39	42	71	70
V	308	294	242	362	533	584
Cu	77	70	58	47	56	128
Pb	11	15	-	4	7	6
Zn	55	83	53	77	72	88
Cd	1.00	1.00	1.00	1.00	1.00	1.00
W	77.00	17.00	27.00	18.00	27.00	121.00
Mo	2.50	2.50	2.50	2.50	2.50	7.30
S	5076.29	816.49	406.88	594.34	1175.17	12585.46
As	2350.00	18.00	241.00	12.00	58.20	16600.00
Se	1.00	1.00	1.00	1.00	1.00	1.00
Sb	33.80	60.90	19.30	7.90	6.80	106.00
Au	555.0	1.0	3.4	1.0	1.0	6530.0
K	7305	2905	16935	3154	1494	5064
Rb	30	14	68	13	6	21
Cs	1.60	3.20	3.50	4.90	3.70	1.70
Ba	114.59	131.66	253.01	174.61	91.69	156.54
Sr	203.68	220.00	360.04	259.34	149.84	197.56
Ga	15	14	13	17	22	24
Li	40.40	127.10	23.80	59.40	48.10	37.90
Ta	0.10	0.53	0.10	0.60	0.81	0.10
Nb	2.5	2.8	1.4	2.3	4.8	5.2
Hf	0.20	2.50	1.50	3.00	4.80	0.20
Zr	91	101	66	121	179	184
Ti	7194	7913	5695	10551	18644	18674
Y	27	28	20	33	48	46
Th	1.40	1.20	0.80	1.80	2.00	0.10
U	0.10	0.10	0.10	0.30	0.60	0.10
La	4.60	6.40	7.20	6.70	9.10	8.50
Ce	16.00	20.00	17.00	23.00	30.00	26.00
Sm	4.00	4.40	3.30	5.50	7.10	6.80
Eu	1.70	1.10	0.25	1.40	2.80	4.40
Tb	0.20	0.76	0.53	1.10	1.30	0.20
Dy	2.90	3.00	2.10	5.00	6.30	4.70
Yb	6.90	4.60	2.80	5.20	6.60	31.00
Lu	0.61	0.58	0.42	0.86	1.00	1.90
Cl	22.81	22.24	25.72	28.11	22.74	24.10
Br	4.60	1.30	1.00	1.00	1.00	20.00
Be	1.00	1.40	1.30	1.30	1.80	1.80

Appendix IIc: (continued)

	DL591 06	DL591 08	DL591 09	DL691-02	DL691-03	DL691-04
%	A Zone	M Zone	M Zone	GMA Zone	M Zone	M Zone
Mg#	27.90	34.23	23.00	63.06	52.21	31.74
SiO ₂	41.00	40.95	47.00	45.90	38.97	45.80
TiO ₂	2.33	2.49	1.20	1.00	1.35	2.11
Al ₂ O ₃	14.19	12.01	14.41	17.53	14.57	9.09
Fe ₂ O ₃	13.68	14.16	10.86	10.28	10.36	12.06
MnO	0.30	0.26	0.19	0.26	0.22	0.25
MgO	2.97	4.14	1.82	9.85	6.36	3.14
CaO	9.19	7.57	5.19	7.42	8.85	6.22
Na ₂ O	5.27	4.49	5.86	3.10	3.21	4.76
K ₂ O	0.07	0.28	0.98	0.55	1.28	0.25
P ₂ O ₅	0.17	0.14	0.37	0.07	0.08	0.05
H ₂ O	3.23	2.47	2.43	5.55	3.64	1.64
CO ₂	9.01	11.10	8.01	0.95	12.66	9.22
LOI	11.11	10.25	11.08	5.84	14.70	13.18
Total	100.28	96.74	98.96	101.80	99.96	96.89
<i>ppm</i>						
Cr	40	14	9	293	167	9
Ni	7	-	-	174	42	-
Cu	48	45	31	62	50	98
Sc	66	40	20	36	45	35
V	367	313	10	220	345	202
Cu	31	40	18	78	68	28
Pb	-	5	4	-	-	6
Zn	58	126	179	77	77	103
Cd	1.00	1.00	1.00	1.00	1.00	1.00
W	43.00	113.00	76.00	27.00	46.00	400.00
Mn	2.50	2.50	2.50	2.50	2.50	2.50
S	1200.80	8705.27	22651.02	353.26	3606.85	31046.40
As	146.00	13300.00	21300.00	4.30	6775.00	38500.00
Se	1.00	1.00	1.00	1.00	1.00	1.00
Sb	10.00	43.80	81.60	1.70	53.00	132.00
Au	17.0	4200.0	5650.0	1.0	2275.0	15500.0
K	581	2324	8135	4566	10667	2034
Rb	2	9	35	24	46	10
Cs	2.30	0.20	4.20	5.30	6.55	1.70
Ba	70.95	100.25	191.69	204.71	240.94	42.81
Sr	187.07	158.07	142.66	302.12	248.25	127.68
Ga	21	24	37	15	17	18
Li	57.10	48.90	4.60	114.30	62.25	2.60
Ta	0.61	0.10	1.10	0.10	0.10	1.60
Nb	4.8	5.0	11.4	2.3	2.3	5.7
Hf	5.70	0.20	11.00	1.50	0.20	6.10
Zr	220	153	461	69	82	255
Ti	13968	14928	7194	5995	8063	12619
Y	52	42	105	22	23	58
Th	2.70	3.00	6.20	0.80	1.40	3.00
U	0.80	0.10	0.10	0.10	0.10	0.10
La	11.00	6.50	19.00	4.70	4.30	10.00
Ce	35.00	26.00	66.00	15.00	15.50	25.00
Sm	8.50	7.20	13.40	3.50	3.55	8.20
Eu	2.40	4.90	4.50	0.25	2.03	2.30
Tb	1.60	0.20	3.50	0.63	0.20	1.80
Dy	6.40	4.60	7.50	3.30	2.50	3.00
Yb	7.90	24.00	7.40	2.90	9.65	0.20
Lu	1.00	2.10	2.10	0.47	0.61	1.40
Cl	41.27	28.03	19.44	32.14	25.05	34.36
Br	1.00	18.00	1.00	1.00	10.50	1.00
Be	1.60	1.40	2.00	1.10	1.05	1.00

Appendix IIc: (continued)

	DL691-05	DL691-06	DL691-07	DL691-08	DL691-09	DL791-02
%	<i>M-Zone</i>	<i>M-Zone</i>	<i>M Zone</i>	<i>M Zone</i>	<i>M Zone</i>	<i>GMA Zone</i>
Mg#	25.37	24.33	24.11	25.17	37.13	62.55
SiO ₂	39.97	42.10	41.63	38.67	32.05	47.85
TiO ₂	2.13	1.53	1.64	2.83	1.21	1.17
Al ₂ O ₃	13.28	15.44	11.06	14.27	15.84	15.23
Fe ₂ O ₃	10.88	11.47	10.91	11.63	14.77	8.46
MnO	0.43	0.26	0.31	0.33	0.25	0.20
MgO	2.08	2.07	1.95	2.19	4.89	7.93
CaO	9.72	7.09	10.07	8.31	6.93	12.47
Na ₂ O	5.34	5.88	4.66	4.33	3.07	3.11
K ₂ O	0.88	0.98	0.54	0.99	1.51	0.40
P ₂ O ₅	0.28	0.34	0.20	0.17	0.08	0.07
H ₂ O	2.05	2.87	2.46	3.23	4.10	4.14
CO ₂	12.78	10.28	11.59	11.13	14.79	0.66
LOI	12.32	11.15	12.62	13.44	17.04	4.05
Total	97.32	98.31	95.58	97.17	97.64	100.94
ppm						
Cr	-	-	9	-	289	592
Ni	-	-	-	-	74	60
Co	29	37	67	51	50	62
Sc	29	26	33	39	47	57
V	78	54	107	209	334	308
Cu	20	23	34	41	61	58
Pb	7	-	-	5	-	4
Zn	177	74	60	115	77	49
Cd	1.00	1.00	1.00	1.00	1.00	1.00
W	68.00	138.00	182.00	157.00	46.00	104.00
Mo	2.50	7.30	2.50	5.00	2.50	2.50
S	17866.24	21931.18	24109.46	22167.14	16670.90	1096.14
As	5270.00	9840.00	30600.00	12900.00	13600.00	1.10
Se	1.00	1.00	1.00	1.00	1.00	1.00
Sb	44.60	38.00	123.00	75.70	88.90	1.10
Au	872.0	1170.0	7280.0	3440.0	2150.0	1.0
K	7347	8135	4483	8177	12576	3321
Rb	30	36	20	43	67	11
Cs	3.00	5.40	3.60	8.90	10.00	2.00
Ba	173.67	180.34	93.02	120.95	305.47	151.42
Sr	194.87	130.07	137.15	145.89	190.36	211.27
Ga	28	32	26	30	25	15
Li	5.70	19.90	25.50	35.20	33.40	52.00
Ta	0.51	0.10	1.10	0.10	0.10	0.91
Nb	10.0	7.6	7.1	8.5	2.6	1.8
Hf	6.30	0.20	7.60	0.20	0.20	2.60
Zr	361	316	286	399	91	75
Ti	12769	9172	9832	16966	7254	7014
Y	96	78	63	79	30	25
Th	4.20	4.40	3.20	5.00	3.50	0.60
U	0.10	0.10	0.10	0.10	0.10	0.10
La	30.00	19.00	11.00	13.00	5.20	4.20
Ce	69.00	56.00	38.00	39.00	18.00	16.00
Sm	14.90	11.70	8.20	9.20	4.00	3.90
Eu	5.20	3.50	2.40	3.40	0.25	2.10
Tb	1.90	0.20	1.90	0.20	0.20	0.78
Dy	6.60	7.00	5.60	5.60	1.90	3.60
Yb	22.00	25.00	0.20	26.00	26.00	2.40
Lu	2.50	2.20	1.10	3.30	1.40	0.51
Cl	19.66	19.27	31.55	18.70	26.40	36.89
Br	7.90	15.00	1.00	18.00	17.00	1.00
Be	1.70	1.80	1.40	2.10	1.90	0.60

Appendix IIc: (continued)

	DL791-03	DL791-04	DL791-07	DL891-03	DL891-06	DL891-07
%	A Zone	M Zone	M-Zone	A-Zone	M-Zone	M-Zone
Mg#	39.74	32.96	28.72	63.28	35.23	16.85
SiO ₂	40.70	37.35	64.93	47.45	43.60	48.50
TiO ₂	2.46	3.65	0.75	1.47	1.23	1.21
Al ₂ O ₃	7.86	10.12	7.11	15.27	13.18	13.82
Fe ₂ O ₃	16.67	15.11	6.64	11.22	9.61	12.84
MnO	0.34	0.28	0.19	0.16	0.28	0.29
MgO	6.17	4.17	1.50	10.85	2.93	1.46
CaO	10.13	9.33	4.84	2.46	8.28	4.26
Na ₂ O	1.77	3.78	3.88	3.23	6.84	5.03
K ₂ O	0.04	0.29	0.20	0.21	0.31	1.08
P ₂ O ₅	0.25	0.06	0.07	0.20	0.08	0.51
H ₂ O	3.08	2.68	0.75	7.32	1.10	3.14
CO ₂	11.97	11.77	7.25	2.43	12.23	5.61
LOI	14.58	11.52	7.18	8.12	11.19	8.08
Total	100.97	95.67	97.28	100.64	97.53	97.08
ppm						
Cr	106	-	10	500	11	-
Ni	46	10	-	328	-	-
Co	64	44	68	73	36	36
Sc	54	65	17	29	35	10
V	546	684	33	219	109	9
Cu	158	57	6	97	24	20
Pb	5	5	-	5	6	5
Zn	140	105	34	70	62	119
Cd	1.00	1.00	1.00	1.00	1.00	1.00
W	30.00	135.00	301.00	22.00	98.00	93.00
Mn	2.50	6.70	2.50	2.50	2.50	5.80
S	2395.29	25535.30	7395.54	1276.78	11031.75	18490.97
As	45.00	11500.00	21600.00	33.00	7320.00	16000.00
Se	1.00	1.00	1.00	1.00	1.00	1.00
Sb	15.10	55.10	79.20	18.40	33.80	71.40
Au	1.0	2690.0	2850.0	1.0	1590.0	4400.0
K	332	2449	1660	1743	2573	8965
Rb	1	8	5	9	9	30
Cs	4.60	2.10	0.20	3.70	0.20	3.10
Ba	-	69.73	-	50.29	69.36	182.92
Sr	92.41	195.11	79.98	78.33	186.77	113.16
Ga	19	18	10	13	17	33
Li	22.80	21.60	4.50	158.80	11.80	31.20
Ta	0.73	0.10	1.70	0.10	0.10	0.10
Nb	6.5	4.4	3.3	4.5	5.7	8.0
Hf	8.20	0.20	2.80	3.00	0.20	0.20
Zr	251	140	125	127	270	327
Ti	14748	21912	4526	8813	7374	7224
Y	91	39	31	20	63	93
Th	3.00	1.40	1.60	1.20	4.60	6.30
U	0.80	0.10	0.10	0.10	0.10	0.10
La	14.00	6.00	7.40	6.40	12.00	21.00
Ce	47.00	22.00	20.00	21.00	27.00	53.00
Sm	14.70	5.90	3.90	4.30	8.00	15.00
Eu	3.50	4.10	1.90	1.90	2.10	7.00
Tb	3.20	0.20	1.10	0.72	1.20	1.50
Dy	12.50	4.50	1.90	2.80	3.40	8.20
Yb	14.00	21.00	0.20	2.60	14.00	31.00
Lu	2.40	1.40	1.10	0.36	1.10	3.10
Cl	23.48	24.65	30.06	24.80	22.58	27.50
Br	1.00	17.00	1.00	1.00	11.00	21.00
Be	1.60	1.50	0.40	1.10	1.10	1.80

Appendix IIc: (continued)

	DL891-08	DL891-09	DL891-10	DL891 11	DL891 12	RC91 14
%	<i>M-Zone</i>	<i>M-Zone</i>	<i>GMA-Zone</i>	<i>A Zone</i>	<i>A Zone</i>	<i>A Zone</i>
Mg#	14.74	21.86	25.59	23.99	22.56	52.98
SiO ₂	41.40	50.70	50.55	51.80	48.55	39.20
TiO ₂	0.98	1.23	2.08	1.08	1.44	0.74
Al ₂ O ₃	10.29	13.54	15.02	14.01	13.00	15.12
Fe ₂ O ₃	10.46	9.43	13.21	11.63	11.68	9.60
MnO	0.32	0.22	0.26	0.26	0.24	0.16
MgO	1.01	1.48	2.55	2.06	1.91	6.07
CaO	12.81	5.02	4.90	5.51	4.94	8.30
Na ₂ O	3.70	5.84	5.73	3.34	4.92	2.05
K ₂ O	1.08	1.13	0.37	1.20	1.23	1.57
P ₂ O ₅	0.31	0.30	0.33	0.56	0.34	0.08
H ₂ O	2.23	2.75	4.83	-	2.77	4.22
CO ₂	12.37	6.28	2.65	-	6.49	16.23
LOI	11.78	8.75	5.72	8.45	9.81	18.11
Total	94.15	97.64	100.72	99.90	98.06	101.00
<i>ppm</i>						
Cr	-	15	-	-	-	22
Ni	-	-	-	-	-	37
Co	34	36	31	34	58	49
Sc	23	20	22	17	22	38
V	13	11	61	-	19	182
Cu	11	7	23	19	23	76
Pb	-	4	-	-	7	-
Zn	62	116	117	127	96	49
Cd	1.00	1.00	1.00	1.00	1.00	1.00
W	103.00	129.00	44.00	106.00	222.00	19.00
Mu	5.20	2.50	2.50	2.50	2.50	2.50
S	18070.05	17560.88	595.73	1500.32	26886.82	1267.37
As	15500.00	20100.00	14.00	782.00	14800.00	86.80
Se	1.00	1.00	1.00	1.00	1.00	1.00
Sb	48.90	60.90	2.80	13.70	43.90	85.80
Au	4390.0	6100.0	1.0	120.0	3830.0	1.0
K	8965	9339	3071	9962	10211	13033
Rb	27	32	11	27	30	51
Cs	0.20	1.70	6.20	1.60	1.60	16.00
Ba	115.03	138.11	98.08	152.98	138.30	142.15
Sr	185.30	120.94	184.63	80.77	139.69	134.30
Ga	24	33	26	28	29	13
Li	7.40	5.30	26.20	40.70	12.20	62.40
Ta	0.10	1.20	0.88	1.00	0.10	0.10
Nb	5.9	8.3	6.6	7.9	8.3	0.9
Hf	0.20	10.00	6.60	7.50	0.20	0.20
Zr	229	419	246	327	309	46
Ti	5845	7374	12470	6475	8633	4436
Y	66	91	66	86	81	15
Th	2.50	5.20	3.40	4.30	3.50	0.10
U	0.10	0.10	0.90	1.10	0.10	0.10
La	21.00	18.00	15.00	18.00	16.00	2.60
Ce	51.00	56.00	47.00	62.00	57.00	10.00
Sm	11.20	12.60	11.40	13.40	10.70	2.50
Eu	4.10	3.40	3.90	3.80	4.40	0.25
Tb	0.20	3.10	2.20	2.50	0.95	0.56
Dy	6.20	6.00	9.50	5.50	7.20	2.00
Yb	29.00	0.20	9.00	13.00	32.00	3.40
Lu	1.30	2.30	1.60	1.90	2.60	0.46
Cl	49.08	59.89	80.02	70.98	64.56	44.65
Br	21.00	1.00	1.00	1.10	20.00	1.50
Be	1.30	1.80	1.80	2.55	1.80	0.80

Appendix IIc: (continued)

	RC91-50	RC91-51	RC91-57	RC91-61	W90-59a	W90-59b
%	<i>GMA Zone</i>	<i>GM 1 Zone</i>	<i>A-Zone</i>	<i>M-Zone</i>	<i>A-Zone</i>	<i>A-Zone</i>
Mg#	36.66	63.86	58.74	16.55	16.44	64.38
SiO ₂	55.45	49.65	42.15	41.48	59.80	45.70
TiO ₂	1.06	1.30	0.96	3.45	0.82	0.92
Al ₂ O ₃	17.70	15.80	16.34	10.57	12.90	17.10
Fe ₂ O ₃	6.99	7.20	8.85	18.12	7.35	9.39
MnO	0.09	0.14	0.16	0.21	0.08	0.14
MgO	2.27	7.14	7.07	2.02	0.73	8.57
CaO	3.78	11.95	9.05	4.79	2.06	5.24
Na ₂ O	8.57	3.50	2.71	3.56	7.66	4.08
K ₂ O	0.06	0.89	1.57	0.89	0.11	0.74
P ₂ O ₅	0.14	0.10	0.06	0.32	0.17	0.07
H ₂ O	2.63	2.66	5.37	2.06	na	na
CO ₂	1.58	0.44	7.02	7.39	na	na
LOI	3.62	3.48	11.74	9.82	na	na
Total	99.73	101.15	100.66	95.22	91.68	91.95
<i>ppm</i>						
Cr	-	544	217	-	31	247
Ni	6	43	97	-	9	175
Co	29	52	47	47	na	na
Sc	-	63	31	23	35	37
V	88	246	185	108	83	181
Cu	14	126	61	52	-	108
Pb	-	-	-	7	12	-
Zr	30	39	55	173	89	60
Cd	1.00	1.00	1.00	1.00	na	na
Vl	81.00	83.00	8.00	162.00	na	na
Mo	2.50	2.50	2.50	2.50	na	na
S	102.95	585.09	464.29	27920.15	381.74	173.05
As	0.90	0.20	2.20	54400.00	-	-
Se	1.00	1.00	1.00	1.00	na	na
Sb	0.36	0.17	8.50	218.00	na	na
Au	1.0	1.0	1.0	36600.0	na	na
K	498	7388	13033	7363	913	6143
Rb	1	24	58	37	118	27
Cs	0.20	3.80	5.70	3.50	na	na
Ba	140.90	453.73	161.39	185.71	398.31	235.25
Sr	174.64	540.84	107.11	129.73	131.42	294.31
Ga	33	13	17	38	23.58	12.84
Li	2.60	32.10	85.00	5.20	na	na
Ta	3.00	1.10	0.10	0.66	na	na
Nb	28.9	6.1	1.3	5.0	13.02	1.70
Hf	25.00	1.90	1.50	5.10	na	na
Zr	1059	73	60	269	274.76	77.49
Ti	6355	7793	5755	20683	4916	5515
Y	104	18	18	66	56	22
Th	4.90	1.10	0.80	3.10	11.61	-
U	1.20	0.10	0.10	0.10	na	na
La	24.00	7.00	3.70	12.00	na	na
Ce	71.00	17.00	11.00	35.00	109.08	-
Sm	14.20	3.70	3.10	10.60	na	na
Eu	2.10	1.30	1.30	1.80	na	na
Tb	2.90	0.70	0.20	2.00	na	na
Dy	10.50	3.10	2.90	4.60	na	na
Yb	20.00	2.60	3.40	0.20	na	na
Lu	3.30	0.44	0.54	1.90	na	na
Cl	151.82	65.33	58.70	24.55	123.72	24.49
Br	1.00	1.00	1.00	1.00	na	na
Be	2.60	0.70	0.60	1.80	na	na

Appendix IIc: (continued)

	W90-59c	W90-59d
%	<i>M-Zone</i>	<i>M-Zone</i>
Mg#	51.17	65.03
SiO ₂	37.70	63.10
TiO ₂	1.10	0.10
Al ₂ O ₃	14.20	4.27
Fe ₂ O ₃	11.49	3.77
MnO	0.17	0.16
MgO	6.08	3.54
CaO	7.02	7.12
Na ₂ O	2.18	1.14
K ₂ O	1.25	0.57
P ₂ O ₅	0.06	0.01
H ₂ O	na	na
CO ₂	na	na
LOI	na	na
<i>Total</i>	81.25	83.78
<i>ppm</i>		
Cr	26	190
Ni	39	17
Co	na	na
Sc	26	24
V	164	83
Cu	63	23
Pb	-	-
Zn	71	20
Cd	na	na
W	na	na
Mo	na	na
S	1213.40	2994.80
As	69.97	4107.70
Se	na	na
Sb	na	na
Au	na	na
K	10377	4732
Rb	46	21
Cs	na	na
Ba	108.99	107.25
Sr	126.45	113.23
Ga	14.13	6.35
Li	na	na
Ta	na	na
Nb	1.98	-
Hf	na	na
Zr	61.93	17.42
Ti	6595	600
Y	18	9
Th	-	-
U	na	na
La	na	na
Ce	34.21	322.90
Sm	na	na
Eu	na	na
Tb	na	na
Dy	na	na
Yb	na	na
Lu	na	na
Cl	18.82	21.10
Br	na	na
Be	na	na

Appendix II: Rare earth element data for select mafic plutonic rocks.

	DL491-10 <i>GMA Zone</i>	DL691-09 <i>M-Zone</i>	DL391-05 <i>A Zone</i>	DL591-06 <i>A-Zone</i>	DL791-02 <i>GMA-Zone</i>	DL191-02 <i>GMA-Zone</i>
Ba	132	253	177	56	138	122
Ta	0.38	0.30	0.35	0.54	0.45	0.15
Nb	5.4	3.5	5.9	6.2	2.2	2.3
Hf	2.30	2.33	3.36	5.72	1.71	1.48
Zr	139	83	194	234	71	80
Y	27	32	34	53	23	18
Th	1.61	1.60	1.26	2.79	0.74	0.77
La	5.66	7.30	7.93	13.05	4.10	5.57
Ce	14.46	18.15	20.60	32.44	10.66	13.49
Pr	2.03	2.53	2.94	4.69	1.58	1.79
Nd	9.24	12.16	14.15	21.78	7.94	8.11
Sm	2.92	3.92	4.37	6.25	2.68	2.19
Eu	0.81	1.26	1.73	2.09	1.06	0.87
Gd	3.81	4.89	5.72	8.62	3.43	2.87
Tb	0.63	0.78	0.88	1.27	0.55	0.42
Dy	4.69	5.77	6.40	9.81	3.91	3.07
Ho	1.05	1.20	1.38	2.06	0.86	0.72
Er	3.31	3.74	4.25	6.34	2.57	2.22
Tm	0.46	0.56	0.61	0.95	0.39	0.29
Yb	3.10	3.34	3.72	6.24	2.50	1.94
Lu	0.50	0.53	0.57	0.91	0.36	0.29

	DL391-11 <i>GMA Zone</i>	DL591-03 <i>GMA-Zone</i>	DL591-05 <i>M-Zone</i>	DL191-10 <i>M-Zone</i>	DL491-17 <i>M-Zone</i>	DL891-08 <i>M-Zone</i>
Ba	78	201	131	146	113	102
Ta	0.29	0.15	0.28	1.00	0.30	0.81
Nb	2.9	2.8	5.7	15.1	5.5	8.8
Hf	1.56	2.61	5.35	8.88	4.18	6.41
Zr	92	115	196	531	146	298
Y	21	32	48	85	44	75
Th	0.57	1.39	2.25	4.42	1.99	3.42
La	3.82	6.57	11.94	21.20	9.91	27.16
Ce	10.43	16.65	28.49	53.13	25.64	62.03
Pr	1.57	2.40	3.95	7.61	3.66	8.41
Nd	7.62	12.35	18.67	36.08	18.20	38.90
Sm	2.62	3.70	5.42	10.60	5.55	10.16
Eu	1.10	1.46	1.83	3.07	2.14	4.44
Gd	3.41	5.19	7.49	13.20	7.47	12.50
Tb	0.52	0.76	1.20	2.14	1.13	1.91
Dy	3.60	5.73	8.89	15.44	8.29	13.50
Ho	0.79	1.28	1.86	3.19	1.79	2.77
Er	2.35	3.90	5.81	9.30	5.22	8.31
Tm	0.35	0.56	0.86	1.40	0.74	1.23
Yb	2.14	3.74	5.97	8.91	4.91	7.99
Lu	0.35	0.55	0.85	1.33	0.70	1.23

Appendix II d: (continued)

	DL691-07	DL691-04	DL491 16	DL891-12	RC91 61
	<i>M-Zone</i>	<i>M-Zone</i>	<i>A-Zone</i>	<i>A-Zone</i>	<i>M-Zone</i>
Ba	91	47	120	124	145
Ta	1.15	1.41	0.68	0.69	0.35
Nb	7.8	7.1	16.7	10.6	7.5
Hf	7.71	6.26	12.48	7.18	6.78
Zr	308	272	761	340	323
Y	63	59	109	85	73
Th	3.98	3.39	6.06	4.07	3.80
La	14.36	13.41	23.74	19.22	16.37
Ce	36.40	33.03	58.76	49.81	41.62
Pr	5.21	4.70	8.34	7.08	6.03
Nd	24.82	22.46	38.38	34.41	29.58
Sm	7.14	6.73	11.27	10.20	8.69
Eu	2.44	2.00	3.37	3.37	2.67
Gd	9.71	9.25	14.60	12.79	11.00
Tb	1.53	1.46	2.48	2.12	1.78
Dy	11.55	10.93	18.99	15.32	12.93
Ho	2.43	2.34	4.12	3.22	2.73
Er	7.61	7.11	12.88	10.05	8.56
Tm	1.12	1.02	1.89	1.44	1.27
Yb	7.50	6.93	12.62	9.69	8.10
Lu	1.13	1.03	1.93	1.53	1.22

Appendix IIe: Major- and trace-element data for sandstone and siltstone lithologies.

	DL191-12	DL191-13	DL291-05	DL391-12	DL491-07	DL491-08
%						
Mg#	32.29	32.74	49.03	30.78	25.48	29.62
SiO ₂	63.55	63.65	64.25	53.00	51.85	68.20
TiO ₂	0.91	0.87	0.82	0.99	1.04	0.81
Al ₂ O ₃	15.26	14.52	11.52	21.01	24.49	12.33
Fe ₂ O ₃	6.54	6.48	4.65	9.82	8.34	7.41
MnO	0.12	0.19	0.15	0.10	0.63	0.18
MgO	1.75	1.77	2.51	2.45	1.60	1.75
CaO	0.79	1.87	4.22	0.33	0.17	0.62
Na ₂ O	1.13	1.93	1.88	1.00	1.31	1.16
K ₂ O	3.20	2.46	2.39	4.20	3.79	2.25
P ₂ O ₅	0.10	0.12	0.16	0.16	0.11	0.15
H ₂ O	2.89	2.83	1.90	5.82	5.26	2.97
CO ₂	2.95	3.80	5.89	0.29	2.83	3.90
LOI	5.72	6.68	8.01	5.40	6.47	4.84
Total	99.07	100.54	100.56	98.46	99.80	99.70
ppm						
Cr	105	98	197	127	125	150
Ni	42	45	48	50	57	55
Co	48	41	47	40	49	70
Sc	18	18	23	25	27	13
V	133	132	86	272	159	151
Cu	18	54	6	87	36	14
Pb	20	17	6	25	19	21
Zn	53	73	49	142	71	66
Cd	1.00	1.00	1.00	1.00	1.00	1.00
W	164.00	133.00	197.00	74.00	32.00	319.00
Mo	2.50	2.50	2.50	13.00	2.50	2.50
S	72.71	379.77	87.29	8919.31	1301.11	308.96
As	44.00	28.00	11.00	38.00	61.00	94.30
Se	1.00	1.00	1.00	1.00	1.00	1.00
Sb	6.40	30.20	4.40	88.10	8.70	4.10
Au	1.0	1.0	7.6	1.0	1.0	1.0
K	26564	20421	19840	34865	31462	18678
Rb	118	98	101	151	169	97
Cs	5.90	4.00	4.10	8.80	9.40	3.90
Ba	554.59	400.85	445.98	550.89	649.61	509.41
Sr	28.36	44.06	110.74	52.87	129.65	44.16
Ga	23	19	14	30	32	17
Li	34.00	42.50	16.80	67.20	53.70	36.70
Ta	2.40	1.90	2.20	2.20	2.00	2.60
Nb	17.6	16.4	15.4	19.3	20.8	14.2
Hf	9.50	8.20	15.00	3.20	3.50	13.00
Zr	254	234	470	161	137	362
Ti	5455	5216	4916	5935	6235	4856
Y	29	33	32	40	23	30
Th	18.00	14.00	15.00	17.00	19.00	14.00
U	4.40	3.30	3.50	7.40	2.50	4.00
La	48.00	32.00	38.00	42.00	50.00	35.00
Ce	108.00	87.00	104.00	102.00	114.00	81.00
Sm	11.00	8.60	10.40	11.20	8.20	10.00
Eu	1.80	1.40	0.25	2.90	1.70	1.40
Tb	1.20	1.00	1.30	1.50	0.57	1.20
Dy	3.50	3.50	3.60	5.70	2.50	3.60
Yb	4.40	4.00	3.70	7.10	3.60	5.00
Lu	0.76	0.57	0.68	0.67	0.33	0.49
Cl	41.29	38.09	63.96	19.87	15.04	31.94
Br	1.00	1.00	1.00	1.90	1.00	1.00
Be	1.90	1.70	1.60	3.40	3.50	1.90

Appendix II: (continued)

	DL491-20	DL491-21	DL591-10	DL791-10	DL891 02	W90 060a
%						
Mg#	30.18	30.42	24.44	33.09	52.86	43.59
SiO ₂	62.60	62.60	63.40	73.00	45.15	70.50
TiO ₂	0.95	0.80	0.78	0.65	0.65	0.14
Al ₂ O ₃	15.17	14.02	13.77	9.66	10.09	9.77
Fe ₂ O ₃	6.76	5.36	6.94	3.82	7.58	4.92
MnO	0.13	0.10	0.09	0.12	0.34	0.10
MgO	1.64	1.32	1.26	1.06	4.77	1.92
CaO	0.74	1.63	1.34	2.44	10.75	1.53
Na ₂ O	1.06	1.13	1.39	1.43	1.84	1.29
K ₂ O	3.49	3.13	2.51	1.96	1.73	1.88
P ₂ O ₅	0.12	0.09	0.02	0.10	0.08	0.08
H ₂ O	2.96	2.62	4.01	1.60	1.53	na
CO ₂	5.33	3.91	3.24	4.13	15.73	na
LOI	7.40	5.71	6.82	5.14	17.87	na
Total	100.06	95.87	98.32	99.38	100.85	92.13
ppm						
Cr	143	95	110	70	176	134
Ni	32	36	27	22	56	37
Co	37	52	33	59	47	na
Sc	17	13	15	12	41	15
V	137	122	140	89	184	80
Cu	27	26	37	7	13	9
Pb	19	24	10	29	10	-
Zn	54	76	70	36	36	52
Cd	1.00	1.00	1.00	1.00	1.00	na
W	102.00	221.00	154.00	287.00	132.00	na
Mo	2.50	6.90	12.00	2.50	2.50	na
S	2608.38	5350.39	12045.43	696.61	1010.43	3565.30
As	2650.00	10900.00	14300.00	50.70	143.00	803.27
Se	1.00	1.00	1.00	1.00	1.00	na
Sb	22.10	35.20	69.10	5.00	10.10	na
Au	764.0	2410.0	2820.0	1.0	13.0	na
K	28972	25942	20836	16271	14361	15606
Rb	115	116	108	74	67	85
Cs	8.30	5.90	6.80	3.00	3.30	na
Ba	602.19	597.92	454.12	275.98	342.67	408.25
Sr	32.93	50.95	54.73	40.67	251.16	96.20
Ga	21	21	27	12	10	14
Li	9.70	7.20	11.80	9.50	7.60	na
Ta	1.50	1.90	0.92	2.30	0.82	na
Nb	16.3	16.8	15.6	12.7	2.5	11.4
Hf	6.20	0.20	0.20	14.00	0.20	na
Zr	280	316	202	401	60	228
Ti	5695	4766	4676	3897	3897	839
Y	34	31	29	28	22	24
Th	16.00	16.00	12.00	13.00	0.80	8.58
U	3.90	3.40	0.10	3.30	0.40	na
La	42.00	42.00	35.00	31.00	6.80	
Ce	92.00	86.00	77.00	71.00	20.00	154.28
Sm	10.30	10.00	8.80	8.30	3.90	na
Eu	0.25	2.50	0.25	1.60	1.60	na
Tb	0.86	0.20	0.20	1.10	0.63	na
Dy	3.80	3.30	2.50	3.10	2.40	na
Yb	8.10	19.00	25.00	3.60	3.10	na
Lu	0.78	0.74	1.10	0.54	0.45	na
Cl	18.47	15.79	15.00	43.70	18.73	17.67
Br	3.90	16.00	20.00	1.00	1.00	na
Be	1.80	1.60	1.40	1.20	1.20	na

Appendix III: Major- and trace-element data for mineralized quartz-carbonate veins.

	RC91-12	RC91-13	RC91-21	RC91-26
%				
TiO ₂	0.01	0.01	0.01	0.01
Al ₂ O ₃	0.20	0.31	0.40	0.28
Fe ₂ O ₃	5.52	8.15	4.53	8.50
MgO	0.74	0.07	0.11	0.01
CaO	2.41	0.42	0.02	0.23
Na ₂ O	0.03	0.05	0.01	0.05
K ₂ O	0.05	0.08	0.07	0.08
P ₂ O ₅	0.12	0.22	0.03	0.22
ppm				
Cr	2	2	5	2
Ni	1	1	4	1
Co	31	34	75	22
V	4	1	9	1
Cu	11	13	6	10
Pb	6	7	4	6
Zn	92	123	55	70
Cd	0.5	0.5	0.5	0.5
W	128	111	245	74
Mo	1	1	1	1
As	<2200	<2200	393	<2200
Sb	44	29	5	10
Au	3050	3910	117	8653
Rb	20	20	20	20
Ba	10	15	22	12
Sr	59	11	2	8
La	10	10	10	10
Ce	18	23	24	27
Be	0.5	0.5	0.5	0.5
	RC91-31a	RC92-02	W90-60b	
%				
TiO ₂	0.01	0.01	0.01	
Al ₂ O ₃	0.09	0.47	0.06	
Fe ₂ O ₃	3.90	3.27	3.67	
MgO	0.14	0.18	0.61	
CaO	0.59	0.10	1.38	
Na ₂ O	0.03	0.01	0.01	
K ₂ O	0.01	0.06	0.03	
P ₂ O ₅	0.08	0.06	0.01	
ppm				
Cr	3	2	2	
Ni	1	1	18	
Co	49	88	39	
V	1	13	2	
Cu	7	3	5	
Pb	5	9	5	
Zn	63	32	17	
Cd	0.5	0.5	0.5	
W	263	370	242	
Mo	1	1	1	
As	<2200	1237	<2200	
Sb	7	3	5	
Au	3213	143	6895	
Rb	20	20	20	
Ba	10	24	15	
Sr	11	5	98	
La	10	10	10	
Ce	11	14	12	
Be	0.5	0.5	0.5	

Appendix IIg: Gold assays and sample intervals for selected diamond drill core samples (data courtesy of Noranda Exploration Company Limited).

Sample	DDH No.	From(m)	To(m)	Interval(m)	Au(g/t)
144401	DL-90-01	3.20	4.20	1.00	0.01
144402	DL-90-01	4.20	5.20	1.00	
144403	DL-90-01	5.20	6.20	1.00	0.02
144404	DL-90-01	6.20	7.20	1.00	
144405	DL-90-01	7.20	8.20	1.00	
144406	DL-90-01	8.20	9.20	1.00	
144407	DL-90-01	9.20	10.20	1.00	
144408	DL-90-01	10.20	11.20	1.00	
144409	DL-90-01	11.20	12.20	1.00	0.03
144410	DL-90-01	12.20	13.20	1.00	
144411	DL-90-01	13.20	14.20	1.00	
144412	DL-90-01	14.20	15.20	1.00	
144413	DL-90-01	15.20	16.20	1.00	
144414	DL-90-01	16.20	17.20	1.00	0.02
144415	DL-90-01	17.20	18.20	1.00	0.09
144416	DL-90-01	18.20	19.20	1.00	0.09
144417	DL-90-01	19.20	20.20	1.00	0.48
144418	DL-90-01	20.20	20.70	0.50	0.02
144419	DL-90-01	20.70	21.70	1.00	2.08
144420	DL-90-01	21.70	22.70	1.00	0.65
144421	DL-90-01	22.70	23.70	1.00	2.89
144422	DL-90-01	23.70	24.70	1.00	5.90
144423	DL-90-01	24.70	25.70	1.00	4.70
144424	DL-90-01	25.70	26.10	0.40	3.83
144425	DL-90-01	26.10	27.10	1.00	0.37
144426	DL-90-01	27.10	27.70	0.60	0.42
144427	DL-90-01	27.70	28.70	1.00	5.14
144428	DL-90-01	28.70	29.70	1.00	6.96
144429	DL-90-01	29.70	30.50	0.80	9.40
144430	DL-90-01	30.50	31.40	0.90	0.02
144431	DL-90-01	31.50	32.50	1.00	
144432	DL-90-01	32.50	33.50	1.00	
144433	DL-90-01	33.50	34.50	1.00	
144434	DL-90-01	34.50	35.50	1.00	
144435	DL-90-01	35.50	36.50	1.00	
144436	DL-90-01	36.50	37.50	1.00	
144437	DL-90-01	37.50	38.50	1.00	
144438	DL-90-01	38.50	38.80	0.30	
144439	DL-90-01	43.20	43.40	0.20	
144440	DL-90-01	46.50	47.00	0.50	1.14
144441	DL-90-02	12.25	12.50	0.25	3.87
144442	DL-90-02	12.50	13.50	1.00	2.52
144443	DL-90-02	13.50	14.50	1.00	2.86
144444	DL-90-02	14.50	15.50	1.00	1.10
144445	DL-90-02	15.50	16.50	1.00	1.72
144446	DL-90-02	16.50	17.50	1.00	0.07
144447	DL-90-02	17.50	18.50	1.00	0.67
144448	DL-90-02	18.50	19.50	1.00	0.05
144449	DL-90-02	19.50	20.50	1.00	
144450	DL-90-02	20.50	21.50	1.00	
144451	DL-90-02	21.50	22.50	1.00	
144452	DL-90-02	22.50	23.50	1.00	
144453	DL-90-02	23.50	24.50	1.00	
144454	DL-90-02	24.50	25.50	1.00	
144455	DL-90-02	25.50	26.50	1.00	
144456	DL-90-02	26.50	27.50	1.00	
144457	DL-90-02	27.50	28.20	0.70	
144458	DL-90-02	29.60	30.30	0.70	
144459	DL-90-02	37.10	37.60	0.50	

Appendix IIg: (continued)

144460	DL 90 03	28.00	28.50	0.50	0.34
144461	DL 90 03	28.50	29.00	0.50	0.01
144462	DL 90 03	30.10	31.10	1.00	-
144463	DL 90 03	31.10	31.60	0.50	0.35
144464	DL 90 03	31.60	32.10	0.50	1.48
144465	DL 90 03	32.10	33.10	1.00	-
144466	DL 90 03	68.00	69.00	1.00	-
144467	DL 90 03	69.00	70.00	1.00	-
144468	DL 90 03	70.00	71.00	1.00	0.10
144469	DL 90 04	17.00	18.00	1.00	-
144470	DL 90 04	18.00	19.00	1.00	-
144471	DL 90 04	94.40	95.40	1.00	0.81
144472	DL 90 04	98.20	99.20	1.00	1.53
144473	DL 90 04	108.80	109.80	1.00	0.70
144474	DL 90 04	109.80	110.80	1.00	0.30
144475	DL 90 04	110.80	111.20	0.40	1.96
144476	DL 90 04	111.20	112.20	1.00	1.09
144477	DL 90 04	112.20	113.20	1.00	0.09
144478	DL 90 04	113.20	114.20	1.00	0.49
144479	DL 90 04	114.20	115.20	1.00	0.79
175401	DL 90 05	42.20	42.50	0.30	-
175402	DL 90 05	46.60	47.60	1.00	-
175403	DL 90 05	58.40	59.30	0.90	1.54
175404	DL 90 05	59.30	60.30	1.00	0.02
175405	DL 90 05	60.30	61.30	1.00	0.23
175406	DL 90 05	61.30	62.70	1.04	0.11
175407	DL 90 05	62.70	63.40	0.70	2.37
175408	DL 90 05	63.40	64.40	1.00	0.09
175409	DL 90 05	64.40	65.90	1.50	0.18
175410	DL 90 05	65.90	67.50	1.60	4.44
175411	DL 90 05	67.50	68.60	1.10	0.18
175412	DL 90 05	68.60	69.10	0.50	1.86
175413	DL 90 05	69.10	70.00	0.90	0.01
175414	DL 90 05	70.00	70.20	0.20	2.32
175415	DL 90 05	70.20	71.00	0.80	0.01
175416	DL 90 05	71.00	71.30	0.30	1.80
175417	DL 90 05	71.30	71.90	0.60	0.38
175418	DL 90 05	71.90	72.90	1.00	1.75
175419	DL 90 05	72.90	73.60	0.70	0.41
175420	DL 90 05	73.60	74.60	1.00	0.02
175421	DL 90 06	48.25	49.25	1.00	0.11
175422	DL 90 06	49.25	50.30	1.05	9.40
175423	DL 90 06	50.30	51.60	1.30	2.42
175424	DL 90 06	51.60	52.60	1.00	6.00
175425	DL 90 06	52.60	54.00	1.40	0.92
175426	DL 90 06	54.00	55.00	1.00	0.03
175427	DL 90 06	55.00	56.50	1.50	3.20
175428	DL 90 06	56.50	57.70	1.20	0.04
175429	DL 90 06	57.70	58.25	0.55	2.21
175430	DL 90 06	58.25	59.00	0.75	0.02
175431	DL 90 06	59.00	59.85	0.85	1.44
175432	DL 90 06	59.85	60.60	0.75	0.04
175433	DL 90 06	60.60	62.00	1.40	0.16
175434	DL 90 05	80.30	81.40	1.10	0.55
175435	DL 90 05	81.40	81.90	0.50	1.22
175436	DL 90 06	47.30	47.90	0.60	0.89
175437	DL 90 06	47.90	48.25	0.35	0.16
175438	DL 90 07	17.70	18.30	0.60	0.02
175439	DL 90 07	24.50	25.10	0.60	1.04
175440	DL 90 07	27.60	27.70	0.10	0.01
175441	DL 90 07	28.90	29.30	0.40	5.00

Appendix IIg: (continued)

175442	DL-90-07	41.30	41.40	0.10	5.00
175443	DL-90-07	42.60	42.70	0.10	5.00
175444	DL-90-07	42.70	43.00	0.30	5.00
175445	DL-90-07	43.00	43.50	0.50	2.27
175446	DL-90-07	43.50	44.40	0.90	0.08
175447	DL-90-07	44.40	44.60	0.20	0.51
175448	DL-90-08	4.80	5.10	0.30	1.18
175449	DL-90-08	5.10	6.00	0.90	0.80
175450	DL-90-08	6.00	7.00	1.00	0.46
175451	DL-90-08	7.00	8.00	1.00	0.18
175452	DL-90-08	8.00	8.90	0.90	0.30
175453	DL-90-08	8.90	9.80	0.90	0.05
175454	DL-90-08	44.60	45.60	1.00	0.04
175455	DL-90-08	45.60	46.20	0.60	1.35
175456	DL-90-08	46.20	47.80	1.60	0.01
175457	DL-90-08	46.80	47.80	1.00	4.67
175458	DL-90-08	49.30	49.60	0.30	4.67
175459	DL-90-08	49.60	50.10	0.50	0.37
175460	DL-90-08	49.60	50.10	0.50	1.38
175461	DL-90-08	50.40	51.40	1.00	0.01
175462	DL-90-08	51.40	51.60	0.20	2.47
175463	DL-90-08	54.90	55.40	0.50	2.08
175464	DL-90-08	62.20	62.60	0.40	1.94
175465	DL-90-08	63.70	64.50	0.80	1.64

APPENDIX III

SAMPLE LOCATIONS

A total of 165 samples were collected from the Duder Lake area comprising outcrop and trench samples (68) and drill core samples (97). Only 85 of the 165 samples were geochemically analyzed, but the remainder were petrographic samples and helped to better constrain the limits of the alteration system.

The following appendices list specific information for all samples. Appendix IIIa contains a listing of trench and outcrop samples with specific sampling site location information such as trench number, UTM northing and easting co-ordinates (if samples were collected outside of the exploration grid) and finally a brief sample description. Appendix IIIb lists the location of samples obtained from drill core and includes diamond drill hole number and depth from which the sample was obtained. In addition it also gives a brief sample description.

Appendix IIIa: Trench and outcrop sample locations.

<i>Sample</i>	<i>Trench¹</i>	<i>Site²</i>	<i>Northing¹</i>	<i>Easting¹</i>	<i>Rock Type</i>
RC-91-001			5465900	670725	Altered Gabbro
RC-91-002			5464300	670475	Mineralized gabbro
RC-91-003			5435000	625300	Altered diorite
RC-91-003a			5435000	625300	Aplite veins in diorite
RC-91-003b			5435000	625300	Unaltered diorite
RC-91-004a			5451500	641750	Coarse-grained conglomerate
RC-91-004b			5451500	641750	Fine-grained conglomerate
RC-91-005			5462750	660000	Caradocian Shale
RC-91-006			5466900	664300	Granodiorite
RC-91-007			5478600	671750	Fe-oxidized sandstone
RC-91-008			5475050	676800	Isoclinally folded sandstone
RC-91-009	TR-89-006	0.3			Altered Gabbro
RC-91-010	TR-89-006	2.3			Altered Gabbro
RC-91-011	TR-89-006	5.3			Altered Gabbro
RC-91-012	TR-89-006	6.3			Mineralized quartz vein
RC-91-013	TR-89-006	8.3			Mineralized quartz vein
RC-91-014	TR-89-006	11.9			Altered gabbro
RC-91-015	TR-89-006	14.3			Unaltered gabbro
RC-91-016	TR-89-005	14.0			Altered Gabbro
RC-91-017	TR-89-005	13.2			Altered Gabbro
RC-91-018	TR-89-005	9.5			Altered Gabbro
RC-91-019	TR-89-005	7.5			Altered Gabbro
RC-91-020	TR-89-09A	3.0			Unaltered Gabbro
RC-91-021	TR-89-09B	4.5			Mineralized quartz vein
RC-91-022	TR-89-004	20.5			Laminated sandstone
RC-91-023a	TR-89-004	16.6			Altered gabbro
RC-91-023b	TR-89-004	16.6			Altered gabbro
RC-91-023c	TR-89-004	16.6			Mineralized gabbro
RC-91-023d	TR-89-004	16.6			Mineralized quartz vein
RC-91-024a	TR-89-004	14.0			Mineralized gabbro
RC-91-024b	TR-89-004	15.0			Altered gabbro
RC-91-025	TR-89-003	15.5			Altered gabbro
RC-91-026	TR-89-003	10.0			Mineralized quartz vein
RC-91-027	TR-89-003	7.0			Altered gabbro
RC-91-028	TR-89-002	7.5			Altered gabbro
RC-91-029	TR-89-002	6.0			Mineralized gabbro
RC-91-030	TR-89-002	5.0			Mineralized gabbro
RC-91-31A	TR-89-002	4.0			Mineralized quartz vein
RC-91-31B	TR-89-002	4.0			Mineralized gabbro
RC-91-032	TR-89-001	4.0			Altered gabbro
RC-91-033	TR-89-001	5.0			Altered gabbro
RC-91-034	TR-89-001	8.0			Mineralized gabbro
RC-91-035			5467375	664750	Tuffaceous siltstone
RC-91-036			5461750	658500	Black shale with pyrrhotite
RC-91-037			5457700	663050	Sheared agglomerate

Appendix IIIa: (continued)

RC-91-038			5457450	663200	Argillaceous siltstone
RC-91-039			5458700	665075	Maroon sandstone
RC-91-040			5463850	667900	Grey micaceous sandstone
RC-91-041			5465450	668500	Diabase dyke
RC-91-042			5459250	662750	Grey micaceous siltstone
RC-91-043			5461500	663400	Argillaceous siltstone
RC-91-044			5462350	663700	Epidotized mafic volcanic
RC-91-045			5469400	666325	Polymict conglomerate
RC-91-046a			5469300	666350	Micaceous siltstone
RC-91-046b			5469300	666350	Siltstone with quartz veins
RC-91-047			5468500	667300	Gossanous Caradocian shale
RC-91-048			5464650	666725	Convolute bedded sandstone
RC-91-049			5468550	668400	Quartz vein breccia
RC-91-050			5468600	668800	Pegmatitic gabbro
RC-91-051			5467450	670900	Bleached gabbro
RC-91-052			5468625	670200	Tuffaceous siltstone
RC-91-053			5468550	670350	Convolute bedded sandstone
RC-91-054			5468600	670600	Gabbro dyke
RC-91-055			5468500	670750	Folded, grey siltstone
RC-91-056			5468375	670850	Siltstone with quartz veins
RC-91-057			5466925	670750	Fine grained altered gabbro
RC-91-058			5476000	674900	Gossanous, veined siltstone
RC-91-059a			5475750	674925	Siltstone
RC-91-059b			5475750	674850	Altered gabbro
RC-91-060			5475000	674875	Gabbro with quartz veining
RC-91-061	TR-89-004	14.2			Mineralized gabbro
RC-91-062			5459650	669200	Basaltic breccia
RC-92-001			5467900	669550	Grey micaceous sandstone
RC-92-002	TR-89-09B	5.0			Mineralized quartz vein
RC-92-003			5464900	671150	Penetratively cleaved siltstone
RC-92-004			5459650	669100	Basalt flow
DE-90-051			5477400	675250	Altered pillow basalts
JH-92-310			5440850	648850	Basaltic fragmental
W-90-059a	TR-89-06	12.5			Altered gabbro
W-90-059b	TR-89-06	12.5			Altered gabbro
W-90-059c	TR-89-06	13.0			Mineralized gabbro
W-90-059d	TR-89-06	13.0			Mineralized gabbro
W-90-060a	TR-89-08	4.0			Sandstone
W-90-060b	TR-89-08	4.0			Mineralized quartz vein

Notes: ¹Refers to the trench from which hand samples were obtained. Also note that plan geology trench maps can be viewed in Appendix IV.

²Site is the distance in metres from the western end of the trench where the sample was obtained.

³Northing and Easting are the UTM co-ordinates within UTM Zone 21 for samples obtained outside the exploration grid.

Appendix IIIb: Location data for samples obtained from diamond drill core.

<i>Sample</i>	<i>DDH</i>	<i>Depth</i> ^s	<i>Rock Type</i>
DL1-91-01	DL-90-01	5.2	Unaltered gabbro
DL1-91-02	DL-90-01	7.0	Altered gabbro
DL1-91-03	DL-90-01	13.3	Altered gabbro
DL1-91-04	DL-90-01	19.5	Altered gabbro
DL1-91-05	DL-90-01	19.7	Mineralized gabbro
DL1-91-06	DL-90-01	23.2	Mineralized gabbro
DL1-91-07	DL-90-01	23.7	Mineralized gabbro
DL1-91-08	DL-90-01	27.3	Mineralized gabbro
DL1-91-09	DL-90-01	25.7	Mineralized gabbro
DL1-91-10	DL-90-01	29.6	Mineralized gabbro
DL1-91-11	DL-90-01	37.7	Altered gabbro
DL1-91-12	DL-90-01	40.9	Siltstone
DL1-91-13	DL-90-01	56.7	Siltstone
DL2-91-01	DL-90-02	19.3	Altered siltstone
DL2-91-02	DL-90-02	25.7	Altered siltstone
DL2-91-03	DL-90-02	32.5	Siltstone
DL2-91-04	DL-90-02	48.0	Sandstone
DL2-91-05	DL-90-02	66.1	Siltstone
DL2-91-06	DL-90-02	48.5	Sandstone
DL3-91-01	DL-90-03	16.7	Siltstone
DL3-91-02	DL-90-03	23.8	Carbonate vein
DL3-91-03	DL-90-03	28.2	Mineralized gabbro
DL3-91-04	DL-90-03	28.8	Altered gabbro
DL3-91-05	DL-90-03	31.3	Altered gabbro
DL3-91-06	DL-90-03	31.9	Altered gabbro
DL3-91-07	DL-90-03	34.2	Unaltered Gabbro
DL3-91-08	DL-90-03	39.5	Altered gabbro
DL3-91-09	DL-90-03	42.5	Altered gabbro
DL3-91-10	DL-90-03	58.8	Unaltered Gabbro
DL3-91-11	DL-90-03	63.9	Mineralized gabbro
DL3-91-12	DL-90-03	67.1	Siltstone
DL3-91-13	DL-90-03	71.0	Unaltered Gabbro
DL4-91-01	DL-90-04	13.3	Altered gabbro
DL4-91-02	DL-90-04	14.2	Altered gabbro
DL4-91-03	DL-90-04	15.7	Altered gabbro with tuchsite
DL4-91-04	DL-90-04	21.4	Altered gabbro
DL4-91-05	DL-90-04	17.2	Altered gabbro
DL4-91-06	DL-90-04	17.5	Quartz-carbonate vein
DL4-91-07	DL-90-04	25.0	Siltstone
DL4-91-08	DL-90-04	38.5	Greywacke
DL4-91-09	DL-90-04	43.7	Siltstone
DL4-91-10	DL-90-04	56.7	Altered gabbro
DL4-91-11	DL-90-04	59.5	Altered gabbro
DL4-91-12	DL-90-04	61.2	Altered gabbro
DL4-91-13	DL-90-04	65.1	Altered gabbro

Appendix IIIb: (continued)

DL4-91-14	DL-90-04	76.0	Altered gabbro
DL4-91-15	DL-90-04	82.8	Altered gabbro
DL4-91-16	DL-90-04	94.4	Mineralized gabbro
DL4-91-17	DL-90-04	98.2	Mineralized gabbro
DL4-91-18	DL-90-04	105.8	Unaltered Gabbro
DL4-91-19	DL-90-04	108.8	Mineralized gabbro
DL4-91-20	DL-90-04	111.0	Siltston.
DL4-91-21	DL-90-04	113.5	Siltstone
DL5-91-01	DL-90-05	29.5	Altered gabbro
DL5-91-02	DL-90-05	46.7	Altered gabbro
DL5-91-03	DL-90-05	50.9	Altered gabbro
DL5-91-04	DL-90-05	60.2	Mineralized gabbro
DL5-91-05	DL-90-05	58.4	Mineralized gabbro
DL5-91-06	DL-90-05	61.4	Altered gabbro
DL5-91-07	DL-90-05	61.6	Mineralized gabbro
DL5-91-08	DL-90-05	63.3	Mineralized gabbro
DL5-91-09	DL-90-05	66.1	Mineralized gabbro
DL5-91-10	DL-90-05	80.3	Siltstone
DL6-91-01	DL-90-06	15.4	Siltstone
DL6-91-02	DL-90-06	38.9	Unaltered gabbro
DL6-91-03	DL-90-06	47.9	Mineralized gabbro
DL6-91-04	DL-90-06	50.5	Mineralized gabbro
DL6-91-05	DL-90-06	50.8	Mineralized gabbro
DL6-91-06	DL-90-06	53.0	Mineralized gabbro
DL6-91-07	DL-90-06	56.4	Mineralized gabbro
DL6-91-08	DL-90-06	57.8	Mineralized gabbro
DL6-91-09	DL-90-06	59.5	Mineralized gabbro
DL6-91-10	DL-90-06	61.1	Siltstone
DL7-91-01	DL-90-07	18.1	Carbonate vein
DL7-91-02	DL-90-07	13.7	Unaltered gabbro
DL7-91-03	DL-90-07	23.3	Unaltered gabbro
DL7-91-04	DL-90-07	24.8	Mineralized gabbro
DL7-91-05	DL-90-07	28.9	Altered gabbro with carbonate vein
DL7-91-06	DL-90-07	34.1	Altered gabbro
DL7-91-07	DL-90-07	43.0	Mineralized gabbro
DL7-91-08	DL-90-07	59.7	Unaltered gabbro
DL7-91-09	DL-90-07	75.6	Unaltered gabbro
DL7-91-10	DL-90-07	88.9	Siltstone
DL8-91-01	DL-90-08	5.0	Siltstone
DL8-91-02	DL-90-08	9.2	Mineralized gabbro
DL8-91-03	DL-90-08	21.3	Unaltered gabbro
DL8-91-04	DL-90-08	25.9	Unaltered gabbro
DL8-91-05	DL-90-08	45.3	Mineralized gabbro
DL8-91-06	DL-90-08	45.8	Mineralized gabbro
DL8-91-07	DL-90-08	49.4	Mineralized gabbro
DL8-91-08	DL-90-08	51.4	Mineralized gabbro
DL8-91-09	DL-90-08	55.2	Mineralized gabbro

Appendix IIIb: (continued)

DL8-91-10	DL-90-08	68.6	Unaltered gabbro
DL8-91-11	DL-90-08	47.0	Altered gabbro
DL8-91-12	DL-90-08	62.2	Mineralized gabbro
DL8-91-13	DL-90-08	80.1	Unaltered gabbro
DL8-91-14	DL-90-08	105.1	Unaltered gabbro

Notes: ¹Refers to the diamond drill hole from which core samples were obtained. Also note that schematic visual drill logs can be viewed in Appendix V.

²Distance in metres from where the core sample was obtained. Measured relative to the top of the hole where the top of hole is assigned a depth of 0m.





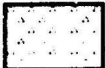





APPENDIX IV

TRENCH MAPS

The following pages in this section are schematic trench plan maps for each of the trenches sampled and studied at Duder Lake. The maps have been modified from original Noranda Exploration Company Limited trench maps during the course of this study with additional information compiled from field research.

The sketches show the lithological subunits that are exposed in the trenches as well as structural information and brief descriptive notes. The legend for the subunits is given below:

Legend for lithological subunits exposed in trenches

	Overburden		Interbedded sandstone and siltstone
	Brittle shears hosting zones of mineralization (Py, Asp, Au)		Siltstone
	Quartz Breccia		Interbedded slate and shale
	Gabbroic Intrusive (Dykes and Sills)		Greywacke
	Sandstone		Shale

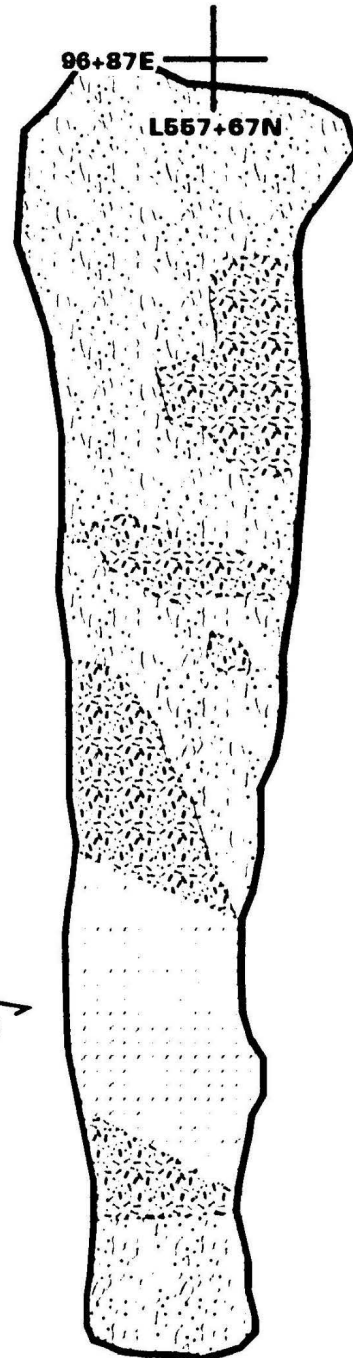
Cgr gabbro with moderate to strong chloritization.

Mgr gabbro with strong chloritization and moderate to strong leucoxene alteration. Trace py.

Fgr gabbro with weak to moderate chloritization with local silicification and leucoxene. Moderate carbonate alteration with 2% py in irregular silicified pods.

Recessively weathered brittle shear zone in fgr gabbro. Shears from 5-10cm in width.

Fgr gabbro with weak chlorite, carbonate, and silicification. Trace py.



0 100 200 300 400 500
CENTIMETRES

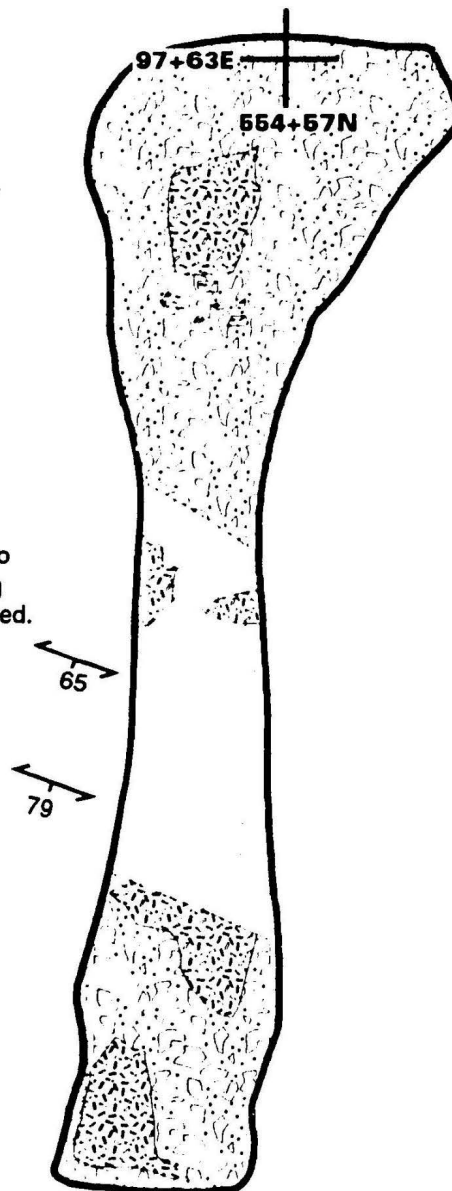
TR-89-01

Coarse grained gabbro with moderate chloritization.

Zone of brittle shearing in gabbro. blocks of gabbro highly silicified with minor carbonate and containing 2-5% Py, Asp. Gossanous and recessively weathered.

Chloritized gabbro, locally silicified, trace to 1% Py and minor mauve leucoxene alteration.

Coarse grained gabbro, weakly chloritized with trace to 1% Py.



0 100 200 300 400 500

CENTIMETRES
TR-89-02

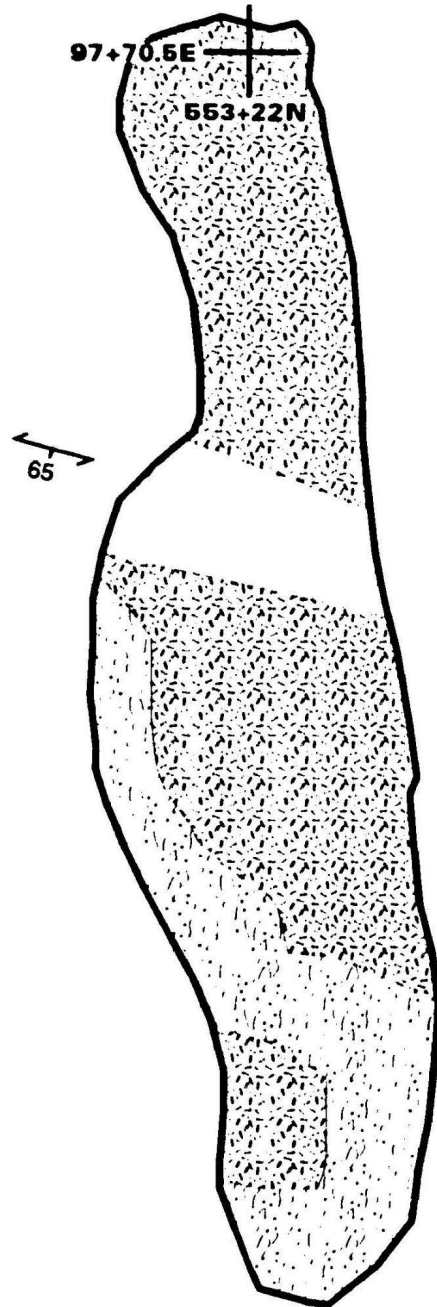
Coarse grained chloritized gabbro with well developed S1 cleavage.

Coarse grained chloritized gabbro weakly silicified.

Gossanous and recessively weathered gabbro containing blocks of silicified gabbro. Mineralization in gabbro as 3-5% Py, Asp. Schistose.

Strongly chloritized coarse grained gabbro exhibiting schistosity. Minor leucoxene alteration with trace to 1% Py.

Coarse grained, weakly schistose gabbro exhibiting moderate chloritization.



0 100 200 300 400 500

CENTIMETRES

TR-89-03

Schistose dark green siltstones and shale.

Schistose light green, finely laminated siltstones with weak carbonatization and trace Py.

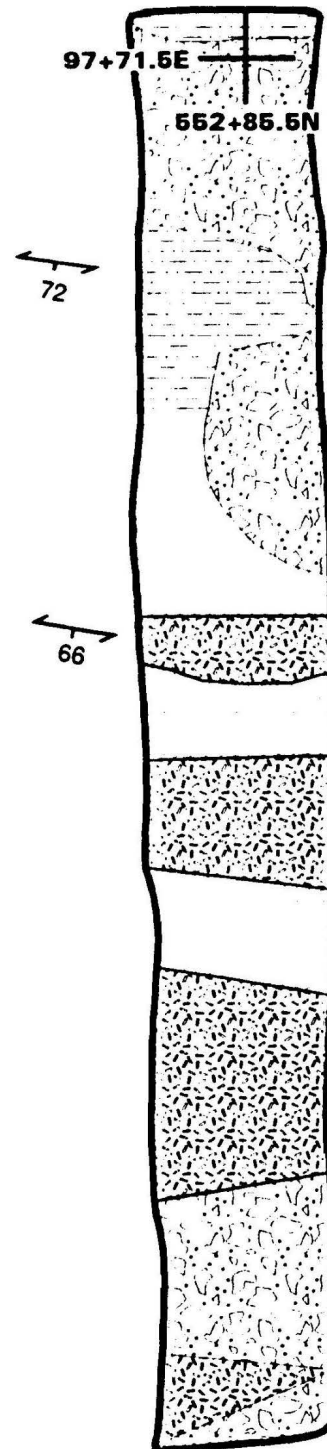
Recessively weathered schistose gabbro with carbonatization, chloritization, and leucoxene alteration. Silicified blocks of gabbro containing up to 27% Py, Asp mineralization.

Schistose medium grained gabbro exhibiting moderate chloritization and pervasive leucoxene alteration. Carbonate and epidote found along fractures. Trace Py in small silicified gabbro pods. Host rock has 1-27% Py, Asp.

Intensely silicified gabbro containing network quartz veining. Disseminated and stringer coarse Py from 3-5% with fine Asp from 3-5%. Minor epidote along fractures.

Recessively weathered gabbro. Intensely silicified with network quartz veining, gossanous, with 4-7% Py, Asp occurring in silicified gabbro blocks.

Schistose medium grained gabbro. Strongly chloritized with weak carbonatization and pervasive leucoxene alteration decreasing away from shear zone. Mn-oxide (pyrolusite) staining noted and trace Py observed.



0 100 200 300 400 500

CENTIMETRES

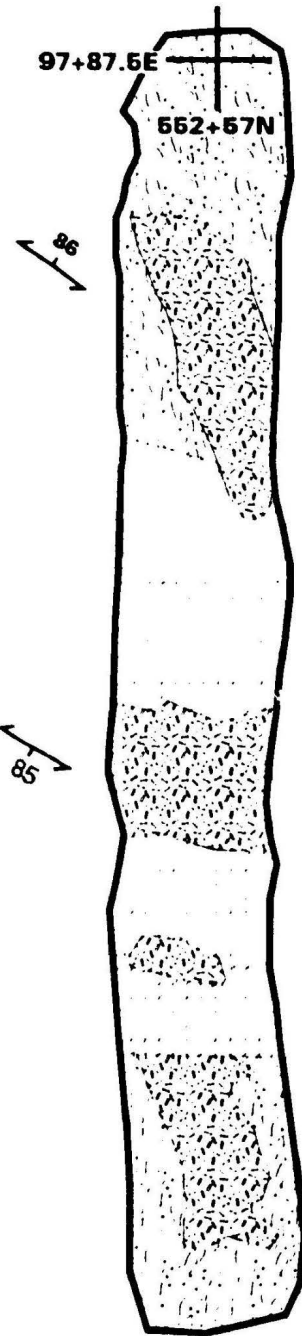
TR-89-04

Strongly schistose coarse grained gabbro with moderate to strong chloritization. Minor leucoxene alteration. Degree of silicification increasing towards shear.

Strongly schistose coarse grained gabbro with moderate silicification and chloritization. Trace to 2% Py. Recessively weathered.

Schistose gabbro.

Strongly schistose gabbro exhibiting strong chloritization and weak leucoxene alteration.



0 100 200 300 400 500

CENTIMETRES

TR-89-05

Mgr gabbro with carbonate, sericite, and leucoxene alteration (locally > 70%). Tr py.

Mgr gabbro with carbonate, chlorite, and sericite. Upwards of 60% leucoxene with trace py. Brittle shear with thin quartz veins cutting through gabbro and hosting 10-15% py-asp.

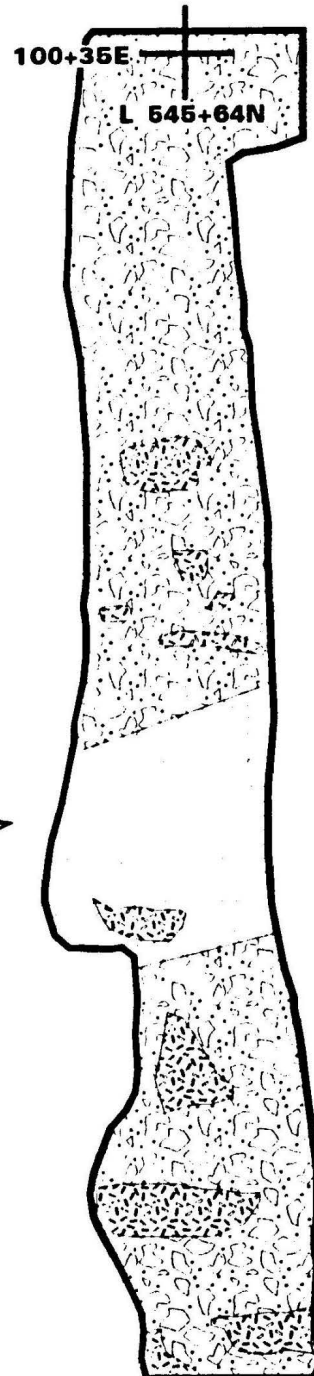
Mgr gabbro with chlorite, sericite, and trace py.

Medium grained gabbro with carbonate and chlorite alteration. Trace py.

0 100 200 300 400 500

CENTIMETRES

TR-89-06



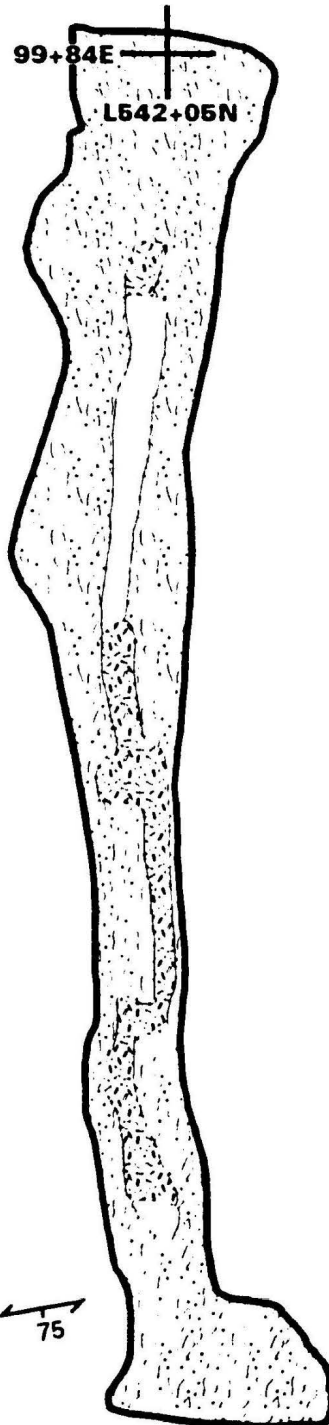
Coarse grained gabbro with strong carbonatization, sericitization, and chloritization. Leucoxene present.

Shear zone in gabbro exhibiting strong carbonatization. Carbonate lenses up to 20cm thick present. Leucoxene, sericitic, and chloritic alteration accompanying local trace py mineralization.

Massive carbonatized gabbro hosting quartz veins and trace py, asp mineralization.

Massive gabbro with thin quartz veins (2-3cm thick).

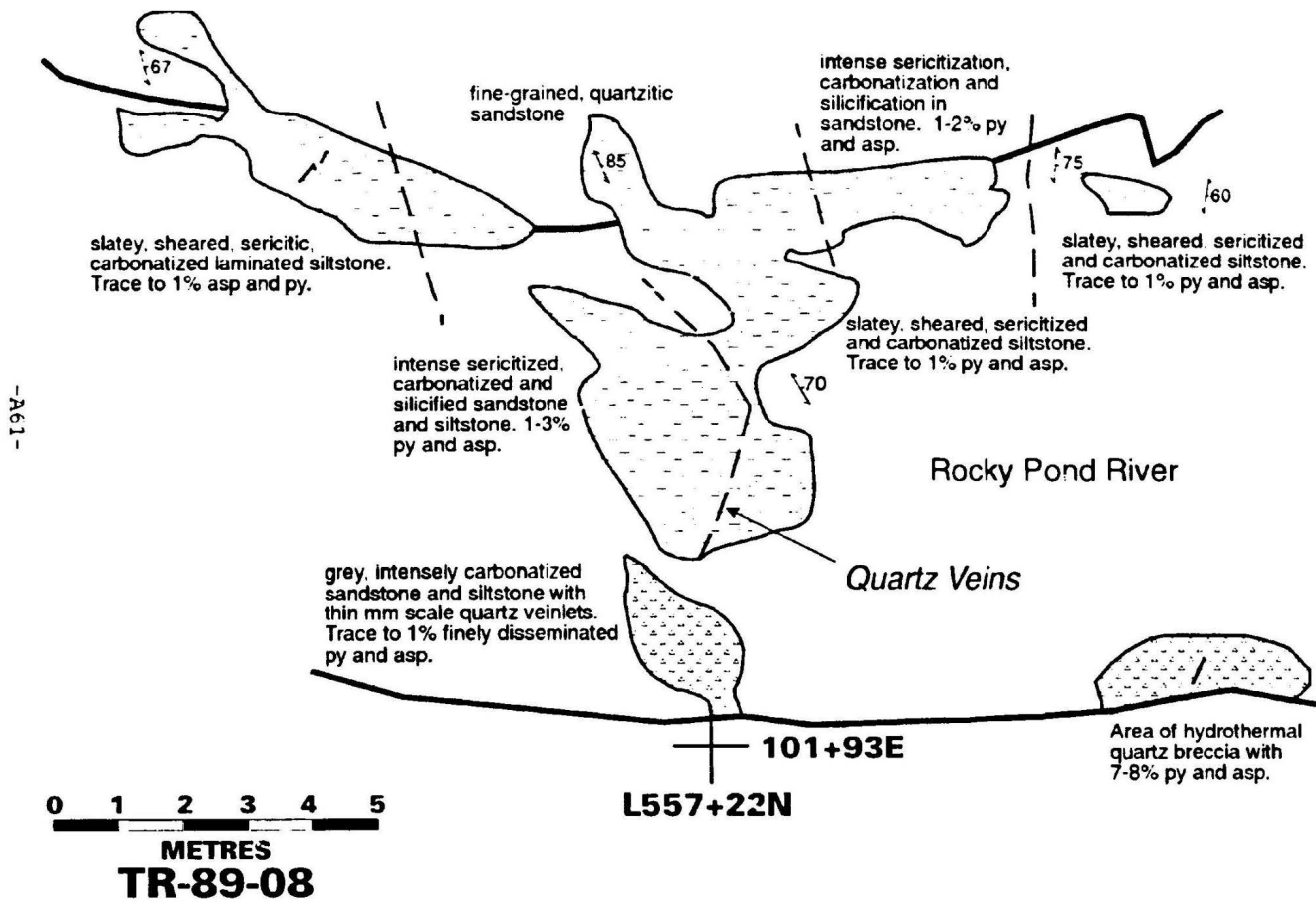
Shear zone in gabbro exhibiting carbonatization.

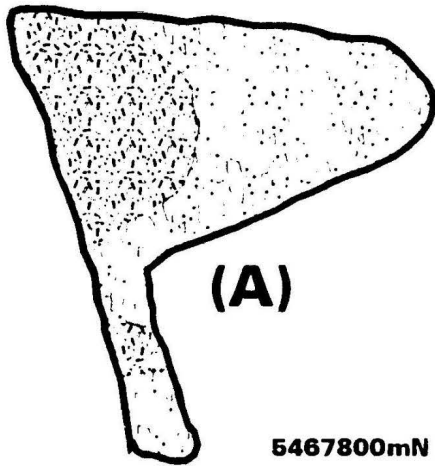


0 200 400 600 800 1000

CENTIMETRES

TR-89-07

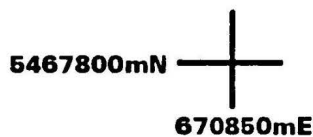




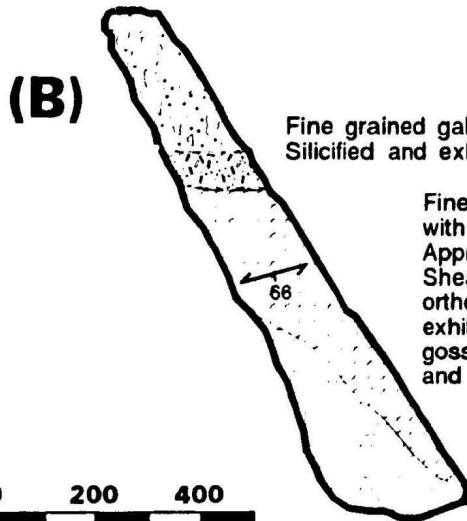
(A)

Fine-grained dark green gabbro. Minor chlorite and carbonate alteration. Trace Py and Asp (<1%).

Fine grained gabbroic dyke less than 1m in width.



Logging Access Road



(B)

Fine grained gabbroic dyke less than 1m in width. Silicified and exhibits minor uralitization.

Fine to medium grained, silicified gabbro dyke with sheared margins observed at contacts. Approximately 1-2% Py and Asp in host rock. Shear parallel quartz veins and second set orthogonal to first also host sulfides and exhibit pinch-and-swell structures. Gabbro gossanous, recessive, strongly sheared, and chloritic.

Fine grained, massive, tuffaceous, grey-green siltstone exhibiting moderate to strong cleavage.



TR-89-09 A/B




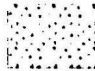



APPENDIX V

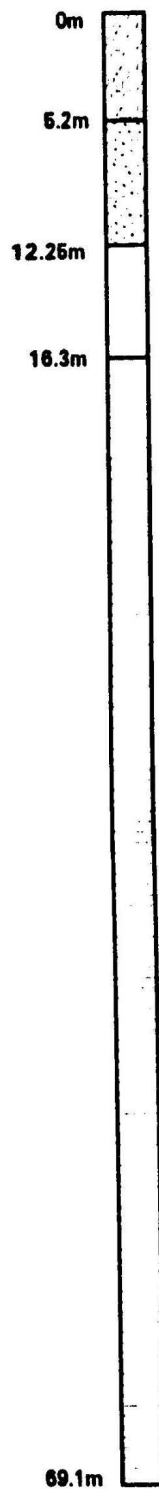
SCHEMATIC VISUAL DRILL LOGS

The following pages in this section are schematic visual drill logs (not drawn to scale) for the eight diamond drill holes sampled and studied. The logs have been compiled and modified from original Noranda written and visual logs as well as information obtained during the course of this study.

The following information is present in the logs: depths represent depths to contacts, lithological subunits that were intersected in drill core, and brief descriptive notes as well as drill hole placement data. The eight drill holes comprise a cumulative meterage of 690.9m and the legend for the subunits is given below:

Legend for lithological subunits intersected in drill core

	Overburden
	Brittle shears hosting zones of mineralization (Py, Asp, Au)
	Gabbroic Intrusive (Dykes and Sills)
	Sandstone
	Interbedded sandstone and siltstone
	Siltstone
	Greywacke



Overburden

Fgr. green-grey sandstone with abundant chlorite.

MINERALIZED ZONE. Quartz brecciated, chloritized and silicified siltstone with stringer and disseminated pyrite associated with most intense brecciation.

Green to olive green, fgr. finely laminated siltstone with trace disseminated Py, Asp. Trace qtz-carb veins and chl alteration grades into sericitized zone with depth.

DDH: DL-90-02
NORTHING: 557+00N
EASTING: 102+15E
DIP: -45
AZIMUTH: 351
DEPTH: 69.1m

0m
2.4m

Overburden

DDH: DL-90-03
NORTHING: 545+65N
EASTING: 100+80E
DIP: -45
AZIMUTH: 292
DEPTH: 75.3m

Interbedded, fgr to mgr, grey to black sandstone and siltstone with schistosity parallel to bedding. Minor sericitization. Lower contact with gabbro sharp and chilled over a 1.5m interval.

24.4m

Cgr to fgr, intensely altered gabbro strongly sheared at base. Chl-lcx-ural alteration and numerous thin quartz veins present.

31.6m
32.0m

MINERALIZED ZONE hosted by strongly sheared gabbro. Approximately 2-3% Py and up to 1% Asp observed.

Intensely altered gabbro with ural-lcx-chl alteration. Extremely cgr with trace Py and numerous qtz-carb veins. Strong schistosity.

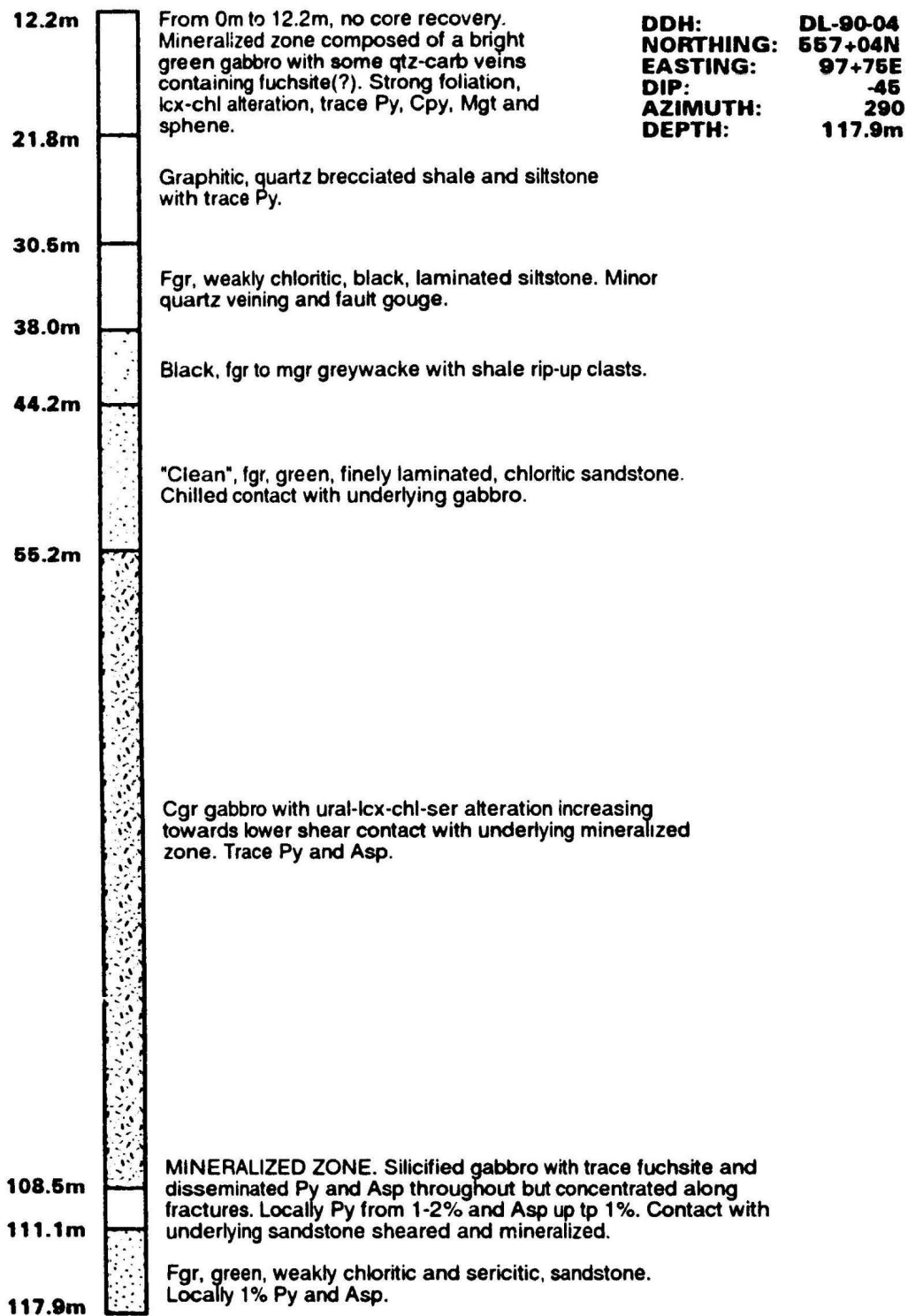
66.5m

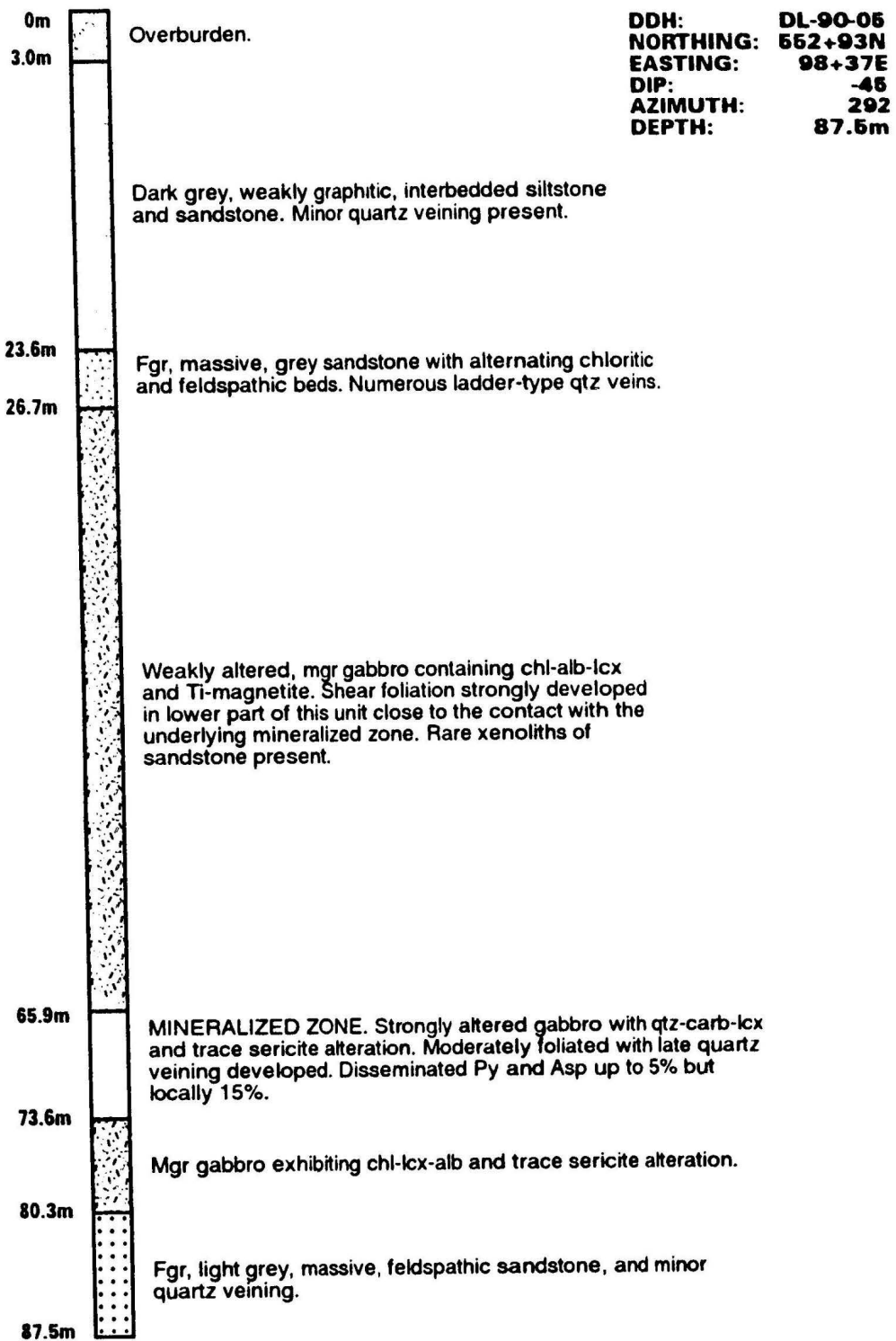
Fgr, intensely fractured, black sandstone with quartz veinlets and minor pyrite stringers.

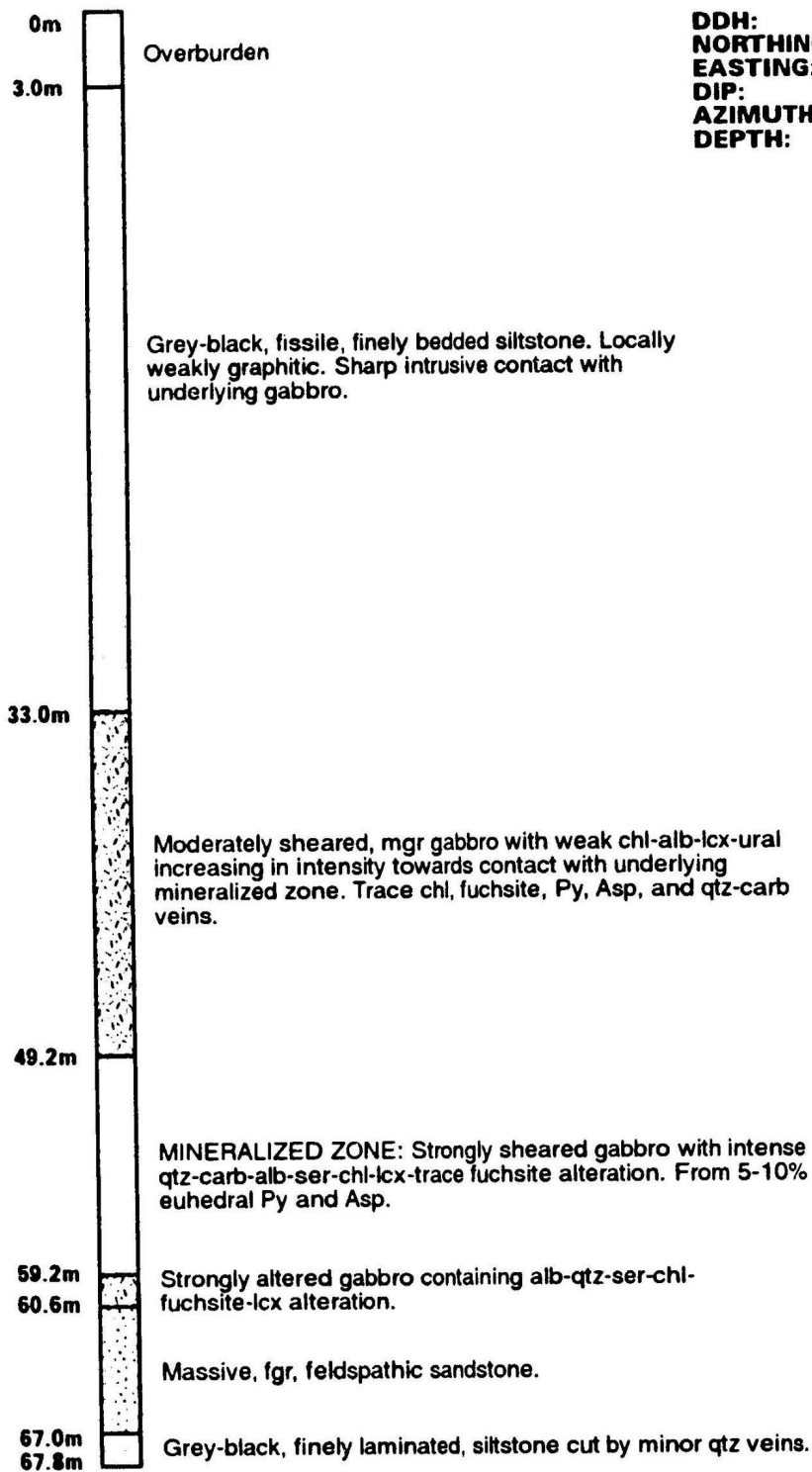
71.0m

Intensely sheared, fgr gabbro with trace Py and Asp. Unit is chilled and contains ural-chl-lcx alteration.

75.3m







DDH: DL-90-06
 NORTHING: 552+50N
 EASTING: 98+36E
 DIP: -45
 AZIMUTH: 292
 DEPTH: 67.7m

0m
1.5m

Overburden.

DDH: DL-90-07
NORTHING: 553+50N
EASTING: 98+05E
DIP: -45
AZIMUTH: 292
DEPTH: 89.9m

Fgr gabbro becoming increasingly altered towards lower contact with mineralized zone. Weak shear fabric. gabbro contains alb-chl-fuchsite-carb alteration. Trace mineralization.

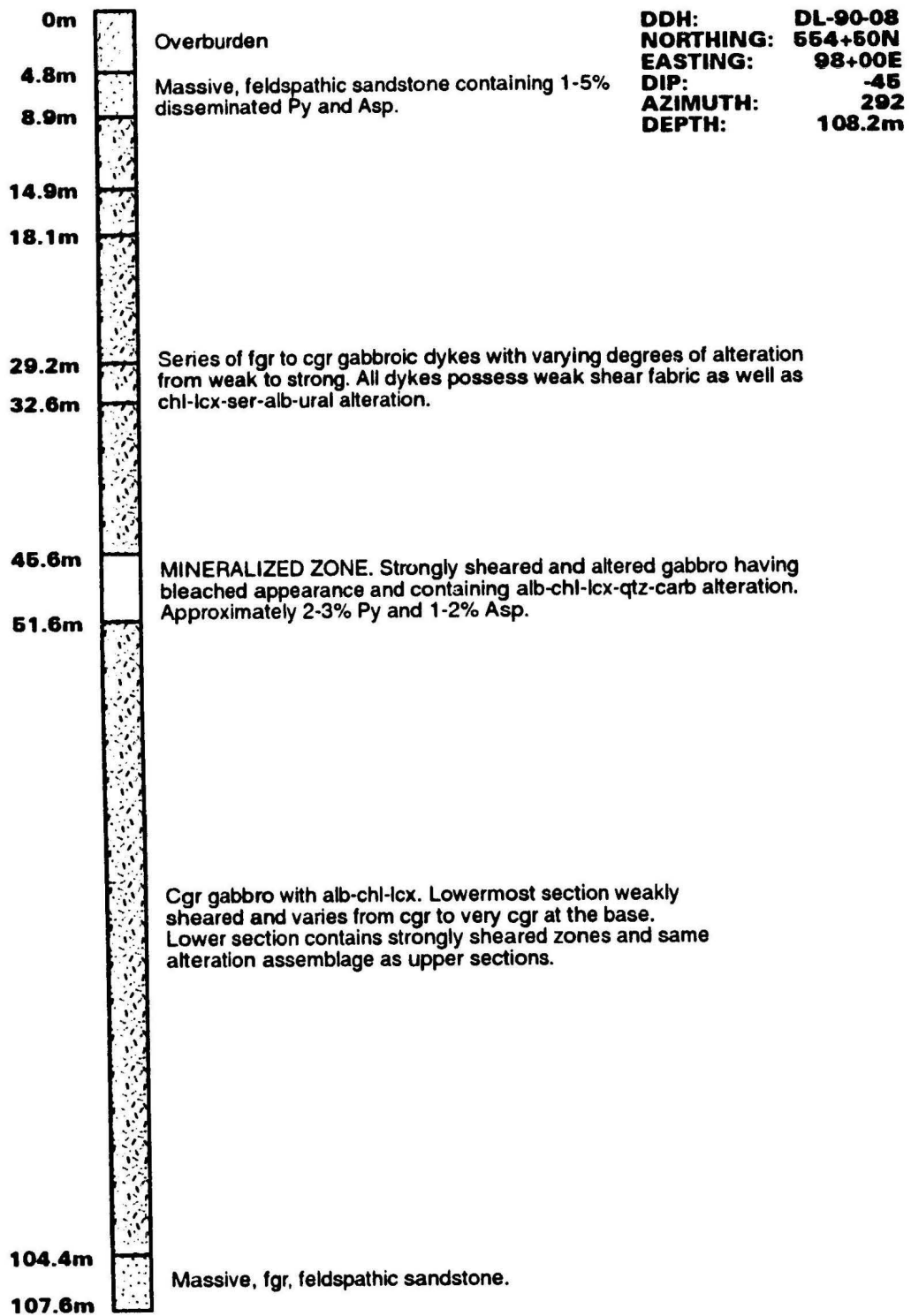
43.1m
44.6m

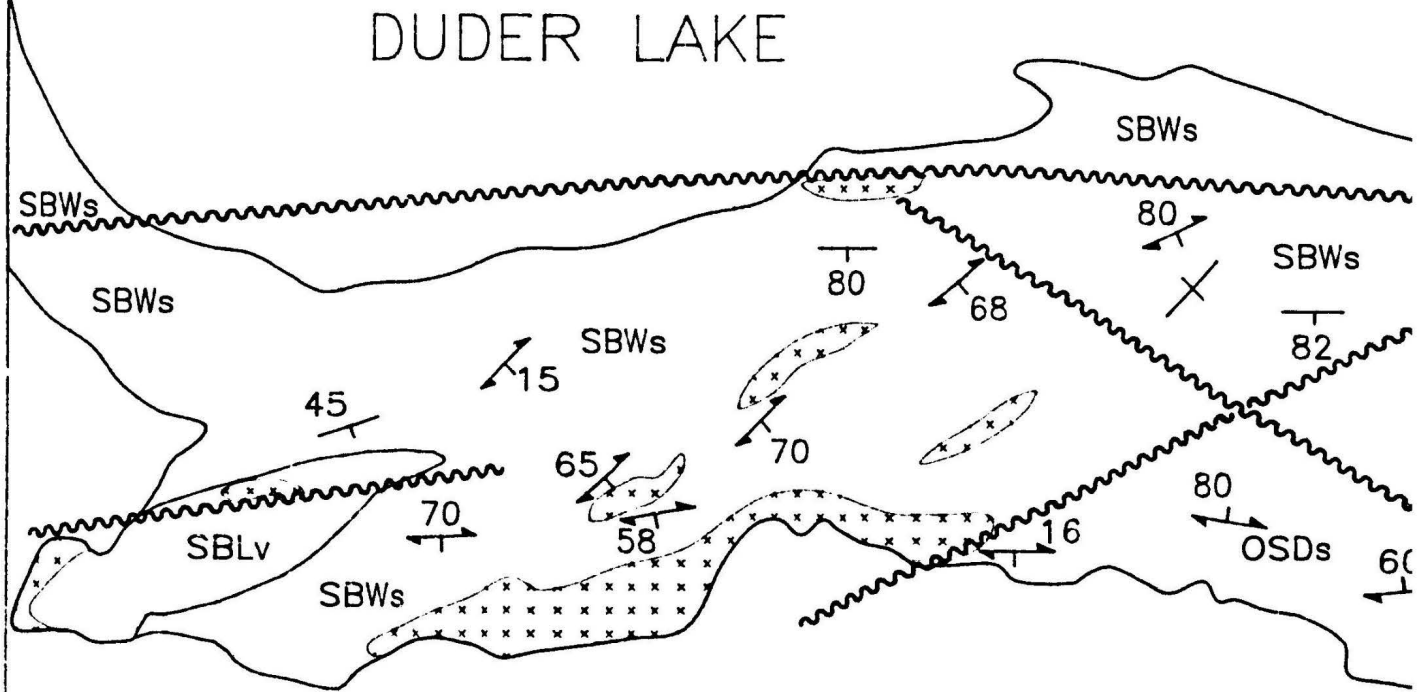
MINERALIZED ZONE. Strongly altered and sheared gabbro containing qtz-alb-carb-trace fuchsite-lcx-chl alteration. Minor quartz veining. 2-3% Py and 1-2% Asp.

Cgr gabbro with varying degrees of alteration from relatively fresh in lower sections to very strong close to contact with the mineralized zone. Alteration phases present include alb-chl-lcx-carb-qtz-fuchsite.

85.1m
89.9m

Fgr, bedded, feldspathic sandstone.





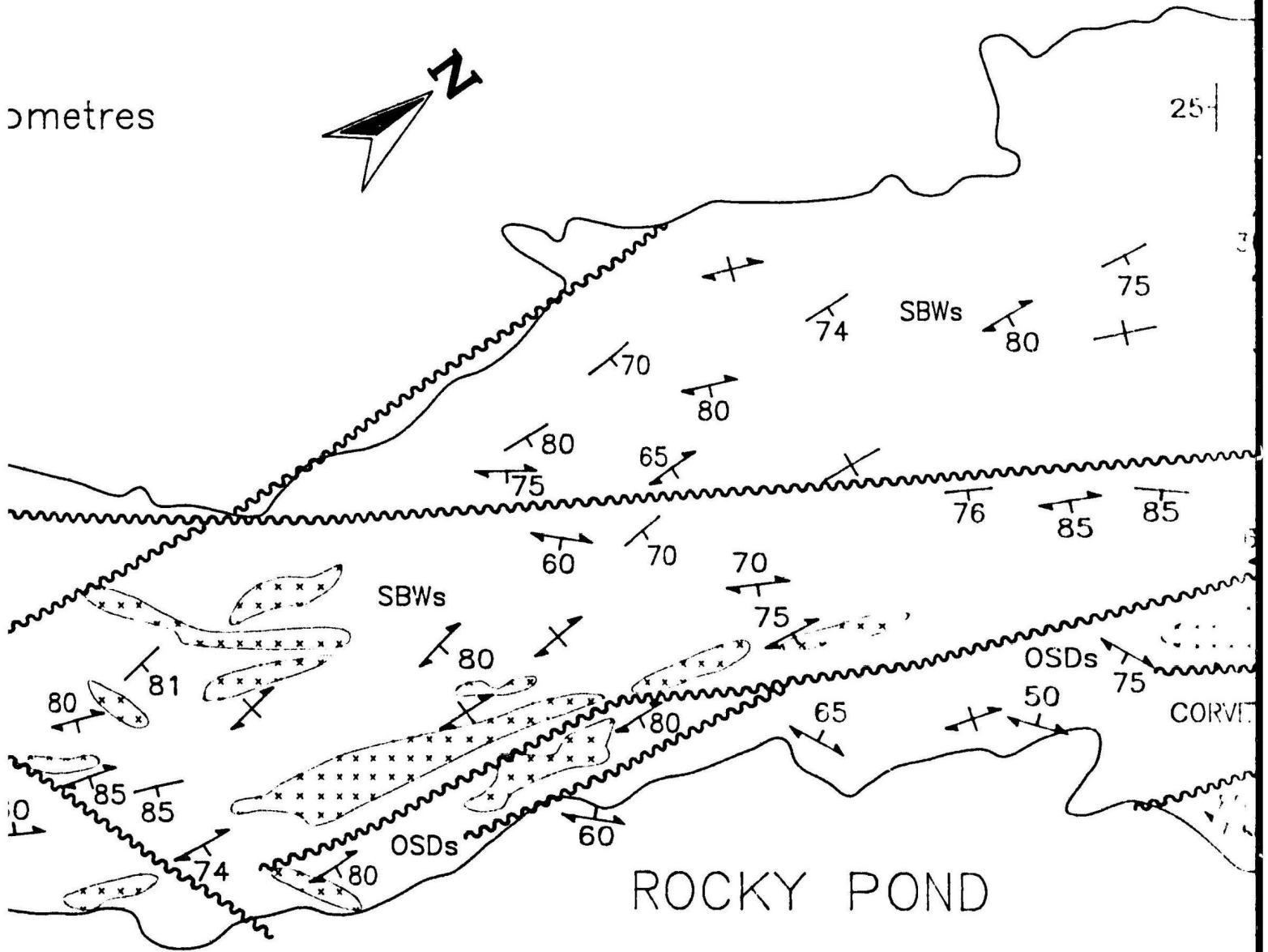
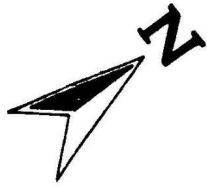
SILURIAN TO DEVONIAN

<table border="0" style="font-family: monospace; font-size: 1.2em;"> <tr><td>x</td><td>x</td><td>x</td></tr> <tr><td>x</td><td>x</td><td>x</td></tr> <tr><td>x</td><td>x</td><td>x</td></tr> </table>	x	x	x	x	x	x	x	x	x	<p>Medium- to coarse grained gabbroic, dioritic and diabasic s possessing pegmatitic textures and primary igneous layering. variably hydrothermally altered and correlatable with elevated</p>
x	x	x								
x	x	x								
x	x	x								

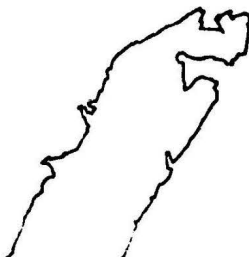
SILURIAN

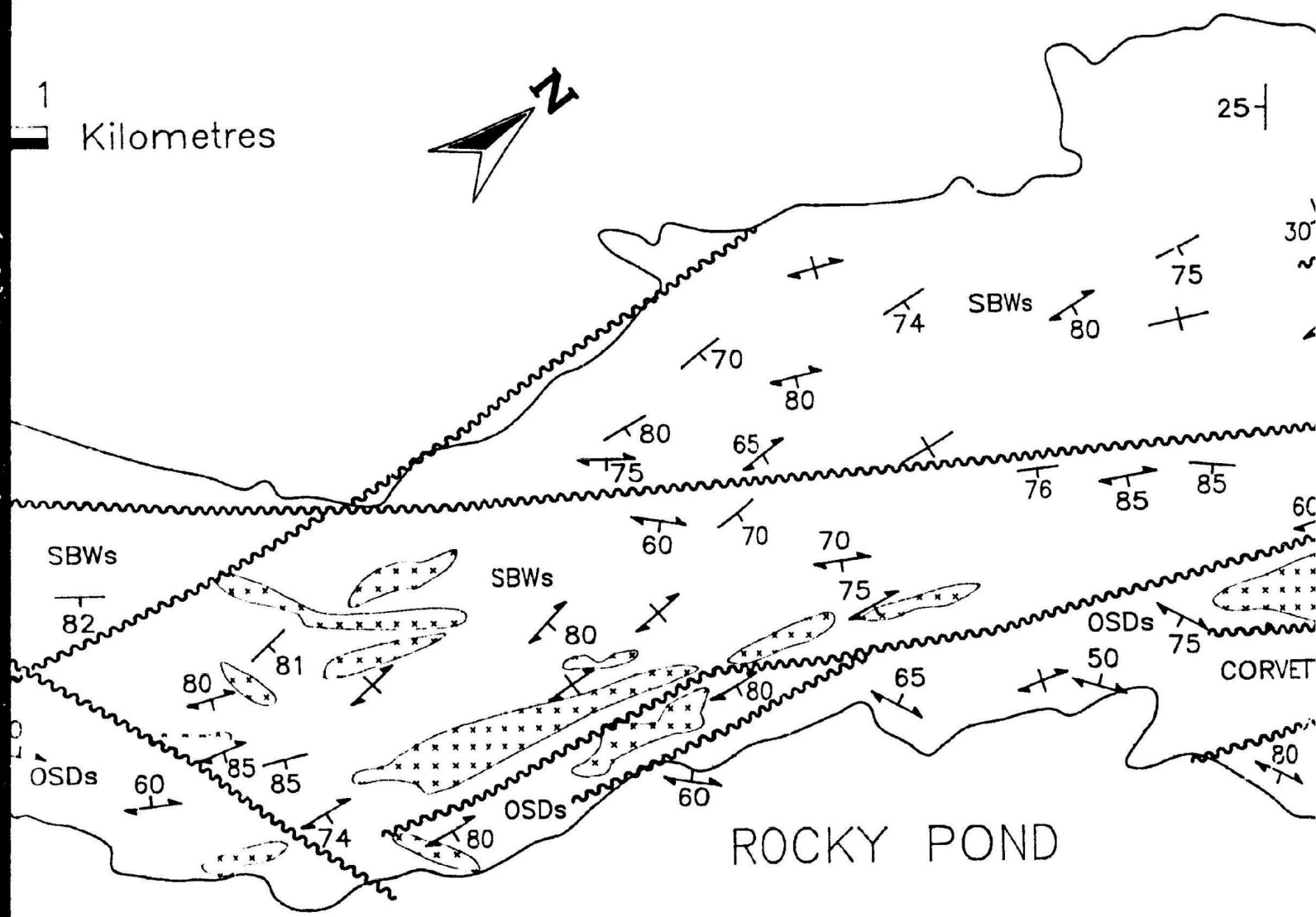
Botwood Group
Wiqwam Formation

metres

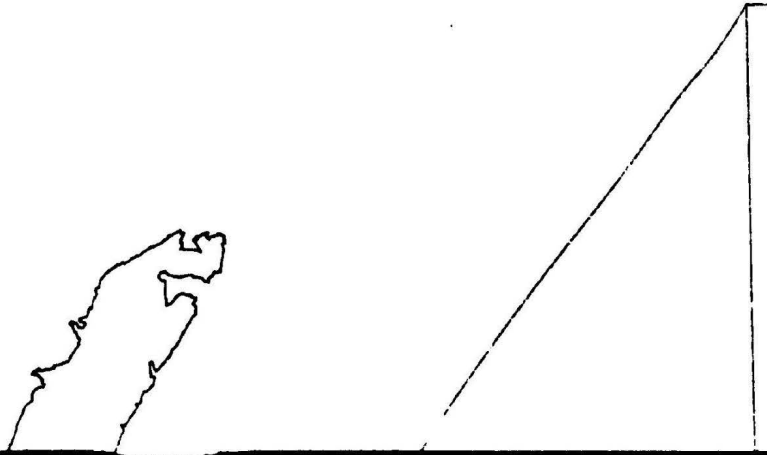


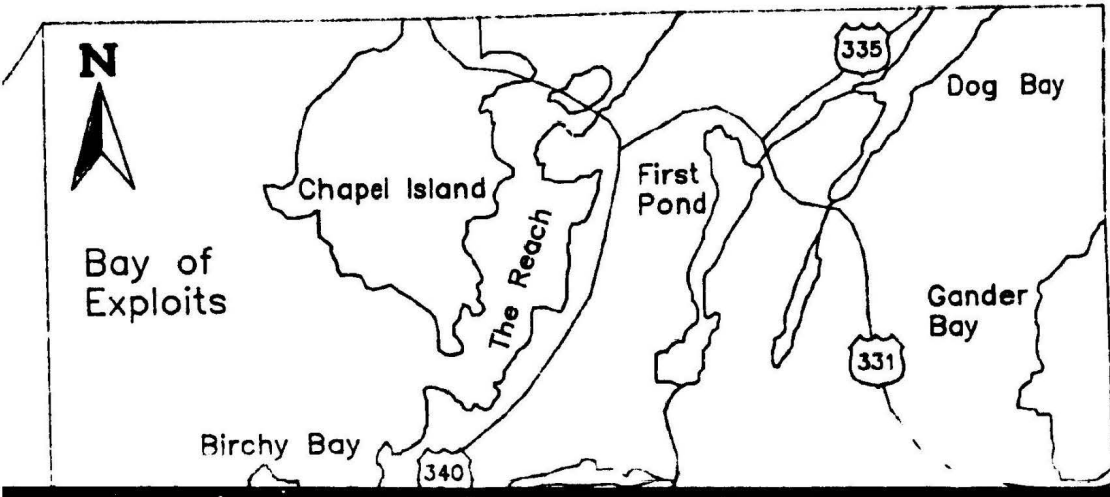
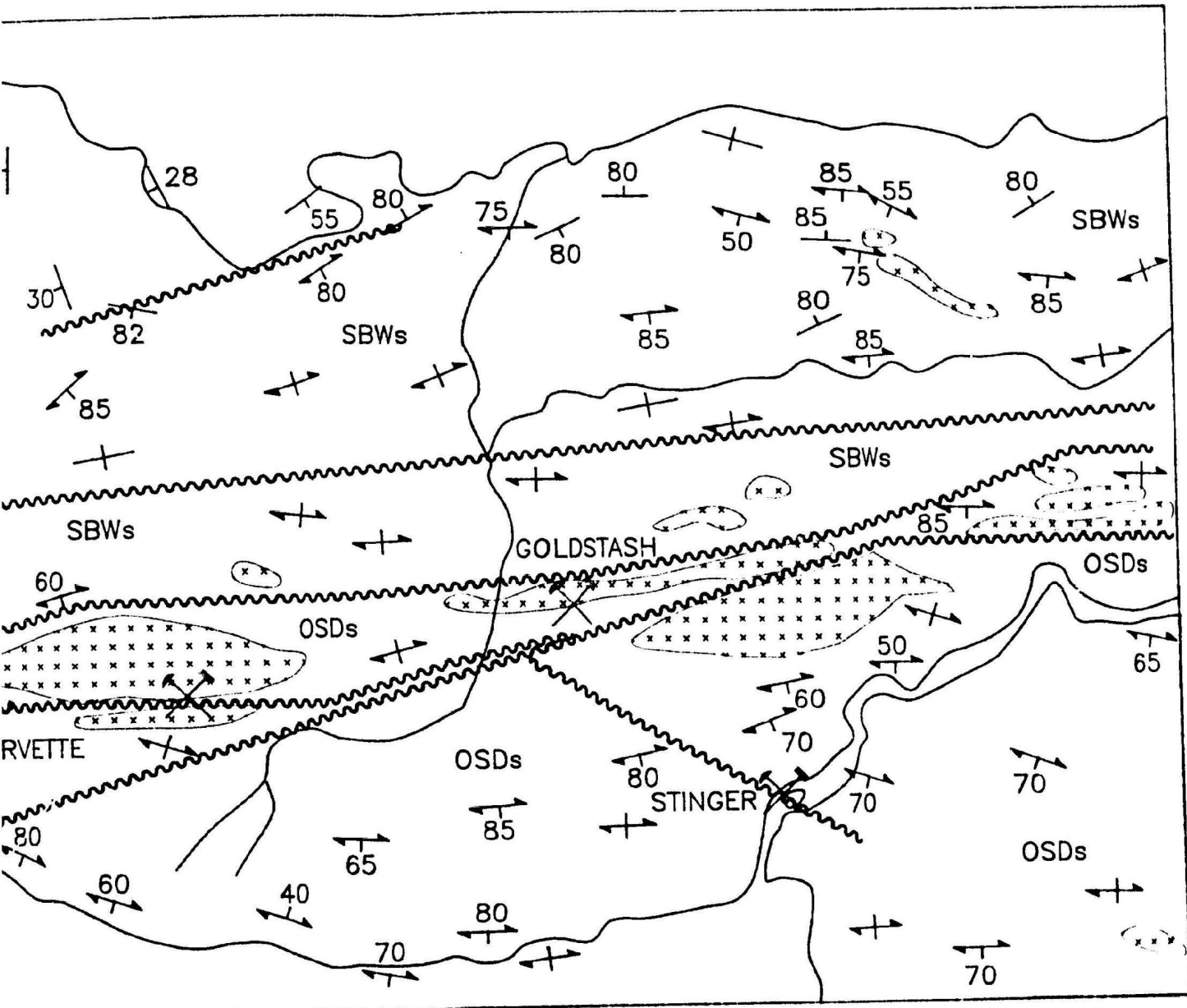
sills and dykes locally
Intrusive bodies
and gold abundances.





diabasic sills and dykes locally
 as layering. Intrusive bodies
 with elevated gold abundances.





SILURIAN TO DEVONIAN

× × × Medium- to coarse grained gabbroic, dioritic and diabasic sills and
× × × possessing pegmatitic textures and primary igneous layering. Intrusives
× × × variably hydrothermally altered and correlatable with elevated gold

SILURIAN

Botwood Group Wigwam Formation

SBWs

Siliceous and micaceous, red to green, massive to laminated shales and
facies sandstone and minor siltstone with locally developed weak
S2 cleavage. Down-section rocks change to deeper marine facies
argillaceous siltstone and shale. Massive units up to 25m in thickness
locally, otherwise thinly interbedded. Moderate to strong cleavage
throughout.

Lawrenceton Formation

SBLv

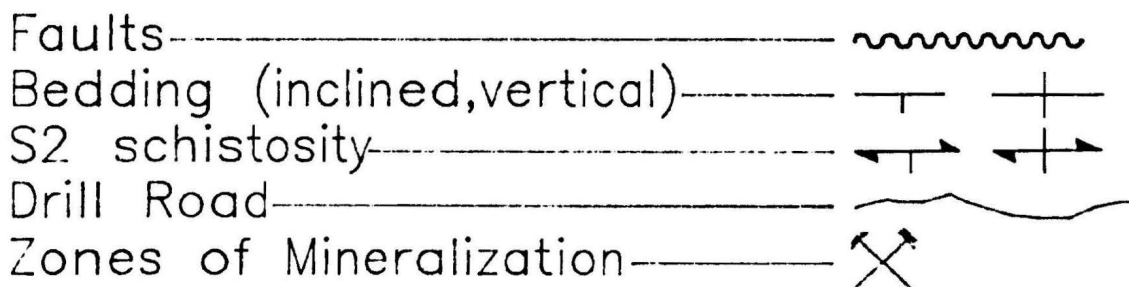
Subaerial, scoriaceous, purple to black basalt flows, pillows and
breccias.

ORDOVICAN TO SILURIAN

Davidsville Group

OSDs

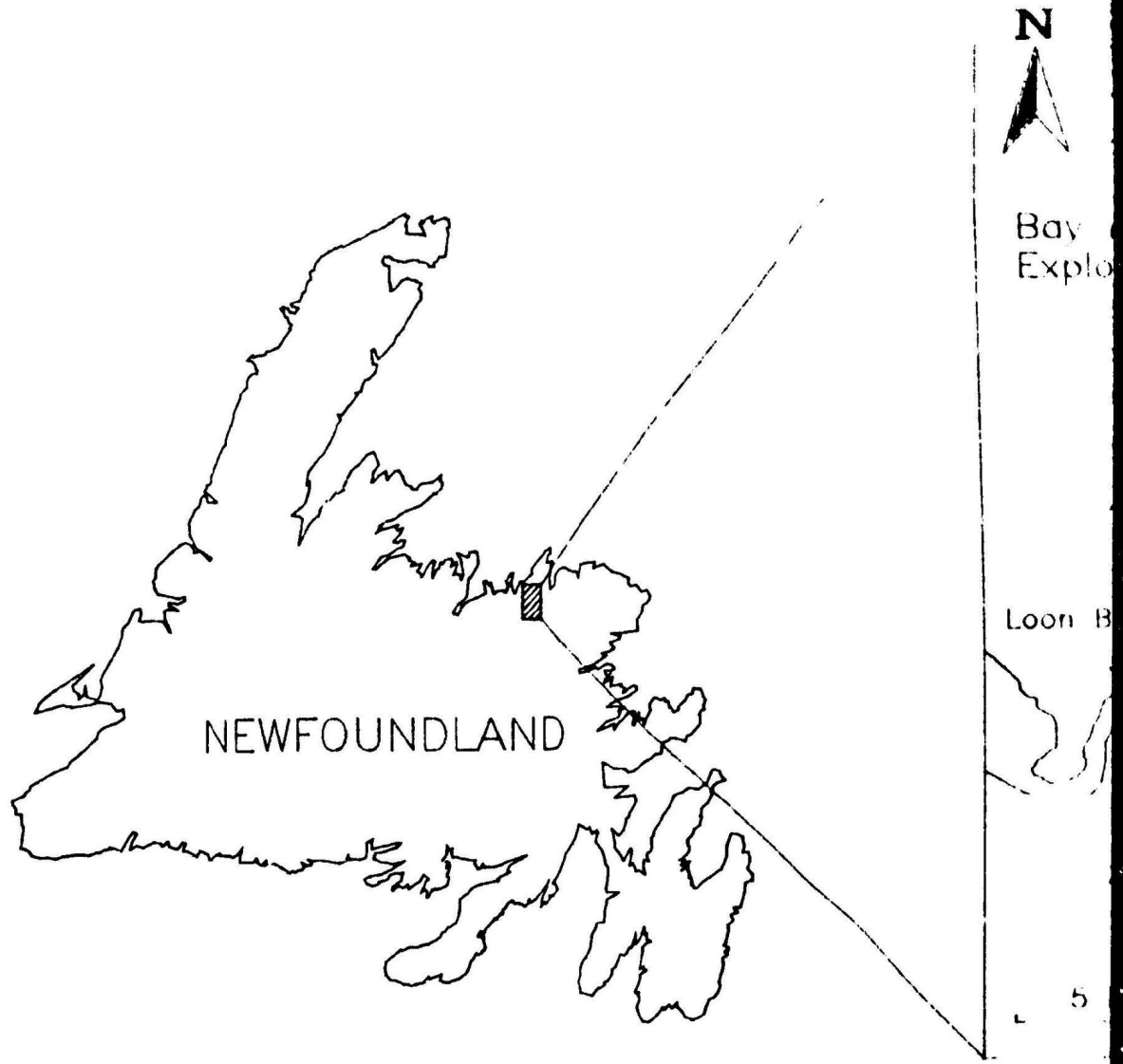
Dark grey, green and black slate with minor argillaceous siltstone
fine-grained graphitic sandstone. Thinly bedded units with penetrative
slaty cleavage.



and dykes locally
intrusive bodies
old abundances.

shallow marine
up to moderate
siltstone,
thickness
developed

one and
strative



*NB: Only three of the four mineralized sites are depicted on this map. The fourth, Flirt, is located approximately 2km NE of the northern end of map area. The geology of the Flirt showing can be observed in Appendix of Trench Maps, page A62.

abasic sills and dykes locally
layering. Intrusive bodies
elevated gold abundances.

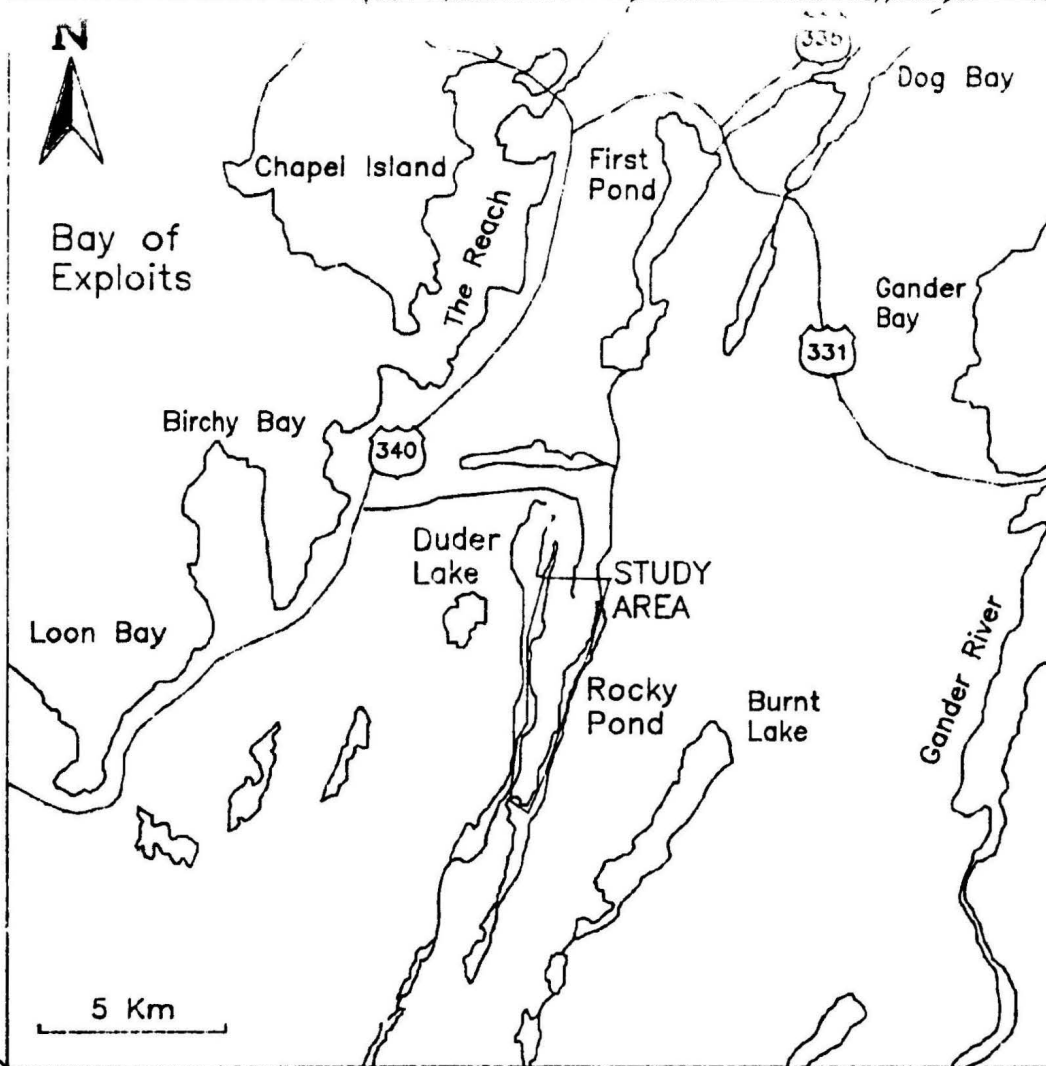
aminated shallow marine
veloped weak to moderate
marine facies siltstone,
25m in thickness
ong cleavage developed

pillows and

aceous siltstone and
s with penetrative



*NB: Only three of the four mineralized sites are depicted on this map. The fourth, Flirt, is located approximately 2km NE of the northern end of map area. The geology of the Flirt showing can be observed in Appendix of Trench Maps, page A62.



DUDER LAKE GEOLOGY

DATE: 12/93

NTS: 2E/07

DRAWN BY: R. Churchill

FILE: dudgeol.dwg

BASELINE AZIMUTH: 023°

Geology modified from Noranda (1989) maps with additional information compiled from Churchill and Evans (1992) and Churchill et al. (1993).

